

**INTEGRATION OF GPS/PSEUDOLITE/INS FOR  
HIGH PRECISION KINEMATIC POSITIONING  
AND NAVIGATION**

By

**Hung Kyu Lee**

B.Sc., Dong-A University, Republic of Korea, 1998

M.Sc., Dong-A University, Republic of Korea, 2000

A thesis submitted to The University of New South Wales  
in partial fulfilment of the requirements for the Degree of  
Doctor of Philosophy

School of Surveying and Spatial Information Systems  
The University of New South Wales  
Sydney NSW 2052, Australia

March, 2004

The integrated GPS/INS system has become an indispensable tool for providing precise and continuous position, velocity, and attitude information for many positioning and navigation applications. Although the integrated GPS/INS system provides augmented solutions that make use of the complementary features of each component system, its performance is still limited by the quality of GPS measurements, and the geometric strength of the satellite constellation. To address such a problem this research has focussed on the integration of GPS, Pseudolite and INS technologies. The main research contributions are summarised below:

- (a) A cost effective GPS/INS integration approach has been developed and tested, consisting of a single-frequency L1 GPS receiver and a tactical-grade strapdown INS. Results of field experiments demonstrate that this approach is capable of delivering position accuracies of the order of a few centimetres under a benign operational environment and provides continuously positioning at sub-decimetre accuracy during GPS signal blockage lasting up to about five seconds.
- (b) A novel kinematic positioning and navigation system based on GPS/Pseudolite/INS integration has been proposed as an alternative to existing GPS/INS systems. With this integration approach, the continuity, integrity, and precision of the GPS/INS system can be significantly improved as the inclusion of pseudolite signals enhances the GPS signal availability and the geometry strength.
- (c) The impact of pseudolite location errors in such pseudolite-augmented systems has been investigated. Theoretical and numerical analyses reveal that the error effects on measurement models, and on final positioning solutions, can be minimised by selecting optimal pseudolite location(s).
- (d) A new ambiguity resolution procedure has been developed for use in the proposed GPS/Pseudolite/INS system. It is designed to rapidly and reliably resolve the single-frequency ambiguities due not only to the aiding by pseudolites and INS, but also by adopting a realistic stochastic model and a statistically rigorous ambiguity validation test. The proposed procedure can indeed improve the performance of the single-frequency ambiguity resolution algorithm in terms of both reliability and time-to-fix-ambiguity.

- (e) An effective cycle slip detection and identification algorithm has been developed, which is suitable for the integrated GPS/Pseudolite/INS system. Test results indicate that induced cycle slips can be reliably detected and instantaneously identified, even if the slips occur at successive epochs.
- (f) Flight trials have been conducted to evaluate the overall performance for aircraft approach and landing using the GPS/Pseudolite/INS system. Results from these trials show that an enhancement in the accuracy and reliability of the vehicle navigation solution can be achieved with the employment of one or more pseudolite.

## ACKNOWLEDGMENTS

---

---

This research was carried out from March 2001 through to February 2004 under the supervision of Dr. Jinling Wang and Professor Chris Rizos. I am sincerely grateful to them for their encouragement, invaluable advice, and patient guidance throughout the course of this study.

I would like to thank Dr. Dorota Grejner-Brzezinska and her research group at Ohio State University not only for providing the elegant AIMS software used in this study, but also for their helpful suggestion and invaluable advice.

I also wish to thank all members of the Satellite Navigation and Positioning (SNAP) group, Mr. Ravindra Babu, Dr. Joel Barnes, Dr. Horng-yue Chen, Dr. Liwen Dai, Dr. Linlin Ge, Mr. Steve Hewitson, Dr. Volker Janssen, Mr. Xiaodong Jia, Dr. Hyung-Keun Lee, Mr. Binghao Li, Mr. Michael Moore, Mr. Peter Mumford, Ms Diana Polonska, Dr. Craig Roberts, Dr. Chalermchon Satirapod, Mr. Ben Soon, Dr. Toshiaki Tsujii, Mr. Tajul Musa, Dr. Clement Ogaja, Mr. Thomas Yan, Dr. Yufei Wang, Mr. Jun Zhang for their support in a variety of ways during this study. Special thanks, in particular, goes to Mr. Soon and Dr. Barnes for their tremendous assistance during the field trials.

I am grateful to Professor Woon-Young Park, Dong-A University, Dr. Kyung-Chul Yun, Hansung UI Engineering Co. Ltd. and Dr. Jae-One Lee, Korean Association of Surveying and Mapping, for their encouragement, valuable advice and inspiration on a variety of research topics. The support of the members of surveying and geo-spatial information system research group at Dong-A University is also acknowledged.

I would also like to sincerely acknowledge the Kwanjeong Educational Foundation, Korea, for awarding me the Postgraduate Research Scholarship to pursue my Ph.D. studies at the UNSW. Much gratitude to the U.S. Institute of Navigation (ION) for awarding me a student competition winner scholarship to support my attendance at the 15<sup>th</sup> International Technical Meeting of the ION Satellite Division, held in Portland, USA, 24-27 September 2001. Thanks to the International Association of Geodesy (IAG)

Special Commission 4 for awarding me a best student paper award to partially support my attendance at the 2<sup>nd</sup> Symposium on Geodesy for Geotechnical and Structural Engineering, held in Berlin, Germany, 21-24 May 2002. In addition, my sincere appreciation to Ohio State University for awarding me a second place in the student paper competition to support my participation at the Heiskanen Symposium in Geodesy, held in Columbus, USA, 1-5 October 2002

Last, but far from least, I would like to extend my deepest appreciation to my family, especially my grandmother Lim-Seng Shin, my father Byeung-Ok Lee, my mother Sun-Hee Lee, my wife Ji-Young Kim and my son Sung-Won, for their love, encouragement and understanding during my PhD studies.

## TABLE OF CONTENTS

---

---

ABSTRACT .....	i
ACKNOWLEDGMENTS .....	iii
TABLE OF CONTENTS .....	v
LIST OF FIGURES .....	xi
LIST OF TABLES .....	xvi
NOTATION .....	xvii

### CHAPTER 1

INTRODUCTION.....	1
1.1 GPS and Pseudolite Background.....	1
1.1.1 Introduction to GPS .....	1
1.1.2 Introduction to Pseudolite.....	3
1.1.3 Fundamental Observables.....	4
1.1.3.1 Pseudo-range observation equation .....	4
1.1.3.2 Carrier phase observation equation .....	6
1.1.3.3 Some comments on the pseudolite observation equations .....	7
1.1.4 Error Sources .....	8
1.1.4.1 Signal transmitter dependent errors.....	8
1.1.4.2 Signal propagation errors.....	9
1.1.4.3 Receiver dependent errors .....	10
1.2 Inertial Navigation System (INS).....	11
1.2.1 Introduction to INS .....	11
1.2.2 Sensor Observations and Errors .....	13
1.3 Motivation .....	15
1.4 Research Objectives.....	16
1.5 Contributions of the Research .....	17
1.6 Outline of the Thesis.....	18

**CHAPTER 2****HIGH PRECISION INTEGRATION OF SINGLE-FREQUENCY GPS WITH TACTICAL-GRADE SDINS ..... 21**

2.1 Introduction.....	21
2.2 Strapdown INS Mechanisation.....	22
2.3 SDINS Error Dynamic Equations.....	25
2.4 Differencing Techniques for GPS Measurement Modelling.....	27
2.4.1 Single-Differences (SD) .....	28
2.4.2 Double-Differences (DD).....	28
2.5 GPS/INS Integration with Kalman Filter .....	29
2.5.1 Kalman Filtering.....	29
2.5.2 State Vector and Dynamic Model .....	32
2.5.3 Filter Update using GPS Measurements.....	35
2.6 Description of Hardware and Software .....	36
2.7 Land Vehicle Experiment.....	38
2.7.1 System Performance Analysis .....	39
2.7.2 Effect of Vehicle Dynamics in the Filter Estimation Performance .....	43
2.7.3 Effect of Vehicle Dynamics in Positioning Accuracy During Complete GPS Signal Blockage .....	46
2.8 Concluding Remarks .....	48

**CHAPTER 3****INTEGRATION OF PSEUDOLITE OBSERVABLES WITH GPS/INS ..... 49**

3.1 Introduction.....	49
3.2 GPS/Pseudolite/INS Integration: Concept and Applications .....	50
3.2.1 General Description of System Concept .....	50
3.2.2 Applications.....	52
3.3 Modelling Pseudolite Measurements.....	53
3.3.1 DD Measurement Model .....	53
3.3.2 Special Considerations for Pseudolite Measurement Modelling.....	53
3.3.2.1 Pseudolite tropospheric delay.....	54

---

3.3.2.2 Pseudolite location error .....	55
3.3.2.3 Pseudolite multipath .....	55
3.4 Geometry Analysis of Pseudolite Augmentation .....	57
3.4.1 GPS Performance Measure.....	57
3.4.1.1 Dilution of Precision (DOP).....	57
3.4.1.2 Ambiguity Dilution of Precision (ADOP).....	58
3.4.1.3 Reliability .....	58
3.4.2 Relative Dilution of Precisions (RDOPs).....	59
3.4.3 Ambiguity Dilution of Precision (ADOP).....	63
3.4.4 Reliability .....	64
3.5 Tests with Simulated Measurements .....	66
3.5.1 Measurement Generation.....	67
3.5.2 Benign Operational Environment.....	69
3.5.3 Adverse Operational Environment .....	72
3.5.4 Pseudolite/INS Integration for Indoor Applications.....	73
3.6 Experiments and Analysis .....	75
3.6.1 Benign Operational Environment.....	76
3.6.2 Adverse Operational Conditions .....	80
3.7 Concluding Remarks .....	81

## **CHAPTER 4**

ANALYSIS OF IMPACT OF PSEUDOLITE LOCATION ERRORS ON POSITIONING .....	83
---	----

4.1 Introduction.....	83
4.2 Theoretical Analysis .....	83
4.3 Numerical Analysis .....	86
4.4 Impacts of Pseudolite Location Errors on Positioning.....	89
4.4.1 Static Positioning Case .....	89
4.4.2 Kinematic Positioning Case.....	92
4.5 Concluding Remarks .....	95



**CHAPTER 5****INTEGER AMBIGUITY RESOLUTION PROCEDURE AIDED BY PSEUDOLITE AND INS..... 96**

5.1 Introduction.....	96
5.2 New Ambiguity Resolution Procedure with Pseudolite and INS.....	98
5.2.1 Measurement Modelling.....	98
5.2.2 Integer Ambiguity Estimation .....	101
5.2.3 Ambiguity Validation .....	103
5.2.4 Discussion on the Proposed Approach .....	104
5.3 Simulation Studies .....	106
5.4 Experiment and results .....	112
5.4.1 General Description of the Tests .....	112
5.4.2 Special Consideration of Pseudolite Multipath .....	114
5.4.3 AR Performance Analysis .....	116
5.5 Concluding Remarks .....	121

**CHAPTER 6****EFFECTIVE CYCLE SLIP DETECTION AND IDENTIFICATION ALGORITHM.....123**

6.1 Introduction.....	123
6.2 A Cycle Slip Detection and Identification Algorithm.....	125
6.2.1 Decision Value and its Statistical Property .....	125
6.2.2 Cumulative Sums (CUSUMS) Test.....	128
6.3 Algorithm Performance Tests.....	134
6.3.1 CUSUM Tuning Parameters and ‘Truth’ for Tests .....	134
6.3.2 Test Results with ‘Data Set I’ .....	135
6.3.3 Test Results with ‘Data Set II’ .....	137
6.4 Concluding Remarks .....	139

**CHAPTER 7****CASE STUDY: GPS/PSEUDOLITE/INS INTEGRATION FOR AIRCRAFT PRECISION APPROACH AND LANDING..... 140**

---

7.1 Introduction.....	140
7.2 An Airborne GPS/Pseudolite/INS System .....	141
7.2.1 Ground Subsystem.....	141
7.2.2 Airborne Subsystem .....	142
7.3 Flight Experiment Design.....	143
7.4 Flight Test Results .....	146
7.4.1 Test Results with Carrier Phase Measurements .....	148
7.4.2 Results with Pseudo-Range Measurements .....	152
7.5 Concluding Remarks .....	156
<b>CHAPTER 8</b>	
SUMMARY AND RECOMMENDATIONS.....	157
8.1 Summary.....	157
8.1.1 High Precision Integration of Single-Frequency GPS with Tactical- Grade SDINS .....	157
8.1.2 Integration of Pseudolite Observables with GPS/INS.....	158
8.1.3 Impact of Pseudolite Location Errors on Positioning.....	159
8.1.4 An Integer Ambiguity Resolution Procedure Using Pseudolite and INS .....	160
8.1.5 An Effective Cycle Slip Detection and Identification Algorithm .....	161
8.1.6 Case Study of GPS/Pseudolite/INS Integration for Aircraft Precision Approach and Landing.....	162
8.2 Recommendations for Future Research.....	163
REFERENCES.....	165
APPENDIX A .....	176
APPENDIX B .....	181

APPENDIX C .....	185
APPENDIX D .....	187
VITA .....	195

## LIST OF FIGURES

---

---

### Figures

1.1	Fundamental Inertial Navigation System concept .....	12
1-2	Inertial sensor bias and scale factor errors (Hewitson et al., 2003).....	14
2-1	Flow chart of the SDINS mechanisation module.....	25
2-2	Tightly coupled GPS/INS integration scheme using carrier phase measurements.	36
2-3	DQI functional block diagram (Boeing, 1997).....	37
2-4	Trial vehicle .....	38
2-5	Vehicle trajectory during the experiment .....	40
2-6	Integrated GPS/INS positioning accuracy comparing with GPS RTK solutions ...	40
2-7	Navigational parameters and their RMS errors .....	41
2-8	Carrier phase residuals based on INS predicted positions.....	41
2-9	INS-predicted antenna position errors during 50 seconds of the signal blockages	42
2-10	Vehicle trajectories and dynamics during the tests.....	44
2-11	RMS errors for horizontal accelerometer bias and heading error estimation .....	45
2-12	Magnified results for heading RMS error in Figure 2-11 .....	45
2-13	Vehicle trajectories and velocities during GPS blockage.....	47
2-14	Error growth of navigation parameters during GPS blockage.....	47
3-1	Tactical-grade INS error behaviour without GPS calibration. ....	51
3-2	Effect of multipath on the double-differenced GPS/pseudolite observations Pseudo-Range (PR) and Carrier Phase (CPH)).....	56
3-3	Satellite constellation and RDOP changes as a function of pseudolite location ....	60
3-4	RDOP simulation results as a function of pseudolite azimuth and elevation.....	62
3-5	Average ADOP with respect to the number of pseudolites.....	64
3-6	Reliability changes without pseudolites .....	65
3-7	Internal reliability (MDB) changes as a function of the number of additional pseudolites.....	65
3-8	External reliability changes as a function of the number of additional pseudolites	66
3-9	The GPS/PL/SDIMU measurement simulator.....	68
3-10	A generated reference trajectory and pseudolite locations .....	69

---

3-11 Standard deviation of position differences in the GPS/PL/INS system as a function of the number of pseudolites .....	70
3-12 Standard deviation of velocity differences in the GPS/PL/INS system as a function of the number of pseudolites .....	71
3-13 Standard deviation of attitude angle differences in the GPS/PL/INS system as a function of the number of pseudolites .....	71
3-14 Standard deviation of DD residuals of the highest satellites in the GPS/PL/INS system as a function of the number of pseudolites.....	72
3-15 Comparison of positioning accuracy between GPS/INS and GPS/PL/INS under adverse operational environment .....	73
3-16 RMS errors for Kalman filter estimation (PL/INS).....	74
3-17 Positioning accuracy of PL/INS .....	74
3-18 DD residual differences of PLs computed by INS predicted positions .....	75
3-19 Coordinate differences in GPS/INS system with/without two pseudolite signals..	77
3-20 DD residuals in four satellites pairs in the GPS/INS case .....	77
3-21 DD residuals in four satellites pairs in the GPS/PL/INS case. ....	78
3-22 RMS value changes in position component.....	78
3-23 RMS value changes in velocity component.....	79
3-24 RMS value changes in attitude component.....	79
3-25 Sky view of satellite and pseudolite distribution.....	80
3-26 Navigation solution comparison with the first test (GPS/PL/INS).....	81
4-1 Special set-ups of the pseudolite and baselines .....	85
4-2 Influence of 5cm pseudolites location bias on the user location B (Worst) .....	87
4-3 Influence of 5cm pseudolite location bias on the location B' (Best).....	87
4-4 Errors in SD varying azimuth at the Location B (Worst).....	88
4-5 Errors in SD varying azimuth at the Location B' (Best) .....	88
4-6 DOP changes in the case of stationary receiver.....	90
4-7 GPS/pseudolite positioning accuracy with/without the pseudolite location errors in the worst case.....	91
4-8 GPS/pseudolite positioning accuracy with/without the pseudolite location errors in the best case .....	91
4-9 Mobile receiver trajectory and pseudolite locations in the test .....	92
4-10 Geometry changes in both scenarios I & II .....	93

4-11 Change of GPS/pseudolite positioning and DD errors (Scenario I).....	94
4-12 Change of GPS/pseudolite positioning and DD errors (Scenario II).....	94
5-1 The proposed ambiguity resolution procedure.....	97
5-2 Impact of Pseudolites on the ADOP (depending on the number of Pseudolites).....	107
5-3 Impact of Pseudolites on ADOP (depending on the vehicle dynamics).....	108
5-4 Impact of INS-predicted position on ADOP (comparison between GPS/INS and GPS/PL/INS systems) .....	109
5-5 Impact of INS-predicted position errors on ADOP during signal blockages (GPS/PL/INS systems).....	110
5-6 INS-predicted position error behaviours during absolute signal outage (30 seconds) and updating the filter by the DD pseudo-ranges in the AR procedure .....	111
5-7 Impact of updating Kalman filter by DD pseudo-ranges on ADOP after 30 second signal blockage.....	112
5-8 Experiment set-up .....	113
5-9 Vehicle trajectory and locations of reference station and pseudolites.....	114
5-10 Pseudolite pseudo-range multipath estimation .....	115
5-11 An effect of including multipath in the pseudolite pseudo-range as an unknown parameter in the float ambiguity estimation.....	116
5-12 W-ratio values for the different system configurations (epoch-by-epoch solution) .....	117
5-13 W-ratio values for the different stochastic models (epoch-by-epoch solution)....	118
5-14 Time-to-fix L1 carrier phase ambiguity after different lengths of signal blockage .....	121
6-1 Cycle slip on GPS carrier phase observables.....	124
6-2 Typical behaviour of the CUSUM decision function calculated by Equation (6.22).....	131
6-3 Typical behaviour of the CUSUM decision function calculated by Equation (6.24).....	132
6-4 Cumulative sums for detecting one cycle slip in L1 carrier phase measurement in the case of positive slip (SV 15).....	133
6-5 Cumulative sums for detecting one cycle slip in L1 carrier phase measurement in the case of negative slip (SV 30).....	133

---

6-6	CUSUM test for PRN 4 (ref SV 7).....	135
6-7	CUSUM test for PRN 9 (ref SV 7).....	136
6-8	CUSUM test for PRN 24 (ref SV 7).....	136
6-9	CUSUM test for SV 7 (ref SV 4).....	138
6-10	CUSUM test for PL 12 (ref SV4).....	138
7-1	L1 C/A pseudolites configuration block diagram.....	142
7-2	Airborne subsystem diagram.....	143
7-3	Airborne system in the aircraft's nose cone.....	143
7-4	Wedderburn Airfield ground configuration (Not to scale).....	144
7-5	Beech Duchess aircraft from the UNSW Aviation Department.....	145
7-6	Plan view of the flight trajectory.....	147
7-7	Vertical view of the flight trajectory chosen for the data processing.....	147
7-8	RDOP changes of an approach with/without pseudolites.....	148
7-9	Position differences of GPS/INS and GPS/PL/INS systems from the dual-frequency GPS-only processing (with DD carrier phases).....	149
7-10	DD carrier phase residuals of the three highest satellites in GPS/INS and GPS/PL/INS systems.....	150
7-11	RMS difference between GPS/INS and GPS/PL/INS systems in the navigation error estimates (with DD carrier phases).....	151
7-12	Internal and external (horizontal and vertical) reliability values during the approach (with DD carrier phases).....	152
7-13	Position differences of GPS/INS and GPS/PL/INS systems from the dual-frequency GPS-only processing (with DD pseudo-ranges).....	153
7-14	DD pseudo-range residuals of the three highest satellites in GPS/INS and GPS/PL/INS systems.....	154
7-15	RMS difference between GPS/INS and GPS/PL/INS systems in the navigation error estimates (with DD pseudo-ranges).....	154
7-16	Internal and External (horizontal and vertical) Reliability during the approach (with DD pseudo-ranges).....	155
D-1	Plan and vertical views of the flight trajectory in ENU frame (origin at reference station).....	187
D-2	Velocities in ENU frame for the vehicle.....	187
D-3	The estimated attitudes for the vehicle.....	188

---

D-4	Estimated position errors from the filter states and their RMS .....	188
D-5	Estimated velocity errors from the filter states and their RMS .....	189
D-6	Estimated three misalignments of the platform frame and their RMS .....	189
D-7	Estimated accelerometer biases from the filter and their RMS .....	190
D-8	Estimated gyroscope biases from the filter and their RMS .....	190
D-9	Plan and vertical view of the flight trajectory in ENU frame (origin at reference station) .....	191
D-10	Velocities in ENU frame for the vehicle.....	191
D-11	Attitudes for the vehicle.....	192
D-12	Estimated position errors from the filter states and their RMS .....	192
D-13	Estimated velocity errors from the filter states and their RMS .....	193
D-14	Estimated three misalignments of the platform frame and their RMS .....	193
D-15	Estimated accelerometer biases from the filter and their RMS .....	194
D-16	Estimated gyroscope biases from the filter and their RMS .....	194



## LIST OF TABLES

---

---

### Tables

3-1	Average RDOP values as a function of the number of pseudolites.....	63
3-2	Mean reliability values as a function of the number of pseudolites (unit: cm) .....	66
5-1	Ambiguity validation test results for different system configurations .....	117
5-2	Ambiguity validation test result for different stochastic models.....	119
5-3	Time-to-fix L1 carrier phase ambiguity after the different length of blockages ..	120
6-1	Cycle slip detection and identification procedure results of ‘Data Set I’ .....	137
6-2	Cycle slip detection and identification procedure results of ‘Data Set II’ .....	139
7-1	Comparison of positioning results of GPS/INS and GPS/PL/INS systems based on DD carrier phases with the independent trajectory obtained from dual- frequency GPS processing (unit: cm) .....	150
7-2	Averaged and standard deviation of DD carrier phase residuals from the three highest satellites (unit: cm) .....	150
7-3	Comparison of positioning results of GPS/INS and GPS/PL/INS systems based on DD pseudo-ranges with the independent trajectory obtained from dual- frequency GPS processing (unit: cm) .....	155
7-4	Averaged and standard deviation of DD pseudo-range residuals from the three highest satellites when pseudolite measurements are available (unit: cm).....	155

## 1. CONVENTIONS

1.1 Rotation Matrix  $R$  is specified by two indices so that the transformation of vector  $r^a$  in the  $a$ -frame to the  $b$ -frame is:

$$r^b = R_a^b r^a$$

1.2 Angular velocity of the  $a$ -frame with respect to the  $i$ -frame, expressed in the  $b$ -frame is described by:

$$\omega_{ia}^b = [\omega_x, \omega_y, \omega_z]^T$$

or by the corresponding skew-symmetric matrix as:

$$\Omega_{ia}^b = \begin{bmatrix} 0 & -\omega_z & \omega_y \\ \omega_z & 0 & -\omega_x \\ -\omega_y & \omega_x & 0 \end{bmatrix}$$

## 2. COORDINATE FRAMES

### 2.1 Inertial Frame ( $i$ -frame)

An inertial frame is a reference frame in which Newton's laws of motion are assumed to apply. Hence, the frame is non-rotating and non-accelerating. The definition of the inertial frame for this thesis is:

- Origin: The earth's centre of mass
- X-axis: Toward the mean vernal equinox
- Y-axis: Complete a right-handed system
- Z-axis: Toward the earth's rotation axis

## 2.2 Earth-Centered Earth-Fixed Frame (*e*-frame)

The ECEF frame is not inertial because it is fixed to the earth. Hence, it rotates relative to the inertial frame with the earth rotation rate (e.g.,  $7.292115 \times 10^{-5}$  rad/s). Its definition is:

Origin: The earth's centre of mass

X-axis: Toward the Greenwich meridian in the equatorial plane

Y-axis: Complete a right-handed system

Z-axis: Toward the earth's rotation axis

## 2.3 Local-Geodetic (Navigation) Frame (*n*-frame)

Local-Geodetic (NED) frame is the right-handed system that is used as a navigation frame in this thesis and its definition is:

Origin: The centre of INS

X-axis: Toward ellipsoidal true north (North)

Y-axis: Toward ellipsoidal east (East)

Z-axis: Downwards direction along the ellipsoidal normal (Down)

## 2.4 Body Frame (*b*-frame)

The body frame is the orthogonal frame in which the measurements of a strapdown INS are made and its definition is:

Origin: The centre of INS

X-axis: Toward the front end of the vehicle

Y-axis: Toward the right side

Z-axis: Downward and perpendicular to the X-Y plane

---

### 3. ABBREVIATIONS

ADOP	Ambiguity Dilution of Precision
AIMS	Airborne Integrated Mapping System
AR	Ambiguity Resolution
C/A-code	Coarse Acquisition or Civilian Access code
cm	Centimetre
CUSUM	Cumulative Sum
CS	Cycle Slip
DD	Double-Differencing
DoD	Department of Defense
DQI	Digital Quartz IMU
CPH	Carrier Phase
MIGITS	Miniature Integrated GPS/INS Tactical System
GCP	Ground Control Points
GINS	Gimballed Inertial Navigation System
GNSS	Global Navigation Satellite System
GPS	Global Positioning System
GDOP	Geometric Dilution of Precision
HDOP	Horizontal Dilution of Precision
Hz	Hertz
INS	Inertial Navigation System
IMU	Inertial Measuring Unit
ION	Institute Of Navigation
ISA	Inertial Sensor Assembly
ISM	Industrial, Scientific, and Medical radio band
KF	Kalman filter
km	Kilometre
L1	First frequency sent out by GPS satellite ( $\approx 1.5\text{GHz}$ )
L2	Second frequency sent out by GPS satellite ( $\approx 1.2\text{GHz}$ )
LAMBDA	Least Squares AMBIGUITY Decorrelation Adjustment
LAAS	Loca Area Augmentation System
m	Metre

---

MDB	Minimum Detectable Bias
MEDLL	Multipath Estimating Delay Lock Loops
mm	millimetre
m/s	Metre per second
NED	Northing Easting Down
NIMA	National Imagery and Mapping Agency (now National Geospatial-Intelligence Agency)
OTF	On-The-Fly
P-code	Precision-code
RINEX	Receiver Independent Exchange Format
PL	Pseudolite
PPM	Part Per Million
PR	Pseudo-Range
QRS	Quartz Rate Sensors
RDOP	Relative Dilution of Precision
PRN	Pseudo-Random Noise
RMS	Root-Mean-Square
RTK	Real-Time Kinematic
SDINS	Strapdown Inertial Navigation System
SDIMU	Strapdown Inertial Measuring Unit
SNAP	Satellite Navigation and Positioning Group
SNR	Signal to Noise Ratio
SPP	Single Point Positioning
SA	Selective Availability
SD	Single-Differencing
SV	Space Vehicle
TEC	Total Electron Content
UNSO	U.S Naval Observatory
UNSW	University of New South Wales
VDOP	Vertical Dilution of Precision
VQA	Vibrating Quartz Accelerometers
WASS	Wide Area Augmentation System
WGS84	World Geodetic System 1984

# CHAPTER 1

## INTRODUCTION

---

---

### 1.1 GPS and Pseudolite Background

#### 1.1.1 Introduction to GPS

The Global Positioning System (GPS) is a satellite-based radio navigation and time determination system, which was developed and is maintained and operated by the U.S. Department of Defense (DoD). The system has the advantage of being globally accessible, functioning independent of local weather conditions, and being able to provide three-dimensional positioning, velocity and time in a common reference system, anywhere on or near the surface of the Earth, on a continuous basis. Hence, although the system was mainly designed for military purposes, it has been widely used in an increasing number of civil applications ranging from vehicle navigation, control and guidance to precise geodetic positioning.

The system consists of three segments, namely the Space, the Control, and the User Segment. The *Space Segment* nominally consists of 24 satellites (21 plus three spares), orbiting within six nearly circular orbital planes of approximately 20,200 km altitude, inclined at about 55 degrees with respect to the equatorial plane. There are four satellites in each orbital plane. The *Control Segment* comprises the ground facilities carrying out the tasks of satellite tracking, orbit computations, telemetry and supervision necessary for the continuous operation of the Space Segment. There are five ground facility stations located around the world. The *User Segment* refers to the entire spectrum of application, equipment and computational techniques that are available to users.

GPS employs the ECEF World Geodetic System 1984 (WGS84), defined and maintained by the U.S National Geospatial-Intelligence Agency (formerly National Imagery and Mapping Agency, NIMA), as the reference frame to which all GPS positioning information is referred. However, GPS time is referenced to the Universal

Coordinated Time (UTC) as maintained by U.S. Naval Observatory (UNSO). The integer offset between the GPS and UTC time scale are the so-called leap seconds.

The present GPS satellites transmit ranging signals on two L-band frequencies, a primary signal (L1) at 1575.42 MHz (corresponding to a wavelength of 19.05 cm) and a secondary signal (L2) at 1227.60 MHz (corresponding to a wavelength 24.45 cm). Modulated on the L1 carrier phase are two pseudo-random noise (PRN) ranging codes. The first code is the 1-millisecond-long C/A-code (Coarse/Acquisition-code) with a chipping rate of 1.023MHz. The second is a week-long segment of the P-code (Precision-code) with a chipping rate of 10.23MHz. In addition, modulated on the carrier phase is the 'navigation message', consisting of satellite health information, satellite ephemeris that describes the predicted position of the satellite and the predicted satellite clock correction terms. The L2 carrier phase is modulated by the P-code and the 'navigation message', but no C/A-code. Whilst the C/A-code is used by the Standard Positioning Services (SPS), the P-code ranging is the basis of the Precise Positioning Service (PPS), which is however reserved for U.S military and other authorised users.

In the near future, two new navigation signals will be available for civil users when the GPS Modernization program is completed. The first of these new signals will be a civilian code (similar to the C/A-code) on the empty box of the existing L2 carrier, for general non-safety critical applications. The other one will be a new civil frequency at 1176.45 MHz, referenced to as L5. Both of these signals will be available for use when the GPS Block IIR-M and IIF satellites are launched, which is scheduled in early 2006. Therefore, the modernized system with new civilian signals will enhance the accuracy, reliability, and robustness of the current GPS navigation performance, resulting in significantly improved system capabilities. Information concerning the modernization status can be found, e.g., at <http://navcen.useg.gov/gps>, and <http://gps.faa.gov>.

Details on the GPS can be found in any of a number of textbooks, see, e.g., Hofmann-Wellenhof et al. (2001); Leick (1995); Parkinson and Spilker (1996); Rizos (1996); Seeber (1993).

### 1.1.2 Introduction to Pseudolite

There are 1024 possible C/A-codes and only 32 C/A-PRN codes are reserved for the GPS satellites, so that other satellites or transmitters may use these unassigned codes. Different PRN codes could be assigned to new satellites, and as far as the user hardware is concerned they would be indistinguishable from the GPS satellite signals. A GPS ‘pseudo-satellite’, commonly referenced to as a ‘pseudolite’, is a ‘satellite-on-the-ground’ that transmits GPS-like ranging signal (Elrod and Van Dierendonck, 1996). The pseudolite is a complementary technology to GPS that offers opportunities for robust positioning and navigation. It can be expected that augmentation of GPS with the pseudolites will improve overall performance as the availability and the geometry of the satellite and pseudolite constellation can be significantly enhanced.

The idea of using pseudolites is older than the GPS itself. Before the U.S. DoD launched the first GPS satellites, it tested the system concept and the initial GPS user equipment with ground-based transmitters (Harrington and Dolloff, 1976). In the early 1980’s, it began to consider the use of pseudolites as a complementary technology for GPS operations (Beser and Parkinson, 1982; Klein and Parkinson, 1984). During the past decade, pseudolite equipment has been available and applied to a range of applications, such as aircraft precision approach and landing (Elrod and Barltrop, 1994; Hein et al, 1997; Bartone, 1997; Henzler and Weiser, 1999), deformation monitoring (Barnes et al., 2002; Dai et al., 2002), precision aircraft approach applications, and other (Barltrop et al., 1996; Dai et al., 2001; Weiser, 1998; Wang et al., 2000; Wang 2002; Stone and Powell, 1999; O’Keefe et al., 1999; Tsujii et al., 2001). For these applications the pseudolites have been implemented as a ground augmentation of satellite positioning and navigation systems, through strengthening the satellite geometry and increasing signal availability. A pseudolite-only positioning system is also possible, replacing the GPS constellation where it is not feasible to use satellite signals, such as indoor positioning (Kee et al, 2000), and for Mars exploration (Lemaster and Rock, 1999).

In principle, pseudolites can be designed to emit their ranging signals on different frequencies. Zimmerman et al (2000) proposed a design of a pseudolite that uses five



frequencies (two in the 900MHz ISM band, two in the 2.4GHz ISM band, and one that is the GPS L1 frequency). An advantage of such multi-frequency pseudolite systems is that the integer carrier phase ambiguities can be resolved instantaneously due to redundant measurements and the extra wide-lane observables that can be constructed from the different frequencies. However, the majority of the pseudolites transmits GPS-like signals at the frequencies of L1 (1575.4MHz), and a few in addition on L2 (1227.6MHz). With such a configuration, and after the appropriate modification of the receiver firmware, standard GPS receivers could be used to track pseudolite signals. It has been recently reported that NovAtel Millennium and CMC Allstar GPS receivers have been used to track pseudolite signals (Dai et al., 2001; Barnes et al., 2002; Tsujii et al., 2001). In addition, some GPS receiver development kits, which include receiver firmware source code, can be modified for pseudolite applications. For example, the Mitel (now Zarlink) GPS Architect 12 Channel Development Kit has been used for this purpose (e.g., LeMaster and Rock, 1999; Stone and Powell, 1998; Wawrzyniak et al., 2002).

### **1.1.3 Fundamental Observables**

The positioning capabilities of GPS and pseudolites are based on the fundamental ranging signal observations. The two most common GPS and pseudolite observables are the pseudo-range and the carrier phase.

#### **1.1.3.1 Pseudo-range observation equation**

The pseudo-range observation is the difference between the transmission time at a signal emitting antenna and the reception time at a receiver, scaled by the speed of light. If the receiver and satellite/pseudolite clocks were synchronised, multiplication of the travel time by the speed of light would yield the true range between a satellite/pseudolite and a receiver. However, the satellite/pseudolite and receiver clocks have different accuracy levels and perfect synchronisation cannot be achieved. In addition, there are many errors and biases affecting the ranging signal as it propagates

through the Earth's atmosphere. Considering these error sources, the mathematical expression for the GPS satellite pseudo-range observations is:

$$R_i^s = \rho_i^s + d\rho_i^s + c(dt^s - dT_i) + di_i^s + dr_i^s + dm_{i,R}^s + \varepsilon_{i,R}^s \quad (1.1)$$

where,

$R_i^s$ :	the pseudo-range observation in units of metres between receiver $i$ to satellite $s$
$\rho_i^s$ :	the true or "geometric" range between receiver $i$ to satellite $s$
$d\rho_i^s$ :	the satellite orbit error
$dt^s$ :	the satellite clock error
$dT_i$ :	the receiver clock error
$di_i^s$ :	the ionospheric effect
$dr_i^s$ :	the tropospheric delay
$dm_{i,R}^s$ :	the multipath on the pseudo-range
$\varepsilon_{i,R}^s$ :	the pseudo-range measurement noise
$c$ :	the velocity of light

The pseudolite pseudo-range observation can be expressed in a manner similar to that of the GPS:

$$R_i^p = \rho_i^p + d\rho_i^p + c(dt^p - dT_i) + dr_i^p + dm_{i,R}^p + \varepsilon_{i,R}^p \quad (1.2)$$

$R_i^p$ :	the pseudo-range observation between receiver $i$ and pseudolite $p$
$\rho_i^p$ :	the true range or "geometric" range
$d\rho_i^p$ :	the pseudolite location error
$dt^p$ :	the pseudolite clock error
$dr_i^p$ :	the tropospheric delay

$dm_{i,R}^p$ :	the multipath on the pseudo-range
$\varepsilon_{i,R}^p$ :	the pseudolite pseudo-range measurement noise

### 1.1.3.2 Carrier phase observation equation

The carrier phase observation is a measure of the phase difference between the carrier signal generated by a receiver oscillator and the carrier signal from a satellite/pseudolite. The carrier phase observation consists of an integer number of full cycles and an additional fractional part. GPS/pseudolite receivers are not able to distinguish one cycle from another, but only measure the fractional part and keep track of changes in the carrier phase. Hence when the receiver locks onto a satellite/pseudolite signal, the number of full cycles is initially unknown, or ambiguous. This is known as the integer carrier phase ambiguity. The mathematical expression for the GPS carrier phase observation is:

$$\lambda_G \cdot \phi_i^s = \rho_i^s + d\rho_i^s + c(dt^s - dT_i) + \lambda_G \cdot N_i^s - di_i^s + dr_i^s + d_{i,\phi}^s + \varepsilon_{i,\phi}^s \quad (1.3)$$

where,

$\phi_i^s$ :	the carrier phase observation between receiver $i$ to satellite $s$
$\lambda_G$ :	the wave length of the GPS carrier phase
$N_i^s$ :	the integer carrier phase ambiguity
$d_{i,\phi}^s$ :	the multipath on the carrier phase
$\varepsilon_{i,\phi}^s$ :	the carrier phase measurement noise

The other terms being the same as Equation (1.1)

The pseudolite carrier phase observation can be expressed in a manner similar to that of the GPS:

$$\lambda_p \cdot \phi_i^p = \rho_i^p + d\rho_i^p + c(dt^p - dT_i) + \lambda_p \cdot N_i^p + dr_i^p + dm_{i,\phi}^p + \varepsilon_{i,\phi}^p \quad (1.4)$$

where,

$\phi_i^p$ :	the carrier phase observation between receiver $i$ and pseudolite $p$
$\lambda_p$ :	the wave length of the pseudolite carrier phase
$dm_{i,\phi}^p$ :	the multipath on the carrier phase
$N_i^p$ :	the integer carrier phase ambiguity
$\varepsilon_{i,\phi}^p$ :	the pseudolite phase measurement noise

The other terms being the same as Equation (1.2)

### 1.1.3.3 Some comments on the pseudolite observation equations

In the above Equations (1.2) and (1.4) for pseudolites observations, it is important to note that there are no signal-propagation correction terms for the ionosphere. This is due to the fact that the pseudolite signal transmitter and the user receiver antenna are both on the ground, and hence the pseudolite signal does not propagate through the ionosphere. In addition, the nature of some error terms, like the pseudolite location error, tropospheric delay, multipath, is different from those of satellites as the pseudolites are located close to users. These issues will be discussed in detail in Chapter 3.

Two different types of pseudolites can be considered, based upon the signal frequencies used to transmit their ranging signals. When pseudolites transmit their ranging signals on frequencies different from those of GPS, modelling strategies developed for GPS and GLONASS measurements can be applied when combining pseudolites with GPS (Wang et al., 2001a). On the other hand, if pseudolites transmit their signals on the same frequencies as GPS, integrating the GPS and pseudolite measurements is straightforward as the pseudolites can simply be considered extra GPS satellites ‘on the ground’. Note that the pseudolite systems used in this research (e.g., IntegriNautics IN200CXL and a prototype system based on Spirent Communications GSS4100P single-channel signal generator) belong to the latter class.

### 1.1.4 Error Sources

As indicated in Equation (1.1) to (1.4), the GPS/pseudolite measurements are contaminated by several error sources. In order to achieve accurate results these errors must be taken into account in the data processing. The errors can be classified as: transmitter related errors, signal propagation errors, and receiver related errors.

#### 1.1.4.1 Signal transmitter dependent errors

The signal transmitter related errors are the satellite orbit error (location error in the case of pseudolite) and the clock error. First of all, the *satellite orbit (or pseudolite location) error* is the discrepancy between the transmitter position information available to the user and the true position. In the case of GPS, the ephemeris available to user at the time of observation is predicted from previous satellite tracking at the ground monitoring stations of the control segment. It is, hence, unfeasible to transmit the exact satellite orbit due to the limitation in the modelling (several metres). On the other hand, GPS or terrestrial surveying techniques are used to determine the coordinates of the pseudolite signal transmitter antennas. Although special precautions are taken, surveying errors are inevitable, resulting in pseudolite location error (albeit small).

The satellite/pseudolite clock bias, drift, and drift-rate from the GPS reference time are referred to as the *satellite/pseudolite clock errors (or uncertainties)*. The behaviour of each satellite clock is monitored with respect to GPS time maintained by the Control Segment. The predicted corrections in the form of a second-order polynomial to the individual satellite clock are transmitted as part of the navigation message to users. Even though the Control Segment monitors and models the clock error behaviour of each satellite, it is impossible to exactly predict these errors. The pseudolite clock bias could be much larger than that of a satellite, unless a special design for the synchronisation of the pseudolites oscillator to GPS time is implemented in the system. Although synchronisation techniques are utilised, the errors are still unavoidable (as with the satellite case). However, a measurement differencing technique between two receivers can eliminate the effect of the satellite/pseudolite clock errors.

#### 1.1.4.2 Signal propagation errors

While propagating from satellites/pseudolites to receivers, the signals are disturbed by atmospheric and multipath effects.

The free electrons in the Earth's ionosphere, extending from a height of about 50km to 1000km, prohibit the GPS signals from travelling at the vacuum speed of light. When passing through the ionosphere, the propagation of the modulation on the carrier is delayed, while the propagation of the carrier wave is advanced. Accordingly, the retardation and advancement are referred to as the *ionospheric effect* (Leick, 1995, Seeber, 1993, Rizos, 1996). In actual fact, the ionospheric effect is proportional to the inverse of the carrier-frequency-squared and to the total electron content (TEC) along the path of the ranging signal. The TEC varies with time, season and geographic location, with the main influences on the signal propagation being the solar activity and the geomagnetic field. In general, the magnitude of the ionospheric delay is of the order of 5m to 15m but can reach over 100m (Parkinson and Spilker, 1996). A differencing technique between two receivers a short distance apart can significantly reduce the impact of the ionospheric due to the fact that the ionospheric delay is highly correlated over distances up to about 15km. However if the baseline length becomes longer than 15km, it is preferable to utilise dual-frequency measurements to estimate the ionospheric effect, as the effect is dependent on the frequency. On the other hand, pseudolites do not have the ionospheric effect term in their observations (Equations (1.2) and (1.4)).

In contrast to the ionosphere, the troposphere is a non-dispersive medium so that the tropospheric effects on GPS/pseudolite signal propagation are independent of the signal frequencies (Spilker, 1996). The troposphere ranges from the Earth's surface up to approximately 50km with the majority being just 10km thick. The effect caused by the atmospheric medium is referred to as the *tropospheric delay (or refraction)*. The magnitude of the tropospheric delay ranges from approximately 2m for signals at the zenith to about 20m for signals at an elevation angle of 10 degrees (Brunner and Welsch, 1993). The delay is a function of elevation angle and is dependent on a number of meteorological factors, such as the atmospheric pressure, temperature and water vapour

content. It should be noted that the tropospheric delay is unable to be estimated by using dual-frequency measurements. Instead, several models can be used to estimate the tropospheric delay (for example, Hopfield, 1969; Saastamoinen, 1973). These models can only compensate for about 90% of the total delay, as it is very difficult to model the wet component of the delay due to its high variability. In addition, the delay can be significantly reduced to a certain level using the differencing technique, as is the case for the ionospheric delay.

*Multipath* occurs when one or more reflected signals arrive at the antenna in addition to the direct signal. The multipath is caused by extraneous reflections from nearby metallic objects, ground or water surfaces reaching the antenna and therefore, is highly dependent on the surroundings of the receiver antenna and the type of antenna used (Seeber, 1993; Leick, 1995; Rizos, 1996). Since the receiver cannot distinguish between direct and reflected signals, the receiver acquires the observables based on the combined signal rather than the direct signal, causing the multipath. If a state-of-art receiver is used under the most severe conditions, the multipath reaches 15m for the PRN ranging measurements and  $\frac{1}{4}$  wavelength for the carrier waves (Ray, 2000). This magnitude corresponds to about 5cm for L1 and L2 phase observations. However, typical magnitude of the multipath effects is up to 3m for the pseudo-range and around 0.5cm for the carrier phase (ibid, 2000). The multipath error can be mitigated by using some appropriate technologies, for example narrow correlator spacing (Van Deirendonck et al, 1992) and Multipath Estimating Delay Lock Loops (MEDLL) (Townsend et al, 1995) or in practice, choosing antenna hardware such as choke rings and ground planes that have been found to be quite effective for reducing multipath (Lachapelle et al, 1989).

#### **1.1.4.3 Receiver dependent errors**

The receiver related errors are mainly caused by the receiver clock error (or uncertainty) and receiver noise. Similar to the satellite clock error, the *receiver clock error* is the offset between the receiver clock time and the GPS reference time system. In general, the receiver clock error is much larger than that of the satellite since relatively inexpensive clocks (e.g., crystal oscillators) are used inside GPS receivers. The option

in the case of Single Point Positioning (SPP) is to treat the error as an additional unknown parameter in the estimation procedure, whereas for relative positioning, measurement differencing between two satellites tracked by the receiver is used.

The *receiver noise* mainly comprises frequency thermal noise and dynamic stress on the tracking loop. The receiver noise for the C/A-code is normally higher than that of the P(Y)-code since the C/A-code chip is ten times wider than that of P(Y)-code. Note that modern GPS receiver technology can maintain a very low noise level, for example a few millimetres for the carrier phase, and several decimetres for the pseudo-range.

## 1.2 Inertial Navigation System (INS)

### 1.2.1 Introduction to INS

An Inertial Navigation System (INS) is a self-contained navigation unit that provides position, velocity and attitude information. It consists of an Inertial Measurement Unit (IMU) and a digital computer. The IMU, comprising accelerometers and gyroscopes, measures motion based on physical laws of nature, while the digital computer performs the mathematical integration operations. The basic concept of INS navigation computation is to integrate the acceleration vector sensed by the accelerometers to determine velocity and position as shown in Figure 1-1. Since the accelerations are measured with respect to the body frame, they have to be transformed to the platform frame and then to the desired navigation frame. The transformation is performed using angular rate or angular displacement sensing instruments (e.g., gyroscopes) physically installed in a known geometrical relationship with respect to the accelerometers. It should be noted that accelerometer-sensed measurements are not *total accelerations* but *specific forces*. Hence, the gravity acceleration compensation should be calculated and added to the specific force (see, Figure 1-1).

Two approaches have been used in INS mechanisation: *gimballed* and *strapdown*. In the older gimballed system, the inertial sensors are mounted orthogonally on a (inner) platform whose orientation is controlled by electric torque motors mounted around the



gimbal bearing axes. The control signals for the torque motors are provided by the respective gyroscope. Hence, the accelerometers are always aligned with the axes of a well-defined frame (e.g., inertial frame and local-level frame) so that the specific forces are measured directly by the accelerometers on the specified frame used in the navigation computation. In contrast, the inertial sensors in the strapdown system are directly mounted within the INS chassis and hence the specific forces are sensed by the accelerometers in a *strapdown sensor coordinate frame*. In order to transform the strapdown sensor frame to the specified navigation frame, the accelerometer orientation parameters should be determined by processing the sensor assembly angular rates sensed by the gyroscopes. This procedure is performed in the system computer using INS navigation software, as opposed to using the mechanical torque in the gimballed system. Comparing the two approaches, the gimballed approach has less computational complexity and a more benign inertial environment, but its disadvantages include relatively large sensor volume and higher system cost. However, it has become possible for the strapdown approach to achieve high accuracy under high angular rates with the advancement of computer technology, so that nowadays strapdown systems are widely used for most navigation and positioning applications.

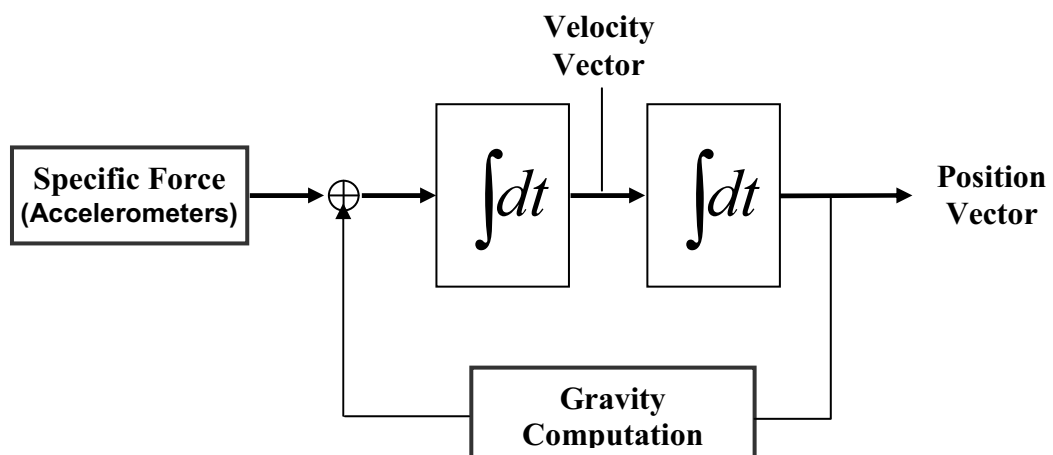


Figure 1.1 Fundamental Inertial Navigation System concept (Savage, 2000a)

More details on the INS can be found in any of a number of textbooks, see, e.g., Broxmeye (1961), Britting (1971), Farrell and Barth (1998), Savage (2000a & b), and Rogers (2000).

### 1.2.2 Sensor Observations and Errors

As already described in the preceding section, the fundamental observables from INS sensors are specific forces sensed by accelerometers and angular velocities measured by gyroscopes. Either of the observables can be described by following simplified expression (Savage, 1983):

$$L = l + b_L + sf_L L + \Omega_L L + \varepsilon_L \quad (1.5)$$

where,

$L$  : the inertial observations (specific force and angular velocity)

$l$  : the inertial observables (specific force and angular velocity)

$b_L$  : the observation bias

$sf_L$  : the diagonal matrix of observation scale factors

$\Omega_L$  : the skew symmetric matrix form of sensor axes misalignment

$\varepsilon_L$  : the observation random noise

The observation *bias* is any non-zero observation obtained from the accelerometer or the gyroscope when the system is stationary as can be seen in Figure 1-2. The ideal zero observation in this situation would indicate a zero bias. The bias is the result of manufacturing imperfection of the sensors, and can be determined by calibrating the system in laboratory tests. Micro-gal ( $\mu g$ ) units are usually used to express the magnitude of the accelerometer bias. On the other hand, the gyroscopes experience three types of biases: a *fixed bias*, *bias stability* and *bias drift*. The fixed bias is a permanent bias, like the accelerometer bias, that is consistent from turn-on to turn-off and need only to be calibrated for once. Bias stability is the variability of the overall bias with each turn-on. It is assumed to remain constant until the next turn-on. The fixed

bias and bias stability components are usually described in units of degree per hour ( $^{\circ}/h$ ). The bias draft occurs after turn-on and is usually specified in terms of  $^{\circ}/\sqrt{h}$  or  $^{\circ}/h/\sqrt{Hz}$ . The bias drift is dependent on the white noise of the sensor and causes the growth of unbounded errors when integrated.

The scale factor is a ratio of the change of the output signal relative to the change in the input signals expressed in parts per million (ppm). Additionally, scale factor asymmetry and non-linearity errors occur (see Figure 1-2). Asymmetry refers to the differences in the magnitude of the output signal between equal but opposite sensor rotations. Non-linearity refers to the systematic errors that arise due to the assumption that the scale factor is linear.

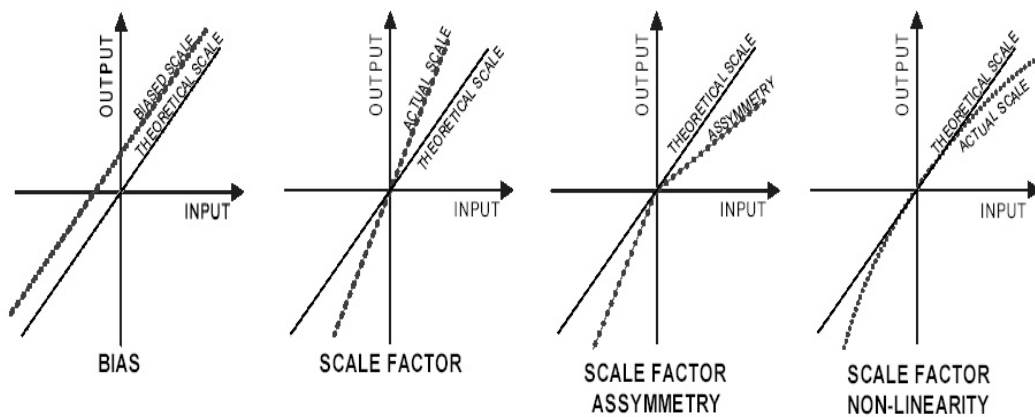


Figure 1-2 Inertial sensor bias and scale factor errors (Hewitson et al., 2003)

The sensor *axes misalignment* refers to the errors caused by mounting imperfections of the sensors with respect to each axis. It results in a non-orthogonality of the axes that define the inertial coordinate system. Hence, each axis is affected by the other two axes of the triad. In kinematic applications, the misalignment effect becomes of less significance if frequent manoeuvres are made so that misalignment error changes in a random manner and can therefore be considered a random error. In contrast, if a strapdown system is mounted in an aircraft that flies in a straight line, the misalignment error effect will be systematic.

The *random noise* refers to errors that cannot be deterministically modelled and are time variable. This implies that the noise represents the overall uncertainty in the inertial sensor model. They are often modelled as first-order Gauss-Markov or random walk processes with model parameters derived from laboratory testing. The stochastic model is used to describe the remaining errors after deterministic models and calibration tests have removed the systematic sensor errors.

### 1.3 Motivation

Position, velocity, and attitude information are crucial in many kinematic surveying and navigation applications. Traditionally, an Inertial Navigation System (INS) has provided this information. The INS system, however, has time-dependent error characteristics when operated in a stand-alone mode, without in-flight alignment. In contrast, GPS provides accurate position, velocity and time data without any impact of mission length or time since update. The main factor limiting the use of GPS is the requirement for line-of-sight between the receiver antenna and the satellites. Additional shortcomings include the low data output rate and the need to deploy more than one GPS antenna in order to obtain full attitude information. Integrated GPS/INS systems have been developed in order to overcome the inherent drawbacks of each system.

Although existing GPS/INS systems can effectively address the inherent drawbacks of each component system, their performance relies greatly on the quality of GPS measurements and the geometry of the satellite constellation. For example, due to the limited number of GPS satellites, a sufficient number of ‘visible’ satellites cannot be guaranteed at all times and all locations. Even when some low elevation satellites can be tracked, the measurements from these satellites may be contaminated by relatively high atmospheric noise. Therefore, this intrinsic shortcoming of satellite-based positioning systems results in, for example, poor accuracy in the vertical coordinate component, which is about three times worse than that of the horizontal coordinate components. Moreover, the performance is degraded in harsh operational circumstances. Some typical examples are when the duration of satellite signal blockage exceeds an INS bridging level, resulting in large accumulated INS errors that cannot be calibrated by

GPS. Such a scenario is unfortunately a common occurrence for certain kinematic applications, and hence the integration of GPS/INS with other technologies needs to be considered. One such technology option is the pseudolite. It is anticipated that pseudolites deployed at appropriate locations can augment the GPS/INS integration system, so that accurate position and attitude information can be obtained for a wide range of operational scenarios.

#### **1.4 Research Objectives**

This thesis deals with the issue of incorporating pseudolite observables into a GPS/INS positioning and navigation system in order to improve signal availability, solution reliability, and accuracy in a localised area. The objectives of this research are summarised below.

A GPS/Pseudolite/INS integration scheme has been proposed, developed and tested in this research to address shortcomings of existing position and navigation systems. Some technical and practical issues concerned with implementing these several integration schemes were investigated. One core issue was to maximise the system performance by choosing an optimal geometric distribution of the pseudolites. Hence, analyses of the effect were carried out through the use of GPS/Pseudolite/INS simulation tools. Further, in order to characterise the system performance in terms of accuracy, precision, and reliability, the results of tests with simulated and real measurements were analysed.

Under some situations, a small pseudolite location error may lead to a larger error in the measurement models and thus impact on the final positioning solutions. In order to obtain precise positioning results, this issue needs to be addressed. This research extends the existing theoretical analysis of pseudolite location errors and new characteristics of the pseudolite location errors in positioning were identified.

In order to achieve an accurate positioning solution from GPS, carrier phase measurements with correctly resolved integer ambiguities must be used. It is well known that ambiguity resolution (AR) “on-the-fly” (OTF) for short-range kinematic

positioning can be easily accomplished with dual-frequency observations. However, for the single-frequency case it is still a challenge to resolve the ambiguities rapidly and reliably. Based on the integration of GPS with pseudolites and INS, this research has developed a novel procedure for single-frequency carrier phase integer ambiguity resolution. With the inclusion of pseudolite and INS measurements, the proposed procedure can speed up the ambiguity resolution process and increase the reliability of the resolved ambiguities. Simulation studies and field experiments were carried out to analyse the impact of the inclusion of pseudolite and INS measurements in the AR process.

The occurrence of an undetected cycle slip significantly degrades the performance of a navigation filter when carrier phase measurements are used. An algorithm that can effectively detect and identify cycle slips has been developed. The algorithm uses additional information provided by the INS, and applies a statistical technique known as the cumulative-sum (CUSUM) test. Cycle slip decision values can be computed from the INS-predicted position due to the fact that its short-term accuracy is very high. The CUSUM test is then very sensitive to abrupt changes of mean values, making it ideal for the detection of cycle slips. To confirm the effectiveness of the proposed algorithm, performance tests were carried out with measurements obtained from field experiments.

In most airborne applications, GPS-based navigation systems cannot fulfil stringent requirements in terms of positioning accuracy, availability and integrity. Airport pseudolites can be used as a means of satisfying the stringent performance requirements. Hence an integrated GPS/INS/pseudolite system was able to improve the system performance under a wide variety of poor operational environments. In this research, flight tests of an aircraft approach and landing system were carried out. The observations were processed to evaluate the system performance.

## **1.5 Contributions of the Research**

The contributions of this research can be summarised as follows:

- A cost effective GPS/INS integration approach has been developed and tested, consisting of single-frequency GPS receivers and a tactical-grade SDINS. Field experiments have been conducted to evaluate the system performance and to investigate the impact of vehicle dynamics on the integration filter performance.
- A new position and navigation scheme based on GPS/Pseudolite/INS integration has been proposed. The pseudolite measurement contribution has been intensively analysed for different operational environments.
- The impact of pseudolite location errors on the final solution has been analysed to identify some new characteristics of pseudolite location errors. It has been found from the results that the optimal locations of pseudolites can minimise the impact of pseudolite location errors on measurement models and on the final positioning solutions.
- A new ambiguity resolution procedure that uses pseudolite and INS observations for single-frequency carrier phase integer ambiguity resolution has been developed. In addition, the effect of the inclusion of pseudolites and INS into the ambiguity resolution has been analysed by simulation studies.
- An effective cycle slip detection and identification algorithm has been developed. The algorithm has been specifically designed for use within integrated GPS/INS/pseudolites systems that use single-frequency receivers. It uses additional information provided by the INS and applies the cumulative-sum (CUSUM) test.
- A GPS/INS/Pseudolite integration system for aircraft precision approach and landing has been tested to evaluate overall system performance.

## 1.6 Outline of the Thesis

This thesis consists of eight chapters. The contents of each chapter are outlined as follows.

*Chapter 2* investigates the issues of integrating a single-frequency GPS receiver with a tactical-grade SDINS. Single- and double-differenced GPS measurement models are presented. This is followed by a detailed description of SDINS mechanisation, dynamic error model, and the Kalman filtering algorithm used for integration of GPS with INS. Finally, field experiment results are discussed to indicate not only the general performance of the integration system, but also to analyse the impact of vehicle dynamics on system performance.

*Chapter 3* proposes a GPS/Pseudolite/INS integration. Some technical and practical issues associated with including pseudolites within GPS/INS system are discussed. Results of extensive geometry simulations are presented to characterise the pseudolite contribution to the integrated system in terms of RDOP, ADOP, and reliability. In addition, test results with simulated and real measurements are presented in order to assess the performance of the proposed integration system.

*Chapter 4* presents results of both theoretical and numerical analyses of the impacts of pseudolite location errors in positioning.

*Chapter 5* proposes a new integer ambiguity resolution procedure suitable for GPS/Pseudolite/INS system. The proposed procedure uses single-frequency GPS data together with pseudolite and INS measurements. Results of simulation studies are presented to examine the effects of the inclusion of pseudolite and INS measurement. Finally, results of field experiments are presented in order to demonstrate the effectiveness of the proposed procedure with respect to different operational conditions.

*Chapter 6* describes an effective cycle slip detection and identification algorithm that can be readily implemented in GPS/Pseudolite/INS system. The algorithm uses the receiver antenna position predicted by INS, and applies the CUSUM test for the detection. Algorithm performance tests were conducted and their results are presented.

*Chapter 7* gives an overview of the GPS/Pseudolite/INS system used for flight tests for precision aircraft approach and landing. This is followed by a description of the flight test, and the preliminary test results.



Chapter 8 summarises the research findings, draws conclusions, and makes recommendations for future investigations.

**CHAPTER 2**

**HIGH PRECISION INTEGRATION OF SINGLE-FREQUENCY  
GPS WITH TACTICAL-GRADE SDINS**

---

---

## **2.1 Introduction**

Global Positioning System (GPS) and Inertial Navigation System (INS) have complementary operational characteristics; GPS has long-term stability with a homogeneous accuracy, while the short-term stability of the INS is excellent with high navigation accuracy but stand-alone INS positioning accuracy deteriorates very rapidly with time. Using these complementary natures, integrating GPS with INS can arguably leverage the best of each component system. The advantages of GPS/INS integration, relative to either GPS or INS only, are reported to be a high data rate of complete navigation solutions (e.g., position, velocity, and attitude) with superior short-term and long-term accuracy, improved availability, smoother trajectories, and greater integrity (Farrell and Barth, 1998; Greenspan, 1996). Hence, these systems have been used for a wide range of applications, for instance aerial photogrammetry and gravimetry, mobile mapping, vehicle navigation, guidance and control (see e.g., Bevely et al., 2000; Da et al., 1997; Grejner-Brzezinska et al., 1998b; Kwon and Jekeli, 2001).

Integrated GPS/INS can be implemented using a Kalman filter in different modes, such as loosely, tightly and ultra-tightly coupled. In these integration modes, the INS sensor error states, together with all navigation error states and other unknown parameters of interest, are estimated using a dynamic model and GPS measurements such as Doppler, pseudo-range, and/or carrier phase. In order to obtain high accuracy of positioning results using such systems, the carrier phase measurements have to be used in the integration filter update. Although integrated GPS/INS systems using carrier phase observations have been developed for applications of high precision positioning applications, most of the systems have been implemented using high cost dual-frequency GPS receivers and/or a navigation-grade INS (e.g., Lapucha, 1990; Da, 1997; Grejner-Brzezinska et al., 1998b; Ford et al., 2001). Hence, this chapter investigates the

issues of a cost effective GPS/INS integration using single-frequency GPS receivers and a tactical-grade Strapdown INS (SDINS), which delivers centimetre-level positioning accuracy even during a few seconds of GPS signal blockage. The SDINS mechanisation and dynamic error model are firstly presented. This is followed by the details of differencing technique for GPS measurement modelling and Kalman filtering which is the core technique for the integration. Finally, field test results will be presented to evaluate not only general performance of the GPS/INS integration approach, but also the impact of vehicle dynamics in the system performance.

## 2.2 Strapdown INS Mechanisation

The strapdown INS (SDINS) mechanisation is the process of transforming specific force measured by accelerometers and angular rates measured by gyroscopes into the navigation parameters: position, velocity, and attitude (Lapucha, 1990). This process is performed through integrating differential equations for the navigation parameters. The time differential navigation equations for the SDINS can be written as follows (*derivation*, see Appendix A):

$$\dot{r}^n = -\Omega_{en}^n r^n + v^n \quad (2.1a)$$

$$\dot{v}^n = f^n - (\Omega_{en}^n + 2\Omega_{ie}^n)v^n + g^n \quad (2.1b)$$

$$\dot{R}_b^n = R_b^n \Omega_{ib}^b - \Omega_{in}^n R_b^n \quad (2.1c)$$

with:

$$\omega_{en}^n = \begin{bmatrix} \dot{\lambda} \cos(\phi) \\ -\dot{\phi} \\ -\dot{\lambda} \sin(\phi) \end{bmatrix}$$

$$\omega_{ie}^n = \begin{bmatrix} \omega_{ie} \cos(\phi) \\ 0 \\ -\omega_{ie} \sin(\phi) \end{bmatrix}$$

$$\omega_{in}^n = \omega_{ie}^n + \omega_{en}^n$$

where,

- $r^n$ : the position vector in the  $n$ -frame
- $v^n$ : the velocity vector in the  $n$ -frame
- $g^n$ : the gravity vector in the  $n$ -frame
- $R_b^n$ : the rotation matrix from the  $b$ -frame to the  $n$ -frame
- $f^n$ : the specific force vector in the  $n$ -frame that is transformed from the specific force vector  $f^b$  sensed in accelerometers
- $\Omega_{ib}^b$ : the skew-symmetric form of angular velocity vector  $\omega_{ib}^b$  sensed in gyroscopes
- $\Omega_{en}^n$ : the skew-symmetric form of the  $n$ -frame rotation rate vector  $\omega_{en}^n$
- $\Omega_{ie}^n$ : the skew-symmetric form of the  $e$ -frame rotation rate vector  $\omega_{ie}^n$
- $\Omega_{in}^n$ : the skew-symmetric form of the  $n$ -frame rotation rate vector  $\omega_{in}^n$

Note that these above Equations (2.1a) and (2.1b) are actually applicable to both gimballed and strapdown systems. The distinct difference between the two systems is the means by which  $f^n$  is obtained. The accelerometers in the former system output  $f^n$  directly in that the sensor platform is torqued to maintain its alignment with the desired navigation frame, while the vector obtained by the latter system should be transformed to the  $n$ -frame using the rotation matrix  $R_b^n$  as the specific force vector is outputted in the  $b$ -frame. It is relatively straightforward to numerically integrate Equations (2.1a) and (2.1b) to calculate position and velocity once the specific force vector  $f^n$  is obtained. However, although the rotation matrix can be determined by directly integrating Equation (2.1c) or using numerical updating of the direction cosine matrix, a numerical quaternion updating approach is widely used in the rotation matrix

integration procedure for the modern SDINS mechanisation due to its relatively less computation burden (Lee et al., 1988; Da, 1997; Savage, 2001a).

‘*Quaternion*’ in SDINS represents the orientation between body and navigation axes using single rotation about a vector through an angle. The quaternion consists of four parameters: the first scalar quantity and the last three parameters representing the components of a vector directed along the Euler axes between the two frames. The quaternion rotating the body to the navigation frame is defined as (ibid):

$$q_b^n = \begin{bmatrix} q_0 \\ q_1 \\ q_2 \\ q_3 \end{bmatrix} \quad (2.2)$$

where  $q_0$  and  $q_i = [q_1 \ q_2 \ q_3]$  are a scalar and a vector component of the quaternion, respectively.

Quaternion  $q_b^n$  can be calculated using a numerical updating algorithm, described in Appendix B in detail. Once a new quaternion at a certain epoch is obtained, the direction cosine matrix  $R_b^n$  and Euler angles (e.g., pitch, roll, and heading) can be obtained using Equations (2.3) and (2.4) respectively (ibid).

$$R_b^n = \begin{bmatrix} (q_0^2 + q_1^2 - q_2^2 - q_3^2) & 2(q_1q_2 - q_0q_3) & 2(q_1q_3 + q_0q_2) \\ 2(q_1q_2 - q_0q_3) & (q_0^2 - q_1^2 + q_2^2 - q_3^2) & 2(q_2q_3 - q_0q_1) \\ 2(q_1q_3 - q_0q_2) & 2(q_2q_3 + q_0q_1) & (q_0^2 - q_1^2 - q_2^2 + q_3^2) \end{bmatrix} \quad (2.3)$$

$$P = \tan^{-1} \frac{-R_{b(3,1)}^n}{\sqrt{(R_{b(3,2)}^n)^2 + (R_{b(3,3)}^n)^2}} \quad (2.4a)$$

$$R = \tan^{-1} \frac{R_{b(3,2)}^n}{R_{b(3,3)}^n} \quad (2.4b)$$

$$H = \tan^{-1} \frac{R_{b(2,1)}^n}{R_{b(1,1)}^n} - \dot{\lambda} \sin \phi \quad (2.4c)$$

where  $P$ ,  $R$ , and  $H$  denotes pitch, roll, and heading, respectively.

A general flowchart for the SDINS mechanisation module with the navigation equations is illustrated in Figure 2-1.

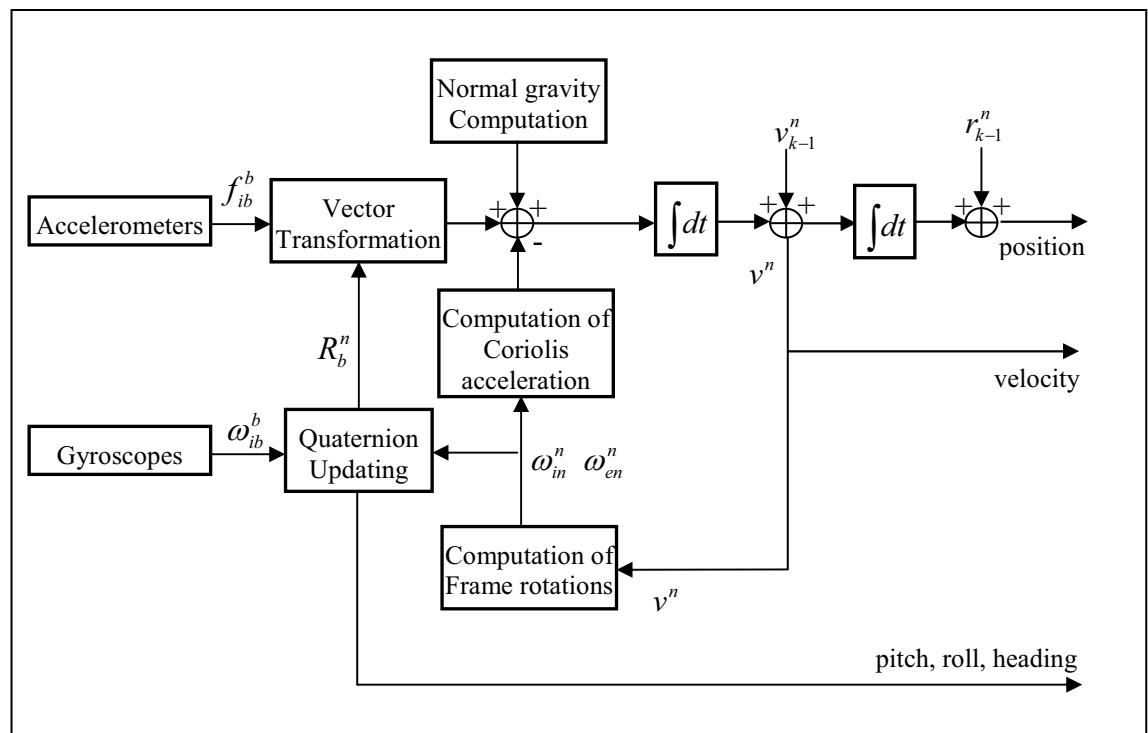


Figure 2-1 Flow chart of the SDINS mechanisation module

### 2.3 SDINS Error Dynamic Equations

There are two widely used INS error models, namely the *perturbation* and *psi-angle* approach. The difference between the two models is the referenced position of INS for deriving the perturbation of the nominal navigation equations (Bar-Itzhak and Bermant, 1987). The psi-angle model, which will be used in this research, is obtained when the nominal equations are perturbed in the local level (geodetic) north-pointing coordinate

system that corresponds to the geographic location indicated by the INS. Hence its derivation can commence by applying the perturbation to the navigation Equation (2.1).

The perturbations of Equations (2.1a) and (2.1b) with respect to the known navigation ( $n$ -) frame yields:

$$\delta\dot{r}^n = -\delta\Omega_{en}^n r^n - \Omega_{en}^n \delta r^n + \delta v^n \quad (2.5)$$

$$\delta\dot{v}^n = \delta f^n - \delta(\Omega_{en}^n + 2\Omega_{ie}^n)v^n - (\Omega_{en}^n + 2\Omega_{ie}^n)\delta v^n + \delta g^n \quad (2.6)$$

Since the coordinates in the  $e$ ,  $n$  and  $i$ -frames and the angular velocities between each two of them are known, it can be assumed  $\delta\Omega_{ie}^n = \delta\Omega_{en}^n = 0$ , then Equation (2.5) and (2.6) can be rewritten:

$$\delta\dot{r}^n = -\Omega_{en}^n \delta r^n + \delta v^n \quad (2.7)$$

where Equation (2.7) is a *position dynamic error equation*,

$$\delta\dot{v}^n = \delta f^n - (\Omega_{en}^n + 2\Omega_{ie}^n)\delta v^n + \delta g^n \quad (2.8)$$

Using the *Translatory Perturbation Rules* (Goshen-Meskin and Bar-Itzhak, 1992a), the perturbation of a specific force can be obtained:

$$\delta f^n = \delta\nabla^n - \Omega_{\psi} f^n \quad (2.9)$$

Substituting Equation (2.9) into Equation (2.8) yields a complete *velocity error equation*:

$$\delta\dot{v}^n = -(\Omega_{en}^n + 2\Omega_{ie}^n)\delta v^n + \delta\nabla^n - \Omega_{\psi} f^n + \delta g^n \quad (2.10)$$

where  $\delta \nabla^n$  are the accelerometer measurement errors in the  $n$ -frame and  $\Omega_\psi$  is the skew-symmetric form of attitude error vector  $\psi$ .

Attitude error vector ( $\psi$ ) is physically induced by the gyro drifts. Thus it can be written as:

$$\dot{\psi}^i = \delta \varepsilon \quad (2.11)$$

where  $\dot{\psi}^i$  is time derivative of the attitude error vector relative to the  $i$ -frame.

The *rule of differentiation in rotating coordinate frame* (Goshen-Meskin and Bar-Itzhak, 1992a) is:

$$\dot{\psi}^i = \dot{\psi}^n + \Omega_{in}^n \psi^n \quad (2.12)$$

where  $\dot{\psi}^n$  is time derivative of the attitude error vector relative to the  $n$ -frame.

Substituting Equation (2.11) into (2.12) results in the following *attitude error equation*.

$$\dot{\psi}^n = -\Omega_{in}^n \psi^n + \delta \varepsilon^n \quad (2.13)$$

## 2.4 Differencing Techniques for GPS Measurement Modelling

Positioning based on GPS observations can be conveniently classified into two different techniques: *Absolute (or Point)* and *Relative Positioning*. The absolute positioning technique utilises only one GPS receiver to provide position information, ignoring the satellite orbit and clock errors. Its accuracy using pseudo-range measurements is currently about 7 metres in the horizontal component and 12 metres in the vertical component (at the 95% confidence level) for civilian users with Selective Availability (SA) removed (Rizos and Satirapod, 2001). Carrier phase measurements can be used to contribute to the velocity determination, or improve the positioning accuracy using the



precise-but-ambiguous carrier measurements to smooth noisy-but-unambiguous pseudo-ranges. On the other hand, the relative technique requires two or more receivers to simultaneously track the satellite signals, and provides the coordinates of an unknown station with respect to a known (reference) station. A differencing technique between satellites and/or receivers is generally used for relative positioning in order to reduce systematic error source in the measurements, resulting in improved positioning accuracy. Thus, such a technique can be used in high precision integration of GPS with INS.

### 2.4.1 Single-Differences (SD)

With two GPS receivers tracking the same GPS satellite at the same epoch, using the *single-differencing* (SD) technique of the pseudo-range and carrier phase can reduce some errors correlated in observations at the two receivers. Mathematical expressions for single differenced pseudo-range and carrier phase measurements can be given as:

$$\Delta R_{ij}^s = \Delta \rho_{ij}^s + \Delta d\rho_{ij}^s + c \cdot \Delta dt_{ij}^s + \Delta di_{ij}^s + \Delta dr_{ij}^s + \Delta d_{ij,R}^s + \Delta \varepsilon_{ij,R}^s \quad (2.14)$$

$$\lambda_G \cdot \Delta \phi_{ij}^s = \Delta \rho_{ij}^s + \Delta d\rho_{ij}^s + c \cdot \Delta dt_{ij}^s + \lambda_G \cdot \Delta N_{ij}^s - \Delta di_{ij}^s + \Delta dr_{ij}^s + \Delta d_{ij,\phi}^s + \Delta \varepsilon_{ij,\phi}^s \quad (2.15)$$

where  $\Delta$  denotes *differencing between two receivers  $i$  and  $j$*  with respect to satellite  $s$ .

The most important characteristic of the SD technique is that the satellite clock error term ( $dt^s$ ) in Equations (1.1) and (1.3) is eliminated. Furthermore, other error terms become differenced errors in the two receivers, so that some errors having strong spatial correlation can be reduced in the case of short baselines. Such error sources include the orbit error, and ionospheric and tropospheric effects. In contrast, the receiver clock error, ambiguity, multipath, and receiver noise do not cancel out, and the receiver noise is increased by the square-root of two times through applying the differencing technique.

### 2.4.2 Double-Differences (DD)

The *double-differences* (DD) are formed by differencing between two single-differences across two different satellites at each epoch. It can be mathematically represented as:

$$\Delta\nabla R_{ij}^{st} = \Delta\nabla\rho_{ij}^{st} + \Delta\nabla d\rho_{ij}^{st} + \Delta\nabla di_{ij}^{st} + \Delta\nabla dr_{ij}^{st} + \Delta\nabla d_{ij,R}^{st} + \Delta\nabla \mathcal{E}_{ij,R}^{st} \quad (2.16)$$

$$\lambda_G \cdot \Delta\nabla\phi_{ij}^{st} = \Delta\nabla\rho_{ij}^{st} + \Delta\nabla d\rho_{ij}^{st} + \lambda_G \cdot \Delta\nabla N_{ij}^{st} - \Delta\nabla di_{ij}^{st} + \Delta\nabla dr_{ij}^{st} + \Delta\nabla dm_{ij,\phi}^{st} + \Delta\nabla \mathcal{E}_{ij,\phi}^{st} \quad (2.17)$$

where  $\nabla$  denotes *differencing between two satellites  $s$  and  $t$* , so that  $\Delta\nabla$  represents a *double-differencing*.

The main benefit of DD is that the receiver clock error term is canceled out in Equations (2.14) and (2.15). The DD technique further reduces the aforementioned spatially correlated errors. To some extent, for baseline length less than 15km, satellite orbit, ionospheric and tropospheric errors can be assumed to be eliminated by applying the DD technique. Hence, in the GPS/INS integration discussed in this chapter, the DD technique will be applied to obtain high precision positioning and navigation.

## 2.5 GPS/INS Integration with Kalman Filter

The Kalman filtering algorithm to the integration of GPS and INS data is discussed in the following with special emphasis on its state vector and dynamic model.

### 2.5.1 Kalman Filtering

Mathematical and stochastic models are required to estimate the state parameters in the Kalman filter. The mathematical models in the continuous time form include the system dynamic model:

$$\dot{x}(t) = F(t)x(t) + Gw(t) \quad (2.18)$$

and the observation model:

$$z(t) = H(t)x(t) + e(t) \quad (2.19)$$

The corresponding stochastic models are assumed as:

$$E[w(t)] = 0 \quad (2.20a)$$

$$E[e(t)] = 0 \quad (2.20b)$$

$$E[w(t_1)w^T(t_2)] = R(t_2)\delta(t_2 - t_1) \quad (2.20c)$$

$$E[e(t_1)e^T(t_2)] = Q(t_2)\delta(t_2 - t_1) \quad (2.20d)$$

$$E[w(t_1)e^T(t_2)] = 0 \quad (2.20e)$$

where,

$F(t)$ :	the system dynamic matrix
$x(t)$ :	the state vector
$z(t)$ :	the measurement vector
$w(t)$ :	the system noise vector
$e(t)$ :	the measurement noise vector
$R(t)$ :	the system plant noise covariance matrix
$Q(t)$ :	the measurement noise covariance matrix
$\delta$ :	the Dirac delta function
$E$ :	the expectation operator

The Kalman filtering computation procedure in discrete time is performed by the '*prediction*' and '*measurement update*' (Brown and Hwang, 1992; Maybeck, 1979).

The prediction of the state vector and its covariance at the  $k$ -th epoch is:

$$\hat{x}_k(-) = \Phi_{k,k-1} \hat{x}_{k-1}(+) \quad (2.21)$$

$$P_k(-) = \Phi_{k,k-1} P_{k-1}(+) \Phi_{k,k-1}^T + R_{k-1} \quad (2.22)$$

where  $x_{k-1}(+)$  and  $P_{k-1}(+)$  are the optimal estimators of the state vector and its covariance matrix at the previous  $(k-1)$ -th epoch respectively, and  $\Phi_{k,k-1}$  is the transition matrix.

As the sampling interval  $\Delta t = t_k - t_{k-1}$  is very small in the integrated GPS/INS implementation, the transition matrix  $\Phi_{k,k-1}$  can be approximated by:

$$\Phi_{k,k-1} = e^{\Delta F} \approx I + F\Delta t \quad (2.23)$$

The system plant noise covariance matrix  $R_{k-1}$  is (Brown and Hwang, 1992):

$$\begin{aligned} R_{k-1} &= E[w(k-1)w(k-1)^T] \\ &= E\left\{ \left[ \int_{(k-1)\Delta t}^{k\Delta t} \phi_{k,k-1}(\xi) G(\xi) w(\xi) d\xi \right] \left[ \int_{(k-1)\Delta t}^{k\Delta t} \phi_{k,k-1}(\eta) G(\eta) w(\eta) d\eta \right]^T \right\} \\ &= \int_{(k-1)\Delta t}^{k\Delta t} \int_{(k-1)\Delta t}^{k\Delta t} \phi_{k,k-1}(\xi) G(\xi) E[w(\xi)w(\eta)^T] G(\eta) \phi_{k,k-1}(\eta)^T d\xi d\eta \end{aligned} \quad (2.24)$$

In this research,  $R_{k-1}$  is, however, approximated using the first order approximation of the transition matrix (i.e. Equation (2.23)) as:

$$R_{k-1} \approx \Phi_{k,k-1} G R G \Phi_{k,k-1}^T \Delta t \quad (2.25)$$

Once measurements are available, the updating procedure to obtain the optimal estimate of the state vector and its covariance matrix is:

$$\hat{x}_k(+) = \hat{x}_k(-) + K_k (Z_k - H_k \hat{x}_k(-)) \quad (2.26)$$

$$P_k(+) = P_k(-) - K_k H_k P_k(-) \quad (2.27)$$

with:

$$K_k = P_k(-)H_k^T [H_k P_k(-)H_k^T + Q_k]^{-1}$$

where  $K_k$  is the so-called Kalman gain matrix.

### 2.5.2 State Vector and Dynamic Model

An exact expression for the system equation for the Kalman filter depends on the error states selected and the type of error model used to describe them. *Psi-angle* model (e.g., Equations (2.11), (2.14), and (2.17)) is adopted in this research to describe the behaviour of INS navigation errors (nine states). Biases and scale factors of the INS sensors are modelled by a random bias and first order Gauss-Markov process, respectively (12 states). Gravity uncertainty is modelled as the first order Gauss-Markov process (3 states). The vector and matrix form of the system dynamic model for the GPS/INS integration in this research is:

$$\begin{bmatrix} \dot{x}_r(t) \\ \dot{x}_v(t) \\ \dot{x}_\psi(t) \\ \dot{x}_\nabla(t) \\ \dot{x}_{\nabla f}(t) \\ \dot{x}_\varepsilon(t) \\ \dot{x}_{gf}(t) \\ \dot{x}_g(t) \end{bmatrix} = \begin{bmatrix} \Omega & I & 0 & 0 & 0 & 0 & 0 & 0 \\ F_{21} & \tilde{\Omega} & F_j & R_b^n & R_f & 0 & 0 & I \\ 0 & 0 & \bar{\Omega} & 0 & 0 & R_b^n & R_\omega & 0 \\ 0 & 0 & 0 & 0 & 0 & 0 & 0 & 0 \\ 0 & 0 & 0 & 0 & F_{55} & 0 & 0 & 0 \\ 0 & 0 & 0 & 0 & 0 & 0 & 0 & 0 \\ 0 & 0 & 0 & 0 & 0 & 0 & F_{77} & 0 \\ 0 & 0 & 0 & 0 & 0 & 0 & 0 & F_{88} \end{bmatrix} \begin{bmatrix} x_r(t) \\ x_v(t) \\ x_\psi(t) \\ x_\nabla(t) \\ x_{\nabla f}(t) \\ x_\varepsilon(t) \\ x_{gf}(t) \\ x_g(t) \end{bmatrix} + \begin{bmatrix} w_r(t) \\ w_v(t) \\ w_\psi(t) \\ w_\nabla(t) \\ w_{\nabla f}(t) \\ w_\varepsilon(t) \\ w_{gf}(t) \\ w_g(t) \end{bmatrix} \quad (2.28)$$

where,  $I$  and  $0$  are the third-order identity and zero matrices;  $x_r$ ,  $x_v$ ,  $x_\psi$ ,  $x_\nabla$ ,  $x_{\nabla f}$ ,  $x_\varepsilon$ ,  $x_{gf}$ , and  $x_g$  are the position, velocity and attitude error, accelerometer bias and scale factor, gyroscope bias and scale factor, and gravity uncertainty vector, respectively. The error states included in those vectors are:

$$x_r = [\delta r_N, \delta r_E, \delta r_D]^T \quad (2.29a)$$

$$x_v = [\delta v_N, \delta v_E, \delta v_D]^T \quad (2.29b)$$

$$x_\psi = [\delta \psi_N, \delta \psi_E, \delta \psi_D]^T \quad (2.29c)$$

$$x_{\nabla} = [\delta \nabla_x, \delta \nabla_y, \delta \nabla_z]^T \quad (2.29d)$$

$$x_{\nabla f} = [\delta \nabla f_x, \delta \nabla f_y, \delta \nabla f_z]^T \quad (2.29e)$$

$$x_\varepsilon = [\delta \varepsilon_x, \delta \varepsilon_y, \delta \varepsilon_z]^T \quad (2.29f)$$

$$x_{\varepsilon f} = [\delta \varepsilon f_x, \delta \varepsilon f_y, \delta \varepsilon f_z]^T \quad (2.29g)$$

$$x_g = [\delta g_x, \delta g_y, \delta g_z]^T \quad (2.29g)$$

where  $\delta \nabla$  and  $\delta \nabla f$  are the accelerometer bias and scale factor;  $\delta \varepsilon$  and  $\delta \varepsilon f$  are the gyro bias and scale factor;  $\delta g$  is gravity uncertainty.

A detailed expression of the dynamic matrix ( $F$ ) can be given by:

$$\Omega = \begin{bmatrix} 0 & \Omega_D & -\Omega_E \\ -\Omega_D & 0 & \Omega_N \\ \Omega_E & -\Omega_N & 0 \end{bmatrix} \quad \text{with} \quad \begin{aligned} \Omega_N &= \dot{\lambda} \cos \phi \\ \Omega_E &= -\dot{\phi} \\ \Omega_D &= -\dot{\lambda} \sin \phi \end{aligned} \quad (2.30)$$

$$\bar{\Omega} = \begin{bmatrix} 0 & \bar{\Omega}_D & -\bar{\Omega}_E \\ -\bar{\Omega}_D & 0 & \bar{\Omega}_N \\ \bar{\Omega}_E & -\bar{\Omega}_N & 0 \end{bmatrix} \quad \text{with} \quad \begin{aligned} \bar{\Omega}_N &= (\omega_{ie} + \dot{\lambda}) \cos \phi \\ \bar{\Omega}_E &= -\dot{\phi} \\ \bar{\Omega}_D &= -(\omega_{ie} + \dot{\lambda}) \sin \phi \end{aligned} \quad (2.31)$$

$$\tilde{\Omega} = \begin{bmatrix} 0 & \tilde{\Omega}_D & -\tilde{\Omega}_E \\ -\tilde{\Omega}_D & 0 & \tilde{\Omega}_N \\ \tilde{\Omega}_E & -\tilde{\Omega}_N & 0 \end{bmatrix} \quad \text{with} \quad \begin{aligned} \tilde{\Omega}_N &= (2\omega_{ie} + \dot{\lambda}) \cos \phi \\ \tilde{\Omega}_E &= -\dot{L} \\ \tilde{\Omega}_D &= -(2\omega_{ie} + \dot{\lambda}) \sin \phi \end{aligned} \quad (2.32)$$

$$F_j = R_b^n \begin{bmatrix} 0 & -f_z & f_y \\ f_z & 0 & -f_x \\ -f_y & f_x & 0 \end{bmatrix} \quad (2.33)$$

$$R_f = R_b^n \begin{bmatrix} f_x & 0 & 0 \\ 0 & f_y & 0 \\ 0 & 0 & f_z \end{bmatrix} \quad (2.34)$$

$$R_\omega = R_b^n \begin{bmatrix} \omega_x & 0 & 0 \\ 0 & \omega_y & 0 \\ 0 & 0 & \omega_z \end{bmatrix} \quad (2.35)$$

$$F_{21} = \text{diag} \left[ -\frac{g}{R_n}, -\frac{g}{R_n}, \frac{2g}{R_n} \right] \quad (2.36)$$

$$F_{55} = \text{diag} [-\xi_x, -\xi_y, -\xi_z] \quad (2.37)$$

$$F_{77} = \text{diag} [-\beta_x, -\beta_y, -\beta_z] \quad (2.38)$$

$$F_{88} = \text{diag} [-\tau_x, -\tau_y, -\tau_z] \quad (2.39)$$

in which  $\omega_{ie}$  is the Earth rate vector;  $\phi$  and  $\lambda$  denote latitude and longitude respectively;  $f_x$ ,  $f_y$ , and  $f_z$  are the accelerometer sensed specified forces;  $g$  is the gravity constant;  $R_n$  represents the radii of parallel curvature;  $\xi$  and  $\beta$ , and  $\tau$  is 1/(correlation time) of the Gauss-Markov process for accelerometer bias, gyro drift, and gravity uncertainty.

### 2.5.3 Filter Update using GPS Measurements

There are two approaches widely used for the GPS/INS integration based on a Kalman filtering scheme, namely *loosely* and *tightly* coupled approaches. The former deals with GPS and INS as independent *navigation systems*. Position or velocity solutions processed in the GPS navigation filter are used in the integration filter to estimate the INS errors. The main drawback of this approach is that the filter update cannot be carried out when the number of tracked GPS signals drops below four. In contrast, the latter approach used in this research treats GPS and INS not as navigation systems, but as *sensors*. A single filter is applied to process both sets of measurements, and hence raw GPS measurements are used. This approach also provides flexibility in GPS data processing in that INS predicts navigation parameters with respect to a subsequent epoch. The DD GPS carrier phase measurements model for short baseline applications (i.e., assuming that satellite orbit error and atmospheric effects are eliminated) is used in this research for high precision positioning and navigation. If integer ambiguities in GPS DD measurements are correctly resolved by an effective procedure (discussed in Chapter 5), the measurement model for updating the integration filter can be expressed as follows:

$$z(t)_{n \times 24} = \begin{bmatrix} A_{n \times 3} R_n^e & 0_{n \times 21} \end{bmatrix} x(t)_{24 \times 1} + e(t)_{24 \times 1} \quad (2.40)$$

where  $A$  is a design matrix for DD GPS measurements that captures the relative receiver-satellite geometry in the  $e$ -frame (see Equation (6-14)).  $R_n^e$  is the transformation matrix from the  $e$ -frame to the  $n$ -frame.

In addition, the closed-loop update technique is used to correct the estimated errors, as indicated in Figure 2-2. The estimated errors are feedback to update the INS navigation solution and sensor measurements. This update limits the position errors to centimetre level when correctly fixed carrier phases are used for the filter updating.



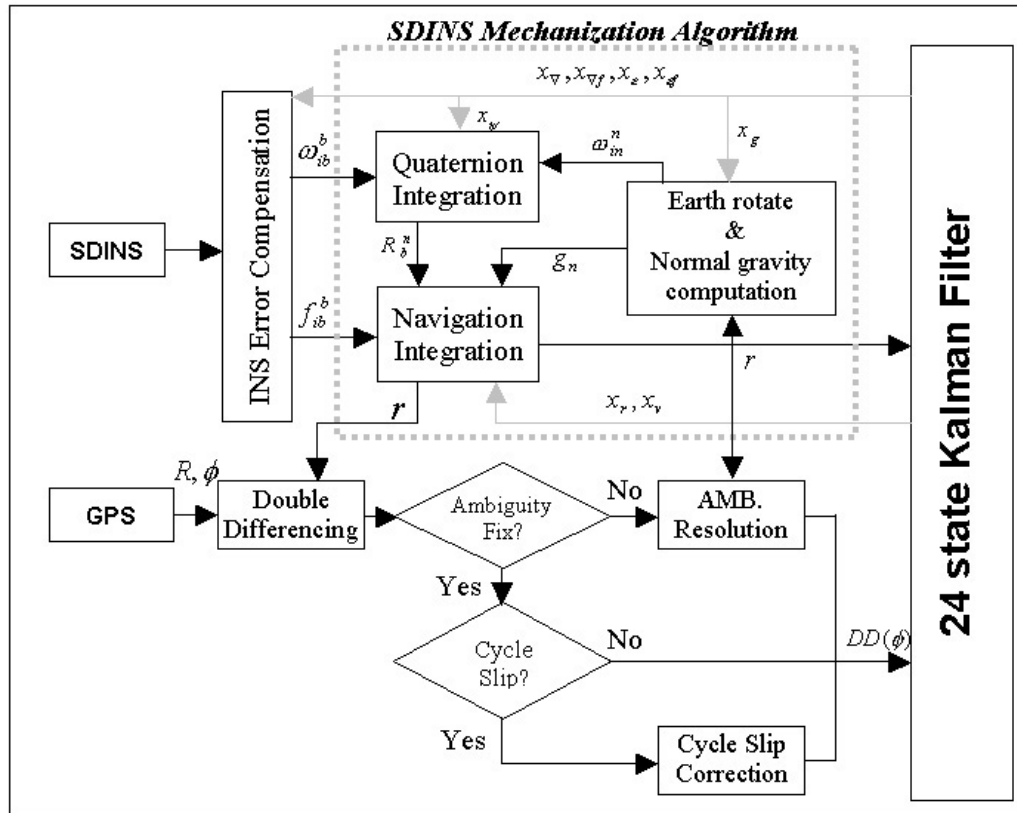


Figure 2-2 Tightly coupled GPS/INS integration scheme using carrier phase measurements

## 2.6 Description of Hardware and Software

The INS used in this research is a Boeing C-MIGITS II system, which is considered to be a tactical-level accuracy unit (5 deg/h, 500 $\mu$ g), compact (8cm  $\times$  9cm  $\times$  12cm), and lightweight (1.1kg). This system is based on a Digital Quartz IMU (DQI) technology. As shown in Figure 2-3, the DQI is designed around an Inertial Sensor Assembly (ISA). The ISA consists of three Quartz Rate Sensors (QRS), three Vibrating Quartz Accelerometers (VQA), the drive electronics, the preamplifier circuitry for the sensor outputs, and the digital conversion electronics. The output of the VQA is digital. The QRS output is an analogue sinusoid, which is converted to a digital signal in the ISA (Boeing, 1997). The ISA also supplies information, which monitors sensor health checks and sensor compensation. The IMU contains the electronics that process the raw sensor signals for compensation, providing delta angle and delta velocity measurements

for navigation solutions at a rate of 100 Hz, as well as acceleration and angular velocity for flight control or sensor stabilization at 600 Hz.

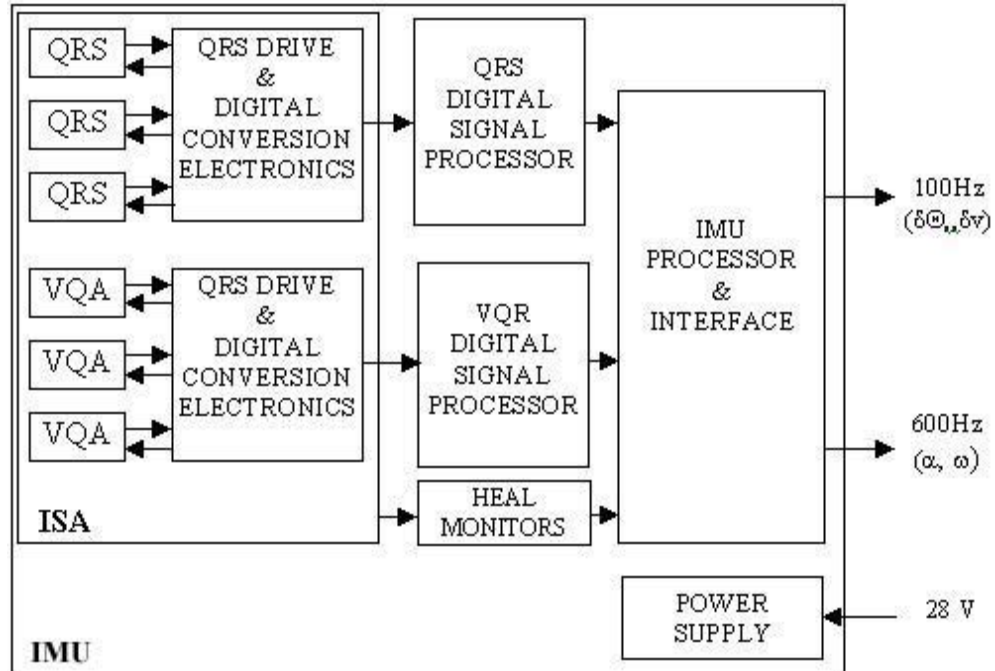


Figure 2-3 DQI functional block diagram (Boeing, 1997)

The GPS receiver used for the integrated GPS/INS system is NovAtel OEM3 Millennium GPS card, which provides high performance code tracking with Narrow Correlator Technology (NovAtel, 1995). Two GPS receivers are used as reference and rover station. More details on the receiver can be found in *ibid*.

The C-MIGITS functions as an integrated GPS (MicroTracker single board)/INS, processing Kalman-filtered navigation solution in real-time. In this study, the raw IMU and GPS data are post-processed using an in-house software AIMS<sup>TM</sup> navigation-processing engine (Grejner-Brzezinska et al., 1998a & b). The software was originally designed for dual-frequency Trimble 4000SSi GPS receivers and navigation-grade Litton LN-100 INS (0.01 deg/h, 30 $\mu$ g). However, it has been modified to be used in the system comprising an integrated tactical-grade INS and single-frequency GPS receivers. Modifications to AIMS software include:

- New implementation of reading and synchronising the INS sensor measurements,

- Redefinition of Kalman filter parameters (e.g., inertial sensor errors, process noises and Morkov process correlation time),
- Modification to the filter update cycle,
- Implementation of new carrier phase processing algorithms suitable for single-frequency carrier phase processing (e.g., ambiguity resolution and cycle slip detection, which will be presented in Chapters 5 and 6).

## 2.7 Land Vehicle Experiment

Kinematic experiments were carried out in Clovelly Bay Carpark, Sydney, on the 24<sup>th</sup> and 25<sup>th</sup> of March 2003. The objectives were (a) to evaluate overall performance of the GPS/INS integration consisting of a tactical-grade INS and single frequency GPS receiver, under benign and harsh (signal blockage) operational environments; (b) to investigate the impact of vehicle dynamics on integration filter initialisation and system performance during GPS signal blockage.



Figure 2-4 Trial vehicle

Both the INS and the GPS antenna were mounted on the roof of the test vehicle (see Figure 2-4). For data acquisition, raw INS sensor measurements were recorded at 100Hz, while GPS data were logged at 1Hz. At the same time, RTK (Real Time Kinematic) processed results were recorded to appraise the position performance of the integrated GPS/INS system. The collected data was processed in post-processing mode (details given in §2.6). It should be noted that double-differenced GPS carrier phase measurements with fixed ambiguities were used to update the system integration filter.

### 2.7.1 System Performance Analysis

The system performance cannot be directly assessed in the kinematic mode, as an accurate reference trajectory is not available. Alternatively, a comparison with the independent trajectory obtained by GPS RTK processing (see Figure 2-5), the Root-Mean-Squares (RMS) errors of the estimated navigation parameters, and the double-differenced residuals are presented here (Grejner-Brzezinska et al., 1998b; Lee et al., 2002) in order to assess the performance of the integrated system. Note that RTK positioning typically provides to a few centimetre level accuracy as long as the carrier phase ambiguities are resolved correctly (Rizos, 1996). As shown in Figure 2-6, the standard deviations of two trajectory differences are 0.39cm, 0.38cm and 1.56cm in the north, east, and height components respectively. In addition, the graphs in the first column of Figure 2-7 show navigation solutions obtained by the integrated GPS/INS system, whereas the plots in the second column depict RMS errors of the estimated navigation parameters. After the filter initialisation, the RMS values are 0.6cm for the horizontal and 1.5cm for the vertical position, better than 0.002cm/sec for velocity as well as in the order of 1.6 arc-minutes for heading and 0.2 arc-minutes for pitch and roll, respectively. Figure 2-8 shows the DD L1 carrier phase residuals for SV 4, 9, and 24 based on the positions that are predicted by the INS. The standard deviation of all the residuals is less than 1.0cm. From these results, it would be possible to conclude that the general positioning accuracy provided by the integration system is up to a few centimetre level under a benign operational environment using six satellites.

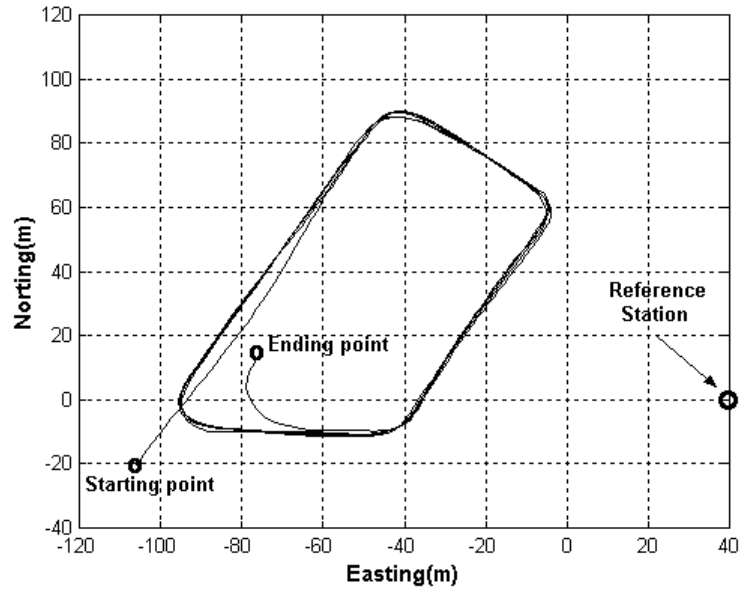


Figure 2-5 Vehicle trajectory during the experiment

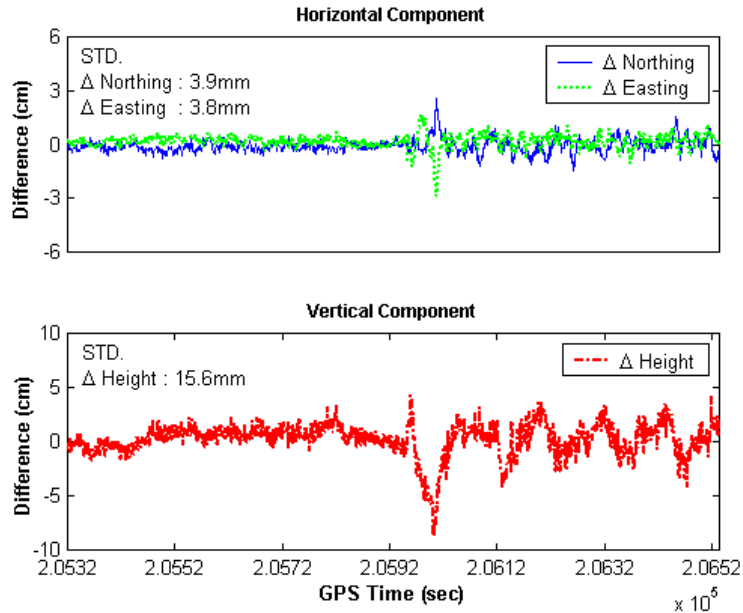


Figure 2-6 Integrated GPS/INS positioning accuracy comparing with GPS RTK solutions

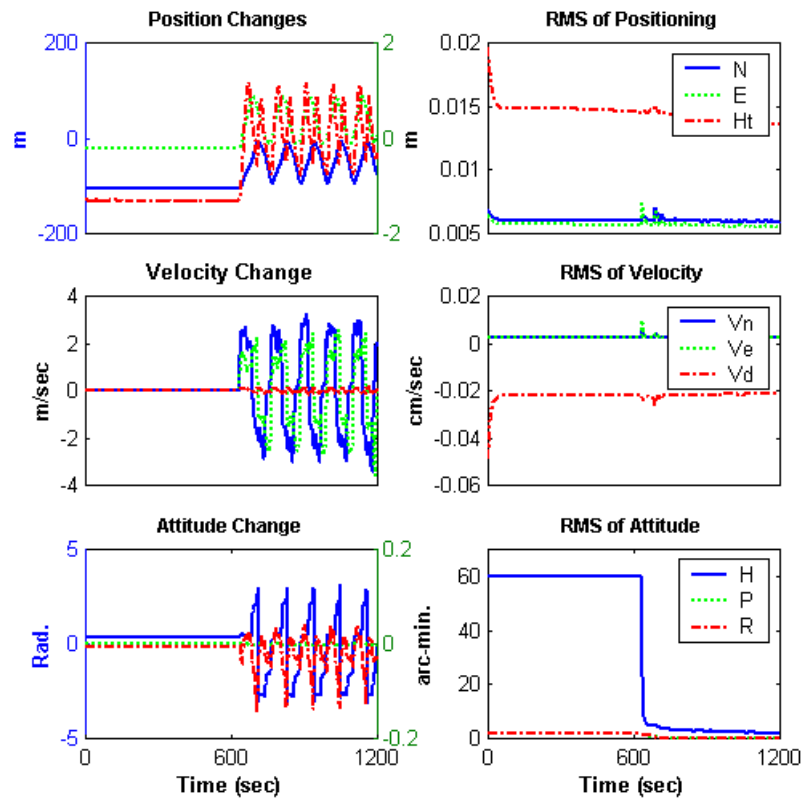


Figure 2-7 Navigational parameters and their RMS errors

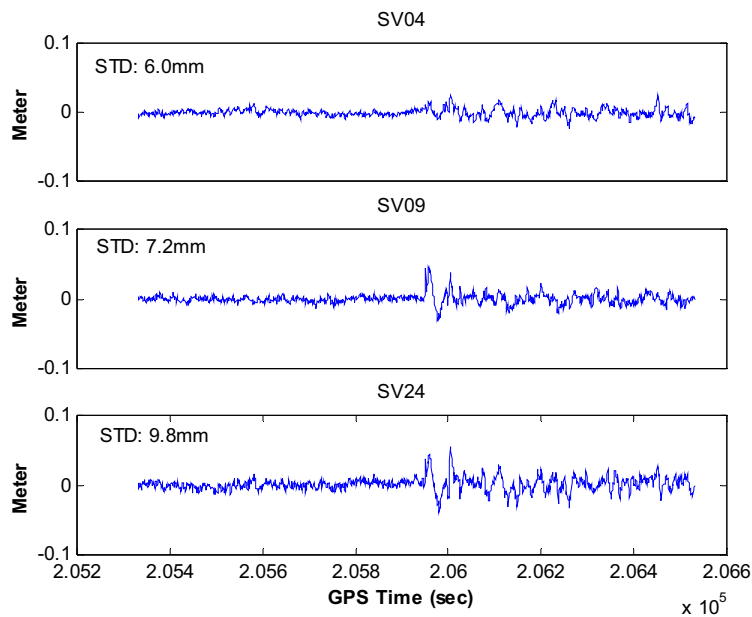


Figure 2-8 Carrier phase residuals based on INS predicted positions

INS-predicted position accuracy during complete GPS signal outage is analysed here. For this analysis, an accurate trajectory is necessary to compare with INS predictions. However, this adverse operational environment hinders such analysis, as an accurate reference trajectory cannot be obtained by a GPS kinematic positioning method due to the lack of satellite visibility. To this end, GPS signal blockages were simulated, although the measurement acquisition was carried out under normal GPS operational conditions, in which six satellites were successfully tracked during the whole experiment period. A total of three periods of GPS blockage (Case I, II, and III) were included in the measurements. Note that all blockages were fifty seconds in length. Graphs in the first column of Figure 2-9 illustrate RMS errors of the INS-predicted antenna position, whereas those in the second column depict the INS-predicted position errors obtained from comparison with positioning results without the signal outages. It can be seen from the results that the system provides sub-decimetres three-dimensional accuracy for the blockage lasting up to about five seconds, while an accuracy of few metres is obtainable after the fifty seconds outage.

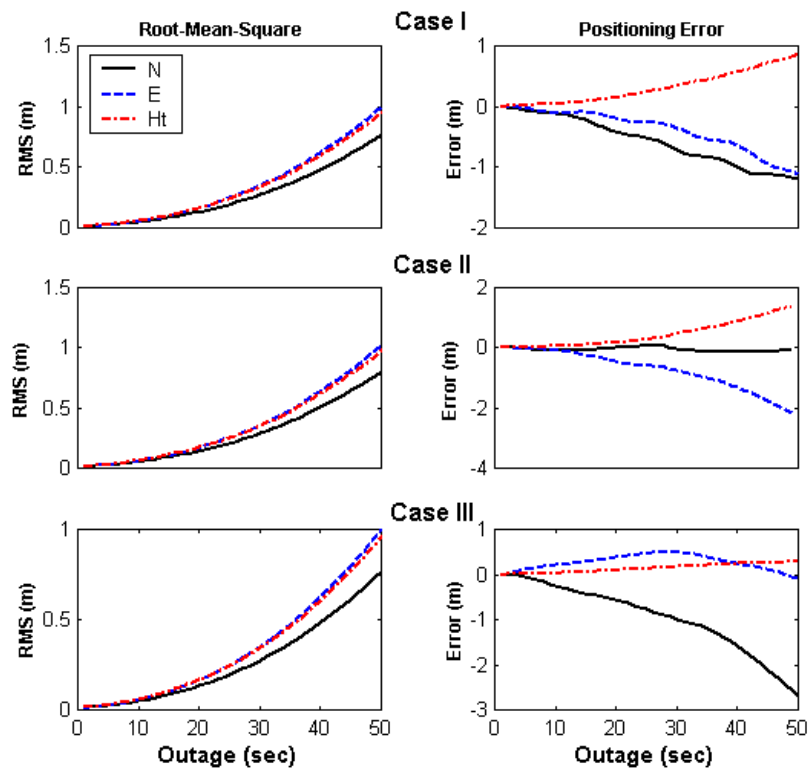


Figure 2-9 INS-predicted antenna position errors during 50 seconds of the signal blockages

### 2.7.2 Effect of Vehicle Dynamics on the Filter Estimation Performance

The observability of a linear system represents the possibility of determining the state parameters using the information on the input and the output of a system (Goshen-Meskin and Bar-Itzhack, 1992b; Rhee et al., 2002). One of the reasons for considering the observability of a dynamic system is the need to determine the efficiency of a Kalman filter designed to estimate the state of that system. When a vehicle is stationary, the GPS/INS integration, comprising a tactical-grade INS and single GPS antenna, is unable to observe the heading error due to deficiency of the filter observability. However, the error state becomes observable if the vehicle starts moving (accelerating). This is due to the fact that lateral acceleration excites the filter observability mode, which is unobservable at rest, and hence the filter observability is enhanced. Moreover, it is crucial to note that even if the filter becomes completely observable with vehicle dynamic changes, all the navigation errors and sensor biases cannot be observed individually (Rhee et al, 2002), which means some error states of the GPS/INS filter are less observable, for example horizontal accelerometer biases (Wang et al., 2003a). Hence, the influence of vehicle dynamics on the estimation of the error states that have less observability is investigated in this section. To this end, four experiments were carried out with controlled-trajectories. Figure 2-10 depicts the vehicle trajectories and dynamics during manoeuvring. For convenience, each of the trajectories is named as CIRCLE, LINE, RECTANGLE, and S-TURN. Note that the vertical dynamics ( $V_d$ ) are very low compared with those of the horizontal components ( $V_n$  and  $V_e$ ).

Figures 2-11 and 2-12 show the Root-Mean-Square (RMS) errors in horizontal accelerometer biases and heading error estimation, indicating the different vehicle dynamic contributions to the Kalman filter estimation procedure. The values were obtained from the diagonal components of the covariance matrix. It can be seen from these results that the filter estimation precision is improved by steady-turn manoeuvres (i.e., CIRCLE, RECTANGLE, and S-TURN), when compared with constant-velocity manoeuvre (e.g., LINE). This improvement can also be verified from the RECTANGLE results showing that the filter precision is considerably increased when the vehicle makes its first right angle turn. In addition, the results in Figure 2-11 and 2-12 show that ‘S-TURN’ provides the best filter estimation performance among the four trajectories



considered in these tests. This is due to reversing of the vehicle's lateral acceleration that occurs in the S-TURN manoeuvre (Porat and Bar-Itzhack, 1981). Note that the precision difference between the S-TURN and LINE cases is about  $200 \mu g$  in horizontal acceleration and 2.5 arc-minutes in heading error estimation at the last epoch (see Figure 2-11 and 2-12).

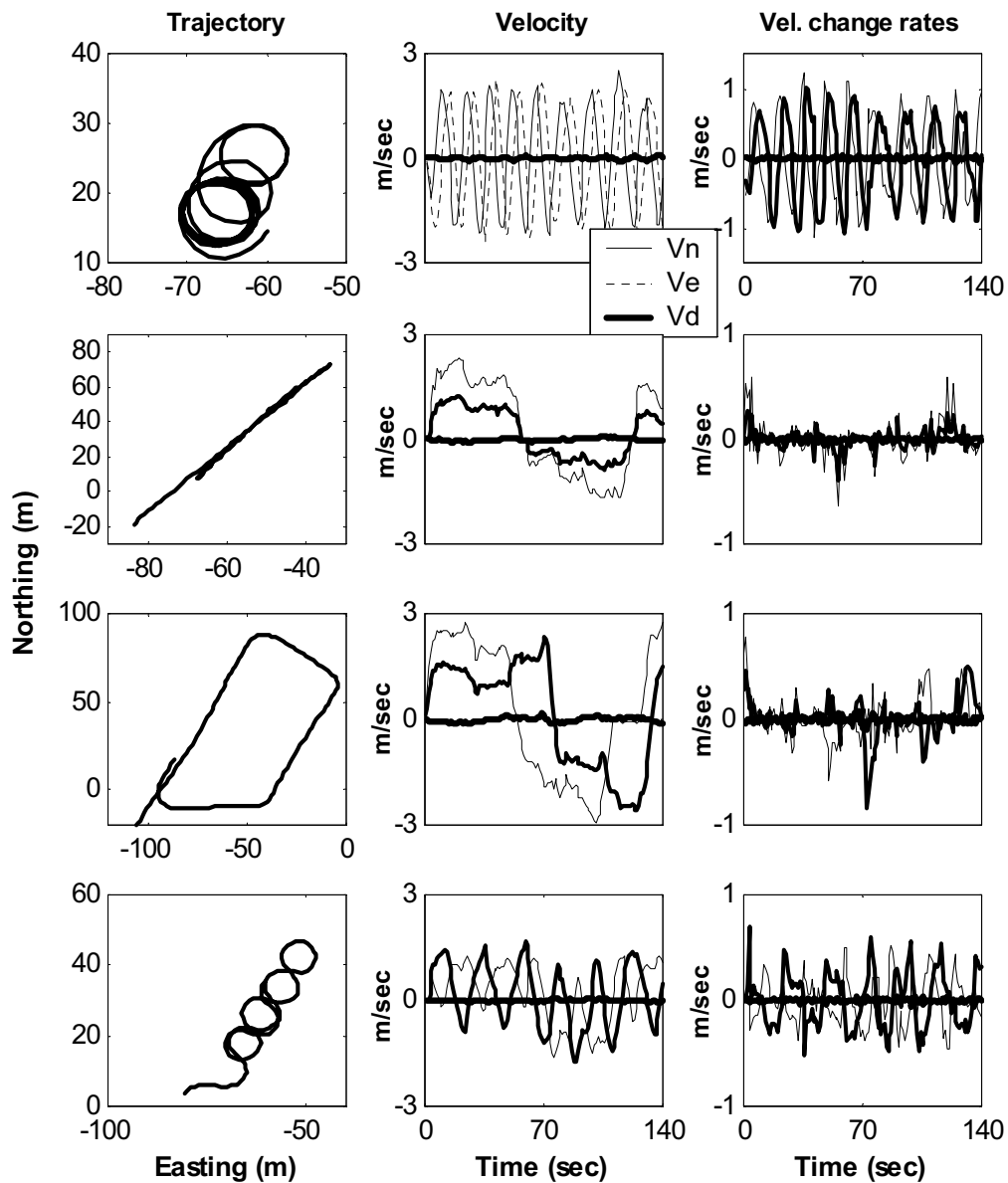


Figure 2-10 Vehicle trajectories and dynamics during the tests

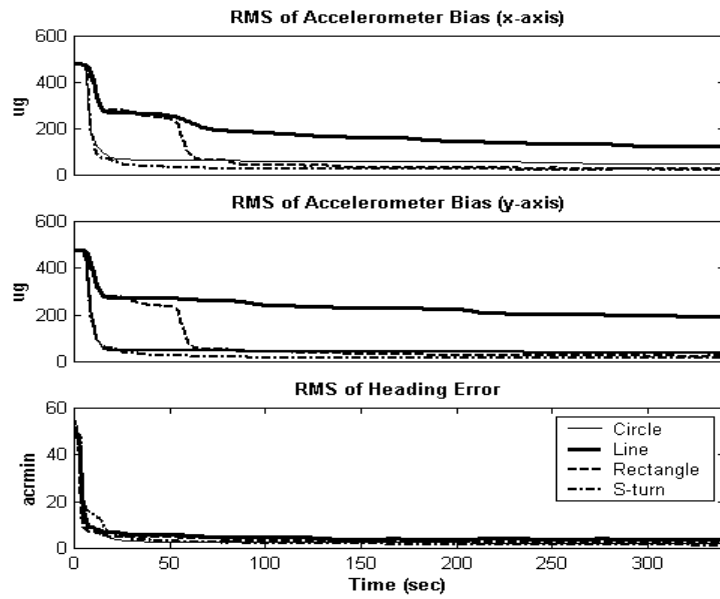


Figure 2-11 RMS errors for horizontal accelerometer bias and heading error estimation

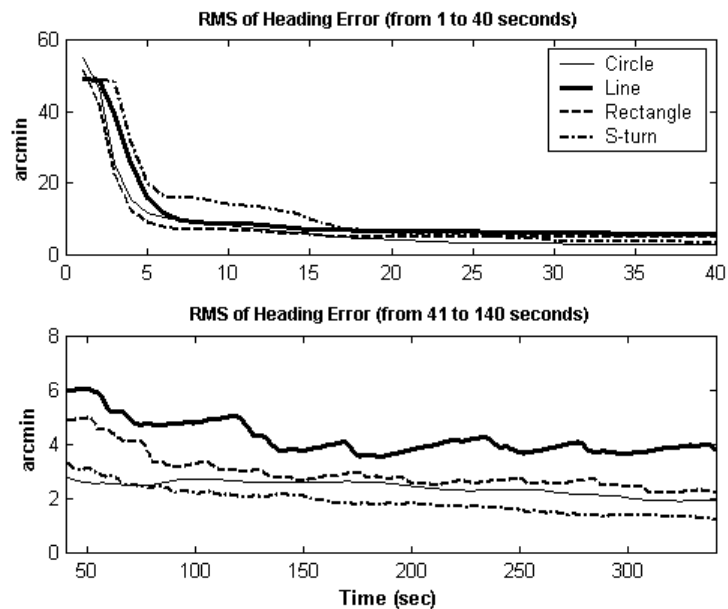


Figure 2-12 Magnified results for heading RMS error in Figure 2-11

### 2.7.3 Effect of Vehicle Dynamics in Positioning Accuracy During Complete GPS Signal Blockage

Two tests were conducted to investigate the effect of vehicle dynamics on navigation error estimation in the Kalman filter during GPS outage. The scenarios for the two tests are as follows (Figure 2-13):

- 1) The vehicle remained in static mode for a duration of 600 seconds (initialisation) before moving in circles within the same trajectory for 420 seconds.
- 2) The vehicle stayed in static mode for a duration of 600 seconds (initialisation) before moving in circles within the same trajectory for 340 seconds, then in a straight line at a constant speed for 80 seconds.

The GPS blockage was simulated for the last 80 seconds. Figure 2-14 depicts test results showing error growth of navigation parameters during GPS blockage. There is no abrupt error growth for the initial few tens of seconds, immediately after the outage. This seems to be due to the navigation and sensor errors being well calibrated during the first cycle with precise double-differenced carrier phase measurement. Otherwise, the results would be different from those presented. As seen from Figure 2-14, the navigation parameter errors in the case of CIRCLE grow more quickly than those in the LINE case during the simulated GPS blockage. Hence, highlighting that the vehicle's lateral acceleration change enhances the integration filter's performance by strengthening observability as long as the filter can be continuously updated by external measurements, while on the other hand it makes these errors to rapidly increase in the INS stand-alone mode (i.e., GPS signal blockage). This may be due to the fact that the equilibrant relationship among error parameters is quickly destroyed, the level of which is dependant on the magnitude of the vehicle dynamic change during the GPS blockage.

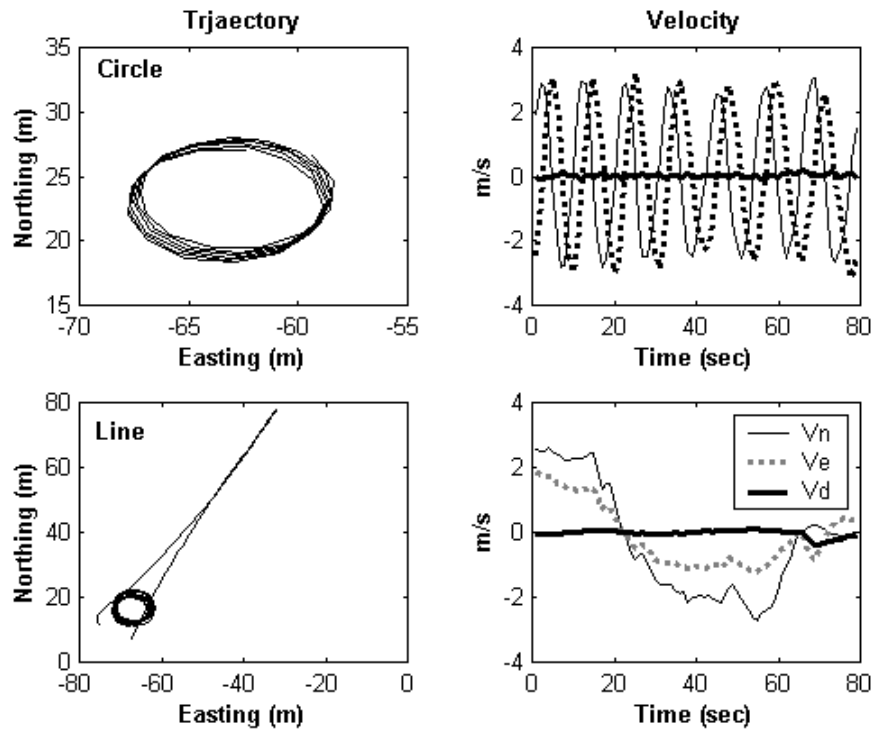


Figure 2-13 Vehicle trajectories and velocities during GPS blockage

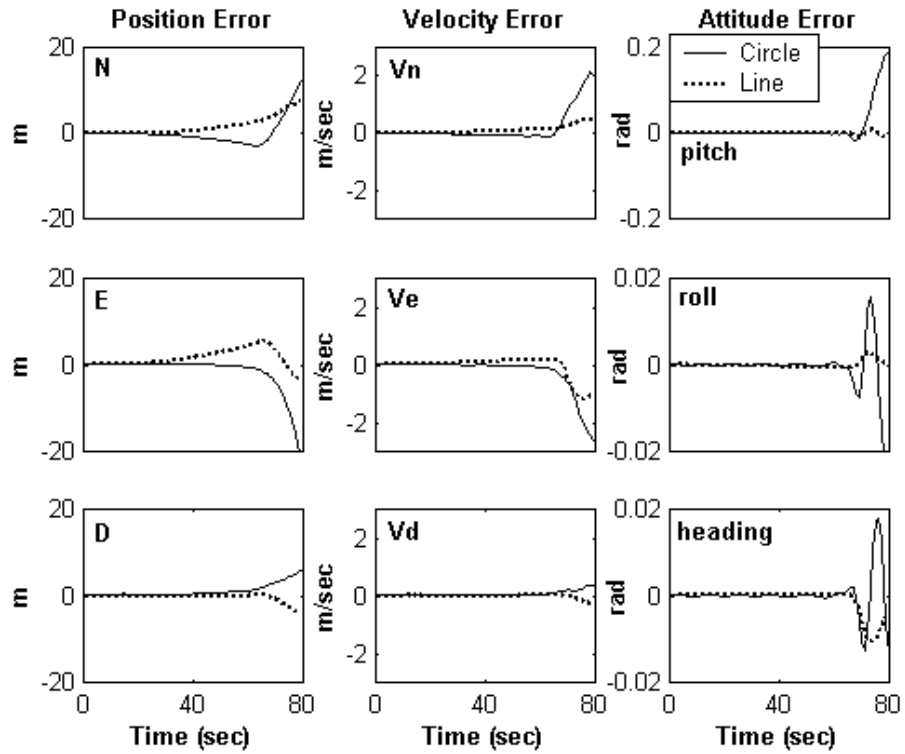


Figure 2-14 Error growth of navigation parameters during GPS blockage

## 2.8 Concluding Remarks

This chapter has described the issues of integrating a single-frequency GPS receiver with a tactical-grade INS, providing a highly precise positioning solution. Emphasis was placed on the integration filter design. Three field tests were designed and carried out, in order to evaluate the usual system performance and the influence of vehicle dynamics in the filter estimation precision and navigation accuracy.

The results of the tests for general system performance evaluation showed that the system was capable of delivering position accuracies in the order of few centimetres under a benign operational environment where six GPS measurements were continuously used for filter updating. On the other hand, simulated GPS signal blockages resulted in INS-predicted three-dimensional accuracies of sub-decimetre level for blockages lasting up to about five seconds, and increased to the few meter level after the fifty seconds outage.

The impact of the vehicle trajectories and dynamics on the performance of the integrated GPS/INS system was investigated using data sets obtained from experiments with controlled-trajectories. When the GPS measurements were used for all the data processing (no blockages), results showed that (a) vehicle dynamics affect the Kalman filter initialisation time and estimation performance, especially the heading component; (b) the higher the dynamic changes in the lateral direction, the shorter the initialisation time and the more precise the filter estimation; (c) the S-turn shaped trajectory provided the best system performance among the four trajectories considered in these tests. When GPS signal blockage was simulated, relatively high dynamic change degrades the system performance; thus implying navigation errors grow more rapidly.

**CHAPTER 3**

**INTEGRATION OF PSEUDOLITE OBSERVABLES WITH**

**GPS/INS**

---

---

### **3.1 Introduction**

Although the GPS/INS integration discussed in Chapter 2 enhances each component system, the performance still relies on the quality of GPS measurements and the geometry of the satellite constellation. For example, due to the limited number of GPS satellites, a sufficient number of 'visible' satellites cannot be guaranteed at all times and all locations. Even when some low elevation satellites can be tracked, the measurements from these satellites may be contaminated by relatively high atmospheric noise. Therefore, this intrinsic shortcoming of satellite-based positioning systems results in, for instance, poor accuracy in the vertical coordinate component, which is about three times worse than that of the horizontal coordinate components. Moreover, the performance is degraded in harsh operational circumstances. Some typical examples are when the duration of satellite signal blockage exceeds an INS bridging level, resulting in large accumulated INS errors that cannot be calibrated by GPS. Such a scenario is unfortunately a common occurrence for certain kinematic positioning and navigation applications.

These two problems of the integrated GPS/INS positioning and navigation can be addressed by the inclusion of additional ranging signals transmitted from ground-based "pseudolites", improving the 'open air' signal availability (Wang et al., 2001). This chapter investigates the issues associated with the introduction of pseudolite observables into the GPS/INS with a view to improving signal availability, solution reliability, and accuracy in a localised area. Two new kinematic positioning and navigation strategies, namely GPS/Pseudolite/INS and Pseudolite/INS integration, are proposed. Typically, the former would be appropriate for a case where the number and geometry of the visible satellites are not sufficient for precise positioning and navigation. The latter is applicable to indoor positioning where the GPS signal is

unavailable for use. This chapter also outlines the modelling issues of pseudolite measurements, which are different to GPS satellites due to the proximity between user and pseudolites as compared to the distance between users and GPS satellites. A series of simulation analyses and field tests have been carried out and are presented in order to analyse the effects of including pseudolites, such as the geometric strength, and to assess the performance of the proposed integrated system.

## **3.2 GPS/Pseudolite/INS Integration: Concept and Applications**

### **3.2.1 General Description of System Concept**

In order to satisfy the objective of this research – to provide high availability, integrity and accuracy continuously in a local area – an integrated GPS/Pseudolite/INS system and an alternative integrated Pseudolite/INS system are proposed. (In practice, the latter system is a special case to the former, for the cases where all GPS signals are blocked.) Pseudolites play three different roles in the proposed integration scheme, depending on the operational environments. Firstly, in cases of 'benign' kinematic GPS operation where there are no signal blockages and more than five satellites are available, additional pseudolites strengthen the GPS satellite-pseudolite geometry.

Secondly, in the cases when there are adverse GPS operational conditions, pseudolites can be used to augment GPS. There are two typical situations. One is when the number of GPS signals is insufficient to generate position solutions. In this situation, although the advantage of a tightly integrated system is to provide Kalman filter updates even when there are less than four satellite signals, the number of measurements cannot satisfy the Kalman filter's observability for three-dimensional positioning. The other situation occurs when the duration of satellite signal blockage is excessive, longer than the INS bridging level, resulting in large accumulated INS errors that cannot be calibrated by GPS. Figure 3-1 shows the simulated 30 second "tactical-grade" SDIMU error behaviour (e.g., gyro drift 5 deg/h and accelerometer bias 500 $\mu$ g) if external measurements are unavailable to update Kalman filter. A good example of GPS positioning in a harsh environment is discussed in Stone and Powell (1998), where the operational time of a GPS-only system can be reduced to 20% if the obstruction angle is

up to  $45^\circ$ . The sky masking at construction or mining sites results in significantly reduced satellite availability, and as a consequence, the geometry is degraded. In such a case, one or more pseudolites deployed at appropriate locations can be used to improve the availability of measurements.

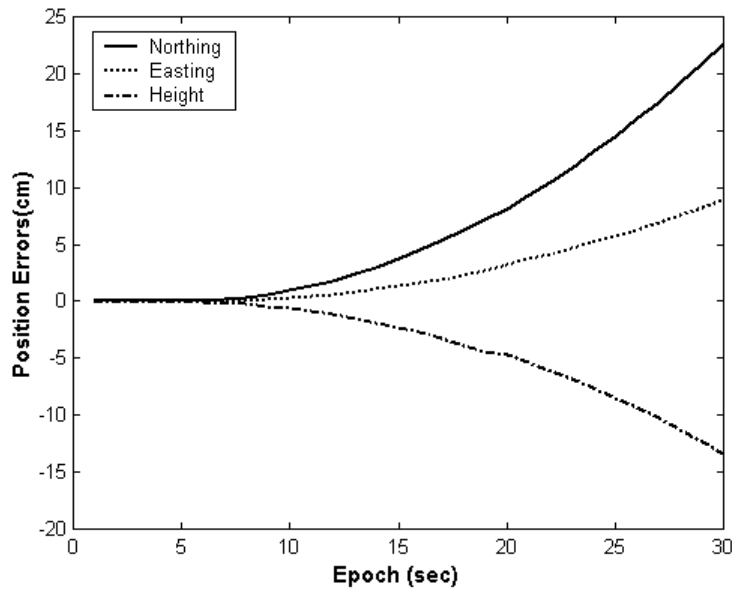


Figure 3-1 Tactical-grade INS error behaviour without GPS calibration.

In the third case, GPS signals are completely unavailable, such as when operating in an indoor environment. In such a case, GPS measurements cannot be used in the Kalman filter updating and the accumulated INS error increases with time as shown in Figure 3-1. The errors in the vertical channel of a Schuler-tuned INS tend to grow exponentially with time, while the errors in the horizontal channels tend to grow no faster than sinusoidally with linearly increasing envelope. However, the pseudolites can replace the satellite constellation, and hence be used to calibrate the INS error states. A pseudolite-based positioning concept has been proposed for indoor positioning (Kee et al., 2000). In this scenario, multipath reflected from the walls will be a major error source, which degrades positioning accuracy (Michalson and Progri, 2000). Another important issue for this application is the deployment of pseudolites, since the positioning results are affected by the pseudolite geometry. This will be discussed in more detail in the following sections.



### 3.2.2 Applications

*Land vehicle control and guidance* is a challenging application, especially for a construction plant, because many obstructions will cause GPS signal blockage. Some examples include drills, shovels, excavators and trucks. Such machinery can be currently controlled through laser guidance systems, or more recently using kinematic GPS techniques. Whilst the laser system can usually only provide height information, the added benefit of a GPS system is that it provides three-dimensional coordinates. However the GPS system cannot provide full orientation information (with one GPS antenna), and its usage is restricted by the requirement for unobstructed line-of-sight between satellites and the receiving antenna (accuracy is dependent on satellite geometry). Unfortunately it is difficult to ensure good satellite geometry and signal availability on construction sites, in open-cut mines, highways, dam construction, etc., where steep pit walls or local terrain may mask some of the GPS signals. An integrated GPS/Pseudolite/INS system provides, in principle, an effective solution for such applications.

*Surveying and mapping* have benefited enormously from the ability of GPS to provide fast and accurate positioning. The GPS/Pseudolite/INS system referred to in this study is able to deliver further benefits by providing accurate attitude information even without satellite signals. The system can provide precise exterior orientation parameters (i.e. position and attitude information) for mobile mapping applications. Hence it is possible to perform direct geo-referencing without Ground Control Points (GCP). In principle, the application of mobile mapping systems can therefore be extended to indoors, and even underground. Another application is the measurement of rail track irregularities (Lück et al., 1999). A GPS/Pseudolite/INS system mounted on a monitoring car can offer an elegant solution to the problem of measuring track geometry in tunnels.

In *aircraft precision approach and landing*, there are stringent requirements in terms of positioning accuracy, availability and integrity. However, it is difficult to meet their requirements using GPS-only or a GPS/INS system due to the limited number of its satellites. Studies have shown that some means of augmentation can address these

shortcomings in order to meet the specified requirements. Airport pseudolites have been suggested as a means of satisfying the stringent performance requirements of CAT II/III approach systems. Further discussion on this application will be given in Chapter 7.

### 3.3 Modelling Pseudolite Measurements

#### 3.3.1 DD Measurement Model

Similar to GPS satellite measurements, the pseudolite DD carrier phase and pseudo-range observations can be modelled as:

$$\nabla\Delta\phi_{PL} = \frac{1}{\lambda_p} \nabla\Delta\rho + \nabla\Delta N + \frac{1}{\lambda_p} \nabla\Delta T_p + \frac{1}{\lambda_p} \nabla\Delta d_p + e_\phi \quad (3.1)$$

$$\nabla\Delta R_{PL} = \nabla\Delta\rho + \nabla\Delta T_p + \nabla\Delta d + e_R \quad (3.2)$$

where

- $\lambda_p$  : the wavelength of the carrier frequency
- $\nabla\Delta T_p$  : the DD tropospheric delay
- $\nabla\Delta d_p$  : the pseudolite location error.

In the above Equations (3.1) and (3.2), unlike the case of GPS measurements, the pseudolite location error and tropospheric delay cannot be removed even though the double-differencing technique is applied for short baseline applications. This is because pseudolites are much closer to the user receivers than the satellites.

#### 3.3.2 Special Considerations for Pseudolite Measurement Modelling

To successfully augment a GPS/INS system by integrating with pseudolites, there are a number of issues that must be considered for pseudolite measurement modelling state. If the issues are appropriately considered, integrating pseudolite observables into the

GPS/INS system is relatively straightforward because the pseudolites can be considered as extra GPS satellites (if the pseudolites transmit signals on the GPS L1 and/or L2 frequency). Hence the system based on GPS/Pseudolite/INS technology can be implemented, using a tightly coupled integration strategy as presented in Chapter 2.

### 3.3.2.1 Pseudolite tropospheric delay

For GPS satellite signals, tropospheric delay can be estimated by using models, such as the Saastomoinen, Hopfield or Black models, as discussed in Chapter 1. The delay estimated from these models is extremely dependent on the GPS satellite elevation angle. Unlike spaceborne satellite signals, pseudolite signals propagate largely through the lower troposphere, as such the effect of tropospheric delays in the pseudolite measurements should be corrected for using a special tropospheric delay compensation model. Hein et al. (1997) has proposed a simple tropospheric delay model, where the refractivity  $n$  at the base of the atmosphere is described as a function of the meteorological parameters:

$$N = (n - 1) \cdot 10^6 = 77.6 \frac{P - e}{T} + 71.98 \frac{e}{T} + 375000 \frac{e}{T^2} \quad (3.3)$$

where  $P$  is the air pressure in hectopascals;  $e$  is the partial pressure of the water vapour in hectopascals; and  $T$  is the absolute temperature in degree Kelvin. The partial pressure of the water vapour can be estimated via the relative humidity ( $RH$ ):

$$e = RH \cdot \exp(-37.2465 + 0.2133T - 0.0002569T^2) \quad (3.4)$$

With the assumption that the meteorological parameters are the same, the tropospheric delay after between-receiver single-differencing can be represented (i.e., Dai et al., 2002) as:

$$\Delta \delta_{trop} = \left( 77.6 \frac{P}{T} + 5.62 \frac{e}{T} + 375000 \frac{e}{T^2} \right) 10^{-6} \Delta \rho_{ij}^p \quad (3.5)$$

where  $\Delta\rho_{ij}^p$  is the single difference in geometric ranges between the pseudolite transmitter (e.g.,  $p$ ) and the two receivers (e.g.,  $i$  &  $j$ ). For the standard meteorological parameters ( $P = 1013\text{mPa}$ ,  $T = 20^\circ$ ,  $RH = 50\%$ ), the tropospheric delay correction can reach 320.5ppm. Under some weather conditions, the influence of the pseudolite tropospheric delay can reach up to 600ppm. Similar conclusions have been drawn by Hein et al. (1997). Clearly the local weather conditions play a significant effect on the magnitude of the correction.

### 3.3.2.2 Pseudolite location error

The orbit error (or error in the coordinates of the phase centres of the transmitter antennas) is one of the major biases in satellite/pseudolites-based positioning. In GPS relative positioning, the impact of the satellite orbital errors on baseline component accuracy is notably mitigated, but ‘pseudolite location error’ can be significant as pseudolites are closer to users. The impact of the pseudolite location errors will be analysed in detail in Chapter 4.

### 3.3.2.3 Pseudolite multipath

One of major error sources for pseudolite measurements is multipath. Compared with multipath from satellite signals, pseudolite multipath has some peculiar characteristics (Ford et al., 1996; Dai et al., 2002). First of all, pseudolite multipath is not only due to reflected signals from surfaces, but also from the signal transmitter itself. Whilst the GPS satellites are orbiting in space and far away, the pseudolite transmitter is generally stationary and nearby. Hence the magnitude of multipath caused by a satellite signal transmitter itself is relatively small and slowly changing, whereas that of a pseudolite is relatively large and rapidly changing in the case of a kinematic environment. If the pseudolite and the receiver were both stationary, the multipath error would be a constant (ibid). In a kinematic environment, the multipath, in particular the ‘*transmitted*’, will significantly increase the noise level of the measurements.

In order to show typical behaviour of GPS and pseudolite multipath in a kinematic mode, DD carrier phase and pseudo-range residuals are illustrated in Figure 3-2. Since the DD technique can remove and/or dramatically reduce the common error sources between reference and remote stations in the case of a short baseline, the residual errors can be considered to be mainly due to multipath. It can be seen from the results that pseudolite measurement residuals (the lower graphs, PL12) are slightly biased and show a lot of fluctuations, compared to the residuals from the satellites (the upper graphs, SV9). The mean value and the standard deviation for the pseudolite carrier phase data are 0.06 and 0.103 cycles respectively, and for the pseudo-range are 0.868 and 1.833 m, respectively. The bias terms in both the carrier phase and pseudo-range residuals seem to be caused by the multipath that is contaminated in the stationary reference station. In addition, the pseudolite multipath presents some patterns related to the vehicle trajectory or dynamics.

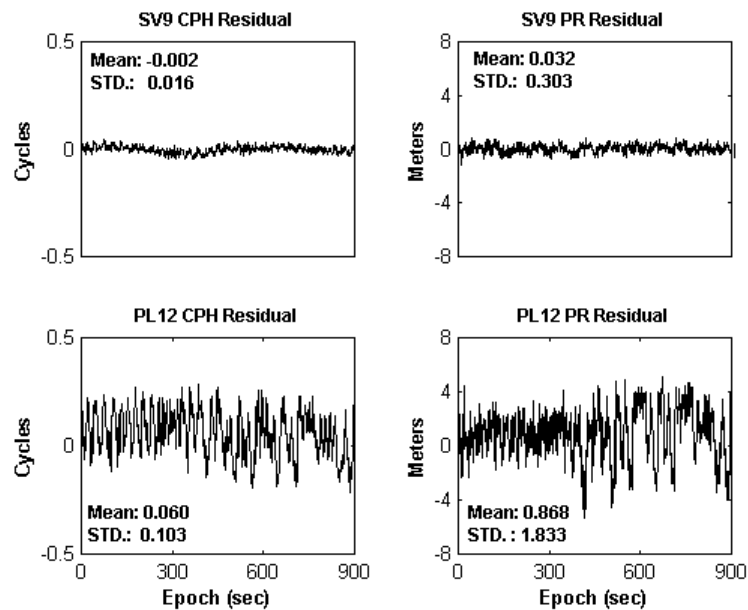


Figure 3-2 Effect of multipath on the double-differenced GPS/pseudolite observations (Pseudo-Range (PR) and Carrier Phase (CPH))

### 3.4 Geometry Analysis of Pseudolite Augmentation

#### 3.4.1 GPS Performance Measure

Geometry simulation analysis for the proposed pseudolite-augmented GPS/INS system will be presented in detail in this section. GPS performance measures used in the following analysis are firstly outlined.

##### 3.4.1.1 Dilution of Precision (DOP)

The *Dilution of Precision* (DOP) is a measure of the geometrical strength of a satellite constellation (Leick, 1995; Rizos, 1996). The DOP values are calculated from the unit line-of-sight vector between a satellite and a receiver, which means the values are dependent on the receiver location and time when carrying out observations. The DOP values are calculated with respect to *Absolute* positioning scenarios. However, Relative Dilution of Precision (RDOP) is widely used for *Relative* Positioning scenarios (Wang et al., 2001a; Lee et al., 2002). Basically, the RDOP computation procedure is the same as that of DOP, but uses a different form of the design matrix suitable for relative positioning.

It is well known that the basic accuracy of GPS can be described as the product of the errors in ranging to the satellites and the dilution of the geometry. Hence, the simplified relationship is (Rizos, 1996):

$$\textit{Positioning Error} = \textit{DOP} \times \textit{Ranging Error} \quad (3.6)$$

where the Geometric Dilution of Precision is a class of multipliers known as DOP (Dilution of Precision), for example HDOP (Horizontal DOP), VDOP (Vertical DOP), RDOP (Relative DOP), or other similar factors. RDOP will be used in this study.

### 3.4.1.2 Ambiguity Dilution of Precision (ADOP)

In addition to DOP and RDOP measures of the geometrical strength of a satellite constellation, *Ambiguity Dilution of Precision* (ADOP) captures the main characteristics of the ambiguity precision and correlation (Teunissen, 1997; Teunissen and Odijk, 1997). It will be obvious that one cannot expect to have a successful validation of the ambiguities when the estimated ambiguities have poor precision. Furthermore, the chance of success is improved if ambiguity precision is augmented, and successful resolution can be expected when the standard deviation, which is expressed in units of cycles, is significantly smaller than one cycle. ADOP (Ambiguity Dilution of Precision) was introduced to represent both precision and correlation characteristics of the estimated ambiguities (ibid):

$$\text{ADOP} = \sqrt{\det Q_{\hat{x}_a}}^{\frac{1}{m}} \text{ (cycle)} \quad (3.7)$$

where  $Q_{\hat{x}_a}$  is the covariance matrix of the float ambiguities (in detail see Chapter 5);  $m$  is the number of the ambiguity variance matrix.

### 3.4.1.3 Reliability

*Reliability* is a measure that describes the quality of the final solution with respect to its ability to detect biases or outliers. For instance, a very reliable solution is one in which quite small biases can be detected. The reliability is dependent upon the redundancy of the system, and how the errors propagate through the system. Reliability has two parts: *internal reliability* and *external reliability*. Whilst internal reliability refers to the capability of the system to detect and localize an error, external reliability is a measure of the effect of an error, which has not been detected, upon the estimated parameters.

The internal reliability is expressed in terms of the Minimum Detectable Bias (MDB), that is the bias that can be detected with a certain probability at a specific significance level. In the calculation of the MDB, the power of the test is usually held fixed at a

reference value of say 80% (Cross et al., 1994). If the measurements are correlated, and it is assumed that there is one outlier present, then the MDB may be calculated as follows (Cross et al., 1994; Moor et al., 2002):

$$\nabla l_i = \sigma_i \frac{\sqrt{\lambda_0}}{\sqrt{c_i^T P Q_v P c_i}} \quad (3.8)$$

where  $c_i = [0, \dots, 1, 0, \dots, 0]$ ,  $i = 1, 2, \dots, m$ ,  $\sigma_i$  is the standard deviation of the  $i^{\text{th}}$  measurement,  $\lambda_0$  is the mean of the non-centrality parameter for  $\alpha$  and  $\beta$  using the normal distribution,  $Q_v$  is the variance-covariance matrix of the residuals, and  $P = Q^{-1}$  is the weight matrix.

The external reliability is computed by propagating the effect of each MDB through the Least Squares process to the final solution. This reliability is concerned only with the effect of undetected outliers upon the final solution. So one can only quantify the probability of detecting them if they do occur, and the effect they will have if they are not detected (ibid):

$$\nabla \hat{x} = (A^T P A)^{-1} A^T P * (c_i * \nabla l_i) \quad (3.9)$$

where  $A$  is the design matrix that captures the relative receiver-satellite geometry, and the other terms are the same as Equation (3.8).

### 3.4.2 Relative Dilution of Precisions (RDOPs)

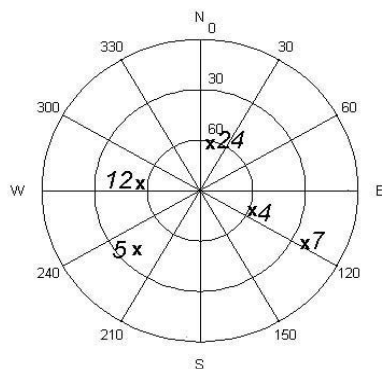
There are two ways to improve GPS positioning accuracy: augmentation of the observation accuracy and/or the geometry of the satellites' distribution (Equation 3.6). Pseudolites can be used to improve the geometrical strength of positioning solutions, particularly for the height component. The pseudolite(s) location with respect to the mobile receiver will be critical. In practice, the possibility that GPS satellite signals may be blocked need to be considered. Optimisation of the pseudolite location(s) is therefore



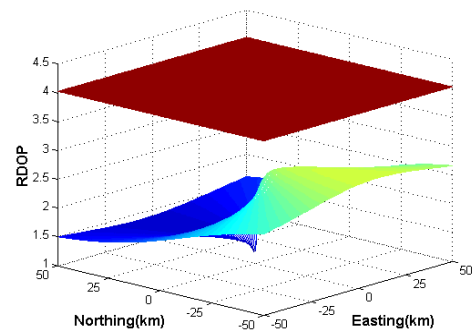
necessary. 'Geometric optimisation' refers to the need to find locations for the pseudolite transmitters that will minimise PDOP, RDOP, or other similar factors.

To analyse the impact of pseudolite location, extensive simulations have been carried out. For this study, the following parameters were considered: the GPS ephemeris on 28<sup>th</sup> June 2002, the sample time interval of 120 seconds, the user location in Sydney, and the cut-off angle of 7.5 degrees.

Firstly, a simulation was performed to investigate how pseudolite location affects satellite geometry. To this end, satellite distribution was fixed at a certain time (see left graph in Figure 3.3), and a single pseudolite location varies from -50,000m to 50,000m with 500m intervals. In addition, the altitudes of a mobile receiver and a pseudolite were fixed at 500m and 50m, respectively. This means that the pseudolite elevation varied through negative values (e.g., airborne applications).



(a) Satellite distribution in the sky



(b) RDOP changes with pseudolite location

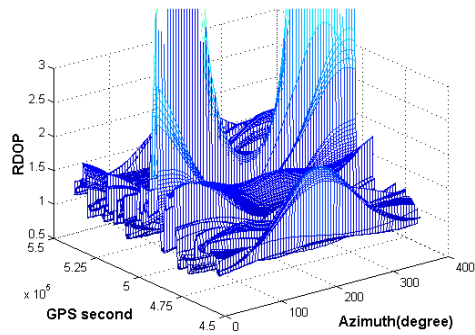
Figure 3-3 Satellite constellation and RDOP changes as a function of pseudolite location

The upper mesh of graph (b) in Figure 3-3 shows the RDOP values without pseudolite augmentation, while that of the lower one represents RDOP changes with the pseudolite location varying across the 500m grids. When comparing the two meshes, one can see that the additional pseudolite significantly improves the satellite geometry. Moreover,

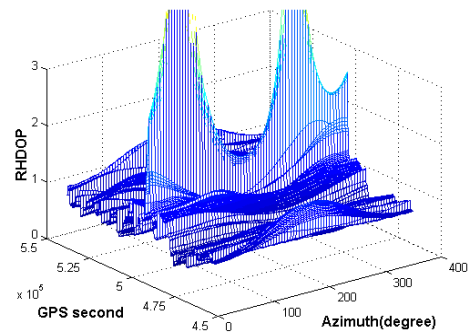
the RDOP values change from 1.2 to 2.8, depending on its location. Generally speaking, excellent RDOP (less than 2) values can be achieved if the pseudolite is located to the north of the GPS receiver. It is therefore obvious that the pseudolite location(s) will change the geometry significantly.

To investigate in more detail how pseudolite location affects GPS satellite geometry, additional geometric simulations for 24 hours were performed where one pseudolite was included, but with varying azimuth from 0 to 360 degrees, as well as elevation angles from -80 to 80 degrees. In addition to RDOP, RHDOP (Relative Horizontal DOP) and RVDOP (Relative Vertical DOP) were also computed. In the case of varying the azimuth, the distance and the elevation angle between the GPS antenna and pseudolite transmitter was 1,500m and -17.5 degrees, respectively. Graphs (a) to (c) in Figures 3-4 show the RDOP, RHDOP, and RVDOP values, while the pseudolite azimuth is varied from 0 to 360 degrees. It can be seen that all three plots have very similar trends, with very large values if the pseudolite is located in the azimuth band 260 to 360, or from 0 to 100 degrees, except for a couple of epochs at the first and last part. Note that varying the pseudolite location affects both the horizontal and vertical components in a similar fashion. Moreover, RVDOP values show better geometric strength than those of RHDOP. This is due to the fact that the pseudolite in this simulation is kept at a low elevation angle.

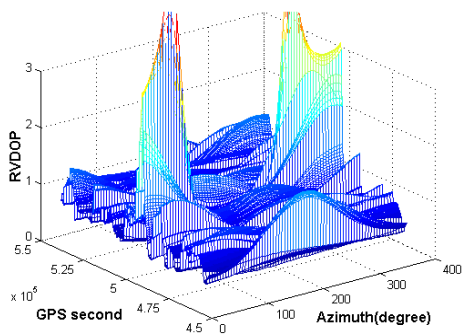
Another simulation was carried out to investigate the effect of varying pseudolite elevation on the GPS-PL geometry. In this study, the distance and the azimuth were kept constant at 1,000m and 45 degrees respectively. Again, 24-hour simulations were carried out, with the results plotted in graphs (d) to (f) in Figures 3-4. It appears that the insufficient constellation of GPS satellites cause the RDOP peaks in these figures. The pseudolite elevation affects the vertical component much more than the horizontal one (comparing graph (d) with (e)). Also, it can be concluded that the lower the pseudolite elevation, the better the RVDOP. One can, therefore, maximize such benefit of pseudolite deployment in the case of airborne applications, even though only one pseudolite is used in the solution. On the other hand, varying the elevation angle does not affect the horizontal component (see graph (e)).



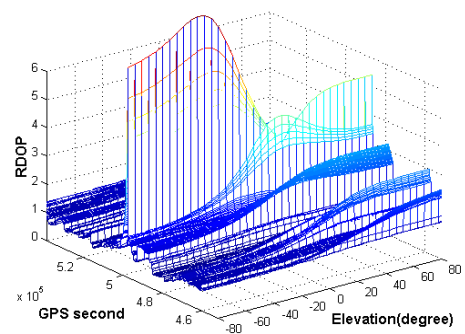
(a) RDOP with varying PL azimuth



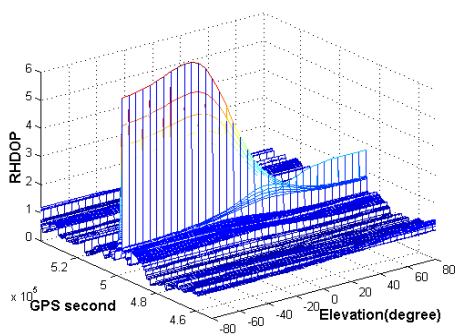
(b) RHDOP with varying PL azimuth



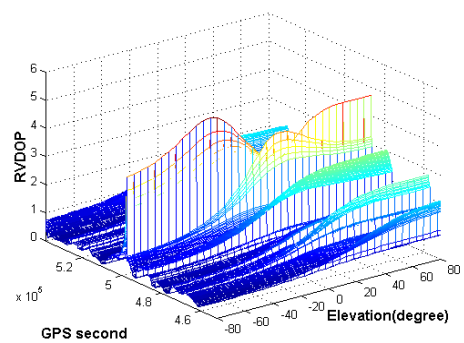
(c) RVDOP with varying PL azimuth



(d) RDOP with varying PL elevation



(e) RHDOP with varying PL elevation



(f) RVDOP with varying PL elevation

Figure 3-4 RDOP simulation results as a function of pseudolite azimuth and elevation

In addition to the pseudolite location effects, further 24-hour simulations were carried out in order to investigate the impact of the number of pseudolites used for augmentation. All of the pseudolites elevations were approximately -17.5 degrees, as in the previous simulation. Table 3-1 shows the average values of RDOP, RHDOP, and RVDOP, as a function of the number of pseudolites. It can be seen that the inclusion of even one pseudolite significantly strengthens the GPS-PL geometry, reducing the RDOP value from 3.2 to 1.5. Comparing RHDOP and RVDOP, with and without pseudolites, it is clear that the employment of pseudolite(s) with an elevation angle below the horizon makes the RVDOP values smaller than the RHDOP values. This is the reverse situation to conventional GPS positioning. Although the geometry can become stronger using more pseudolites, it is unlikely that more than three pseudolites need to be used. This is due to the fact that three or four pseudolites only affect GPS satellite geometry marginally, if it is assumed that all signals from the deployed pseudolites can be successfully tracked during the whole mission.

Table 3-1 Average RDOP values as a function of the number of pseudolites

Number of PL	0	1	2	3	4
RDOP	3.1	1.5	1.1	1.0	0.8
RHDOP	1.9	1.1	0.9	0.8	0.7
RVDOP	2.8	1.0	0.7	0.6	0.5

### 3.4.3 Ambiguity Dilution of Precision (ADOP)

ADOP values using the single-frequency single-epoch measurement model were computed using Equation (3.7) for two minutes with respect to the number of pseudolite(s) used. In this computation the standard deviation of the code and carrier phase measurements was 0.3m and 0.002m respectively. As can be seen from Figure 3-5, additional pseudolites improve ambiguity precision (i.e. lower the value of ADOP). For example, comparing the GPS-only case with the scenario that includes four pseudolites, the ADOP value was improved by about 57%. Note that the inclusion of even one pseudolite can help in this regard.

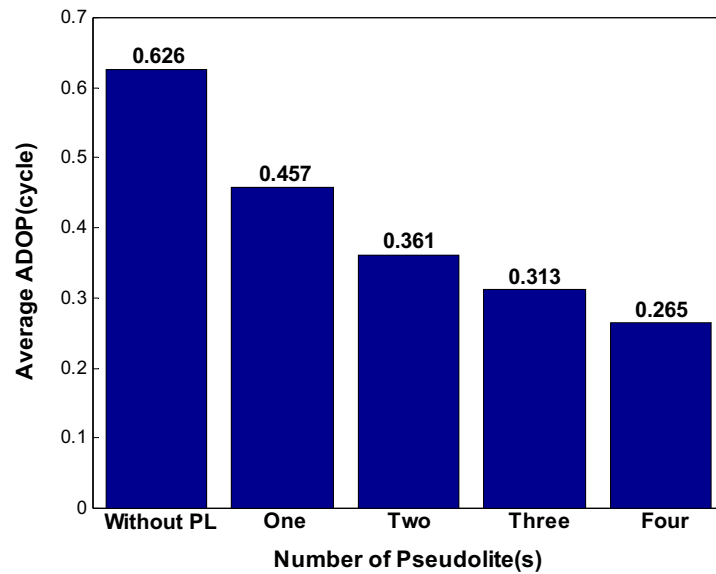


Figure 3-5 Average ADOP with respect to the number of pseudolites

#### 3.4.4 Reliability

To investigate how the inclusion of a pseudolite influences both internal and external reliability, simulations were carried out for a period of 3 hours, when the satellite geometry was relatively poor. Up to four pseudolites were included. Note that the basic simulation parameters were the same in the previous studies, and Equations (3.8) and (3.9) were used to calculate the values. Figures 3-6 to 3-8 demonstrate that pseudolites can improve the reliability of the GPS solution. Table 3-2 shows the average values of the computed internal and external reliability. With respect to the first and second columns in Table 3-2, it is interesting that the reliabilities were dramatically improved, even with the inclusion of only one pseudolite. This result can be attributed to the fact that high reliability peaks of 0.03m (internal reliability) and a few metres (external reliability) were significantly reduced when using a pseudolite.

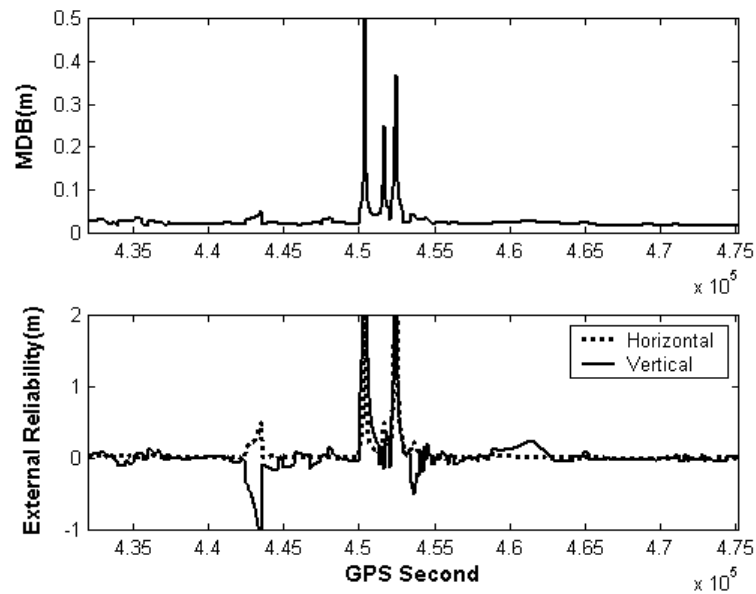


Figure 3-6 Reliability changes without pseudolites

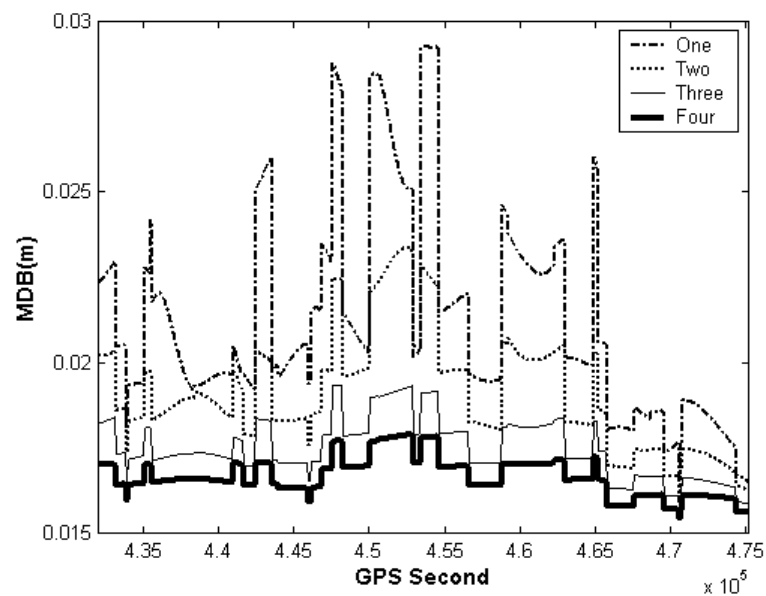


Figure 3-7 Internal reliability (MDB) changes as a function of the number of additional pseudolites

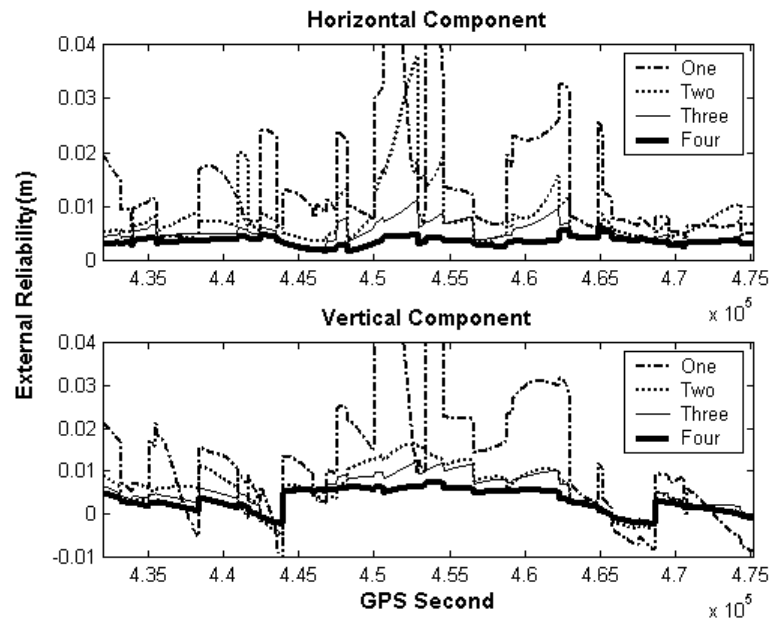


Figure 3-8 External reliability changes as a function of the number of additional pseudolites

Table 3-2 Mean reliability values as a function of the number of pseudolites (unit: cm)

Number. Of PLs	0	1	2	3	4
Internal (MDB)	2.89	2.12	1.90	1.74	1.66
External (Horizontal)	6.52	1.43	0.83	0.53	0.35
External (Vertical)	8.91	1.36	0.59	0.52	0.32

### 3.5 Tests with Simulated Measurements

During the early stages of the development of an integrated positioning and navigation system, it is necessary to test the components, assess the behaviour of the various integration strategies and to verify the performance of the system algorithms. It is often not practical to collect data under all possible scenarios. Furthermore, in many kinematic scenarios the true trajectory is not known precisely. By processing the simulated data, a reference trajectory can be generated, and then compared with the results from the integrated system.

### 3.5.1 Measurement Generation

Simulation software has been developed in this study. It comprises three components as shown in Figure 3-9: the trajectory profile, and the SDIMU and GPS/pseudolite measurement simulation modules. Both the GPS/pseudolite and SDIMU data simulation require a reference trajectory (a flight profile) for the moving vehicle. The reference trajectory is defined by the time, coordinate, velocity and attitude angle values. The inputs for the software include the initial coordinates, velocity, attitude, update rate, starting and ending times. In addition, to define the vehicle's movement change, segment parameters, for example acceleration, velocity and heading changes, need to be defined. The generated trajectory profile is output at 1Hz rate.

In the case of the SDIMU, specific force (acceleration) and angular velocity are firstly generated, based on the given trajectory profile. Then, the related sensor errors, accelerometer/gyro bias, scale factor and noise, as well as effects associated with Earth rotation and gravity, are computed and added to the generated 'true' measurements. All the data generated are stored in a binary format at a rate of 64Hz.

GPS/pseudolite data generation starts with the computation of the coordinates of the satellites. While GPS satellite coordinates are computed using an ephemeris data file (converted from the almanac file), those for the pseudolites need to be provided by the user. Subsequently, based on the coordinates of the receiver antenna and the satellites, the distances between the two points in space are computed. The biases, errors and measurement noise defined by the appropriate models (0.4 m for pseudo-range and 0.5 cm for carrier phase measurement), are then added. Multipath is not taken into account in this simulation study. Some points need to be considered at this stage. One is the lack of an ionospheric delay model for the pseudolite measurements, as presented in Equations (1.2) and (1.4). Secondly, a different tropospheric effect model (e.g., Equation (3.5)) must be used for each pseudolite, as the standard GPS tropospheric models cannot compensate for the pseudolite tropospheric effect. A GPS/pseudolite simulation output rate of 1Hz was used. The simulated data is outputted in RINEX V2 format.



The simulation was carried out with respect to an integrated "tactical-grade" IMU (e.g., gyro drift 5 deg/h and accelerometer bias 500 $\mu$ g) and a single-frequency GPS receiver. Using the software, GPS/pseudolite and SDIMU measurements were generated, including a reference (true) trajectory for the simulation tests as shown in Figure 3-10.

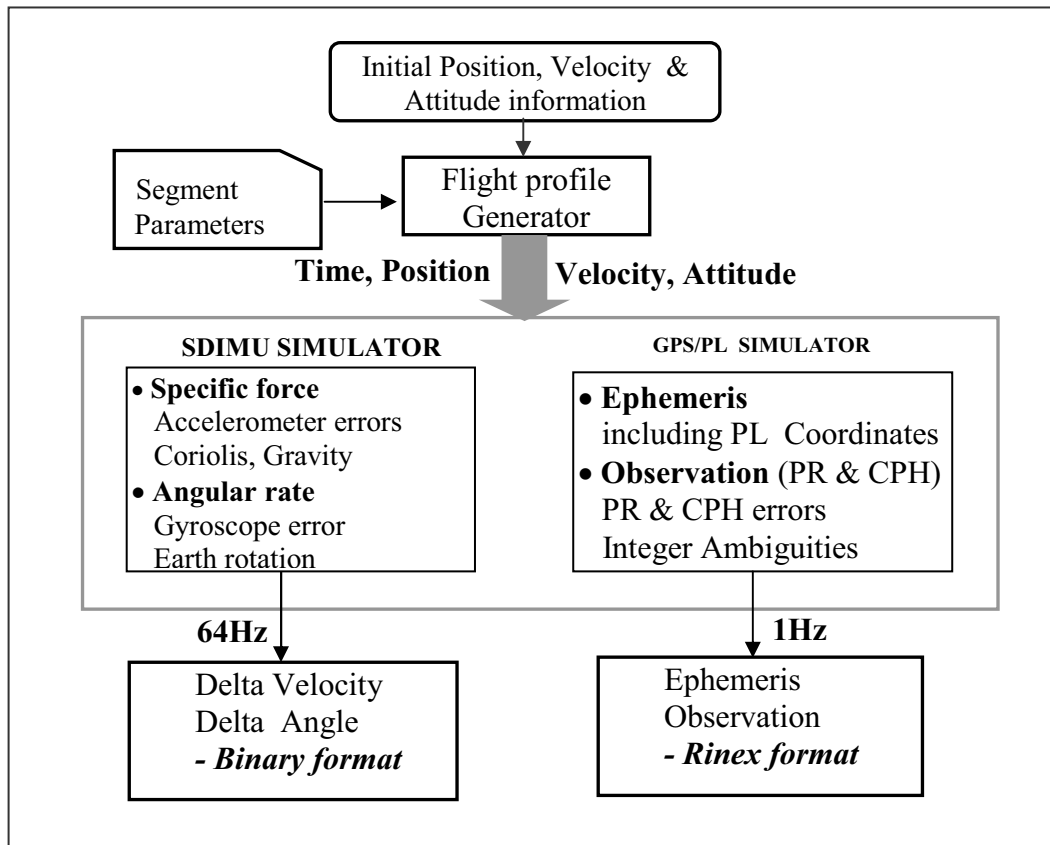


Figure 3-9 The GPS/PL/SDIMU measurement simulator

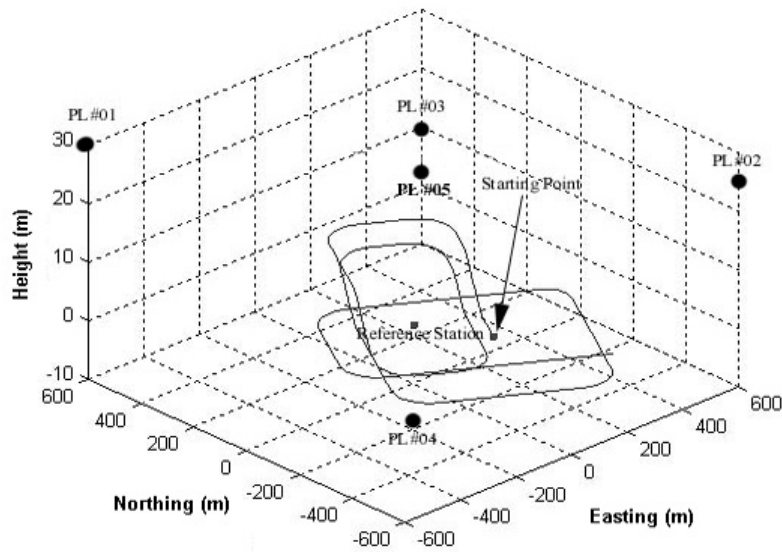


Figure 3-10 A generated reference trajectory and pseudolite locations

### 3.5.2 Benign Operational Environment

The objective of this test was to compare the performance of standard GPS/INS with a GPS/Pseudolite/INS system, as well as to evaluate the accuracy of the integrated GPS/Pseudolite/INS system as a function of the number of pseudolites used. To this end, GPS measurements from five satellites were used under benign operational conditions, whilst an additional four pseudolite measurements were included in turn. To evaluate the system accuracy, a comparison between positions, velocities, and attitude angles on the reference and computed trajectory is given in Figure 3-11 to 3-13. As mentioned in the previous section, the reference trajectory in the simulation studies provides the best means of analysing achievable accuracy and system performance. In addition, standard deviations of the double-differenced (DD) residuals of the three highest satellites in each epoch are compared (see Figure 3-14). As discussed in § 3.4.3, the addition of pseudolites strengthens the existing GPS satellite geometry. The enhanced geometry may result in accurate INS error estimation in the integration filter, and subsequently improved accuracy for the integrated system. Comparisons of the standard deviation values of the computed positions, velocities, and attitude angles, as well as the double-differenced residuals show that the addition of pseudolites has improved the accuracy of

the GPS/INS system. Therefore, the deployment of the pseudolite(s), including the number and their location, should be carefully considered with the aid of a geometric simulation process. Moreover, Figures 3-11 and 3-12 show that the quality of results can be significantly improved with the inclusion of only one pseudolite. In contrast, with the case of position and velocity, the improvement of attitude accuracy is more modest because the accuracy of the attitude components in the INS is strongly dependent on the gyroscope performance.

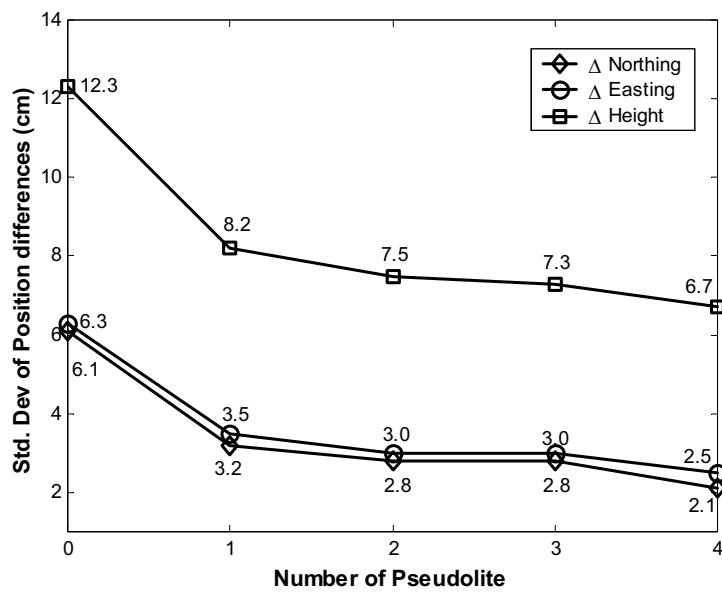


Figure 3-11 Standard deviation of position differences in the GPS/PL/INS system as a function of the number of pseudolites

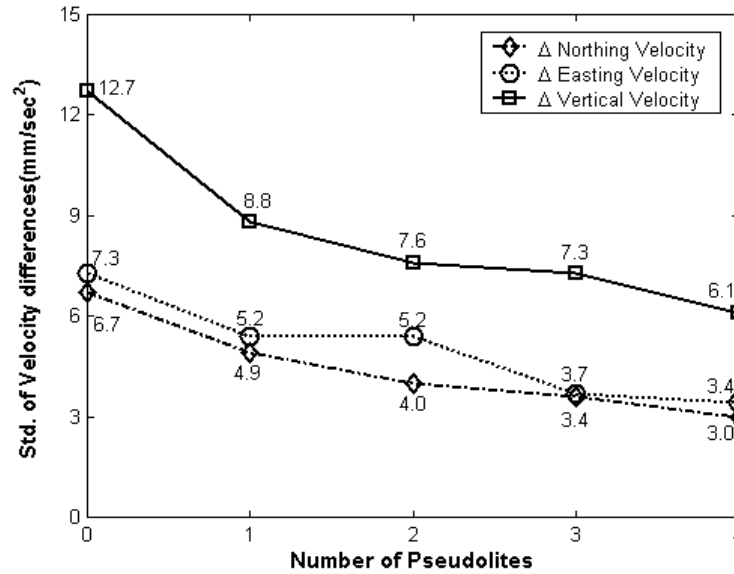


Figure 3-12 Standard deviation of velocity differences in the GPS/PL/INS system as a function of the number of pseudolites

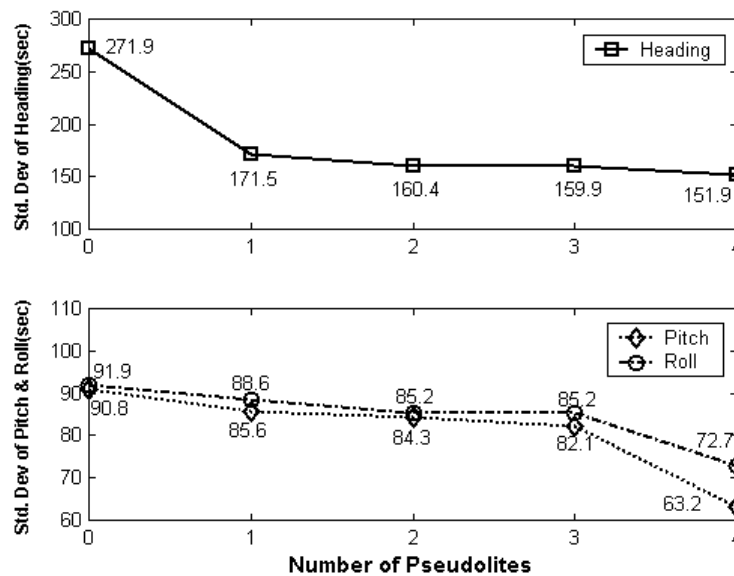


Figure 3-13 Standard deviation of attitude angle differences in the GPS/PL/INS system as a function of the number of pseudolites

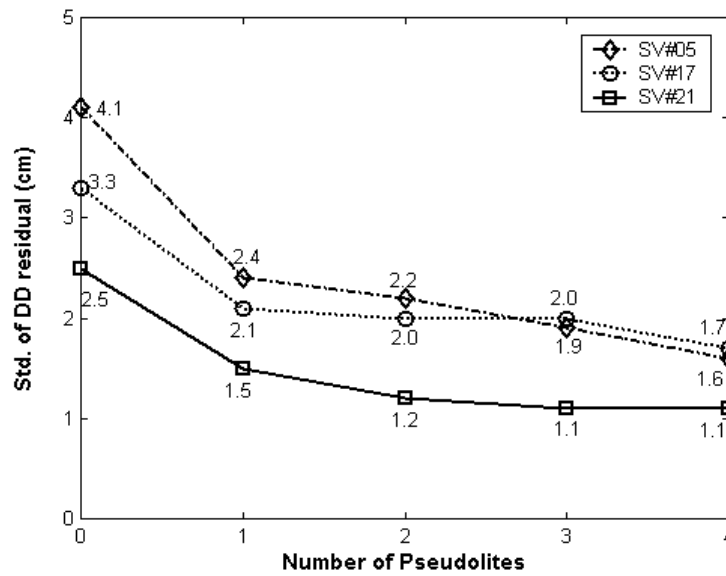


Figure 3-14 Standard deviation of DD residuals of the highest satellites in the GPS/PL/INS system as a function of the number of pseudolites

### 3.5.3 Adverse Operational Environment

For this test, five satellite and three pseudolite measurements were generated. Signal blockages from satellites 5, 17, and 21 were introduced in order to simulate a harsh operational environment. The difference between coordinates of the reference trajectory and those obtained by the system are presented in Figure 3-15. It is expected that the Kalman filter update will not be of high quality due to insufficient external measurement (only one GPS DD measurement) in the case of the GPS/INS system. Consequently the inappropriate filter update results in a significant position error increase, as shown in the upper graph of Figure 3-15. In contrast, the lower graph in Figure 3-15 gives almost identical results with/without the blockages because four DD measurements were used in the filter update (using the additional measurements of the three pseudolites). This means that the additional pseudolite signals can play a significant role in maintaining stable system accuracy, especially in harsh operational environments such as urban canyons and on construction sites.

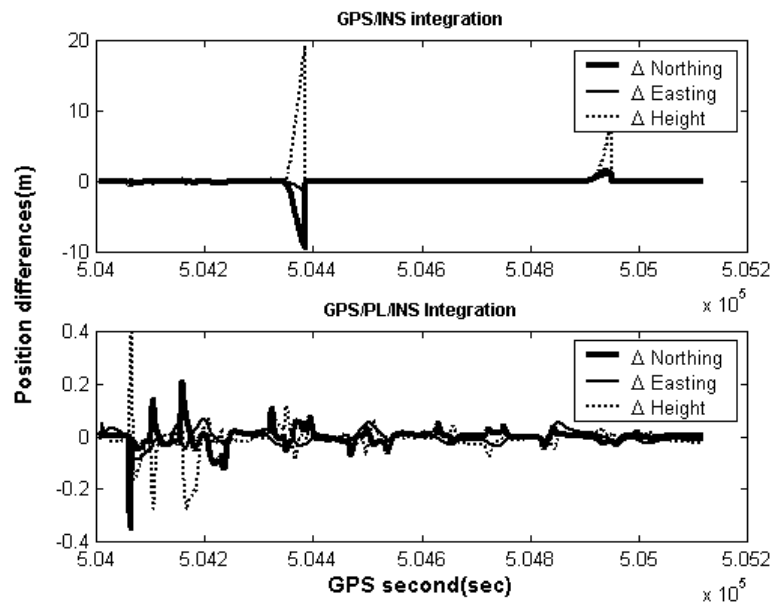


Figure 3-15 Comparison of positioning accuracy between GPS/INS and GPS/PL/INS under adverse operational environment

### 3.5.4 Pseudolite/INS Integration for Indoor Applications

This test involves the 'harshest' satellite-based positioning environment, where GPS signals from satellites are unavailable, as in the case of indoor positioning. As shown in Figure 3-1, the INS error increases without external calibration. This test is focused on whether pseudolite signals can replace those of satellites in the indoor case.

The test assumed five pseudolites in an integrated Pseudolite/INS configuration as shown in Figure 3-10. To evaluate the filter performance, Figure 3-16 depicts the RMS values of position, velocity, and attitude angle estimation derived from the covariance matrix. The estimated values are several centimetres for the position, better than 0.003m/sec for the velocity, and around 5 and 1 arc-minute for the heading, pitch & roll, respectively. These values demonstrate that pseudolite measurements have successfully replaced those from satellites in the filter update period. In addition, Figures 3-17 and 3-18 show the position differences and carrier phase double-differenced residuals computed by INS prediction. Again, these results indicate that an integrated Pseudolite/INS system with double-differenced carrier phase measurements is able to

meet centimetre-level accuracy positioning as long as the pseudolite signals are continuously tracked.

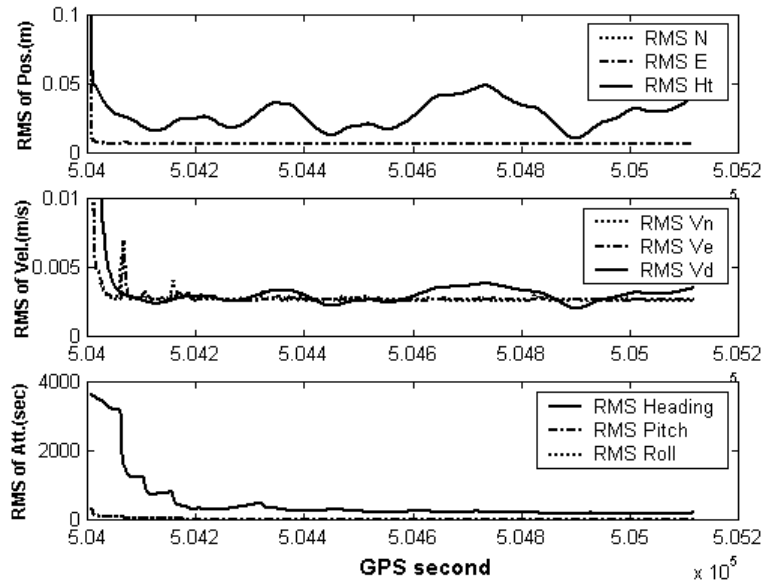


Figure 3-16 RMS errors for Kalman filter estimation (PL/INS)

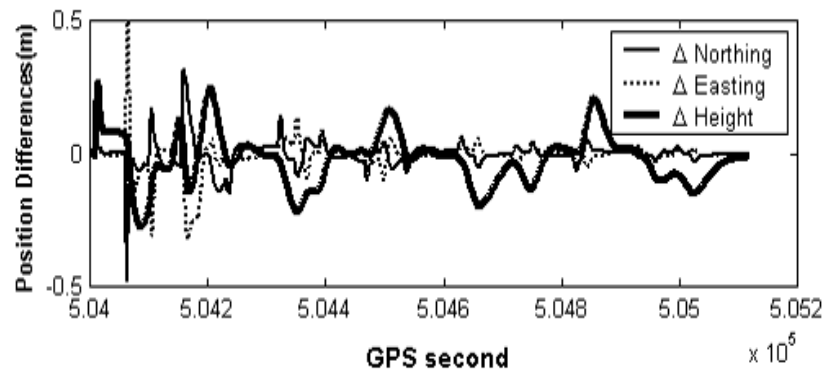


Figure 3-17 Positioning accuracy of PL/INS

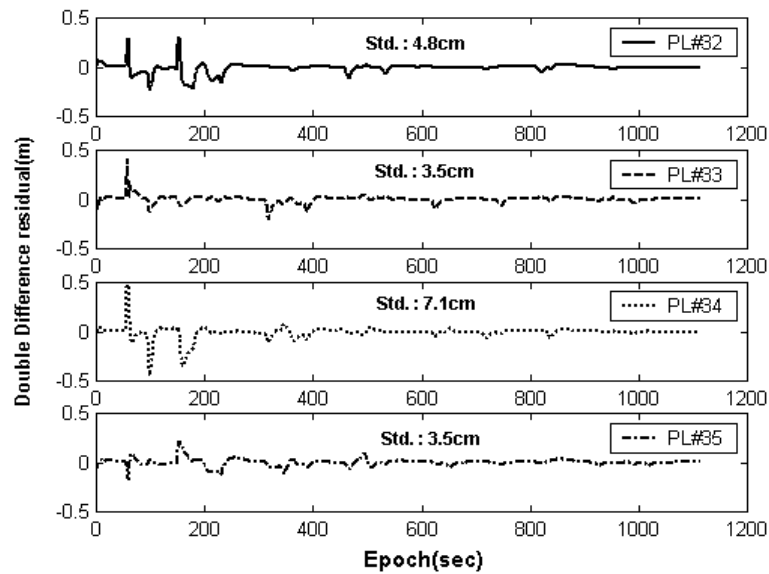


Figure 3-18 DD residual differences of PLs computed by INS predicted positions

### 3.6 Experiments and Analysis

To investigate the effect of using additional pseudolite signals in the final navigation solution, kinematic experiment was carried out in UNSW campus on 26<sup>th</sup> June 2002. The system consisted of NovAtel Millennium GPS receiver, IntegriNautics IN200 pseudolite, and Boeing MIGITS strapdown INS. Two pseudolite signal transmitters (PL#12 and PL#32 were assigned) were used in the test. GPS data were collected at 1Hz data rate, whereas those of the INS were at 100Hz data rate. Both the GPS rover receiver and INS were installed on an electric vehicle. The data were collected over a duration of thirteen minutes, including a 3.5 minute period in the static mode. During the experiment, an average of 6 visible satellites were tracked (with masking angle of 15°). The AIMS<sup>TM</sup> navigation-processing engine was modified for single-frequency receiver and tactical-grade INS as mentioned in Chapter 2. The software was further modified to process additional pseudolite observations. The following modifications were made:



- 1) Implementation of user-defined values for the pseudolite coordinates, and measurement variances,
- 2) Disabling of the ionospheric delay correction calculation for the pseudolite observations, and modification of pseudolite tropospheric delay correction calculation.

With the collected measurement set, two types of tests were performed for different operational environments, through a manipulation of the GPS measurements.

### **3.6.1 Benign Operational Environment**

This test was carried out with five satellite and two pseudolite transmitters in order to investigate the pseudolite signal contribution to the integrated system. To this end, a comparison between GPS/INS and GPS/Pseudolite/INS results was made with respect to position, velocity, and attitude results (see Figures 3-19 to 3-24). As mentioned previously, the inclusion of the pseudolite measurements improves the precision for three-dimensional coordinates, and in particular the height component. It is noted from Figure 3-19 that the vertical coordinate differences between the two types of solutions are larger than those of the horizontal components. In addition, Figures 3-20 and 3-21 show the double-differenced residuals for the four satellite pairs computed using the INS-predicted coordinates. It can be concluded that the position component accuracy obtained from the GPS/Pseudolite/INS system is at the few centimetre-level.

Figures 3-22 to 3-24 show the Root-Mean-Square (RMS) errors in the position, velocity, and attitude components, indicating the pseudolite contribution to the Kalman filter estimation. The values were obtained from the diagonal components of the covariance matrix. Comparing the results of GPS/INS with the GPS/Pseudolite/INS solution, a few millimetres to one centimetre in position accuracy and a few mm/second-level velocity accuracy improvement is observed in Figures 3-22 and 3-23. On the other hand, it is noted from Figure 3-24 that the accuracy improvement of 5-10 arc-second for pitch and roll, as well approximately 100 arc-second for heading can be achieved.

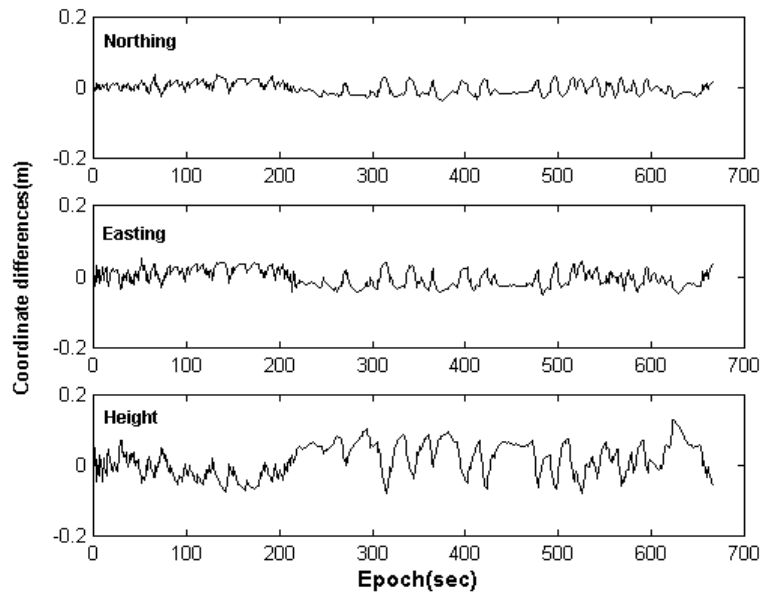


Figure 3-19 Coordinate differences in GPS/INS system with/without two pseudolite signals

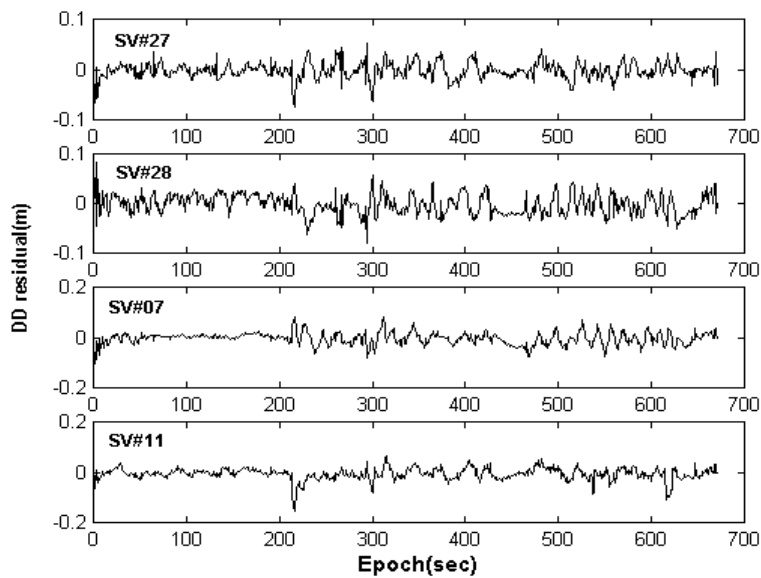


Figure 3-20 DD residuals in four satellites pairs in the GPS/INS case

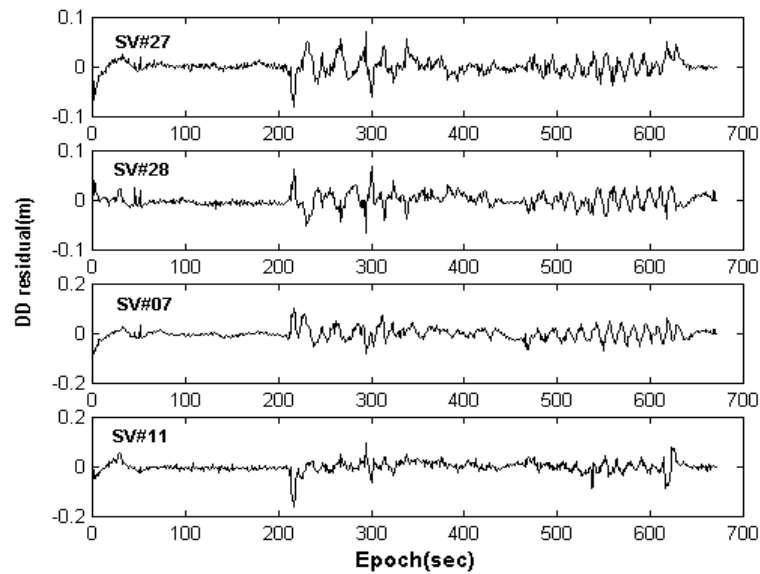


Figure 3-21 DD residuals in four satellites pairs in the GPS/PL/INS case.

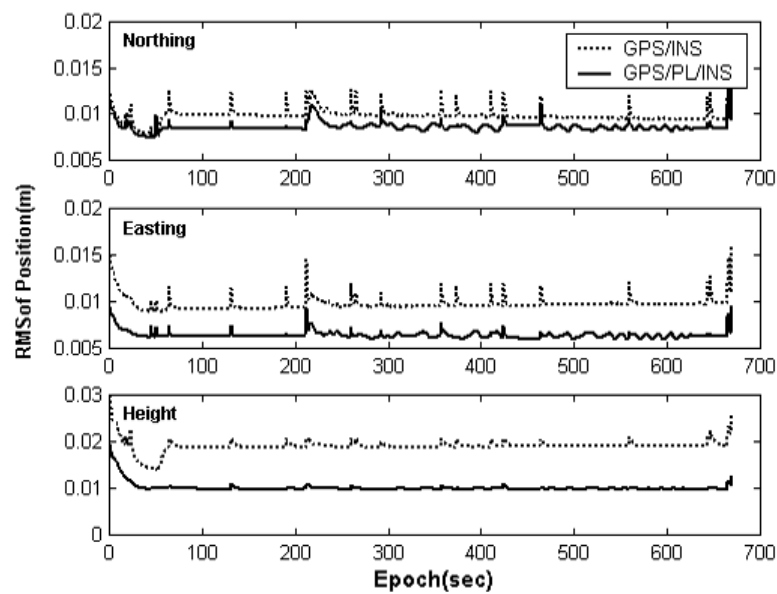


Figure 3-22 RMS value changes in position component

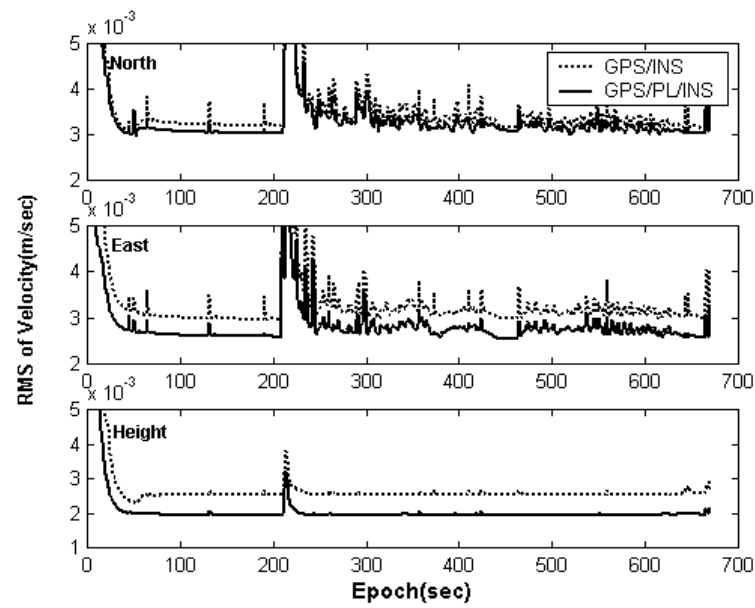


Figure 3-23 RMS value changes in velocity component

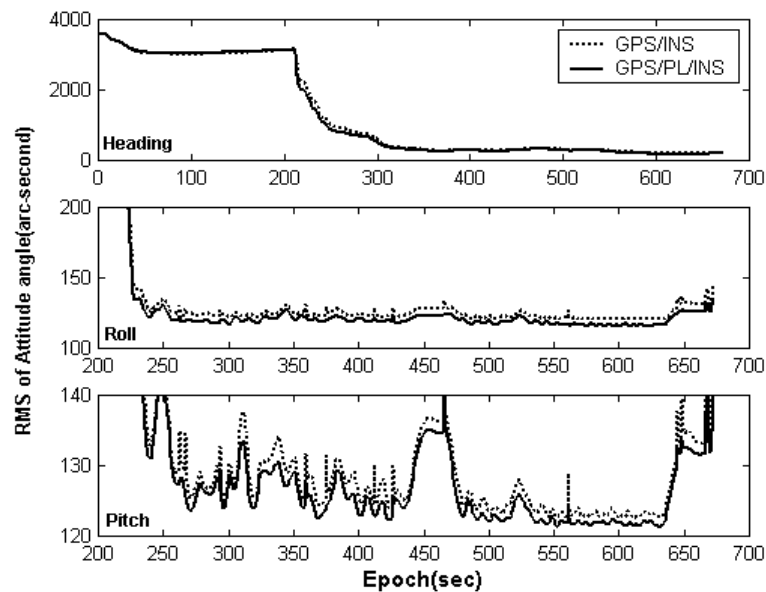


Figure 3-24 RMS value changes in attitude component

### 3.6.2 Adverse Operational Conditions

The test described above demonstrated that the inclusion of two pseudolite transmitters augments GPS/INS solutions. However the benefit of using pseudolites is obtained in the case of adverse operational conditions, where the number and geometry of the visible GPS satellites is insufficient for updating the integration filter of a GPS/INS system. It should be mentioned that typically more than five satellite measurements are necessary to fix integer ambiguities by means of OTF searching methods. To investigate the pseudolite measurement contribution to an integrated system in such an environment, measurements to three GPS satellites were selected for data processing (even though six satellites were visible). Two pseudolites were included in data processing. Figure 3-25 illustrates the geometry of the satellites and pseudolites.

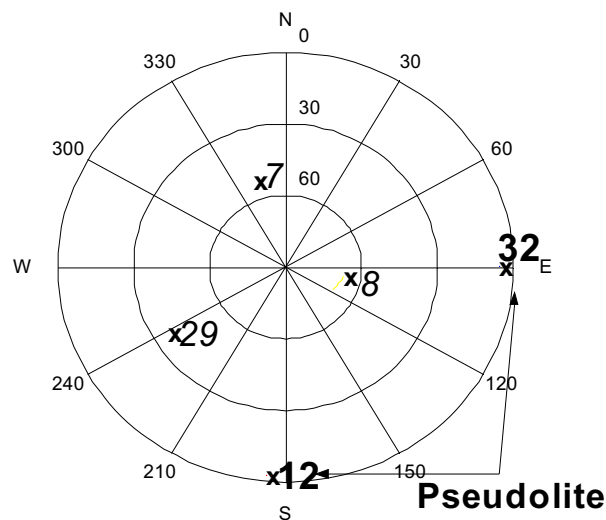


Figure 3-25 Sky view of satellite and pseudolite distribution

In this test (with three GPS measurements and two pseudolite measurements per epoch) ambiguities could be successfully resolved within a few seconds. In addition, another contribution of pseudolites for ambiguity resolution is the reduction in ambiguity search time because in the kinematic mode the line-of-sight vector between epochs changes by a large angle, which results in a well-conditioned matrix for ambiguity parameters. The processed results were compared with the ones obtained by the first test, which used

five satellites and two pseudolites, as shown in Figure 3-26. The results indicate that there is no significant system degradation even if only three measurements from the satellites were used in the processing. This means that the pseudolite measurements can indeed substitute for satellite measurements in a GPS/INS system when the number and geometric quality of the GPS satellites is insufficient.

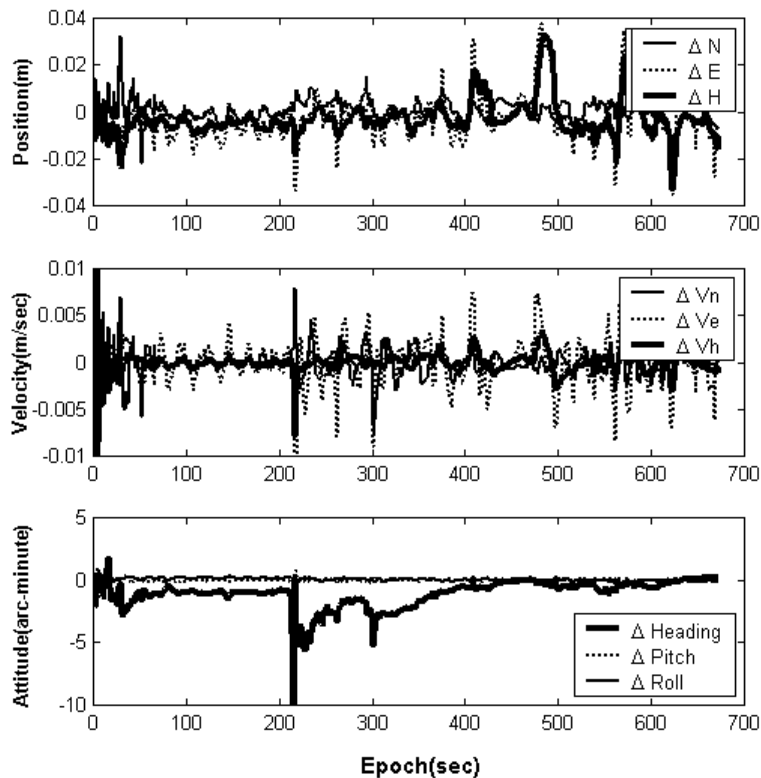


Figure 3-26 Navigation solution comparison with the first test (GPS/PL/INS)

### 3.7 Concluding Remarks

In this chapter, an integrated GPS/Pseudolite/INS system for high precision kinematic positioning and navigation has been proposed, with a view to improving signal availability, solution reliability, and accuracy. Emphasis was given to the discussion on issues of pseudolite double-differenced measurements modelling. A series of simulation studies and field experiments were conducted to investigate the effect of employing additional pseudolite observables in the system performance.

Geometry analyses has shown that appropriately located pseudolites could strengthen the GPS satellite geometry and signal availability, so that a large impact on the reliabilities and precision could be achieved, especially in the vertical component. The best pseudolite location(s) at a certain time depends on the satellite positions and is certainly not continuously the best since satellites are in motion.

It has been found from the first test with the simulated measurements that the more pseudolites used, the more accurate the navigation solutions (position, velocity, and attitude). However, more than three pseudolites used in the GPS/INS system have marginally improved solution accuracy. The second simulation test results demonstrated that pseudolite signals have successfully replaced those of satellites in the Kalman filter update. This is useful for indoor applications.

The field experiment has proved that the two pseudolites employed improved the precision of positioning, in particular the vertical component, and other parameters in the filter. The test under harsh GPS operational condition has shown that two pseudolite transmitter deployments made centimetre-level accuracy positioning possible, even if there are insufficient GPS signals available.

**CHAPTER 4**

**ANALYSIS OF IMPACT OF PSEUDOLITE LOCATION ERRORS  
ON POSITIONING**

---

---

### **4.1 Introduction**

From the positioning point of view, a pseudolite can be viewed as a ‘satellite-on-the-ground’ as it transmits GPS-like ranging signals. However, the space-borne satellites and the ground-based pseudolites do have different implications to some aspects of positioning operations as discussed in §3.3. One of them is the *satellite orbit* (or *pseudolite location*) *error*. Such an error is negligible for the satellites, but could be significant in the case of pseudolites (Hein et al., 1997; Morley and Lachapelle, 1997). The reason for this is that the pseudolites are much closer to user receivers than the satellites are.

In this chapter, the impact of pseudolite location errors in such pseudolite-augmented positioning systems will be investigated. Theoretical and numerical analyses will be conducted to identify some new characteristics of the pseudolite location errors on positioning.

### **4.2 Theoretical Analysis**

The satellite orbit error is one of the major error sources in GPS positioning as presented in §1.4. In GPS relative positioning applications, the impact of the satellite orbit error on baseline length can be approximately appraised using the following ‘rule of thumb’ formula (Bauersima, 1983; Wells et al., 1987):

$$\frac{db}{b} = \frac{dr}{r} \tag{4.1}$$

where,



$db$ :	the baseline error
$dr$ :	the satellite orbital error
$b$ :	the baseline length
$r$ :	the distance between satellites and users

Equation (4.1) indicates that satellite orbit error would have negligible impact on the baseline solutions in the application of short-range GPS relative positioning. However, as pseudolites are close to users, careful analysis is required.

Assuming that  $dx$ ,  $dy$  and  $dz$  are the errors in the coordinates of pseudolite transmitter antenna  $(x, y, z)$ , and  $(0,0,0)$  and  $(0,b,h)$  are three-dimensional coordinates of station  $A$  and  $B$  respectively, the impact of these errors on the single-differenced (SD) measurements between stations  $A$  and  $B$  can be expressed as (Wang et al., 2000; Wang and Lee, 2002):

$$dS_{AB} = x \left( \frac{1}{S_A} - \frac{1}{S_B} \right) \cdot dx + \left( \frac{y}{S_A} - \frac{y-b}{S_B} \right) \cdot dy + \left( \frac{z}{S_A} - \frac{z-h}{S_B} \right) \cdot dz \quad (4.2)$$

with

$$S_A = \sqrt{x^2 + y^2 + z^2} \quad (4.3a)$$

$$S_B = \sqrt{x^2 + (y-b)^2 + (z-h)^2} \quad (4.3b)$$

Above Equations (4.2) and (4.3) show that the pseudolite location errors are geometry-dependent. For example, assuming that distances from the transmitter to the two receivers are the same (i.e.,  $S_A = S_B = S$ ), Equation (4.2) can be rewritten:

$$dS_{AB} = \frac{b}{S} \cdot dy + \frac{h}{S} \cdot dz \quad (4.4)$$

In this situation, whilst the term  $dx$  causes no model errors, the impacts of term  $dy$  and  $dz$  on the measurement model are inversely proportional to  $S$  (the separation between the transmitter and the user) and are proportional to  $b$  (horizontal baseline distance) and  $h$  (the baseline height difference). If the baseline height difference is equal to zero (i.e.,  $h = 0$ ), then  $dS_{AB}(z)$  becomes zero as well. In such an event the ‘rule of thumb’ in Equation (4.1) is identical to Equation (4.4). Therefore, Equation (4.1) is a special case of Equation (4.2), which provides a general tool for analysing the impact of orbit errors on the SD measurement model.

In some situations, the geometric relationship between the pseudolite transmitter and the user is quite different from that between the satellite transmitter and the user. Hein et al. (1997) and Morley & Lachapelle (1997) discussed two special set-ups for the pseudolite and user, as shown in Figure 4-1. These set-ups can be easily analysed using Equation (4.2).

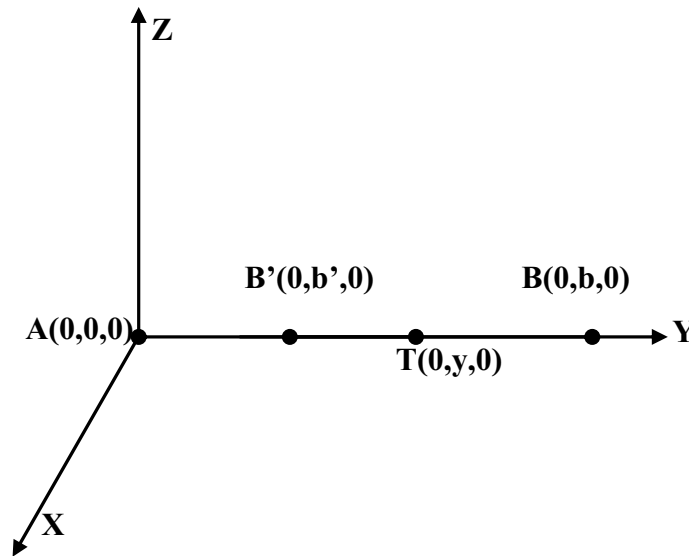


Figure 4-1 Special set-ups of the pseudolite and baselines

In the case of baseline  $AB$ ,  $y = S_A$  and  $S_A + S_B = b$ . Then, from Equation (4.2)  $dS_{AB} = 2 \cdot dy$ , indicating that the single-differencing procedure doubles the size of the pseudolite location error in the measurements. However, for baseline  $AB'$ , since  $S_A - S_{B'} = b'$ ,  $dS_{AB'} = 0 \cdot dy$ , the location error is cancelled out in differencing.

The above theoretical analysis provides an insight into the pseudolite location error issue. These formulas can be used in the following numerical analysis, leading to a derivation of the characteristics of the pseudolite location errors and their impact.

### 4.3 Numerical Analysis

To investigate the impact of pseudolite location errors on single-differenced (SD) measurements, a numerical analysis was conducted with the Equations (4.2) and (4.3). Figures 4-2 and 4-3 illustrate the effect of a 5.0cm pseudolite location error on SD measurements at two user locations:  $B$  (*Worst*) and  $B'$  (*Best*), as shown in Figure 4-1. Both figures show that the effects of the pseudolite location errors vary with the elevation and azimuth of the mobile pseudolite ( $T$ ). In the worst case, shown in Figure 4-2 for user location at  $B$ , the influence of the pseudolite location error on the SD measurements can reach up to 12.5cm, more than twice the original pseudolite location error. In contrast, Figure 4-3 shows that the influence of pseudolite location error can be significantly reduced when the pseudolite is located in the best site. Therefore, the conclusion drawn from these results is that the impact of pseudolite location errors in the SD measurements can be either expanded or contracted depending on the selection of the transmitter location.

To investigate in more detail how the pseudolite location error affects the SD measurements according to its horizontal location, another numerical analysis was carried out as a function of pseudolite's azimuth with respect to both the 'worst' and 'best' cases, as shown in Figure 4-1. The results are presented in Figures 4-4 and 4-5.  $S_a$  and  $S_b$  in these figures are the distances between pseudolite-reference receiver and pseudolite-mobile receiver, respectively. Figure 4-4 shows that the largest errors obtained are approximately 12cm when the azimuth is 45 degrees, while they are dramatically reduced to almost zero when the pseudolite is situated around 180 and 270 degrees. It can be seen from Figure 4-5 that the effect of the pseudolite location error is minimised at 45, 90, 225, and 270 degrees. Comparing top graphs in these two figures, the best case always yields smaller SD measurement errors than those of the worst case. In addition, Figure 4-5 shows the bigger the  $S_a - S_b$ , the smaller the errors.

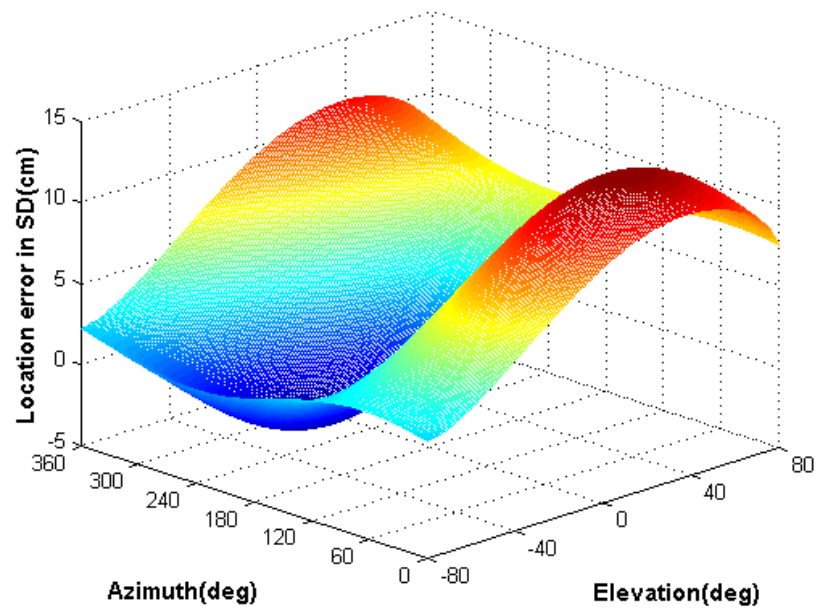


Figure 4-2 Influence of 5cm pseudolites location bias on the user location B (Worst)

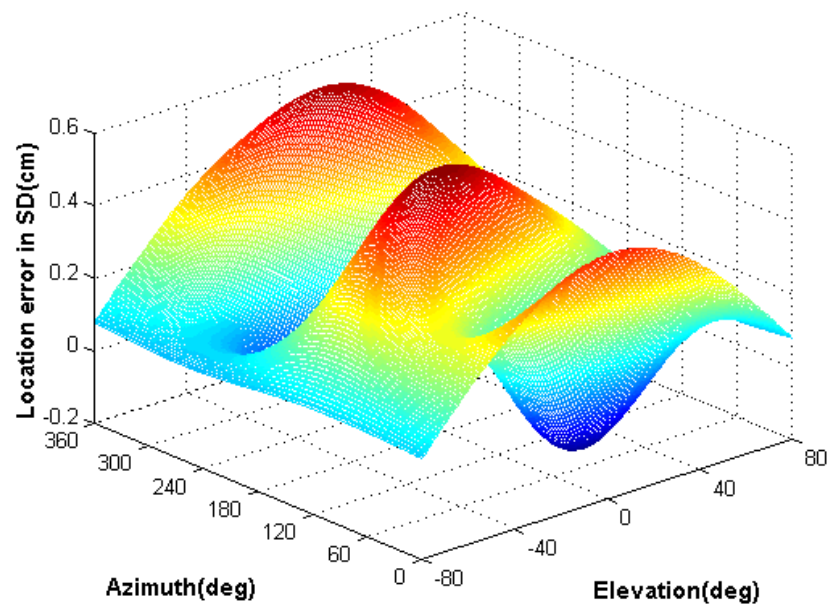


Figure 4-3 Influence of 5cm pseudolite location bias on the location B' (Best)

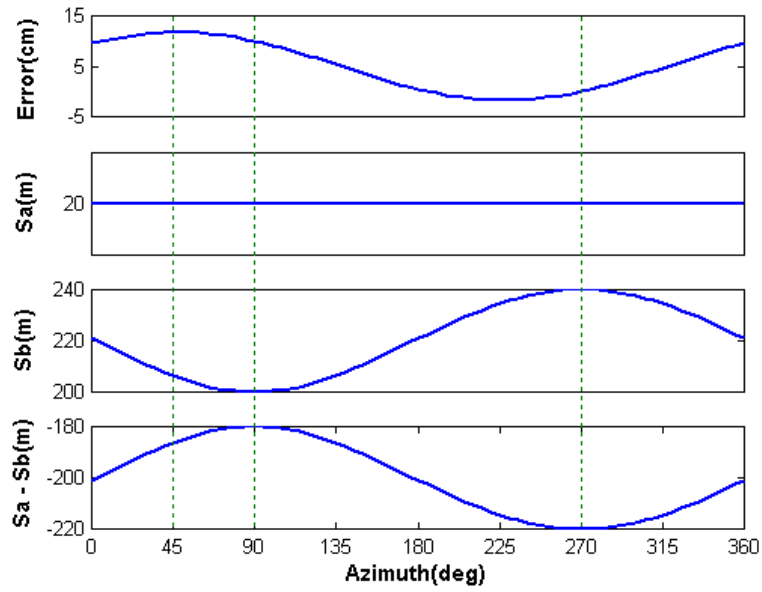


Figure 4-4 Errors in SD varying azimuth at the Location B (Worst)

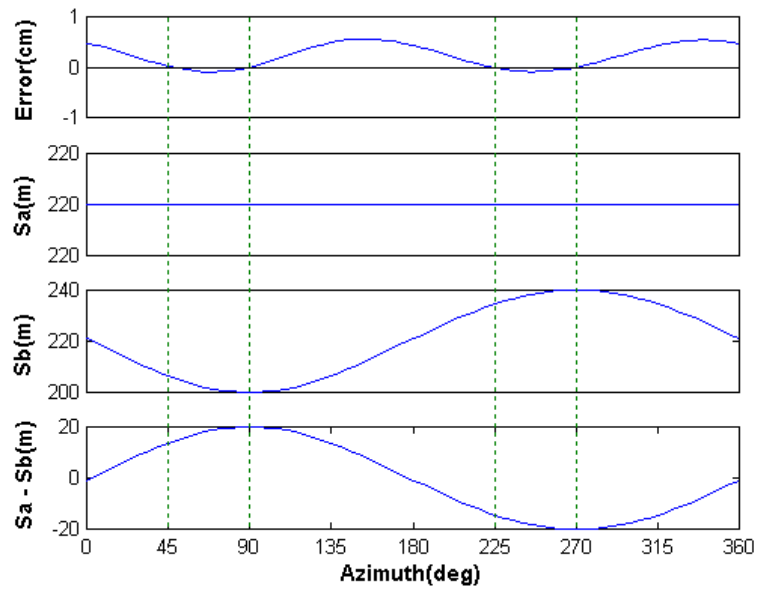


Figure 4-5 Errors in SD varying azimuth at the Location B' (Best)

#### 4.4 Impacts of Pseudolite Location Errors on Positioning

In addition to the numerical analysis with the derived formulas, a series of tests with simulated measurements were carried out to examine the effects of pseudolite location errors in integrated GPS/pseudolite positioning solutions, with respect to different receiver dynamics and pseudolite locations.

In the following tests, the GPS/pseudolites simulation software developed in Chapter 3 was used to generate raw GPS and pseudolite observations. Measurements for the stationary and moving receiver were generated for a period of 600 and 1064 seconds, respectively. All the simulated measurements were processed using the SNAP kinematic GPS/pseudolite processing software.

##### 4.4.1 Static Positioning Case

The objective of the first analysis was to investigate how the pseudolite location errors influence the final solutions of an integrated GPS/pseudolite positioning solution (based on carrier phase measurements) in static applications. The comparison was made as a function of pseudolite horizontal location, just as in the previous theoretical and numerical analyses, namely for the *best* and *worst* location. For this simulation, GPS measurements from five satellites and one pseudolite were used in the solution. To evaluate the accuracy of GPS/pseudolite positioning solutions, a comparison between true position used for measurement generation and the resulting coordinates of the mobile receiver estimated from the data processing was made.

Figure 4-6 shows the RDOP values for both the best and worst scenarios. Although these values are similar in both cases, the positioning results are quite different due to the impact of pseudolite location errors (see Figure 4-7), indicating that the induced 1cm pseudolite location error leads to around 1 cm and 1.5 cm errors in horizontal and vertical components of the positioning solutions, respectively. As the reference and mobile receiver are both stationary, the pseudolite location error causes invariant biases in the positioning solution, as depicted in Figure 4-7. On the other hand, the results

from the best pseudolite location case illustrate that there is no significant positioning accuracy degradation, even if a pseudolite location error of 5cm is considered (see Figure 4-8). Hence, the results confirm that the selection of optimal pseudolite location is crucial in an integrated GPS/pseudolite positioning, as this is not only to ensure a strong positioning geometry, but also to minimise the impact of pseudolite location errors.

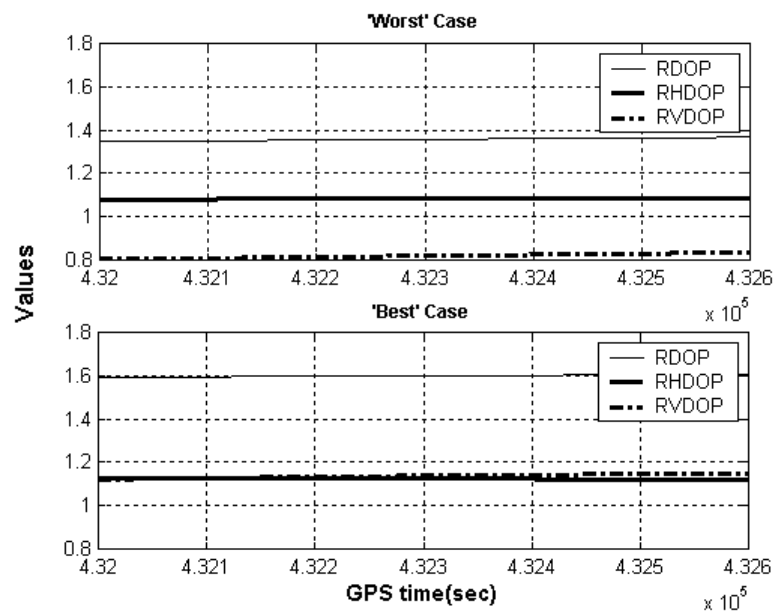


Figure 4-6 DOP changes in the case of stationary receiver

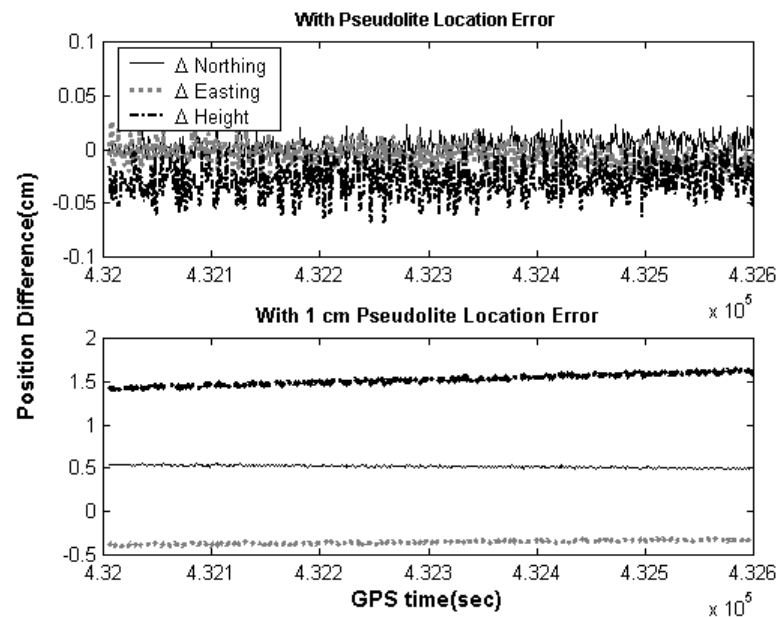


Figure 4-7 GPS/pseudolite positioning accuracy with/without the pseudolite location errors in the worst case

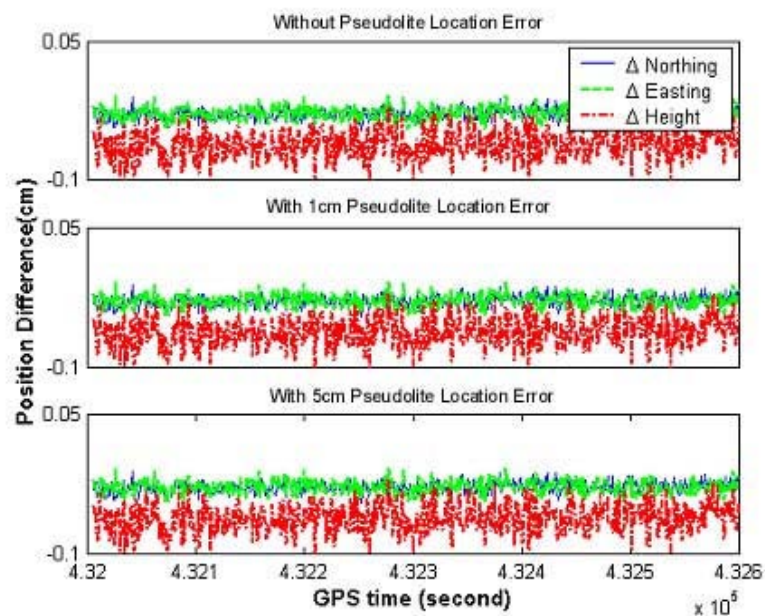


Figure 4-8 GPS/pseudolite positioning accuracy with/without the pseudolite location errors in the best case



#### 4.4.2 Kinematic Positioning Case

From the previous simulation tests, the pseudolite location errors resulted in a constant bias in the final positioning solution. However, if the receiver were moving, the results would become different. In order to perform the tests in the kinematic environment, a mobile receiver trajectory was generated as shown in Figure 4-9. Again, the measurements from one pseudolite and five satellites were included in the data processing, and a comparison between the reference trajectory used for the measurement simulation and the resulting trajectory from the data processing was made to evaluate the positioning accuracy. Moreover, it should be mentioned that a pseudolite location error of 2cm in each of three-dimensional coordinate components was considered in the analysis.

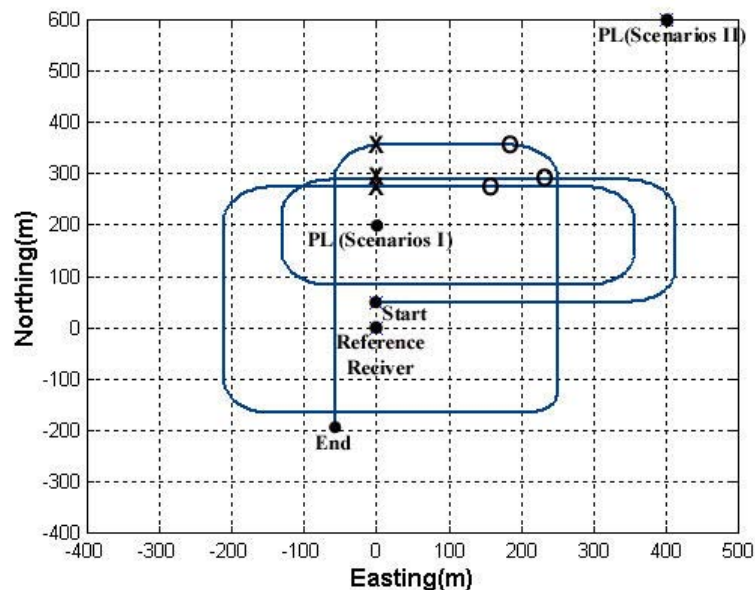


Figure 4-9 Mobile receiver trajectory and pseudolite locations in the test

Two pseudolite locations, Scenarios I & II in Figure 4-9, were considered in the tests. In the case of scenario I, the mobile receiver trajectory is located between the reference receiver and the pseudolite, whereas the mobile receiver is mainly located on the left side of the pseudolites in the case of scenario II. Figure 4-10 illustrates the satellite/pseudolite geometry changes during the test for both scenarios. Note that the

bold dashed-line in both the graphs represents the double-differenced measurement errors caused by the simulated pseudolite location errors.

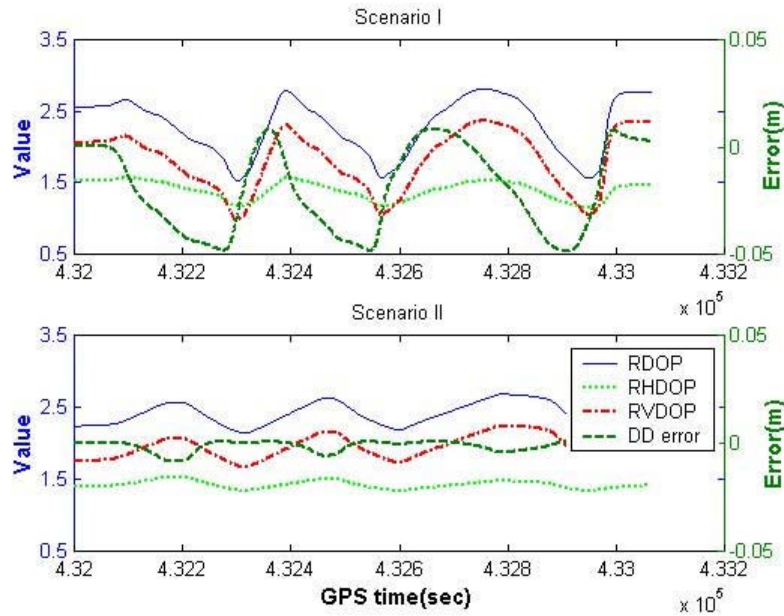


Figure 4-10 Geometry changes in both scenarios I & II

Figure 4-11 depicts the results from GPS/pseudolite positioning based on scenario I (i.e., ‘worst case’). Similar to the results presented in Figure 4-4, the lower graph in Figure 4-11 shows that DD measurement errors reach up to twice the size of the simulated pseudolite location errors (e.g., 3.8, 3.9 and 4.1cm, respectively), when the two receivers and pseudolites are almost collinearly located (see ‘x’ marks in Figure 4-9). In addition, as presented in Figure 4-3, the lower graph also indicates that the largest DD errors occur when angles between reference to mobile receiver and reference to pseudolite vector are around 45 degrees (see ‘o’ marks in Figure 4-9). Hence, it can be recognised that these results are identical with those obtained by the preceding theoretical and numerical analyses based on Equation (4-2).

Figure 4-12 illustrates the results with the best pseudolite location (see Figure 4-9), indicating that there is no significant accuracy degradation even if a pseudolite location error of 2cm was considered. Therefore, it should be emphasised that, for kinematic applications, either the pseudolites location is precisely determined using GPS surveying, total station or other traditional surveying techniques, or optimal pseudolite

locations must be selected to minimise impact of the pseudolite location errors on positioning.

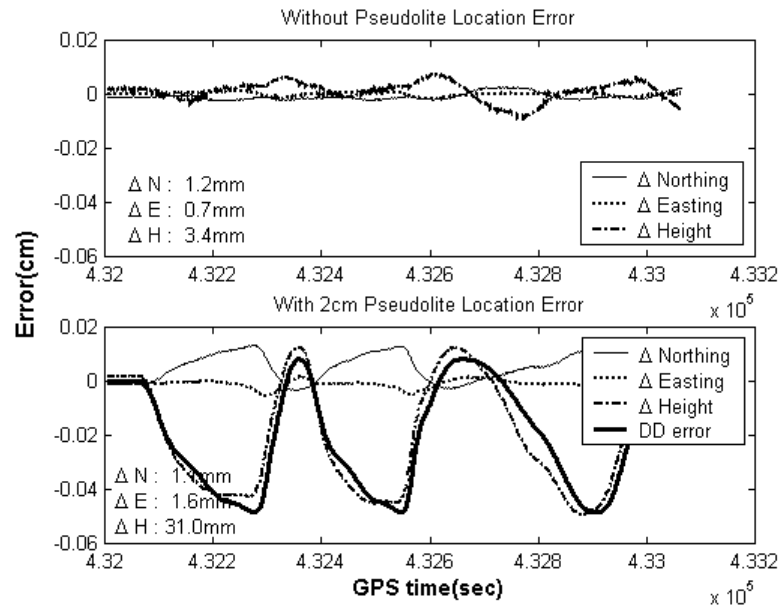


Figure 4-11 Change of GPS/pseudolite positioning and DD errors (Scenario I)

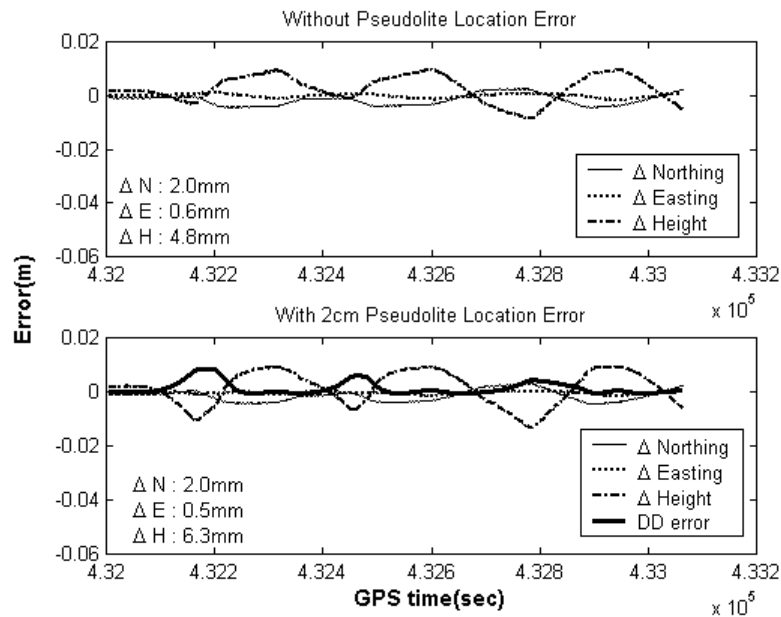


Figure 4-12 Change of GPS/pseudolite positioning and DD errors (Scenario II)

#### **4.5 Concluding Remarks**

The pseudolite location error is one major source that leads to biased solutions of satellite/pseudolite based positioning. In this chapter, the impact of pseudolite location errors in positioning has been theoretically and numerically analysed. Furthermore, a series of tests with simulated GPS/pseudolites observations have been carried out with respect to static and kinematic environments.

The analysis results have indicated that special attention should be given to the pseudolite location error in order to ensure precise positioning solutions. In particular, the tests with simulated GPS/pseudolite observations have shown that the optimal locations of pseudolites can minimise the impact of pseudolite location errors on measurement models and on the final positioning solutions. Hence, for the development of a GPS augmentation system with pseudolites, it is strongly recommended to carefully select the pseudolite locations, not only to maximise the satellite/pseudolite geometry constellation but also to minimise their error effects in positioning.

Finally, due to the consistent results between the numerical analyses and simulation tests, it is also possible to conclude that Equation (4.2) can be efficiently used for a thorough analysis of the potential effects of pseudolite location (orbit) errors for any specific application.

**CHAPTER 5**

**INTEGER AMBIGUITY RESOLUTION PROCEDURE AIDED  
BY PSEUDOLITE AND INS**

---

---

### **5.1 Introduction**

Ambiguity resolution (AR) is the most crucial procedure to achieve the goal of high accuracy carrier phase-based navigation and positioning. This process consists of two main steps: ‘*ambiguity estimation*’ and ‘*ambiguity validation*’. Whilst the former involves least squares estimates of the integer ambiguities, the latter is concerned with the question of whether one is willing to accept the outcomes of the integer least squares solution. An ability to resolve the integer ambiguities is determined by the float ambiguity precision and correlation. The float ambiguities unfortunately have poor precision and high correlation, making the AR cumbersome. This is attributed to the fact that the low precision and high correlation of the float ambiguities makes the searching space enlarged, elongated, and rotated (Teunissen, 1997). In contrast, the AR becomes easy and trivial if the precision can be somehow improved and/or the correlation can be dwindled. Therefore, it is necessary to note that the shape of ambiguity searching space is dominated by a covariance matrix of the float ambiguities, which contains information regarding the float solution’s precision and correlation. On the other hand, the matrix characteristics can be determined by several facts, for instance the measurement precision, the number of satellites tracked, and observation epoch used, as well as the change over time in the relative receiver-satellite geometry (ibid).

It is well known that AR “on-the-fly” (OTF) for short-range kinematic positioning can be readily accomplished with dual-frequency observations, and under the assumption that the satellite ephemeris error and differential atmospheric delay can be ignored (Han and Rizos, 1997; Teunissen, 19997; Kim and Langly, 2000). However, for the single-frequency case it is still a challenge to resolve the ambiguities rapidly and reliably (Wang et al., 2003b). In this chapter, a new single-frequency ambiguity resolution

procedure is proposed for use within the proposed GPS/Pseudolite/INS system. This procedure uses single-frequency GPS data together with pseudolite and INS measurements. A more realistic stochastic modelling and a statistically rigorous ambiguity validation test scheme are also adopted to enhance the quality of ambiguity resolution. Results from covariance simulations based on the Ambiguity Dilution of Precision (ADOP) factor are presented to examine some effects of the inclusion of pseudolites and INS on the integer ambiguity estimation. The effects of pseudolite multipath in a kinematic environment are discussed, and three approaches that can be used to handle the error sources will be proposed to avoid the potential biases in the estimates of real-valued integer ambiguities – which is critical for achieving reliable ambiguity resolution. Finally, the results from field experiments will be presented to demonstrate the effectiveness of the proposed procedure with respect to different operational conditions.

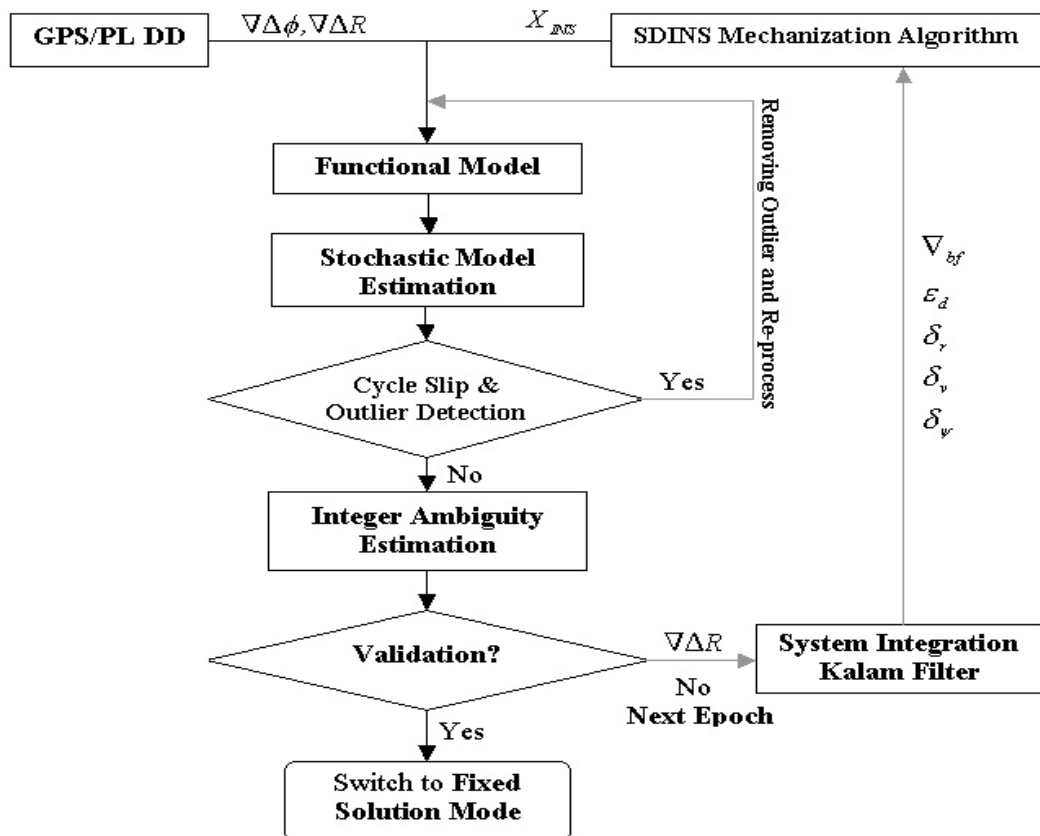


Figure 5-1 The proposed ambiguity resolution procedure

where  $\nabla\Delta\phi$  and  $\nabla\Delta R$  is DD carrier-phases and pseudo-ranges;  $X_{INS}$  is the INS predicted-position;  $\hat{x}_k(+)$  is the estimated filter state vector at  $k^{th}$  epoch (e.g., errors of sensors and navigation solutions)

## 5.2 New Ambiguity Resolution Procedure with Pseudolite and INS

This section describes a proposed approach for integer ambiguity resolution based on double-differenced (DD) GPS/pseudolite carrier phase and pseudo-range measurements from single-frequency receivers, and an Inertial Navigation System (INS). Figure 5-1 outlines the proposed procedure.

### 5.2.1 Measurement Modelling

There are a number of error sources that contaminate GPS measurements, including satellite ephemeris and clock biases, atmospheric delays, multipath, and receiver clock bias, as discussed in Chapter 1. However, for short baseline applications such as those considered in this research (<15km), most of these errors are eliminated or significantly reduced through the use of the double-differencing (DD) methodology. If the pseudolites transmit their ranging signals on the same frequency as GPS satellites, and their location and tropospheric errors are modelled and/or mitigated by appropriate technologies described in Chapters 3 and 4, single-frequency DD carrier phase and pseudo-range observation equations for GPS/pseudolite can be defined as the following based on Equations (2.16), (2.17), (3.1), and (3.2):

$$\nabla\Delta\phi_{GPS/PL} = \frac{1}{\lambda}\nabla\Delta\rho + \nabla\Delta N + \nabla\Delta\varepsilon_\phi \quad (5.1a)$$

$$\nabla\Delta R_{GPS/PL} = \nabla\Delta\rho + \nabla\Delta\varepsilon_R \quad (5.1b)$$

where  $\lambda$  is the wavelength of the L1 GPS/pseudolite carrier phase measurement,  $\nabla\Delta\rho$  is the DD true geometric distances,  $\nabla\Delta N$  is the DD integer ambiguity,  $\nabla\Delta\varepsilon_\phi$  and  $\nabla\Delta\varepsilon_R$  are the remaining measurement noise for DD carrier phase and pseudo-range, respectively.

On the other hand, the INS position solution is obtained from its mechanisation as described in §2.2. Considering the position component, the INS delivers a three-dimensional coordinate at the  $k$ -th epoch:

$$r_k(-) = r_{k-1}(+) + \Delta r \quad (5.2)$$

where  $r_{k-1}(+)$  is the filter-updated position at the  $(k-1)$ -th epoch, and  $\Delta r$  is the position increments obtained from integrating Equation (2.1a) between two consecutive epochs.

Linearisation of the DD GPS/pseudolite observation equations with the INS-predicted antenna positions yields the following expression:

$$L = AX + V \quad (5.3)$$

where  $L$  is the measurement vector,  $A$  is the design matrix, and  $V$  is the residual vector:

$$A = \begin{bmatrix} A_b & \lambda_1 I_{m \times m} \\ A_b & 0_{m \times m} \\ I_{3 \times 3} & 0_{3 \times m} \end{bmatrix} \quad (5.4)$$

$$X = \begin{bmatrix} X_b \\ X_a \end{bmatrix} \quad (5.5)$$

$$L = \begin{bmatrix} \nabla \Delta \phi_{GPS/PL} - \nabla \Delta \rho_0 \\ \nabla \Delta R_{GPS/PL} - \nabla \Delta \rho_0 \\ r_{k-1}(+) + \Delta r - r_0 \end{bmatrix} \quad (5.6)$$

where  $A_b$  is the  $m \times 3$  DD design matrix that contains information on the relative receiver-satellite geometry;  $X_b$  is the 3-vector of the unknown increments of the three-dimensional baseline components, and  $X_a$  is the  $m$ -vector of the real-valued unknown



DD integer ambiguities;  $\nabla\Delta\phi_{GPS/PL}$ ,  $\nabla\Delta R_{GPS/PL}$ , and  $\nabla\Delta\rho_0$  are the  $m$ -vector of the DD GPS/pseudolite carrier phase, pseudo-range measurements, and the DD geometric distance, respectively (computed with respect to an approximate antenna position  $r_0$ ).

A corresponding covariance matrix for the observation equation can be written as:

$$Q_l = \sigma_0^2 \begin{bmatrix} Q_{\nabla\Delta\phi} & 0 & 0 \\ 0 & Q_{\nabla\Delta R} & 0 \\ 0 & 0 & Q_{\Delta r} \end{bmatrix} \quad (5.7)$$

where  $Q_{\nabla\Delta\phi}$  and  $Q_{\nabla\Delta R}$  is the  $m \times m$  cofactor matrix for the DD GPS/pseudolite carrier phase and pseudo-range observations respectively, and  $Q_{\Delta r}$  is the  $3 \times 3$  cofactor matrix for the INS positioning solution, which is obtained from the position component of the covariance matrix of the predicted states (e.g., Equation 2.22).

Stochastic modelling, which determines the values of Equation (5.7), is one of crucial steps for AR.  $Q_{\Delta r}$  matrix can be obtained from the system integration filter (e.g. Equation (2.22)). An on-line stochastic estimation scheme for GPS and pseudolite observations based on post-fit residuals is adopted in this procedure to determine  $Q_{\nabla\Delta\phi}$  and  $Q_{\nabla\Delta R}$ . A realistic covariance matrix for the observations can be estimated based on the residual series from previous epochs as follows (Wang, 1999):

$$Q_{\nabla\Delta\phi, R} = Q_{\hat{V}_{GPS/PL}} + A_{GPS/PL} Q_{\hat{X}} A_{GPS/PL}^T = \frac{1}{N} \sum_{i=1}^N \hat{V}_{k-i} \hat{V}_{k-i}^T + A_{k_{GPS/PL}} Q_{\hat{X}_k} A_{k_{GPS/PL}}^T \quad (5.8)$$

where  $Q_{\hat{V}_{GPS/PL}}$  is the covariance matrix for the residuals of GPS/pseudolite measurements;  $A_{GPS/PL}$  is the design matrix that contains line-of-sight vectors for GPS/pseudolite;  $Q_{\hat{X}}$  is the covariance matrix for the unknown parameters;  $k$  denotes the current epoch;  $N$  is the width of the moving data ‘window’ (ibid).

Special attention should be paid to the selection of the window width. According to *ibid*, an optimal width of the window is in the range of 10-30 epochs with one second sampling rate. One of the main benefits of this approach is that it is not necessary to separately model satellite and pseudolite measurements. Using the estimated covariance matrix for the observations, the precision of the estimation results can be improved, and therefore a better AR performance can be expected.

### 5.2.2 Integer Ambiguity Estimation

The integer ambiguity estimation is performed in two steps: a) real-valued (float) ambiguities are estimated, and b) the best integer ambiguity combination is searched. Based on the least squares principle, the estimates of the unknown parameters  $\hat{X}$  in Equation (5.3) can be obtained:

$$\hat{X} = (A^T P A)^{-1} A^T P L, \quad (5.9)$$

with:

$$Q_{\hat{X}} = (A^T P A)^{-1} = \begin{bmatrix} Q_{\hat{X}_b} & | & Q_{\hat{X}_b \hat{X}_a} \\ \hline Q_{\hat{X}_a \hat{X}_b} & | & Q_{\hat{X}_a} \end{bmatrix} \quad (5.10)$$

where  $\hat{X} = (\hat{X}_b, \hat{X}_a)^T$ ;  $\hat{X}_b$  and  $\hat{X}_a$  is the baseline and the real-valued (float) ambiguity vector;  $Q_{\hat{X}}$  is the cofactor matrix of the estimated unknown parameters  $\hat{X}$ . Furthermore, from Equations (5.3), (5.9) and (5.10), the least squares residuals are obtained as:

$$\hat{V} = L - A\hat{X} = Q_{\hat{V}} P L \quad (5.11)$$

where  $Q_{\hat{v}} = Q - AQ_{\hat{x}}A^T$  is the cofactor matrix of the residuals. With the estimated residual vector  $\hat{V}$  and weight matrix  $P$ , the a *posteriori* variance cofactor can be estimated as:

$$\hat{s}_0^2 = \frac{\Omega_0}{f}, \quad (5.12)$$

where

$$\Omega_0 = V^T P V = L^T P L - L^T P A \hat{X} \quad (5.13)$$

and  $f$  is the degree of freedom.

The unity test of a *posteriori* variance  $s_0^2$  can be used to indicate whether or not the adjustment model is satisfactory and hence *detects* the presence of any gross anomalies. In order to check the fidelity of the stochastic and functional models, unity of a *posteriori* variance  $s_0^2$  is set up as follows with the null hypothesis  $H_0$  and the alternative hypothesis  $H_1$  (Baarda, 1968; Cross, 1983):

$$H_0 : \hat{s}_0^2 = 1 \quad (5.14a)$$

$$H_1 : \hat{s}_0^2 \neq 1 \quad (5.14b)$$

The rejection regions are:

$$s_0^2 > F_{(f, \infty; 1-\alpha/2)} \quad (5.15a)$$

$$s_0^2 < F_{(f, \infty; \alpha/2)} \quad (5.15b)$$

where  $F_{(f,\infty;\alpha/2)}$  and  $F_{(f,\infty;1-\alpha/2)}$  are the lower and upper bounds of the  $1-\alpha$  confidence level for  $F$ -distributed statistic, respectively. If the null hypothesis is rejected by Equation (5.15a), the outlier identification procedure should be applied because the outliers may exist in the observations, such as cycle slips, multipath, biases in INS-predicted positions, or a priori standard deviations of the observations do not reflect the accuracies of these observations. If the null hypothesis is rejected by Equation (5.15b), a check should be made in order to test whether the functional and stochastic model is correct or not.

After estimating the float ambiguities, a search procedure is performed to obtain the integer-valued ambiguities. The Least squares AMBiguity Decorrelation Adjustment (LAMBDA) method (Teunissen, 1993; 1996; Tiberius and de Jonge, 1995) is used for this purpose. The main feature of the method is the decorrelation of the ambiguities via the Z-transformation. If the ambiguity elements  $\hat{X}_a$  are fixed to the integer values  $\tilde{X}_a$  using the searching method, the ambiguity-fixed baseline solution can be obtained:

$$\tilde{X}_b = \hat{X}_b - Q_{\hat{X}_b, \hat{X}_a} Q_{\hat{X}_a}^{-1} (\hat{X}_a - \tilde{X}_a) \quad (5.16)$$

$$Q_{\tilde{X}_b} = Q_{\hat{X}_b} - Q_{\hat{X}_b, \hat{X}_a} Q_{\hat{X}_a}^{-1} Q_{\hat{X}_a, \hat{X}_b} \quad (5.17)$$

and

$$\tilde{\Omega}_0 = \Omega_0 + (\hat{X}_a - \tilde{X}_a)^T Q_{\hat{X}_a}^{-1} (\hat{X}_a - \tilde{X}_a) \quad (5.18)$$

### 5.2.3 Ambiguity Validation

When one or more integer ambiguity combinations are accepted in the process of ambiguity search, the integer ambiguity combination resulting in the minimum quadratic form of the least squares residuals (Equation (5.18)) will be considered as the most likely (best) solution. However, it is crucial to ensure that the most likely integer

ambiguity combination is statistically better than the second best combination as defined by the second minimum quadratic form of the least squares residuals. This is called the '*ambiguity validation test*'.

A recently developed validation test scheme is implemented to overcome the drawback of the traditional method (e.g., *F*-ratio test), for which the probability distribution is unknown. The procedure is based on the ratio (called the *W*-ratio) of the difference between the minimum and second minimum quadratic forms of the least squares residuals and its standard deviation. The *W*-ratio value can be defined as (Wang et al., 1998):

$$W = \frac{d}{\hat{s}_0 \sqrt{Q_d}} \quad (5.19)$$

where

$$d = \tilde{\Omega}_{0(sec\ ond)} - \tilde{\Omega}_{0( first)} \quad (5.20)$$

$$Q_d = \left( \tilde{X}_{a(sec\ ond)} - \tilde{X}_{a( first)} \right)^T Q_{\tilde{X}_a}^{-1} \left( \tilde{X}_{a(sec\ ond)} - \tilde{X}_{a( first)} \right) \quad (5.21)$$

where  $Q_d$  is the cofactor of  $d$ , and  $s_0^2$  is the *a posteriori* variance. In this situation, the *W*-ratio has a Student's *t*-distribution. A critical value for the test statistic is determined based on the given test confidence level and the level of redundancy.

#### 5.2.4 Discussion on the Proposed Approach

In order to discuss the effectiveness of the proposed ambiguity resolution procedure which makes use of pseudolite and INS measurements, a covariance matrix for the estimated float ambiguities obtained using single epoch data is derived as follows (*proof*. See Appendix C):

$$Q_{\hat{x}_a} = \frac{1}{\lambda_1^2} (Q_{\nabla\Delta\phi} + Q_{\hat{r}}) \quad (5.22)$$

with:

$$Q_{\hat{r}} = A Q_{\hat{x}_b} A^T \quad (5.23a)$$

$$Q_{\hat{x}_b} = \left( Q_{\hat{x}_b, \nabla\Delta R}^{-1} + Q_{ins}^{-1} \right)^{-1} \quad (5.23b)$$

where  $Q_{\hat{r}}$  is the covariance matrix for the DD range estimate,  $Q_{\hat{x}_b}$  is the covariance matrix of the (float) baseline solution;  $Q_{\hat{x}_b, \nabla\Delta R}$  denotes the covariance matrix of the carrier phase-only baseline solution.

Equation (5.22) is the covariance matrix of the float ambiguities, indicating the precision and correlation characteristics of the estimated float ambiguities. This matrix is influenced by the covariance matrices of the DD carrier phase measurements ( $Q_{\nabla\Delta\phi}$ ) and the DD range estimates ( $Q_{\hat{r}}$ ). In reality, AR performance is dependent on the covariance matrix of the estimated float ambiguities because it defines the ambiguity searching space and the quality of the real-valued ambiguity estimates (Teunissen, 1997). For instance, the search for the integer ambiguities becomes difficult in the cases where the float ambiguities are less precise, and are highly correlated as the search space becomes elongated. The search is easier when the ambiguities are more precise and less correlated. Therefore, this study aims to improve the covariance matrix of the float ambiguities in terms of its precision and correlation characteristics by improving the precision of the DD range estimates. This is attributed to the fact that the covariance matrix of the float ambiguity estimates is mainly driven by the precision of the DD range estimates.

Now another question arises: ‘How can we improve the precision of the range estimates?’ Equation (5.23) provides a clue to the answer. First of all, an examination of Equation (5.23a) reveals that the covariance matrix for the range estimates is influenced

by the geometry of the GPS/pseudolite constellation, and the covariance matrix for the ambiguity float baseline solution. This means that the less correlated and more precise float ambiguities can be obtained if better geometry is used and/or the baseline solution is improved. In the proposed procedure, the former can be achieved using pseudolite signal(s), as the proper inclusion of pseudolites can enhance the geometry (in that the number of satellites tracked is increased, and the line-of-sight vector between epochs changes significantly). On the other hand, the latter can also be achieved by introducing INS-predicted position observations, due to the fact that Equation (5.23b) implies that the baseline solution becomes more precise when using additional measurements. Hence the use of PL and INS measurements should significantly improve the performance of single-frequency AR process.

### 5.3 Simulation Studies

A series of simulation studies based on Ambiguity Dilution of Precision (ADOP) values, which represents both the precision and the correlation characteristics of the estimated ambiguities (Teunissen, 1997; Teunissen and Odijk, 1997), were carried out to investigate the impact of including INS and pseudolite observations on the AR process. In the analyses, a GPS satellite and pseudolite transmitter constellation was generated using a GNSS simulation tool (see Chapter 3), while the covariance matrix for the INS-predicted positions was obtained by covariance simulation (Farrell and Barth, 1998; Savage, 2000b). Note that the observation precisions ( $1\sigma$ ) of GPS/pseudolite pseudo-range and carrier phase measurements were considered to be 0.3m and 0.005m, respectively. The IMU instrument was considered to be of a ‘tactical-grade’ (gyro drift 5 deg/h and accelerometer bias 500 $\mu$ g).

Figure 5-2 depicts the ADOP changes for a 30 second sequential solution as a function of the number of pseudolites used. Note that the INS-predicted positions are also included in the solutions. As expected, the result reveals that the more pseudolite measurements used, the better the AR performance. It is of interest to note that the ADOP is significantly decreased even if only *one* pseudolite is added to the GPS

constellation. However, if more than three pseudolites are used, this does not improve the ADOP values much further.

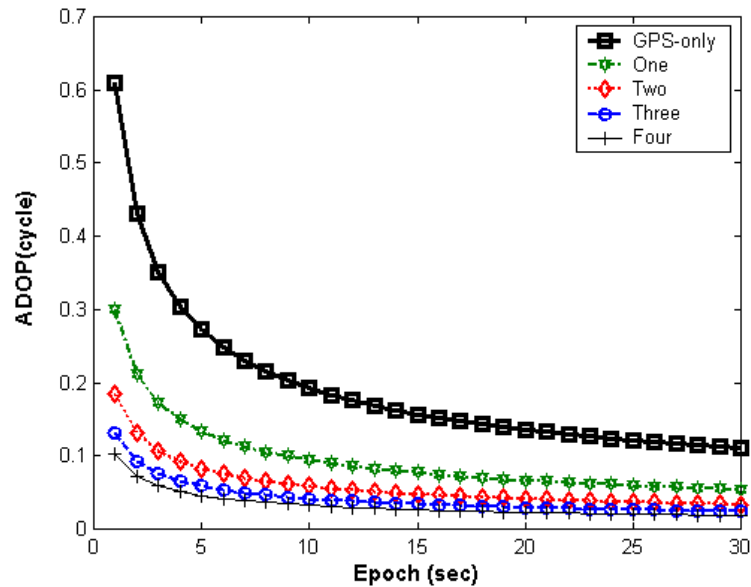


Figure 5-2 Impact of Pseudolites on the ADOP (depending on the number of Pseudolites)

Another benefit associated with the inclusion of pseudolites in the AR process is the relatively rapid change of the line-of-sight vector, which in turn enhances the performance of the AR process. This is because the relative change in *satellite-receiver geometry* plays a crucial role in AR. In order to investigate such an effect, three different user dynamics, defined by the accelerations of  $0.1 \text{ m/sec}^2$ ,  $0.5 \text{ m/sec}^2$ , and  $1.0 \text{ m/sec}^2$  respectively, were considered. It should be noted that the line-of-sight is completely determined by the user's dynamics as the locations of the pseudolites are fixed. Figure 5-3 illustrates the *vehicle dynamics effect* in AR due to the change in relative pseudolites-receiver geometry. Of course, the overall trend indicates that the higher the dynamics, the smaller the ADOP values (hence enhanced AR performance). However the performance cannot be improved over time (increased velocity). For instance, the cases with  $0.5 \text{ m/sec}$  and  $1.0 \text{ m/sec}$  accelerations become identical at the 30-second epochs, but on the other hand the ADOP difference reaches the maximum value around the 10-second epoch. This is because although the velocity is continuously



increasing, the user is getting further away from the pseudolite locations, and thus the relative change of the geometry becomes less.

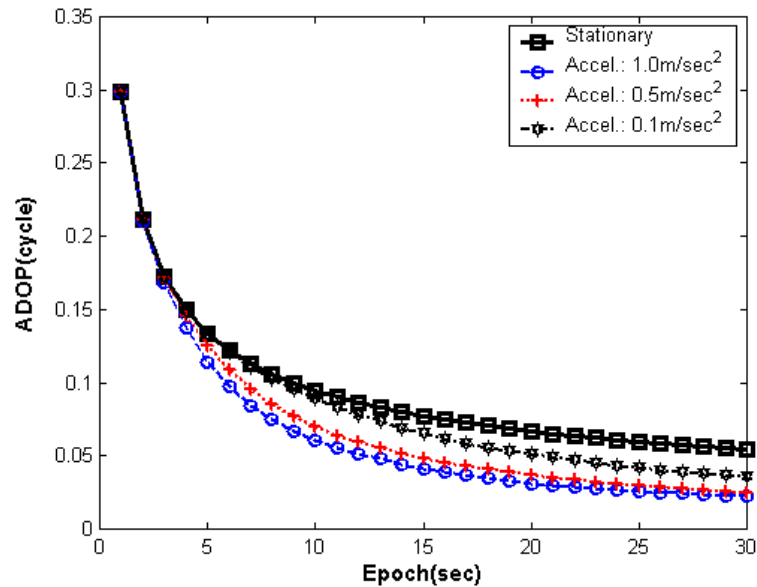


Figure 5-3 Impact of Pseudolites on ADOP (depending on the vehicle dynamics)

More analyses were performed to assess the impact of including INS-predicted position on the AR procedure. However an important consideration is the length of time of the assumed GPS/pseudolite signal blockage, since during a blockage, an integration filter (typically a Kalman filter) is unable to be updated, resulting in an error growth of the INS-predicted position. The magnitude of the error depends on the length of the blockage and the quality of the INS instrument. Moreover, during the AR procedure the filter cannot be updated by the accurate (ambiguity-fixed) carrier phase solution. These facts were considered in the analyses. Four scenarios, with different signal blockage lengths, were considered: *instantaneous* (normally caused by a cycle slip), 10, 20, and 30 seconds. Figure 5-4 depicts the influence (on the ADOP value) of introducing the INS-predicted position (and/or pseudolites) into the AR process as a function of the four different scenarios. All of the results, in the case of both GPS/INS and GPS/PL/INS integrated systems, indicate that the inclusion of an INS significantly reduces the ADOP values, and hence improves the AR performance.

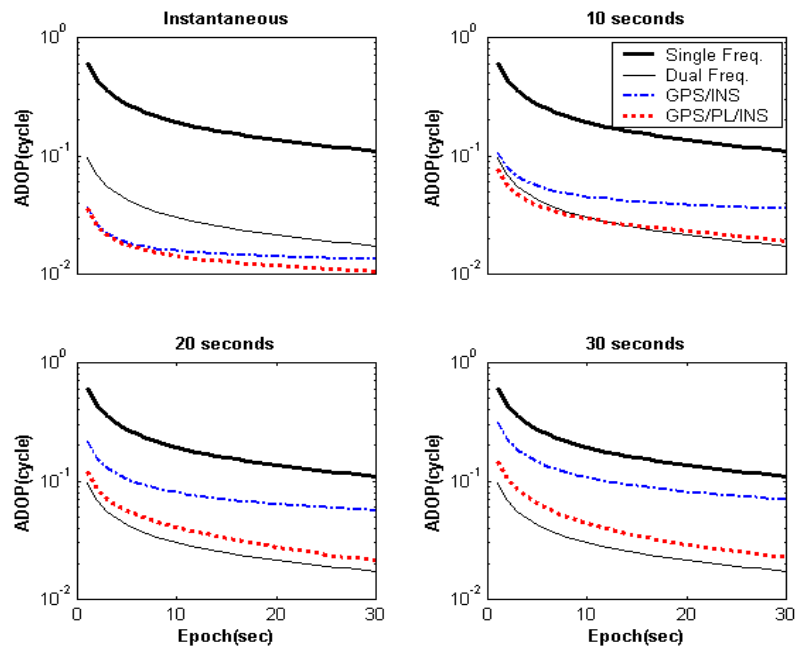


Figure 5-4 Impact of INS-predicted position on ADOP (comparison between GPS/INS and GPS/PL/INS systems)

Analysing the results in more detail, one can also identify the impact of the different behaviours of INS-predicted position error. The ‘*Instantaneous*’ blockage (the smallest error growth), for both GPS/INS and GPS/PL/INS systems, using single-frequency receivers is indeed superior to that of the dual-frequency GPS-only case. In other words, it appears that single epoch AR could be possible with such integrated systems. In the case of the 10 second blockage, even though the three sets of results (dual-frequency GPS-only, GPS/INS, and GPS/PL/INS) are similar at the beginning, the GPS/PL/INS results are much better than those of GPS/INS. Note that the results from the dual-frequency GPS case are always better than those of the integrated systems in the case of 20 and 30 second blockages. However although epoch-by-epoch AR with dual-frequency GPS data for short baselines is possible, using GPS/INS and GPS/PL/INS systems can permit the resolution of the ambiguities within a couple of seconds.

Figure 5-5 illustrates the change of ADOP (and hence the AR performance) as a function of the length of the signal outage. It can be seen from the figure that the ADOP values vary significantly, depending on the magnitudes of the initial position errors. However, those values become similar after a 30 second sequential solution, which

means the time-to-fix will be different, depending on the length of the signal blockage. However, the most impressive output of the results is that augmentation with pseudolite and INS measurements would significantly improve the single-frequency AR performance.

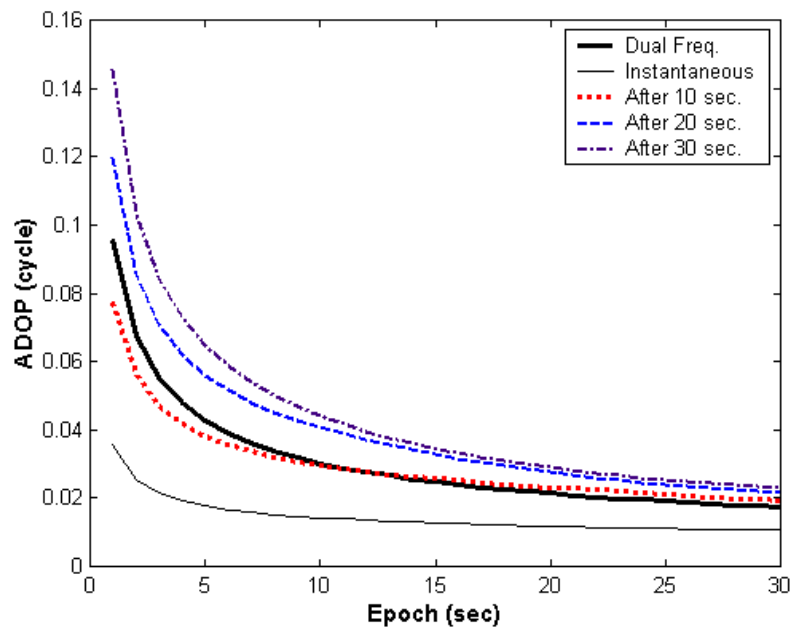


Figure 5-5 Impact of INS-predicted position errors on ADOP during signal blockages (GPS/PL/INS systems)

In order to solve the problem of position error growth during the AR procedure, one can consider the use of the DD pseudo-range measurements for the Kalman filter update as indicated in Figure 5-1, once the signals are reacquired. Even though the precision of the pseudo-ranges is not as good as that of carrier phase measurements with correctly fixed ambiguities, pseudo-ranges can be helpful in preventing the errors from increasing exponentially.

Figure 5-6 depicts the position error changes during the signal blockage (30 seconds). In this case study, the DD pseudo-range measurements are used in the filter update, after the signals are required. The error growth stops and drops down to a certain level, which reflects the level of DD pseudo-range errors.

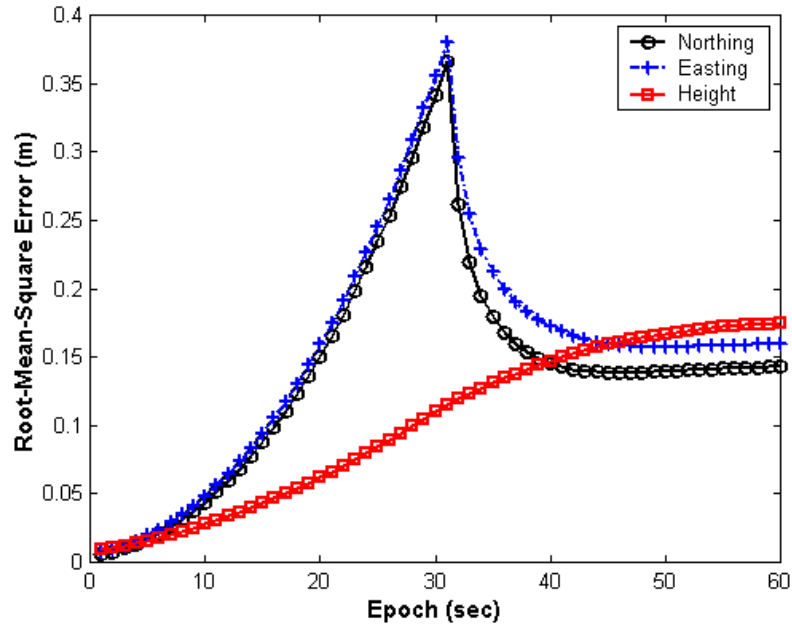


Figure 5-6 INS-predicted position error behaviours during absolute signal outage (30 seconds) and updating the filter by the DD pseudo-ranges in the AR procedure.

Figure 5-7 shows the ADOP changes with and without the use of DD pseudo-range data in the filter updating during the AR procedure. The results indicate that the AR performance will be improved by using pseudo-range measurements. Even though the degree of improvement of the ADOP values is small just after regaining the ranging signals (e.g., at the first epoch in Figure 5-7), the magnitude becomes significant with increasing time elapsed since the first epoch. Therefore this is a useful method to enhance the AR performance after a long signal blockage.

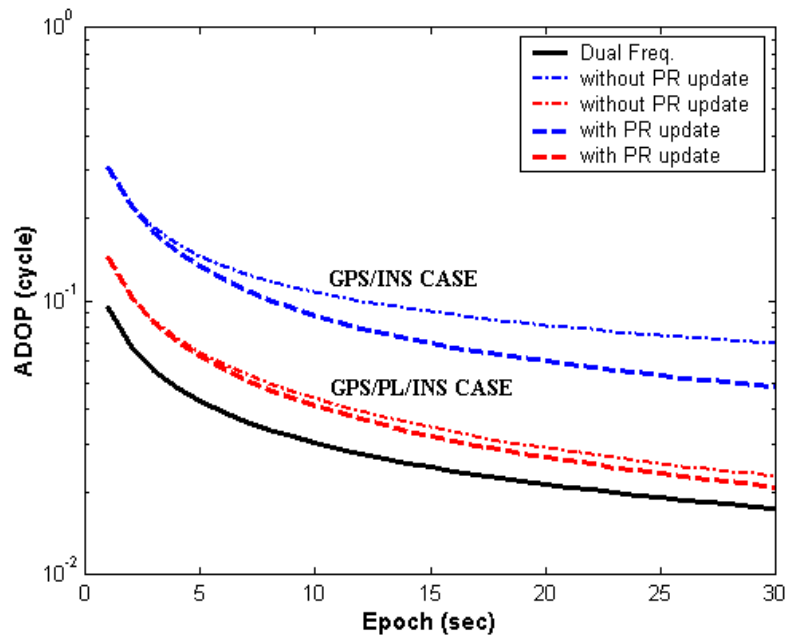


Figure 5-7 Impact of updating Kalman filter by DD pseudo-ranges on ADOP after 30 second signal blockage.

## 5.4 Experiment and results

Land vehicle experiments were carried out on 23<sup>rd</sup> April 2003 at the Clovelly Bay Carpark in Sydney. The objective of these experiments was to evaluate ambiguity resolution performance of the integrated GPS/Pseudolite/INS system based on the proposed procedure.

### 5.4.1 General Description of the Tests

A prototype pseudolite system developed at DSO National Laboratories of Singapore and UNSW was used in the test (described in detail in Chapter 7). The locations of the pseudolite and the reference station were precisely surveyed using Leica GPS system 500 receivers. During the trial, the pseudolite signal was configured to transmit with the power of  $-10$  dB (assigned PRN 12). The GPS/INS system developed in Chapter 2 was used for the data acquisition. Furthermore, Leica AT504 choke-ring antennas were used

at both the reference and rover (vehicle) stations to track the GPS and pseudolite signals. The antenna and INS were mounted on the roof of the test vehicle. Figure 5-8 illustrates the experiment set-up. Raw IMU measurements (accelerations and angular velocities) were recorded at 100Hz, while the single-frequency GPS/pseudolite data were logged at 1Hz. During the experiment there were 6 visible satellites (above the cut-off angle of  $15^\circ$ ) and one pseudolite (PRN 12) was set up. The maximum baseline length between the reference station and the rover was of the order of 50 metres, as shown in Figure 5-9.

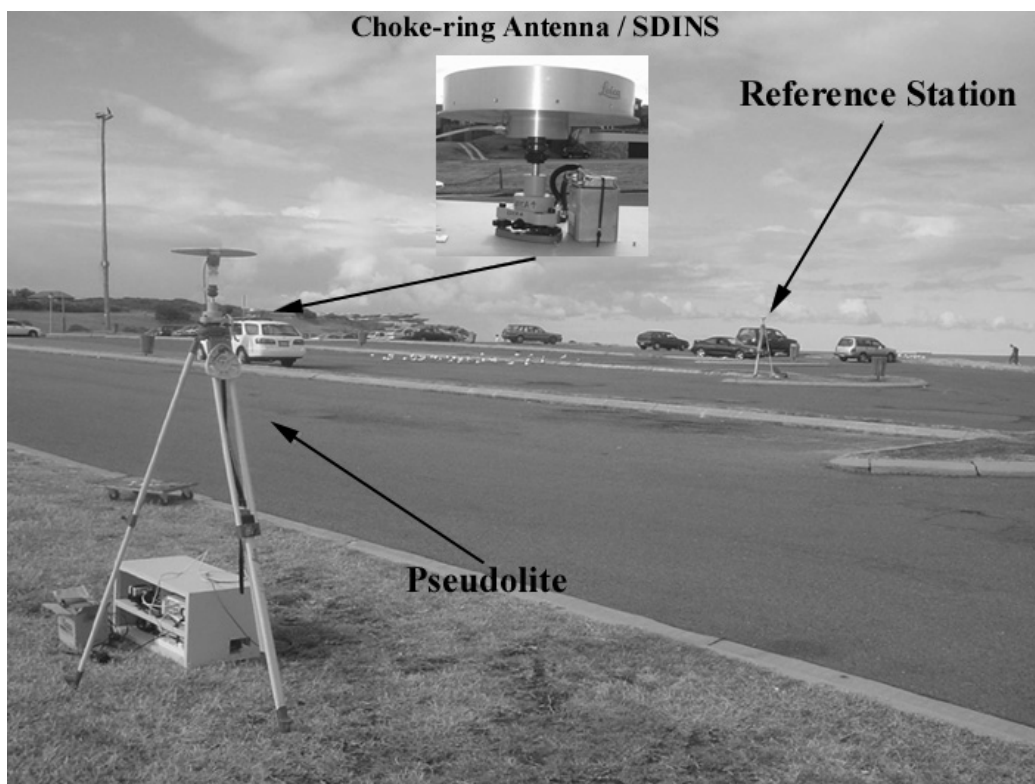


Figure 5-8 Experiment set-up

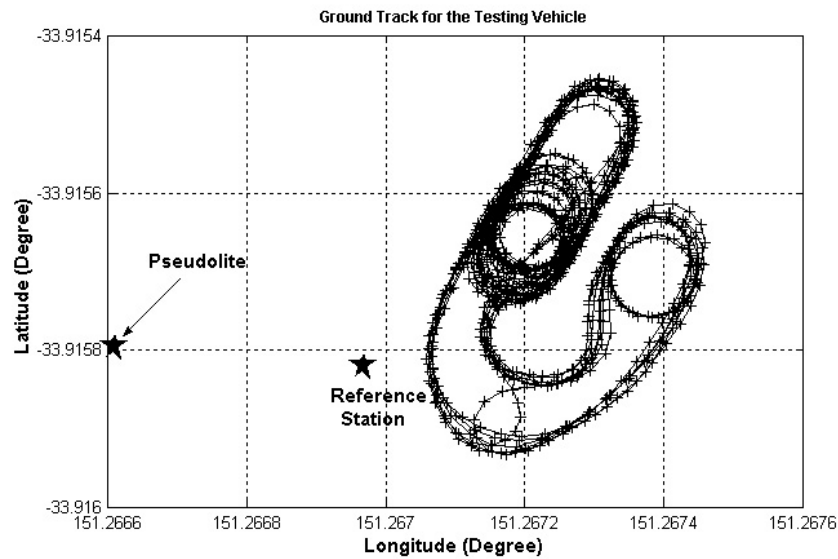


Figure 5-9 Vehicle trajectory and locations of reference station and pseudolites

#### 5.4.2 Special Consideration of Pseudolite Multipath

Chapter 3 showed the peculiar nature of pseudolite multipath, compared with that of GPS. Therefore, more attention should be paid to mitigate and/or handle the pseudolite-caused multipath. Three different methods are considered here in this study. The first method is to use choke-ring antennas at the reference stations and the rover. The second method is to realistically weight the pseudolite observations, by employing a realistic stochastic model (i.e. Equation (5.8)). The third method is to estimate the multipath effect in the pseudolite pseudo-range using one additional unknown parameter in the least squares solution. It should be noted that the third method would be only applicable when the number of satellites is greater than four. Therefore, this method will be of benefit to avoid the model infidelity problem due to the relatively severe multipath in the pseudo-range data.

Figure 5-10 illustrates the precision of the multipath error estimation with two system configurations: GPS/pseudolite and GPS/Pseudolite/INS. The values were calculated from a comparison of the residuals computed about positions obtained from RTK solution. The results indicate that the GPS/Pseudolite/INS solution provides more precise estimates. On the other hand, one may ask the question: ‘Does the inclusion of

the new parameter degrade the float ambiguity estimation?’ To answer this question analyses based on the ADOP factor were carried out using the same data set as the test discussed above. Figure 5-11 illustrates the analysis results with respect to three different methods, such as GPS/INS as well as GPS/Pseudolite/INS without/with the inclusion of the new parameter. It can be seen from Figure 5-11 that the inclusion of the pseudolite is helpful in improving the float solutions (smaller ADOP values), and the ADOP values are almost the same even though the additional unknown parameter is included in the least squares processing. It can therefore be concluded that the inclusion of the new unknown parameter does not degrade float ambiguity estimation.

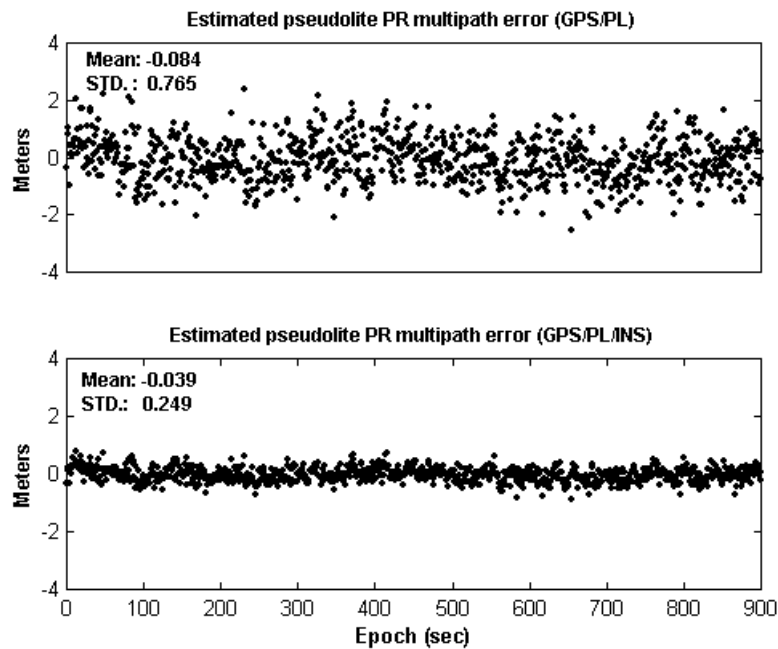


Figure 5-10 Pseudolite pseudo-range multipath estimation



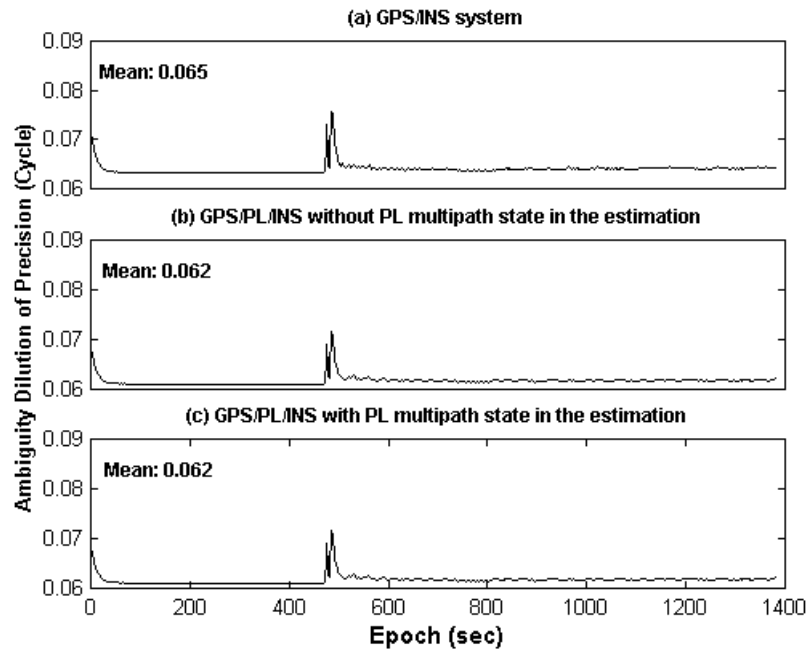


Figure 5-11 An effect of including multipath in the pseudolite pseudo-range as an unknown parameter in the float ambiguity estimation

### 5.4.3 AR Performance Analysis

In order to demonstrate the performance of the proposed AR procedure, a comparison between different system configurations was conducted. Three different configurations (GPS-only, GPS/INS, and GPS/Pseudolite/INS) were applied for all the data processing in the single-epoch solution mode. The AR performance can be evaluated by the comparison of ambiguity validation test statistics ( $W$ -ratio) obtained by Equation (5-19), in that the larger values for the statistics the higher the probability of correctly fixing the integer ambiguity (Wang, 1999; Wang et al., 2003b).

Figure 5-12 shows the  $W$ -ratio values in the case of using only GPS data; they are mostly less than their critical values (4.5 with the 99% confidence level). This means that most of the integer ambiguity combinations cannot be successfully validated. However the ratios obtained by either integrated GPS/INS or GPS/Pseudolite/INS are sufficiently large to validate the correct ambiguity for critical values (3.2 and 3.0 with the 99.9% confidence level respectively). Comparing the results from the GPS/INS case

with the GPS/INS/Pseudolite case, it can be seen that the ratios from the latter are usually larger than those obtained from the former (see also the averaged  $W$ -ratios in Figure 5-12). Therefore, the inclusion of PL observations enhances the AR performance. Table 5-1 summarises the ambiguity validation test results. The successful validation rates for the three different system configurations based on the aforementioned critical values are 0.4%, 97.4%, and 99.3%, respectively. Hence, it has been demonstrated that the proposed procedure based on GPS/Pseudolite/INS integration does indeed perform better.

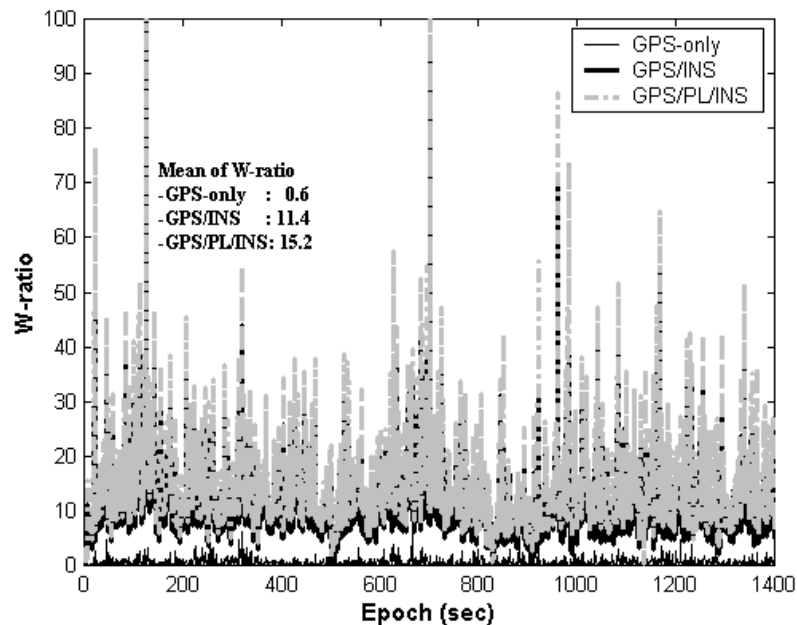


Figure 5-12  $W$ -ratio values for the different system configurations (epoch-by-epoch solution)

Table 5-1 Ambiguity validation test results for different system configurations

System Configuration	Num. Of Validated Ambiguity combinations	Num. Of Not Validated Ambiguity Combinations	Validation Rate (%)
GPS-only	5	1395	0.4
GPS/INS	1363	37	97.4
GPS/PL/INS	1390	10	99.3

A realistic estimation of measurement covariance matrices provides reliable statistics for AR. In order to clearly demonstrate this fact, the solutions based on the two different types of stochastic model, namely the ‘Preset’ and ‘Estimated’, are obtained. The ‘Preset’ model is based on an apriori assumption of the measurement precision. For the ‘Estimated’ model, a realistic measurement covariance matrix is estimated using Equation (5-8). Figure 5-13 depicts the validation test statistics ( $W$ -ratios), indicating that the ambiguity validation test statistics with the ‘Estimated’ measurement covariance matrices are better than those with the ‘Preset’ measurement covariance matrices. On the other hand, Table 5-2 shows that the successful validation rates for the ‘Estimated’ and ‘Preset’ are 92.1% and 99.3%, respectively, which demonstrates the AR performance with ‘Estimated’ model is superior to that of the ‘Preset’ models.

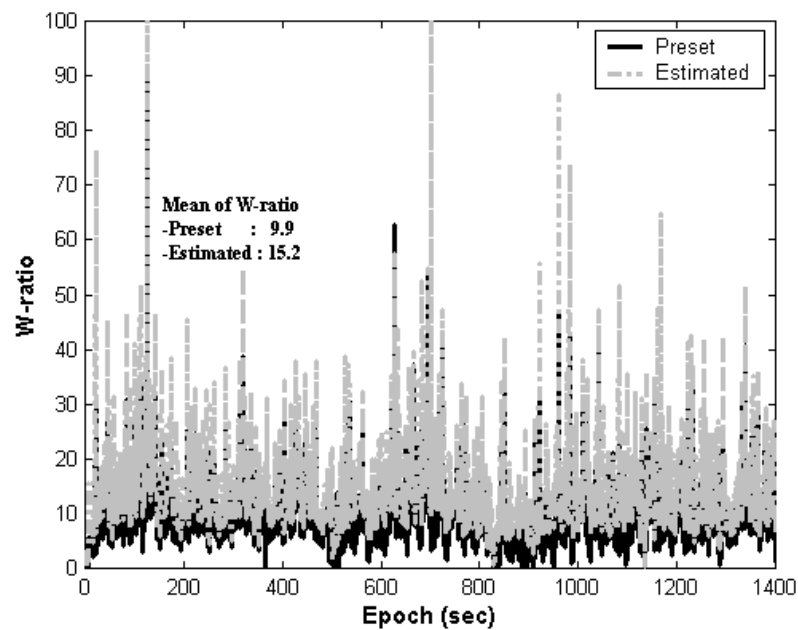


Figure 5-13 W-ratio values for the different stochastic models (epoch-by-epoch solution)

Table 5-2 Ambiguity validation test result for different stochastic models

Model	Num. Of Validated Ambiguity combinations	Num. Of Not Validated Ambiguity Combinations	Validation Rate (%)
Preset	1289	111	92.1
Estimated	1390	10	99.3

The ability of an integrated system to recover from complete GPS/pseudolite signal blockages, and return to a positioning solution with correctly resolved ambiguities, is critical to maintaining high system performance. Therefore the impact of including the pseudolite and INS observations on the AR performance after complete GPS/pseudolites signal blockage was also investigated. For this test, signal blockages of 2, 5, 10, 20, 30, 40, and 50 seconds with respect to three different locations in the observation files (referred to as Case I, II, and III) are simulated through modifying the RINEX data files. Note that DD pseudo-range measurements are used in the filter update for the AR procedure, and a sequential solution is applied to estimate the initial float ambiguities.

Table 5-3 and Figure 5-14 shows the time-to-fix of L1 carrier phase ambiguities after complete GPS/pseudolite signal blockages. The results manifest two important characteristics. First, the GPS-only solutions are the poorest in all cases. Second, the AR performances of GPS/INS and GPS/Pseudolite/INS are similar after a short signal outage (up to 10 seconds). However, the AR performance is significantly improved by including pseudolite measurements for outages of 20 seconds and above, except for the 30 second blockage for Case III. Special attention should be paid to ‘Case I’, because the most significant improvement was obtained. Hence, it is demonstrated from the results that the proposed AR procedure based on GPS/Pseudolite/INS integration makes it possible to resolve the ambiguities within a couple of seconds if the outage is relatively short. Moreover, the AR performance can be considerably enhanced even in the case of a blockage of 50 seconds. The different performances among the three cases appear to be caused by the different error growth rates of the INS-predicted positions, satellite geometry and/or measurement errors.

Table 5-3 Time-to-fix L1 carrier phase ambiguity after the different length of blockages

Case	Outage Duration (Sec)	Time to fix ambiguities (sec)		
		GPS-only	GPS/INS	GPS/PL/INS
Case I	2	61	1	1
	5		5	5
	10		10	8
	20		20	14
	30		31	22
	40		36	20
	50		43	24
Case II	2	34	1	1
	5		1	1
	10		1	1
	20		5	2
	30		10	8
	40		16	11
	50		20	13
Case III	2	32	1	1
	5		3	1
	10		5	4
	20		6	4
	30		8	8
	40		15	8
	50		19	10

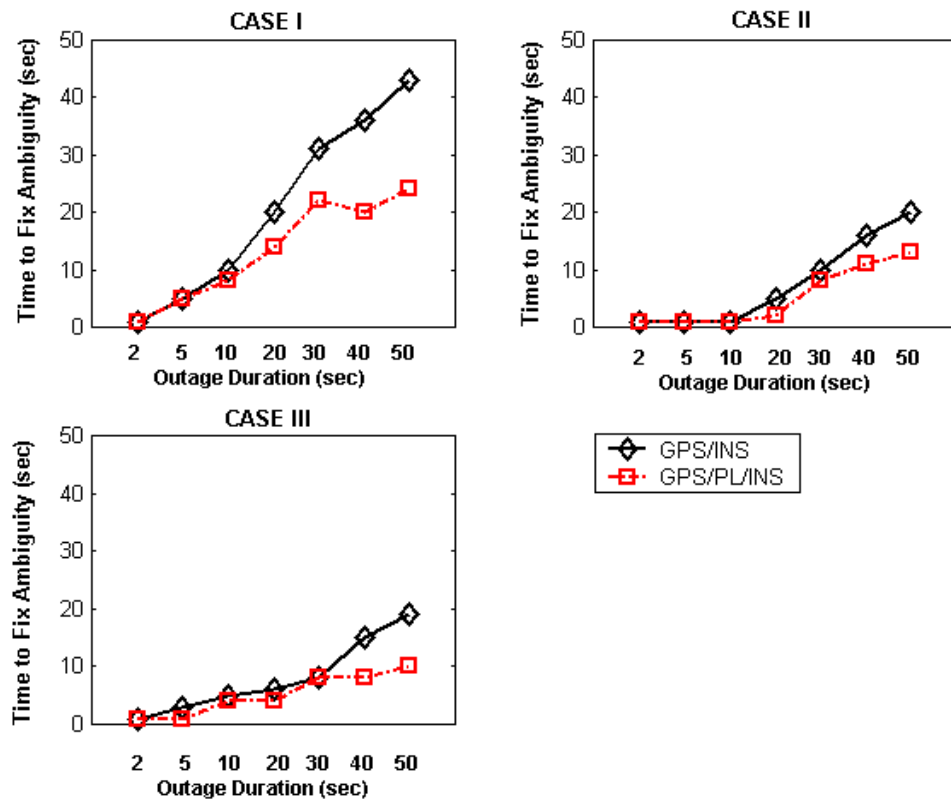


Figure 5-14 Time-to-fix L1 carrier phase ambiguity after different lengths of signal blockage

## 5.5 Concluding Remarks

Ambiguity resolution is one of the most crucial steps in achieving high accuracy positioning results using the proposed GPS/Pseudolite/INS system. In this chapter an ambiguity resolution procedure which uses GPS, pseudolite and INS measurements has been proposed, that improves the performance of single-frequency on-the-fly AR. In the proposed procedure, realistic stochastic modelling and a statistically rigorous ambiguity validation scheme were adopted to enhance the reliability of ambiguity resolution.

The potential benefits of the proposed procedure have been discussed with the derivation of single epoch covariance of float ambiguities within the integrated GPS/Pseudolite/INS system. The impacts of including pseudolite and INS observations in the AR procedure have been investigated through simulation studies based on

Ambiguity Dilution of Precision (ADOP) values. These analysis results show that the INS predicted-position included in the ambiguity resolution could substantially improve the precision and correlation of the float ambiguities (e.g., enhanced AR performance). In addition, it was found that the pseudolite measurements play an important role in the proposed AR procedure as ADOP values can be largely decreased even if only *one* pseudolite is added to the GPS constellation. Another benefit of including the pseudolite is the relatively rapid change of the line-of-sight vector that enhances the performance of the AR process.

The experimental results have shown that appropriate stochastic modelling for the satellite and pseudolite measurements are important in enhancing the performance of ambiguity resolution. It was also demonstrated that ‘instantaneous’ resolution was possible if the duration of the signal blockage was up to a couple of seconds. Moreover even if the signal blockage was up to 50 seconds, the ambiguities could be fixed within a few tens of seconds, depending on the satellite/pseudolite geometry and the measurement precision.

**CHAPTER 6**

**EFFECTIVE CYCLE SLIP DETECTION AND  
IDENTIFICATION ALGORITHM**

---

---

### **6.1 Introduction**

To obtain high precision of positioning and navigation performance with the proposed GPS/Pseudolite/INS system, carrier phase observations have to be used in the integration filter update. However, it was emphasised in Chapter 5 that the carrier phase integer ambiguities must be resolved before the measurements were utilised in the update. The resolved (or fixed) ambiguities remain constants as long as no loss of signal lock occurs. In the event of signal loss, the integer counter is reinitialised, effectively causing a jump in the instantaneous accumulated phase by an integer number of cycles. Such a jump (as indicated in Figure 6-1) is called a ‘cycle slip’, which corrupts the carrier phase measurement causing the unknown ambiguity value to be different after the cycle slip compared with its value before the slip. Hence it must be ‘repaired’ before the phase data is processed as double-differenced observations (Rizos, 1996 & 1999).

There are mainly three causes of cycle slips (Hofmann-Wellenhof et al., 2001). First, cycle slips are induced by the obstructions of the satellite signal due to trees, buildings, etc. The second cause is a low SNR due to extreme ionospheric conditions, multipath, high receiver dynamics, or low satellite elevation. The third cause is internal receiver tracking problems, reflected in incorrect signal processing. The occurrence of a cycle slip which is undetected will significantly degrade the accuracy of the navigational solution obtained from the integrated system. Therefore a number of techniques for the detection and identification of cycle slips have been developed. Some examples, in the case of standalone GPS, include: the use of GPS Doppler frequency (Cannon, 1987); linear combinations of L1 and L2 observations such as the geometry-free combination (Blewitt, 1990; Dedes and Mallett, 1995); and wide-lane phase minus narrow-lane pseudo-range (Han, 1997; Gao and Li, 1999). On the other hand, integration of GPS with INS is ideal for the detection and identification of small cycle slips. In such a



system, the high relative accuracy of the INS output can be used to predict the GPS antenna position at the measurement, with periodic INS errors updated by GPS observations (Wei et al., 1992; Schwarz et al., 1994). In addition, such an approach can overcome the drawbacks of GPS standalone techniques, which are not sensitive to dynamics, as it does not rely exclusively on GPS measurements (Gao, 1992; Altmayer, 2000).

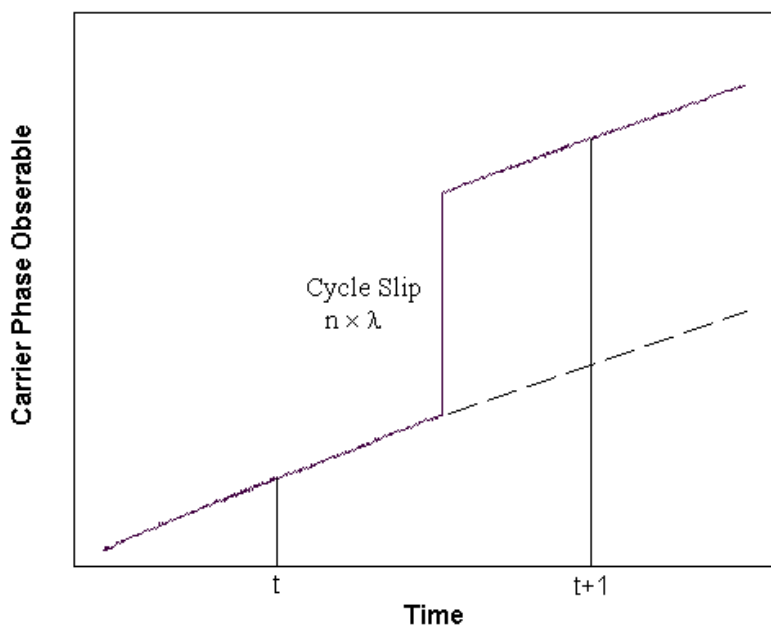


Figure 6-1 Cycle slip on GPS carrier phase observables

In this chapter a cycle slip detection and identification algorithm, which can be readily implemented in an integrated GPS/Pseudolite/INS system, will be proposed. The algorithm uses the GPS/pseudolite antenna position provided by the INS to calculate cycle slip decision values, and then applies the cumulative-sum (CUSUM) test to small persistent changes in the mean and/or standard deviation of the measurements (Mertikas and Rizos, 1997; Mertikas, 2001). The algorithm performance will be evaluated using two data sets in order to demonstrate the effectiveness of the proposed cycle slip detection/identification scheme.

## 6.2 A Cycle Slip Detection and Identification Algorithm

### 6.2.1 Decision Value and its Statistical Property

The basic task of the algorithm is to compare the double-differenced (DD) GPS/pseudolite carrier phase observations  $\nabla\Delta\phi_{GPS/PL}$  with the DD geometric distances  $\nabla\Delta\phi_{INS}$  computed using INS-predicted GPS/pseudolite antenna positions:

$$\delta\nabla\Delta\phi = \nabla\Delta\phi_{GPS/PL} - \nabla\Delta\phi_{INS} \quad (6.1)$$

Denoting  $\delta\nabla\Delta\phi$  to be the cycle slip decision values. In Equation (6-1), the GPS/pseudolite DD observation for short baseline applications can be defined as follows:

$$\nabla\Delta\phi_{GPS/PL} = \frac{1}{\lambda} \nabla\Delta\rho + \nabla\Delta N + \nabla\Delta\varepsilon_{\phi} \quad (6.2)$$

Note that in this algorithm development (i.e., Equation (6.2)), it is assumed that multipath error can somehow be modelled and/or mitigated by appropriate technologies. Such techniques may include narrow correlator spacing (Van Deirendonck et al., 1992) and Multipath Estimating Delay Lock Loops (MEDLL) (Townsend et al., 1995) or in practice, choosing antenna hardware such as choke rings and ground planes that have been found to be quite effective for reducing multipath (Lachapelle et al., 1989).

On the other hand, the computation of the double-differenced geometric distances is based on the INS-predicted positions:

$$\nabla\Delta\phi_{INS} = \frac{1}{\lambda} \nabla\Delta\rho + \nabla\Delta\varepsilon_{INS} \quad (6.3)$$

where  $\nabla\Delta\varepsilon_{INS}$  represents the error introduced by the INS-predicted GPS antenna positions and the satellite ephemeris error. Hence, the decision value  $\delta\nabla\Delta\phi$  (i.e., Equation (6-1)) can be rewritten as:

$$\delta \nabla \Delta \phi = \nabla \Delta N + \nabla \Delta \varepsilon_{GPS/PL} + \nabla \Delta \varepsilon_{INS} \quad (6.4)$$

If it is further assumed that the ambiguities were successfully resolved before a certain time using the procedure proposed in Chapter 5 (and then eliminated from the model as an unknown), the ambiguity term in Equation (6.2) also disappears. As a consequence, Equation (6.4) becomes:

$$\delta \nabla \Delta \phi = \nabla \Delta \varepsilon_{GPS/PL} + \nabla \Delta \varepsilon_{INS} \quad (6.5)$$

The expected value of the measurement noise ( $\nabla \Delta \varepsilon_{GPS/PL}$ ) would be:

$$E[\nabla \Delta \varepsilon_{GPS/PL}] \approx 0 \quad (6.6)$$

If two DD measurements are available, the homogeneous covariance matrix is:

$$cov[\nabla \Delta \varepsilon^{GPS/PL}] = 2\sigma^2 \begin{bmatrix} 2 & 1 \\ 1 & 2 \end{bmatrix} \quad (6.7)$$

Hence, the variance of one DD measurement is  $4 \cdot \sigma^2$  (Hofmann-Wellenhof et al., 2001).

On the other hand, the errors ( $\nabla \Delta \varepsilon_{INS}$ ) in the DD geometric distances are mostly induced by the INS-predicted position errors. In order to analyse this error, both the receiver antenna position and satellite ephemeris biases have to be mapped into distance errors. The distance between a GPS/pseudolite signal transmitter and user receiver ( $\rho_i^s$ ) can be linearised with respect to their approximate values  $x_0^s, y_0^s, z_0^s$  and  $x_{i0}, y_{i0}, z_{i0}$ :

$$\rho_i^s = \rho_0 + \underbrace{\frac{x_{i0} - x_0^s}{\rho_0}}_{a_x} (\delta x_i - \delta x^s) + \underbrace{\frac{y_{i0} - y_0^s}{\rho_0}}_{a_y} (\delta y_i - \delta y^s) + \underbrace{\frac{z_{i0} - z_0^s}{\rho_0}}_{a_z} (\delta z_i - \delta z^s) \quad (6.8)$$

Assuming that these initial coordinates are true values, the distance errors of the reference and mobile receivers caused by the satellite ephemeris and receiver position errors are:

$$\delta\rho_R^s = a_X^s(\delta x_R - \delta x^s) + a_Y^s(\delta y_R - \delta y^s) + a_Z^s(\delta z_R - \delta z^s) \quad (6.9)$$

$$\delta\rho_M^s = a_X^s(\delta x_M - \delta x^s) + a_Y^s(\delta y_M - \delta y^s) + a_Z^s(\delta z_M - \delta z^s) \quad (6.10)$$

If it is assumed that the satellite ephemeris errors are eliminated by double-differencing, the error ( $\nabla\Delta\varepsilon_{INS}$ ) is:

$$\nabla\Delta\varepsilon_{INS} = \underbrace{(a_X^s - a_X^t)}_{A_X}\delta x_M + \underbrace{(a_Y^s - a_Y^t)}_{A_Y}\delta y_M + \underbrace{(a_Z^s - a_Z^t)}_{A_Z}\delta z_M \quad (6.11)$$

If the expected values of the GPS/Pseudolite/INS system's position error ( $x_r$ ) is zero with the assumption that the navigation parameters and sensor errors are reliably estimated (and corrected), and its covariance matrix can be obtained from the Kalman filter (e.g, Equation (2.22)):

$$E(x_r) \approx 0, \quad Q_r = \begin{bmatrix} \sigma_{xx} & \sigma_{xy} & \sigma_{xz} \\ \sigma_{yx} & \sigma_{yy} & \sigma_{yz} \\ \sigma_{xz} & \sigma_{yz} & \sigma_{zz} \end{bmatrix} \quad (6.12)$$

then the expected values of  $\nabla\Delta\varepsilon_{INS}$  are zero as well, if the remaining error sources are assumed eliminated by double-differencing. On the other hand, the covariance matrix can be derived using the covariance propagation law:

$$\text{cov}[\nabla\Delta\varepsilon_{INS}] = A_b Q_r A_b^T \quad (6.13)$$

where,

$$A = \begin{bmatrix} A_X^{aj} & A_Y^{aj} & A_Z^{aj} \\ A_X^{bj} & A_Y^{bj} & A_Z^{bj} \\ \vdots & \vdots & \vdots \\ A_X^{ij} & A_Y^{ij} & A_Z^{ij} \end{bmatrix} \quad (6.14)$$

Assuming that GPS carrier phase measurements are uncorrelated with respect to time, the predicted position by INS and the actual carrier-phase measurements can also be assumed statistically uncorrelated as the predicted position is only affected by previous GPS measurements. Thus the expected values of the decision values are (Altmayer, 2000):

$$E[\delta\nabla\Delta\phi] \approx 0 \quad (6.15)$$

and the variance can be obtained as follows:

$$\sigma^2[\delta\nabla\Delta\phi] = \sigma^2[\nabla\Delta\varepsilon_{GPS/PL}] + \sigma^2[\nabla\Delta\varepsilon_{INS}] \quad (6.16)$$

Finally, cycle slip detection and identification can be carried out through continuously performing a hypothesis test with respect to the decision values under the aforementioned assumptions.

### 6.2.2 Cumulative Sums (CUSUMS) Test

The decision values ( $\delta\nabla\Delta\phi$ ) represent the cycle slip indicating signal which makes the detection of slips, and permits determination of their magnitude. Assuming that the signal is characterised by a Gaussian distribution with the static properties described in the preceding section, the CUSUM algorithm can be applied to detect the cycle slips.

Define the two statistical hypotheses  $H_0$  and  $H_a$ . A sequence of  $\delta\nabla\Delta\phi$  can be obtained, which is assumed to be a white noise process with the constant mean value  $\mu_i$  ( $i=0, a$ ):

$$\delta\nabla\Delta\phi = \begin{cases} \mu_0 + e_t & \text{if } T \leq u-1 \\ \mu_a + e_t & \text{if } T > u \end{cases} \quad (6.17)$$

where  $\mu_0$  is the mean value for the decision values before a cycle slip,  $\mu_a$  is the mean value after the cycle slip and  $e_t$  is a white noise sequence with variance  $\sigma^2[\delta\nabla\Delta\phi]$ .

Given a sample of size  $T$ , the null hypothesis  $H_0$  denotes no change or departure from the initial conditions has taken place during the entire time sequence, while the alternative hypothesis  $H_a$  corresponds to a slip occurring at the sampling position  $u$ . These hypotheses can therefore be expressed as:

$$\begin{cases} H_0 : \mu = \mu_0 & \text{if } u \geq T \\ H_a : \mu = \mu_a & \text{if } u \geq T \end{cases} \quad (6.18)$$

The probability density functions of the decision values are:

$$f_i(x) = \begin{cases} f(x|H_0) = \frac{1}{\sigma\sqrt{2\pi}} \exp\left(-\frac{(x-\mu_0)^2}{2\sigma^2}\right) & \text{if } H_0 \text{ is true} \\ f(x|H_a) = \frac{1}{\sigma\sqrt{2\pi}} \exp\left(-\frac{(x-\mu_1)^2}{2\sigma^2}\right) & \text{if } H_a \text{ is true} \end{cases} \quad (6.19)$$

where  $x$  represents the decision value  $\delta\nabla\Delta\phi$ . Since successive decision values are statistically independent, the logarithms of the likelihood of joint distribution density at the  $n$ -th sampling point can be written as a cumulative sum (CUSUM) (Mertikas and Rizos 1997; Mertikas 2001):

$$s(n) = \ln \frac{f_a(x_1)}{f_0(x_1)} + \dots + \ln \frac{f_a(x_n)}{f_0(x_n)} = z_1 + z_2 + \dots + z_{n-1} + z_n \quad (6.20)$$

where the single increment  $z_n$  can be derived from Equation (6.19):

$$\begin{aligned}
z_n &= \ln f_a(x_n) - \ln f_0(x_n) = \frac{1}{2\sigma^2} \left\{ (x_n - \mu_0)^2 - (x_n - \mu_a)^2 \right\} \\
&= \frac{\mu_a - \mu_0}{2\sigma^2} \left( x_n - \frac{\mu_a + \mu_0}{2} \right) = \frac{\delta\mu}{2\sigma^2} \left( x_n - \mu_0 - \frac{\delta\mu}{2} \right)
\end{aligned} \tag{6.21}$$

Generally, the single increment  $z_n$  is negative if the null hypothesis  $H_0$  is true, whereas it is positive if the alternative hypothesis  $H_a$  is true in the case of positive shift. Thus a shift in the mean value of the decision values (a cycle slip occurrence) is reflected as a change in the sign of the average value of the single increment of the log-likelihood ratio (Mertikas and Rizos 1997; Mertikas 2001).

The CUSUM algorithms can be classified into two types. The first type is the one-sided CUSUM, which can be used when both the means before and after the change are known. The second type is the two-sided CUSUM, to be used when the change magnitude is unknown. It is the two-sided CUSUM test that should be used for the cycle slip detection algorithm with a minimum detectable jump ( $\delta\mu_{min}$ ). It uses two CUSUM algorithms in parallel; the first one for detecting an increase in the mean, and the second for detecting a decrease in the mean of the sequence (Basseville, 1988; Basseville and Nikiforov, 1993; Hinkley, 1970). Thus, a slip will be detected if:

$$\begin{cases} g_n^* = s_n - \min_{0 \leq t \leq n} s_t \geq \lambda^* \\ g_n^\bullet = \max_{0 \leq t \leq n} s_t - s_n \leq \lambda^\bullet \end{cases} \tag{6.22}$$

where

$$s_t = s_{t-1} + \frac{\delta\mu_{min}}{2\sigma^2} \left( x_t - \mu_0 - \frac{\delta\mu_{min}}{2} \right), \quad s_0 = 0 \tag{6.23}$$

The typical behaviour of CUSUM values computed by Equation (6.22) is illustrated in Figure 6-2.

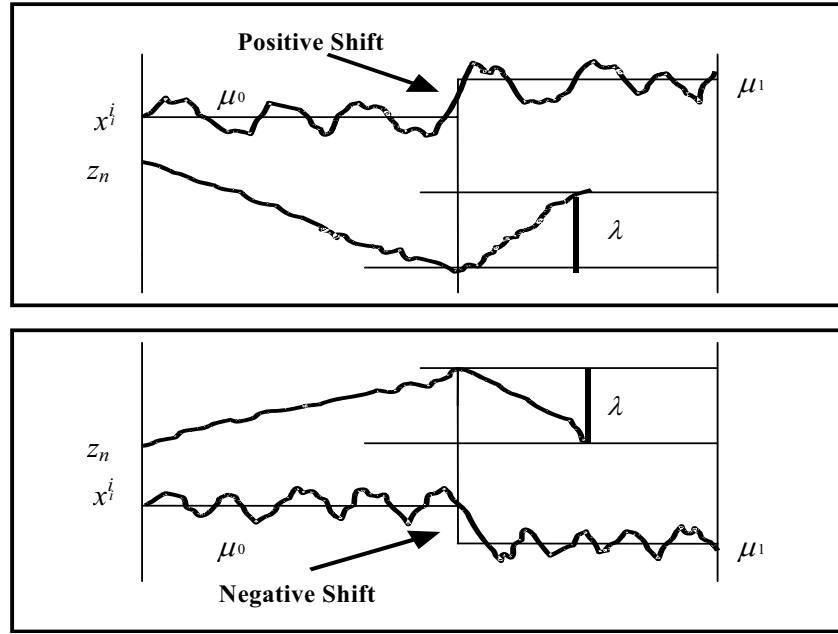


Figure 6-2 Typical behaviour of the CUSUM decision function calculated by Equation (6.22)

To avoid the downward drift of the CUSUM across and out of the page limits, an algebraic equivalent of Equation (6.22) is used (Hawkins and Olwell 1998; Mertikas 2001):

$$\begin{cases} C_n^* = \max(0, C_{n-1}^* + g_n) \geq \lambda^* \\ C_n^\bullet = \min(0, C_{n-1}^\bullet + g_n) \leq \lambda^\bullet, C_n^* = C_n^\bullet = 0 \end{cases} \quad (6.24)$$

The typical behaviour of CUSUM values computed by Equation (6.24) is sketched in Figure 6-3.

The resulting alarm time is given by (Ogaja, 2002):

$$t_a = \min\{t \geq 1 : (g_t^* \geq \lambda) \cup (g_t^\bullet \geq \lambda)\} \quad (6.25)$$

In most cases very little is known about the change magnitude  $\delta\mu_{\min}$ . Three possible *a priori* choices can be made with respect to this parameter. The first is to choose  $\delta\mu_{\min}$  as a minimum possible jump magnitude (limit case being  $\delta\mu_{\min} = 0$ ). The second is to choose *a priori* the most likely jump magnitude. The third choice is the worst-case



value from the point of view of the cost of missed detection(s). If the actual change in mean is less than that specified in the CUSUM test, then the single increments  $z_n$  of the log-likelihood ratio will always have a positive mean and the CUSUM scheme will be ineffective as a detector of change. It is common to specify a “rejectable level”  $\delta\mu_{\min}$ , and then determine the threshold value  $\lambda$  so that the CUSUM test has a specified maximum rate of detection alarm with a minimum delay. A more detailed description of CUSUM parameter tuning is given in Hawkins and Olwell (1998) and Mertikas and Rizos (1997).

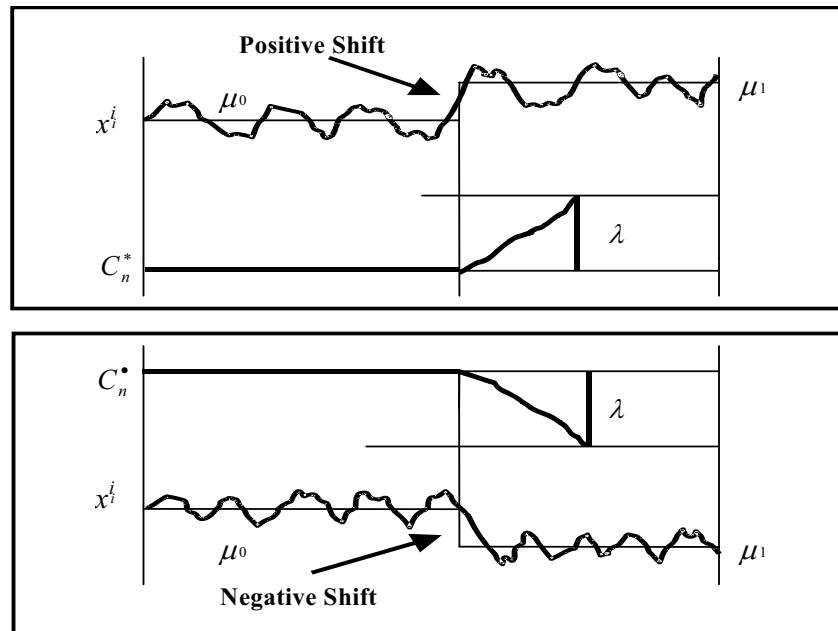


Figure 6-3 Typical behaviour of the CUSUM decision function calculated by equation (6.24)

Figures 6-4 and 6-5 show typical examples of the cumulative sum tests for detecting cycle slips. In these figures, the upper graphs depict the calculated decision values, whereas the lower ones show the CUSUM values computed from Equation (6.25). Cycle slips were simulated in L1 carrier phase measurements, namely +1 cycle on SV 15 and -2 cycles on SV 30. A cycle slip at the  $n = 130$  sampling step in these two cases is reflected as a change of the positive and negative trend in the cumulative sum. The onset time could be reliably determined as the last time a minimum value of the log-likelihood occurred.

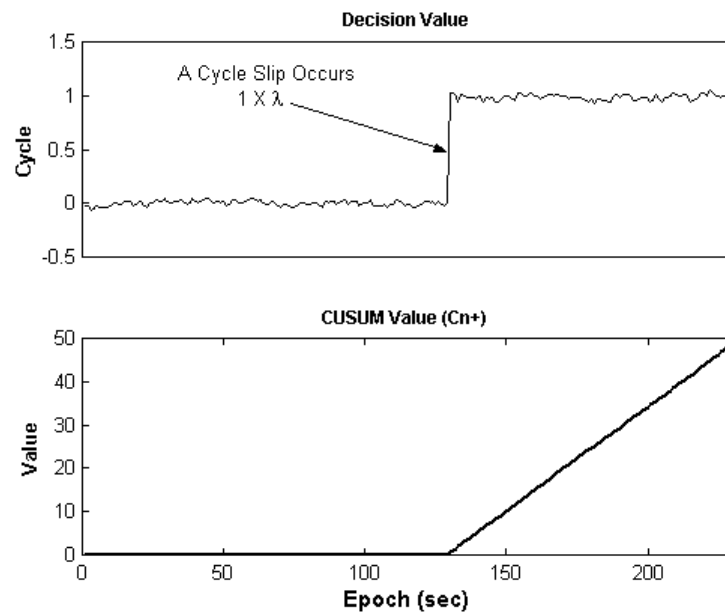


Figure 6-4 Cumulative sums for detecting one cycle slip in L1 carrier phase measurement in the case of positive slip (SV 15)

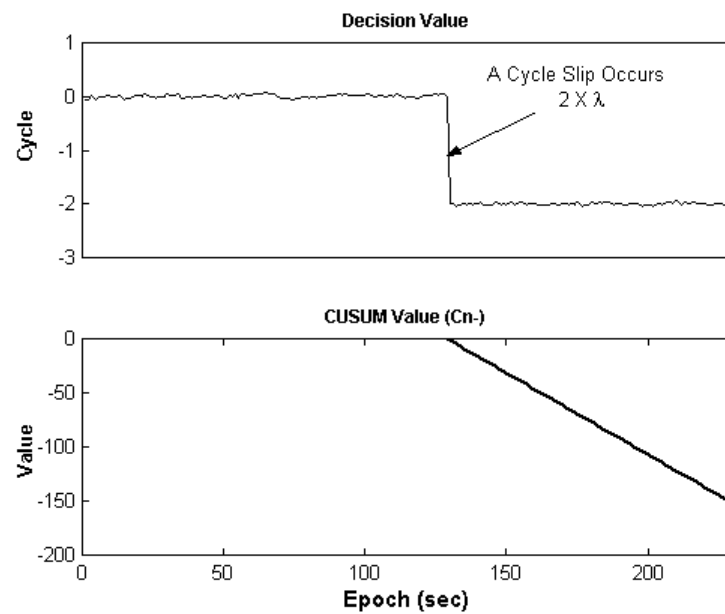


Figure 6-5 Cumulative sums for detecting one cycle slip in L1 carrier phase measurement in the case of negative slip (SV 30)

### 6.3 Algorithm Performance Tests

In order to demonstrate the effectiveness of the proposed cycle slip detection/identification scheme, algorithm performance tests were carried out using two data sets. One set of data was collected using GPS/INS integration system (denoted as '*Data Set I*'), which was analysed in Chapter 2. The second set was collected using integrated GPS/Pseudolite/INS system (denoted as '*Data Set II*') that was used for ambiguity resolution test in Chapter 5. Details on these test descriptions can be found in Chapters 2 and 5.

#### 6.3.1 CUSUM Tuning Parameters and 'Truth' for Tests

First of all, CUSUM parameters were set at 0.5 cycles (approximately 9cm) and 0.4 for the minimum detectable value ( $\delta\mu_{\min}$ ) and the threshold ( $\lambda$ ) respectively, as suggested in the CUSUM parameter tuning procedure proposed by Mertikas and Rizos (1997).

A pre-processing step was performed to obtain the 'truth', before analysing the algorithm performance. A method used in this research is to scrutinise the DD carrier phase residuals with respect to antenna positions obtained from GPS RTK positioning. Note that such a data processing scheme provides a few centimetre-level accuracy when the carrier phase ambiguities are resolved correctly (Rizos, 1996). It was revealed from the pre-processing that no cycle slips existed in all the GPS carrier phase observations of both *Data Set I* and *II*, while thirteen slips were identified in the pseudolite measurements in the *Data Set II*. This result highlights that the pseudolite signal is more vulnerable to cycle slips than the satellite signal. This is likely to be due to the low pseudolite elevation angle and some obstructions in this test.

For analysis purposes, cycle slips were *simulated* on three satellites (SV 4, 9, 24) in *Data Set I* and one satellite (SV 7) in *Data Set II*, by editing the RINEX observation files. Note that the simulated slips were considered as the 'truth' in the following tests. The simulated cycle slip scenarios of different magnitudes are shown in Table 6-1 and

6-2. On the other hand, the identified cycle slips of pseudolite (PL12) were left in the data files and considered as the ‘truth’ for pseudolite test (see Table 6-2).

### 6.3.2 Test Results with ‘Data Set I’

Figures 6-6 to 6-8 illustrate decision values and two-sided CUSUM values of PRN 4, 9, and 24 to give a closer insight into how the algorithm is performing during data processing. The top graphs in these figures depict the decision values with imposed cycle slips in raw measurements. The middle and bottom graphs show CUSUM values are kept as zero when no cycle slip occurs. At the presence of a cycle slip, the detection threshold is exceeded and the cycle slip determination process identifies the affected DD observations. It can be seen in Table 6-1 that the algorithm performs well, since the magnitudes and epochs of the slipped carrier phase measurements are accurately identified even if the magnitude of the slip is one cycle.

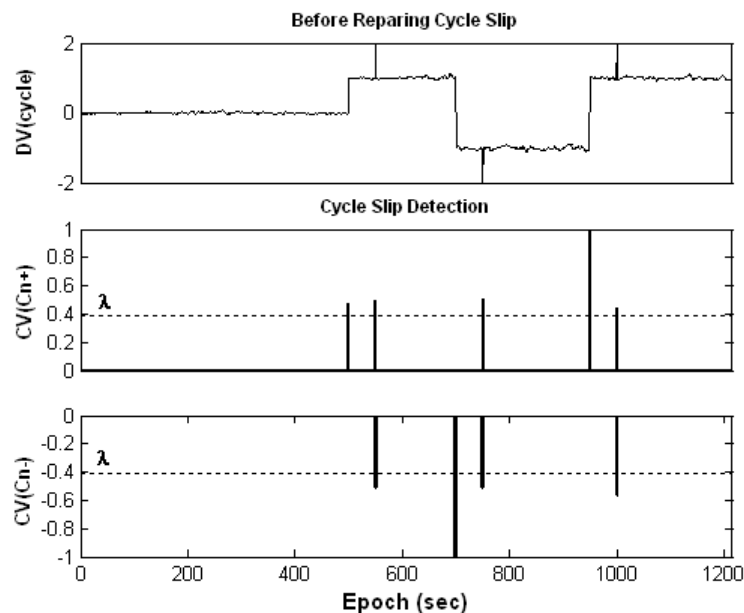


Figure 6-6 CUSUM test for PRN 4 (ref SV 7)

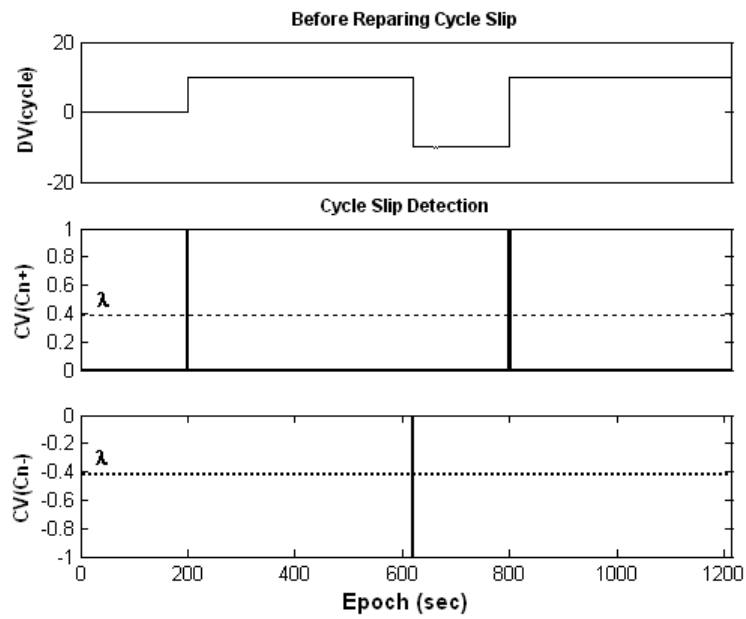


Figure 6-7 CUSUM test for PRN 9 (ref SV 7)

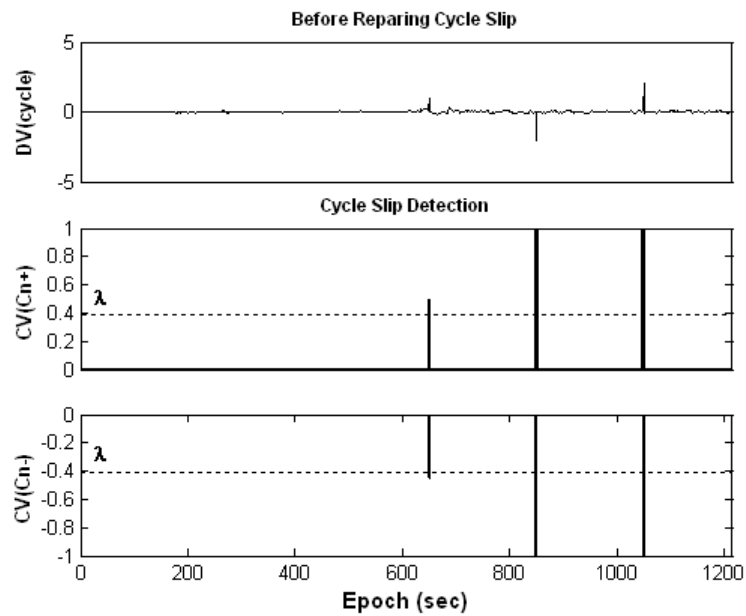


Figure 6-8 CUSUM test for PRN 24 (ref SV 7)

Table 6-1 Cycle slip detection and identification procedure results of ‘Data Set I’

PRN number	Epoch	Truth	Identified
4	500	+ 1	+ 1
	550	+ 1	+ 1
	551	- 1	- 1
	700	- 2	- 2
	750	- 1	- 1
	751	+ 1	+ 1
	950	+ 2	+ 2
	1000	+ 1	+ 1
	1001	- 1	- 1
9	200	+10	+10
	620	- 20	- 20
	800	+10	+10
24	650	+ 1	+ 1
	651	- 1	- 1
	850	- 2	- 2
	851	+ 2	+ 2
	1050	+ 2	+ 2
	1050	- 2	- 2

### 6.3.3 Test Results with ‘Data Set II’

Similar to the previous section, Figures 6-9 and 6-10 illustrate the decision values and two-sided CUSUM values of SV 7 and PL 12. The top graphs in these figures depict the decision values with the introduced cycle slips in the raw measurements. The second and third graphs show that the CUSUM values remain at zero when no cycle slip occurs. At the occurrence of a cycle slip, the detection threshold is exceeded and the cycle slip determination process identifies the affected double-differenced observations. Table 6-2 shows locations and magnitudes of the truth, and the ones identified from the proposed procedure. It is seen from the results how well the algorithm performs in the data processing as slipped carrier phase measurements are successfully detected and identified without missing any cycle slips, despite some slips occurring at two successive epochs.

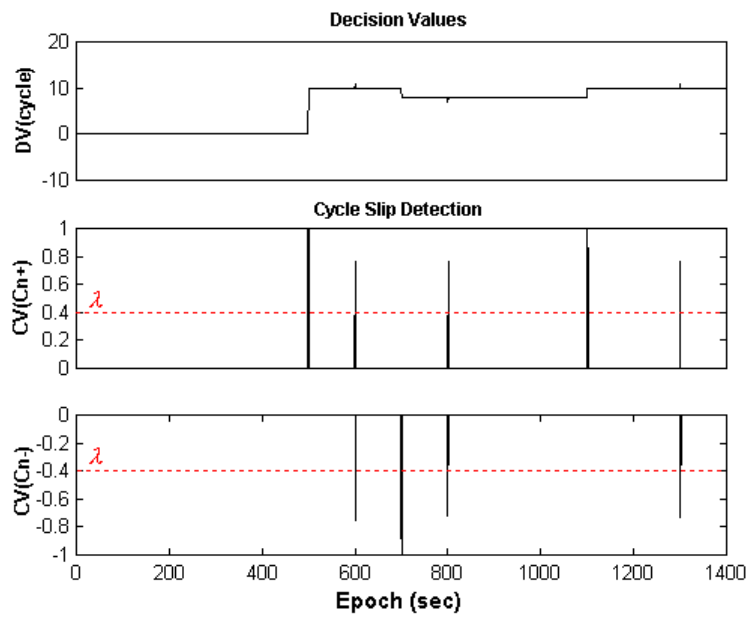


Figure 6-9 CUSUM test for SV 7 (ref SV 4)

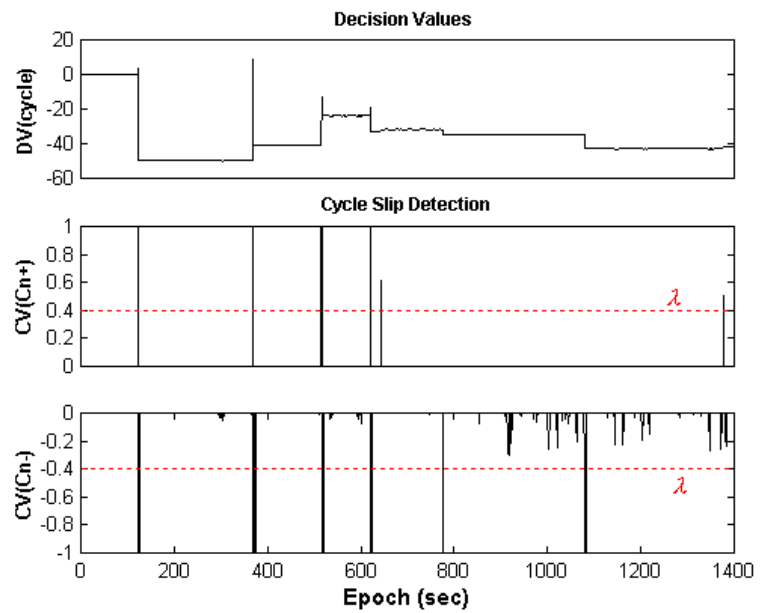


Figure 6-10 CUSUM test for PL 12 (ref SV4)

Table 6-2 Cycle slip detection and identification procedure results of ‘Data Set II’

Satellite PRN 09			Pseudolite PRN 12					
Epoch	Truth	Identified	Epoch	Truth	Identified	Epoch	Truth	Identified
500	+10	+10	123	+3	+3	644	+1	+1
600	+1	+1	124	-53	-53	776	-3	-3
601	-1	-1	368	+58	+58	1081	-8	-8
700	-2	-2	369	-48	-48	1307	+1	+1
800	-1	-1	374	-1	-1			
801	+1	+1	516	+28	+28			
1100	+2	+2	518	-11	-11			
1300	+1	+1	621	+5	+5			
1301	-1	-1	622	-14	-14			

#### 6.4 Concluding Remarks

Cycle slip detection/identification is a crucial step to ensure high accuracy of carrier phase-based GPS/Pseudolite/INS integration. In this Chapter, an effective cycle slip detection and identification scheme for single-frequency measurements using an integrated GPS/Pseudolite/INS system has been proposed and described. The algorithm makes use of the additional GPS antenna position information given by the INS navigation solutions, and cumulative-sum (CUSUM) test is applied to detect the slips in the decision values. Hence it is possible to simply implement the algorithm within the integrated system software. In addition, algorithm performance tests have been carried out to examine its effectiveness. The results indicate that the pseudolite signal is more vulnerable to cycle slips than the satellite signal. This is probably due to the low pseudolite elevation angle and some obstructions in this test. Moreover, the test results for the proposed algorithm have indicated that cycle slips can be effectively detected and instantaneously identified using the proposed algorithm, even if the slips occur at two successive epochs.



**CASE STUDY: GPS/PSEUDOLITE/INS INTEGRATION FOR  
AIRCRAFT PRECISION APPROACH AND LANDING**

---

---

**7.1 Introduction**

The performance of GPS/INS integration systems relies heavily upon the quality of GPS measurements and the geometry of the satellite constellation. In most airborne applications, however, there are stringent requirements in terms of positioning accuracy, availability and integrity that cannot always be met. For instance, due to the limited number of GPS satellites, a sufficient number of ‘visible’ satellites cannot be guaranteed at all times and locations. Even when some low elevation satellites are tracked, relatively high atmospheric effects contaminate the observations from these satellites. Therefore, this intrinsic shortcoming of satellite-based navigation systems leads to, for example, poor accuracy in the vertical component, which is approximately three times worse than that of the horizontal component. Literature has shown that these drawbacks can be addressed by the integration of GPS with other sensors and/or GPS augmentation using airport pseudolites (Elrod and Barltrop, 1994; Pervan, 1996; Bartone, 1997; Hein et al., 1997; Henzler and Weiser, 1999).

The airport pseudolites are ground-based GPS-like signal transmitters described in Chapter 3, which can be readily installed wherever they are needed. Hence, the pseudolite-augmented GPS/INS system (i.e., GPS/Pseudolite/INS integration) will be able to improve system performance in terms of availability, accuracy, and integrity under a wide variety of poor operational environments. Availability is increased because the airport pseudolites provide additional ranging sources to augment the GPS constellation. Navigation accuracy improvement can occur due to better local geometry, as measured by a lower vertical dilution of precision (VDOP), which is crucial in aircraft precision approach and landing applications. In addition, integrity enhancement is achieved by increased redundant measurements.

In this chapter the issue of the integration of pseudolites into GPS/INS for aircraft precision approach and landing will be discussed. A prototype airport pseudolite has been configured for this application. To evaluate overall navigation performance, flight tests were carried out in April/May 2003 at the Wedderburn Airfield, Sydney. An overview of the equipment used for the flight tests will be presented. This is followed by a description of the flight tests and the preliminary test results, with an emphasis on effects of including the airport pseudolite in the navigation solution.

## **7.2 An Airborne GPS/Pseudolite/INS System**

In this section, an airborne GPS/Pseudolite/INS integration for aircraft precision approach and landing will be presented in detail. The system essentially consists of two components: a ground and an airborne subsystem.

### **7.2.1 Ground Subsystem**

A ground subsystem comprises a pseudolite and a ground reference system. The prototype pseudolite system intended for airborne/land applications is configured as shown in Figure 7-1. The pseudolite system primarily consists of a GPS signal generator with low noise amplifier (LNA) and a rubidium frequency reference clock. The pseudolite signals are provided by a Spirent Communications GSS4100P single-channel signal generator pulsing at a 1/11 duty cycle, with a 10MHz oven-controlled crystal oscillator (OCXO) frequency reference. The pseudolite signals are compatible with the GPS signal, i.e. a  $1575.42 \pm 2.046\text{MHz}$  carrier coherently modulated with a C/A code (1.023MHz) and navigation message (50bps).

The reference station consists of a NovAtel Millennium receiver with Leica AT504 choke-ring antenna, and a wireless data-link transmitter. Note that use of the choke-ring is for the mitigation of GPS/pseudolite multipath. Raw measurements from the GPS/pseudolite signals tracked on the reference receiver are recorded using a laptop

computer, simultaneously output over a serial communications interface and broadcast over the wireless data-link.

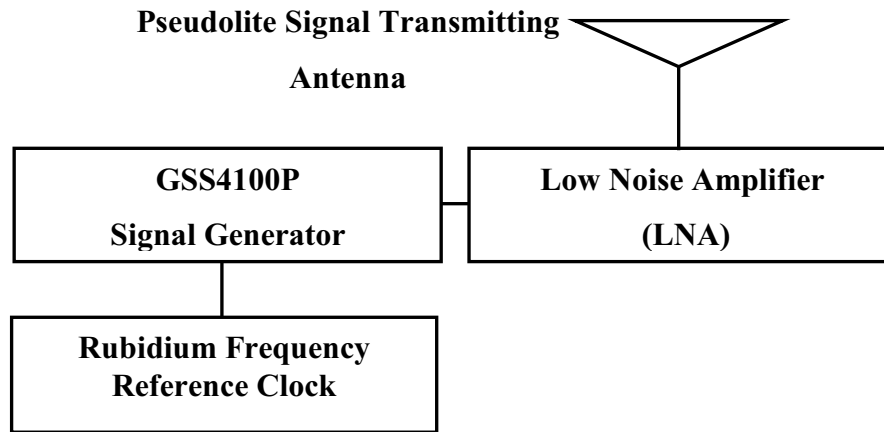


Figure7-1 L1 C/A pseudolites configuration block diagram

### 7.2.2 Airborne Subsystem

The block diagram of the airborne system shown in Figures 7-2 and 7-3 consists of two GPS/pseudolite receivers (NovAtel Millennium) including antennas (#1 and #2), a main processor, an Inertial Navigation System (INS) and a wireless data-link receiver/antenna. The INS is the Boeing C-MIGITS II system, which was described in Chapter 2. The system has two GPS antennae mounted on the aircraft; one upward-looking antenna is mounted on the top of the aircraft, whereas the second is attached to a downward-looking antenna mounted on the belly of the aircraft. Both antennas can be used to track signals from the GPS satellites and pseudolites. There are two configurations in which the subsystem functions as a navigation system: a system using only the top-mounted antenna for tracking both GPS and pseudolites, and a system using the top-mounted antenna for GPS and bottom-mounted antenna for pseudolites. However, note that the flight test results presented in this chapter are processed using the GPS and pseudolite measurements from the receiver connected to the top-mounted antenna only.

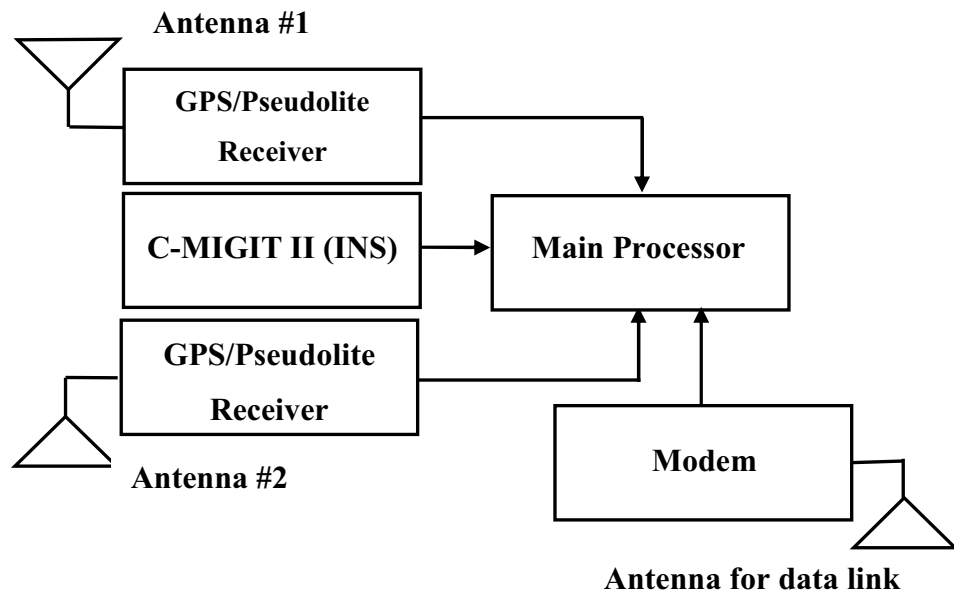


Figure7-2 Airborne subsystem diagram

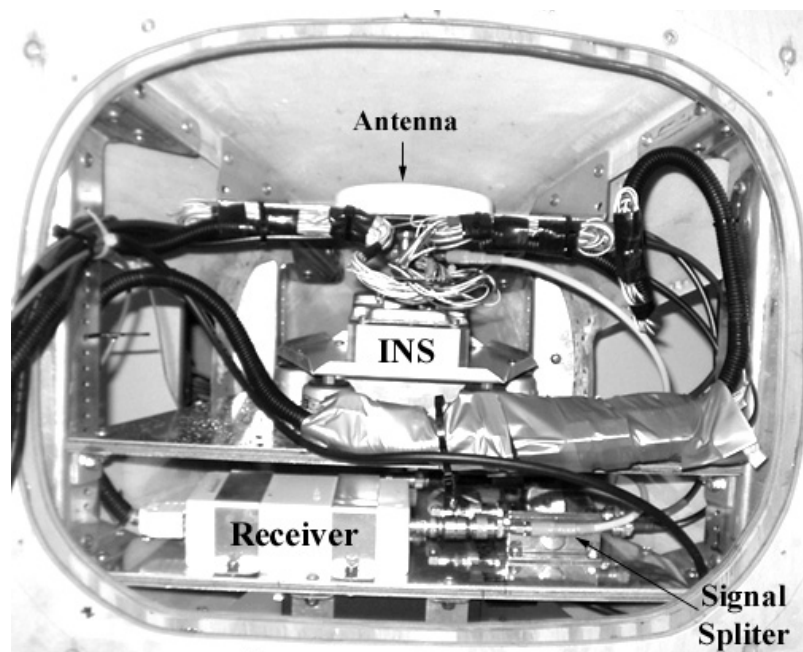


Figure7-3 Airborne system in the aircraft's nose cone

### 7.3 Flight Experiment Design

The Satellite Navigation and Positioning (SNAP) group at The University of New South Wales and DSO National Laboratories, Singapore carried out flight tests at Wedderburn Airfield, Sydney, in April/May 2003, to assess the capabilities and limitations of both integrated GPS/pseudolite and GPS/Pseudolite/INS systems. Figure 7-4 illustrates the setup of the ground subsystem around the runway.

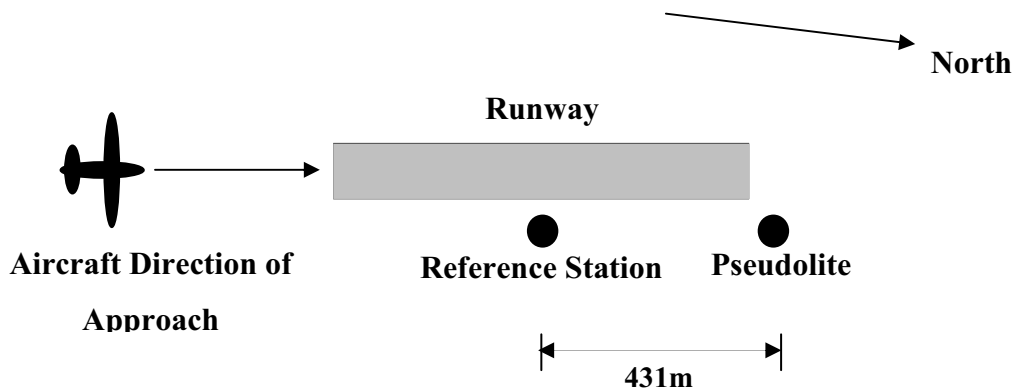


Figure 7-4 Wedderburn Airfield ground configuration (Not to scale)

The location of the pseudolite transmission antenna and the GPS reference antenna were precisely surveyed using Leica GPS system 500 (dual-frequency) receivers, post-processed using the Lieca SKI-Pro software. The ground reference station was set up approximately 431.0m away from the pseudolite system. The power level for the pseudolite transmission was able to support an operational range of approximately 10 – 15km. However, the power level was reduced due to the proximity of the pseudolite signal transmitter to the reference station, since high level power transmission could interrupt the reference station's ability to track GPS signals.

The flight test aircraft used was a Beech Duchess aircraft from the Department of Aviation, The University of New South Wales, as shown in Figure 7-5. Data was collected for three flight days of the test period (29<sup>th</sup> April, 6<sup>th</sup> May and 8<sup>th</sup> May 2003). During these days no changes were made to the ground configuration.



Figure 7-5 Beech Duchess aircraft from the UNSW Aviation Department.

The raw INS sensor and GPS data from the NovAtel Millennium receivers were processed using an in-house software package - the modified version of the AIMS<sup>TM</sup> navigation processing software described in Chapter 3. Note that only L1 measurements were used for the Kalman filter update in this study as the pseudolite system used in the tests transmits single frequency-signals.

The system accuracy cannot be directly evaluated in the kinematic mode, as an accurate reference trajectory is not available. Alternatively, a comparison with the independent trajectory obtained by dual-frequency GPS post-processing using the GrafNav/GrafNet software and the double-differenced (DD) residuals computed from INS-predicted GPS antenna positions are used to analyse the prediction accuracy of the INS. In addition, the RMS errors of the estimated navigation parameters from the Kalman filter (Grejner-Brzezinska et al., 1998b; Lee et al., 2002) are analysed to evaluate the performance of the integrated system. Full satellite measurements were processed to generate the independent trajectory. However, in the integrated GPS/Pseudolite/INS processing, five of these satellites and one pseudolite was used in order to simulate a harsh operational environment. Two different system configurations dependent on using double-

differenced (DD) carrier phase and pseudo-range observations for Kalman filter updating were considered for the data processing and the system evaluation.

#### **7.4 Flight Test Results**

Figure 7-6 depicts the typical trajectory of the aircraft approach during the flight test. A specified period within the data sets, which was from start of the approach (the highest altitude) to the lowest altitude, was selected for the processing in order to evaluate the precise approach and landing system performance. Figure 7-7 illustrates the vertical view of the flight trajectory chosen for data processing. It can be seen from the figure that the highest altitude of the aircraft at the starting point of the approach is approximately 850 metres and the lowest point is about 290 metres. Note that the ellipsoidal height of the reference station is 284.731 metres. In addition, tracking of pseudolite signal began at an altitude of 480.5 metres, at a distance of 3.8 km from the reference station. This is attributed to the fact that the power of the pseudolite signal could not be optimally adjusted because of experiment restriction (i.e., the proximity of the pseudolite signal transmitter to the reference station).

Figure 7-8 shows the RDOP values during the aircraft approach, with/without pseudolite. It can be seen that the RPDOP value is significantly reduced when the pseudolite observable is introduced into the navigation solution. It is interesting to note that the greatest reduction occurs in the RVDOP value, indicating that in the case of airborne application, the inclusion of the pseudolite largely affects the vertical component in the positioning solution. It should be noted that no attempt was made to optimally place the pseudolite transmitter to maximise the signal availability, nor was the time of the day for the flight tests chosen to minimise the VDOP.

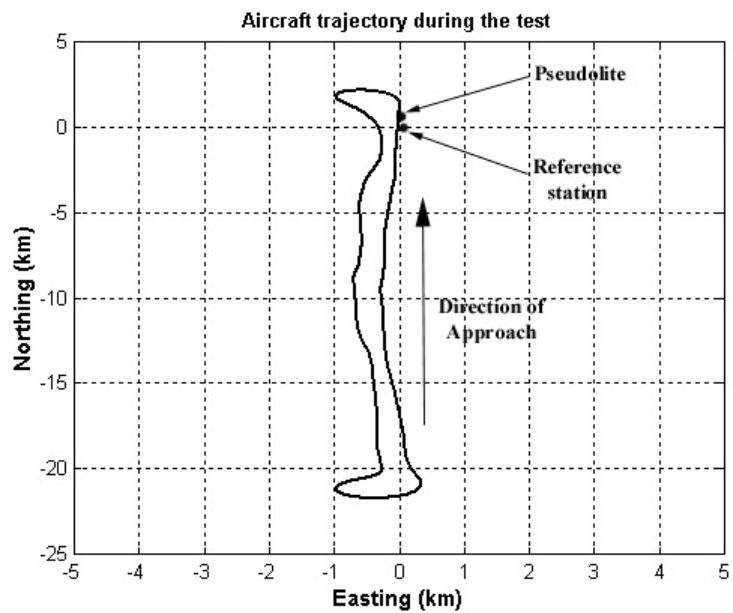


Figure7-6 Plan view of the flight trajectory

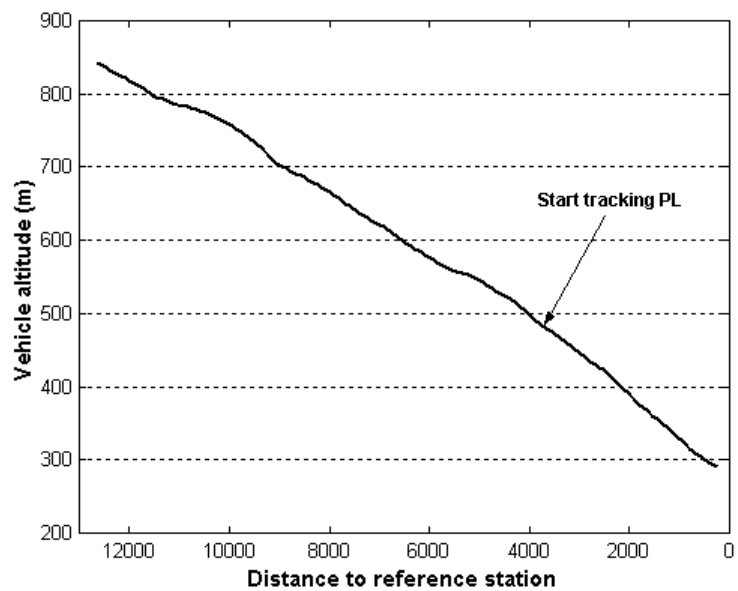


Figure 7-7 Vertical view of the flight trajectory chosen for the data processing



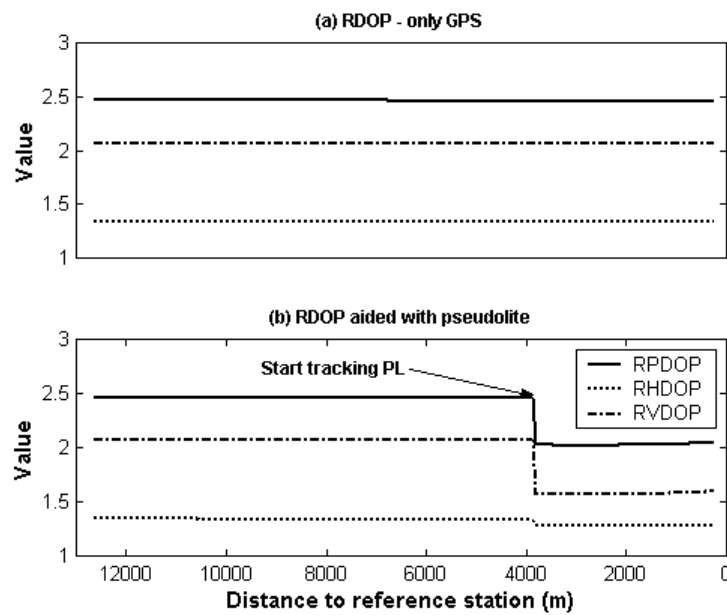


Figure 7-8 RDOP changes of an approach with/without pseudolites

#### 7.4.1 Test Results with Carrier Phase Measurements

Figure 7-9 illustrates positioning performance of GPS/INS and GPS/Pseudolite/INS integrations, obtained from a comparison of the positioning results provided by each of the system with the aforementioned independent trajectory as reference. Carrier phase integer ambiguities are resolved using the technique proposed in Chapter 5. Overall results show that the position differences in both the systems are within a few centimetres, and the differences in the vertical component fluctuate more than the horizontal component (note that different sets of satellites are used in the integrated processing). Two interesting points can be observed from these results. One is the position differences with/without the pseudolites augmentation; the differences in the vertical component are relatively larger than that of the horizontal component, which means the inclusion of pseudolites largely impacts the vertical positioning performance (as demonstrated in the geometry analysis shown in Figure 7-8). The other point observed in Figure 7-9 is that the position difference with/without pseudolite increases when the aircraft gets closer to the runway (i.e., pseudolite signal transmitter). However, the results could be different if the pseudolite location is changed, as demonstrated by the geometry simulations in the Chapter 3. The mean and standard deviation of the

positioning differences obtained from the two different system configurations are tabulated in Table 7-1. It can be seen from the results that a slight improvement in the vertical component (of the order of one centimetre) is achieved with the employment of a pseudolite. On the other hand, Figure 7-10 depicts double-differenced carrier phase residuals for the three satellite pairs computed using the INS-predicted coordinates. Similar to Figure 7-9, these results show that a gap of the two residual sequences obtained from GPS/INS and GPS/Pseudolite/INS configurations becomes larger as the aircraft approaches the pseudolites. Table 7-2 represents the statistics of the residuals. In general, these results indicate that the residuals of the GPS/Pseudolite/INS system are slightly better than those of GPS/INS system (i.e., closer to zero value). Considering the results presented in Figures 7-9 & 10 as well as Tables 7-1 & 2, it can be summarised that the position component accuracy obtained from the GPS/Pseudolite/INS system is slightly better than that of GPS/INS system. However, the accuracy improvement is as much as has been expected from the satellite/pseudolite geometry analysis. This is due to the pseudolite residual errors mainly caused by multipath.

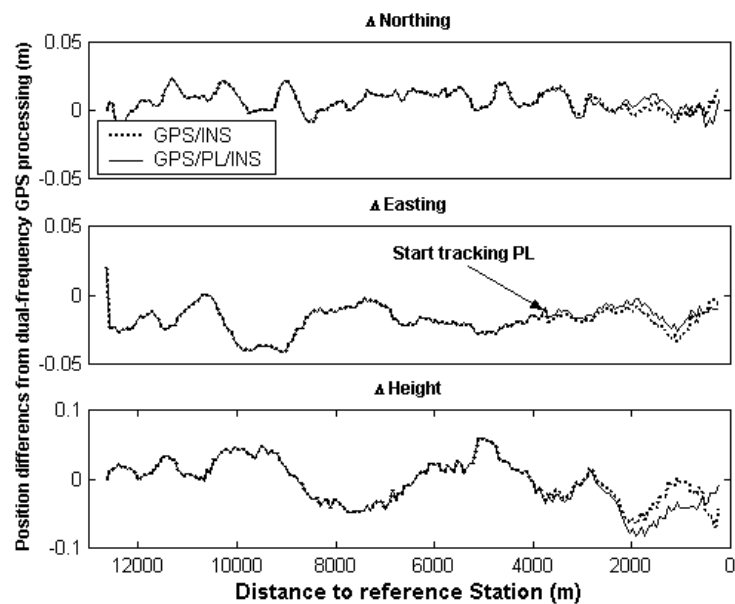


Figure 7-9 Position differences of GPS/INS and GPS/PL/INS systems from the dual-frequency GPS-only processing (with DD carrier phases)

Table 7-1 Comparison of positioning results of GPS/INS and GPS/PL/INS systems based on DD carrier phases with the independent trajectory obtained from dual-frequency GPS processing (unit: cm)

	GPS/INS System		GPS/Pseudolite/INS System	
	Averaged	Std.	Averaged	Std.
$\Delta$ Northing	0.3	0.7	0.4	0.6
$\Delta$ Easting	-1.3	0.5	-1.7	0.7
$\Delta$ Height	3.7	2.4	2.5	2.0

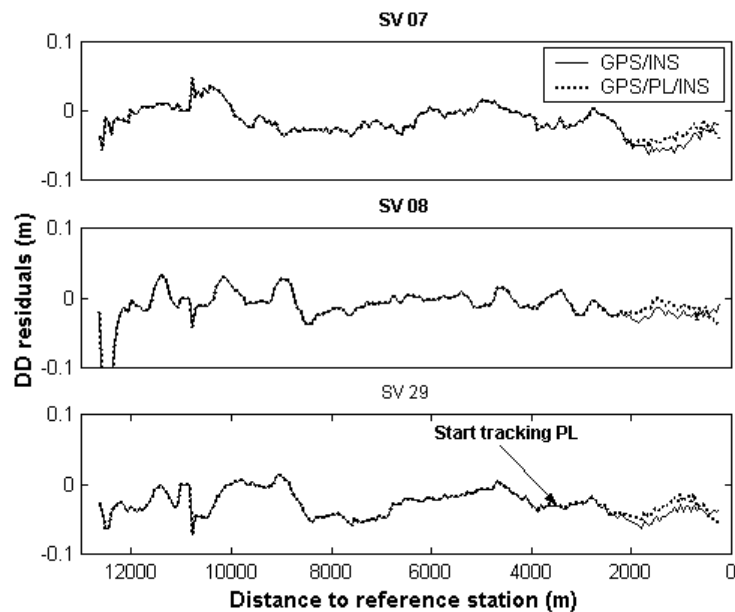


Figure7-10 DD carrier phase residuals of the three highest satellites in GPS/INS and GPS/PL/INS systems

Table 7-2 Averaged and standard deviation of DD carrier phase residuals from the three highest satellites when pseudolite measurements are available (unit: cm)

	GPS/INS System		GPS/Pseudolite/INS System	
	Averaged	Std.	Averaged	Std.
SV 07	-1.5	1.9	-1.4	1.4
SV 08	1.2	1.1	-1.0	1.1
SV 29	2.9	1.0	-2.7	1.0

Figure 7-11 shows the Root-Mean-Square (RMS) error differences between GPS/INS and GPS/Pseudolite/INS systems in the position, velocity, and attitude components, indicating the pseudolite contribution to the Kalman filter estimation procedure. The actual values can be calculated by subtracting the RMSs of GPS/Pseudolite/INS from those of GPS/INS. Therefore, if the performance of the GPS/Pseudolite/INS system were better than that of GPS/INS, the values would be positive, otherwise it would be negative. Note that the RMS values are obtained from the diagonal components of the integration filter's covariance matrix. It can be seen from the figure that the pseudolite augmented results are slightly better (more precise), the greatest improvement is observed in the vertical position component.

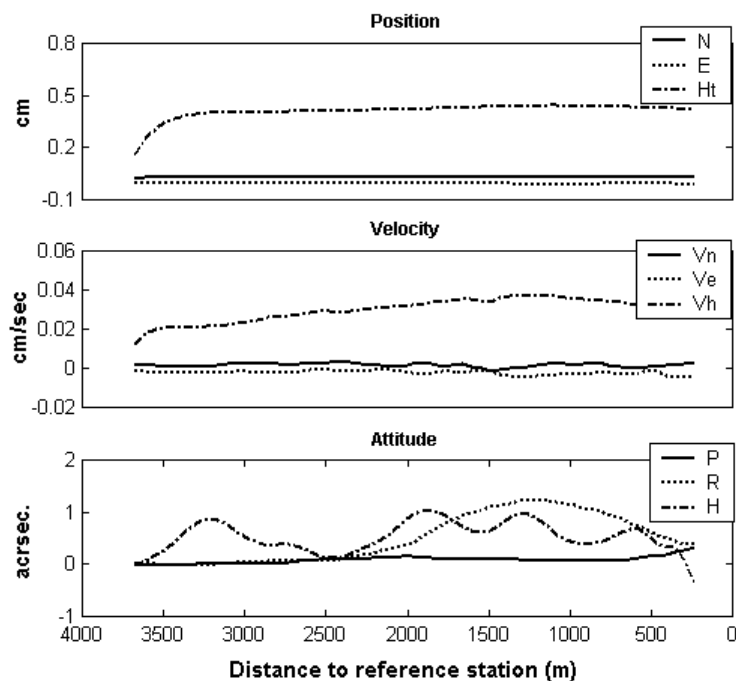


Figure 7-11 RMS difference between GPS/INS and GPS/PL/INS systems in the navigation error estimates (with DD carrier phases)

In addition to the solution accuracy and precision, reliability should be considered in a navigation system design and implementation. As mentioned in Chapter 2, the reliability has two distinct forms: internal and external reliability. The internal reliability is the ability of a system to detect biases in the observations. These biases are referred to as Minimal Detectable Bias (MDB), which describes the size of model errors that can

be detected using the appropriate test statistics. On the other hand, the external reliability is the effect of undetected biases on positioning, which can be computed by propagating the effect of each MDB in the solution. Both the reliabilities are critical for monitoring the navigation solution integrity. Figure 7-12 illustrates the internal and external reliability changes. Even though the inclusion of pseudolite enhances both reliabilities, it is important to note that a significant improvement (e.g., from 28 cm to 6 cm) of the external reliability is in the vertical component. Such an enhancement in the reliability can be described by increased redundancy in the navigation solution. The greater redundancy, the easier it is to detect outliers due to less correlation among the test statistics (see in detail in Hewitson et al., 2004).

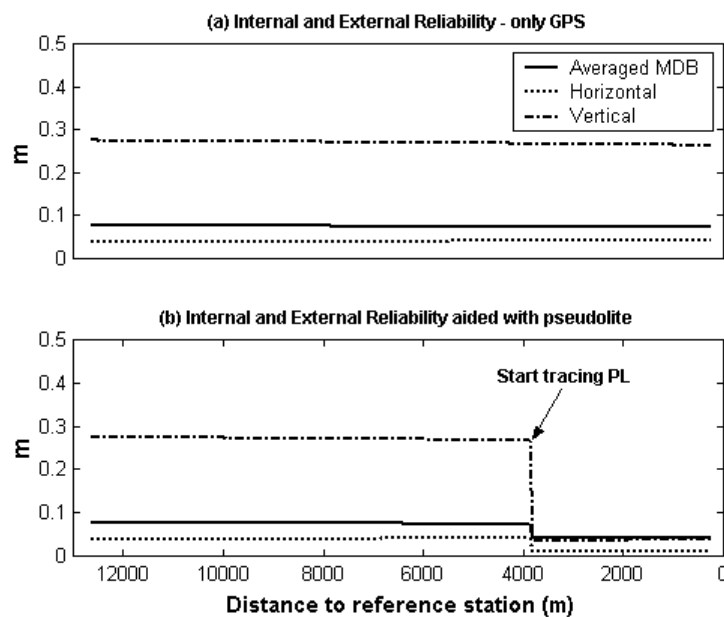


Figure 7-12 Internal and external (horizontal and vertical) reliability values during the approach (with DD carrier phases)

#### 7.4.2 Results with Pseudo-Range Measurements

This subsection presents the processed results using GPS/pseudolite pseudo-range observations for the integration filter update. Performance evaluation and comparison methodologies are identical with the preceding subsection. Figure 7-13 and Table 7-3

depict the position difference of two system configurations (e.g., GPS/INS, GPS/Pseudolite/INS) from an independent trajectory obtained using the dual-frequency GPS-only solution. Figure 7-14 and Table 7-4 show DD pseudo-range residual changes of three high elevation satellites. Furthermore, Figure 7-15 depicts the RMS error differences between GPS/INS and GPS/Pseudolite/INS. High precision is obtained using the DD carrier phase measurements during the initial thirty seconds, which quickly initialises the Kalman filter. The results look similar to those using the carrier phase observations, though there are improvements of around 10 centimetres in the vertical position component, about 0.2 cm/sec in the vertical velocity error estimation, and a couple of arc-seconds in the heading error estimation. On the other hand, Figure 7-16 depicts the reliabilities, and illustrates a dramatic enhancement in the external reliability of the vertical component (an improvement from 23 m to 6 m).

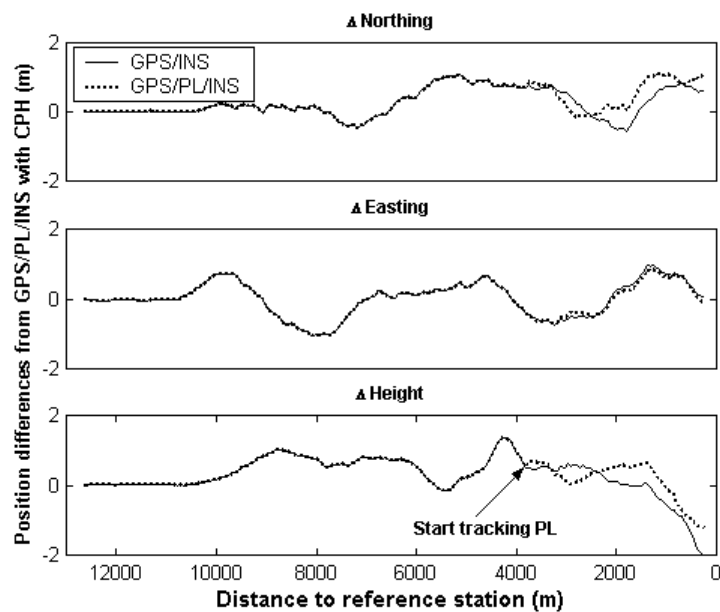


Figure 7-13 Position differences of GPS/INS and GPS/PL/INS systems from the dual-frequency GPS-only processing (with DD pseudo-ranges)

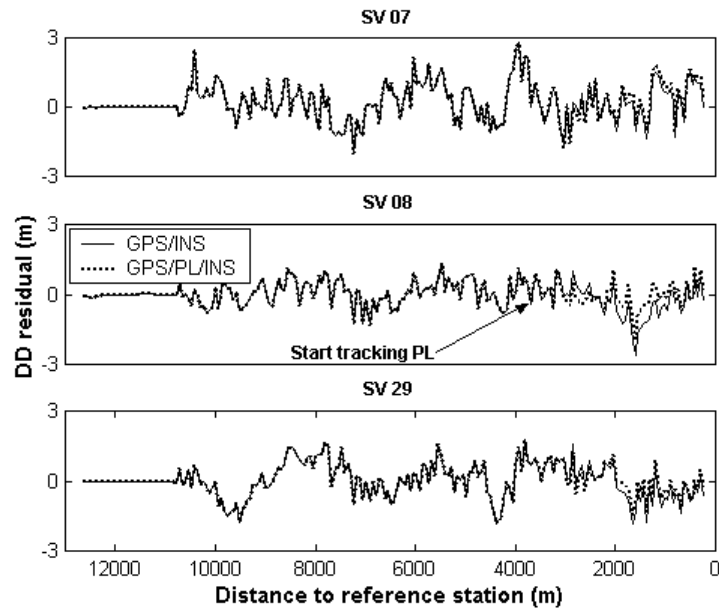


Figure 7-14 DD pseudo-range residuals of the three highest satellites in GPS/INS and GPS/PL/INS systems

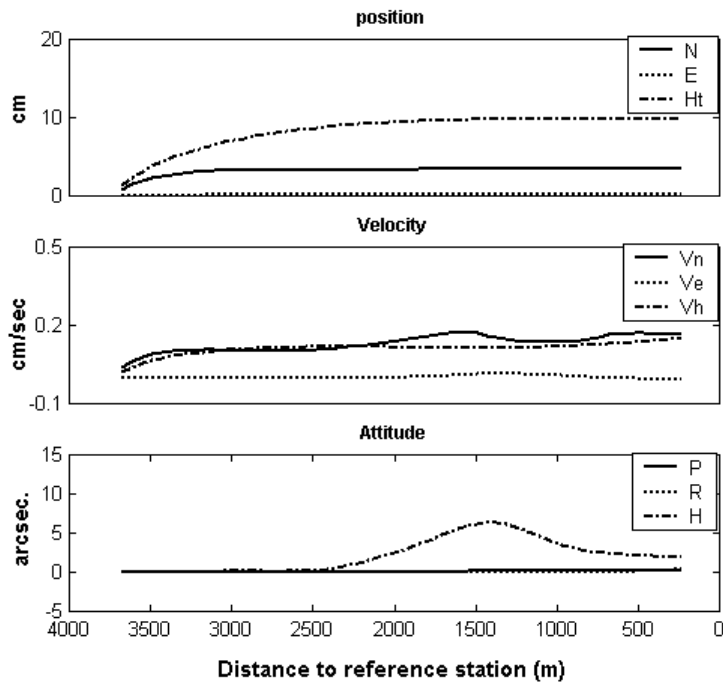


Figure 7-15 RMS difference between GPS/INS and GPS/PL/INS systems in the navigation error estimates (with DD pseudo-ranges)

Table 7-3 Comparison of positioning results of GPS/INS and GPS/PL/INS systems based on DD pseudo-ranges with the independent trajectory obtained from dual-frequency GPS processing (unit: cm)

	GPS/INS System		GPS/Pseudolite/INS System	
	Averaged	Std.	Averaged	Std.
$\Delta$ Northing	30.8	44.7	38.5	44.2
$\Delta$ Easting	7.2	57.4	2.5	51.9
$\Delta$ Height	13.3	72.8	11.4	56.8

Table 7-4 Averaged and standard deviation of DD pseudo-range residuals from the three highest satellites (unit: cm)

	GPS/INS System		GPS/Pseudolite/INS System	
	Averaged	Std.	Averaged	Std.
SV 07	16.0	78.9	22.2	80.7
SV 08	-28.2	73.8	2.4	57.8
SV 29	-9.6	75.9	4.9	64.7

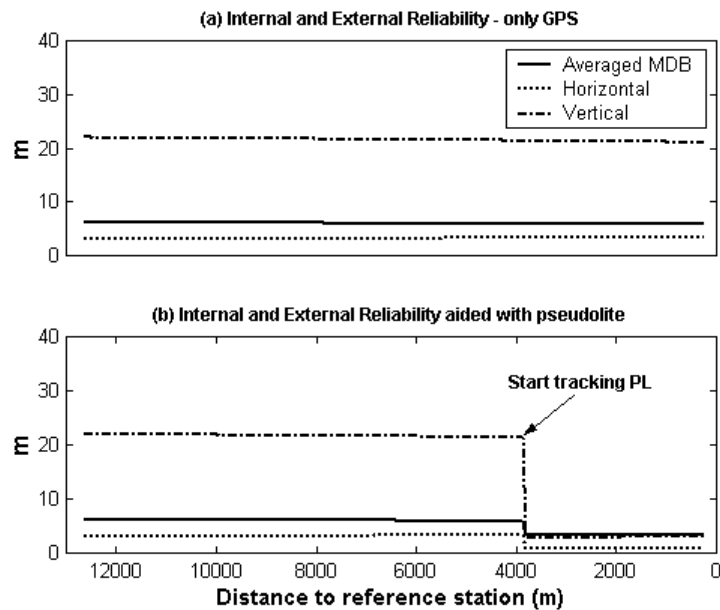


Figure 7-16 Internal and External (horizontal and vertical) Reliability during the approach (with DD pseudo-ranges)

Note that detailed results of the data processing can be found in Appendix D.



## 7.5 Concluding Remarks

The precision and reliability of a satellite-based navigation system to support aircraft precision approach and landing is highly dependent on both the number of visible GPS satellites and their geometric distribution. Integrating pseudolite with GPS/INS is one option to improve these system performances, particularly in poor operational environments. Hence, this chapter has explored the GPS/Pseudolite/INS integration for aircraft precision approach and landing.

In order to evaluate the overall system performance of the airborne GPS/Pseudolite/INS integration system, flight experiments were carried out. The results presented in this chapter have shown that the pseudolite signal can strengthen the signal availability and the satellite geometry. Significant geometry enhancement was observed in the vertical component, resulting in improvement in the aircraft's altitude. However, the actual positioning accuracy improvement in the vertical component was not as much as had been expected from the satellite/pseudolites geometry (e.g., RVDOP), and was relatively smaller than the improvement in the filter estimation precision (e.g., RMS errors). This contradiction seems to be attributed to the impact of pseudolite measurement residual errors mainly caused by multipath. Hence, if such errors are mitigated and/or modelled, it is expected that the positioning accuracy be further improved.

Reliability parameters are critical as they provide a measure for monitoring the navigation solution integrity. The results from the tests have revealed that the inclusion of pseudolite enhances both internal and external reliabilities due to the increased number of redundant measurements. A dramatic improvement in the external reliability of the vertical component was observed.

**8.1 Summary**

Integrated GPS/INS systems have been developed during the past two decades to overcome the inherent drawbacks of each component system, and such integrated systems are popularly used in many kinematic surveying, geodesy and navigation applications that require precise and continuous position, velocity and attitude information. However, the system performance still relies upon the quality of GPS measurements and the satellite geometry. Due to the limited number of GPS satellites, a sufficient number of ‘visible’ satellites cannot be guaranteed at all times and/or locations. Moreover, if GPS signal blockage occurs, the system navigation errors rapidly increase with time (Section 3.2), as the system operation mode is switched to INS stand-alone. Such a scenario is unfortunately a common occurrence for certain kinematic applications. Therefore, the GPS/INS integration with other technologies needs to be considered to strengthen availability, accuracy and integrity of the navigation solution. To address these problems, this study has focussed on an integration of GPS, Pseudolite and INS technologies for high precision kinematic positioning and navigation.

**8.1.1 High Precision Integration of Single-Frequency GPS with Tactical-Grade SDINS**

Although integrated GPS/INS systems using carrier phase observations have been developed for applications of high precision positioning, most of the systems have been implemented using high cost dual-frequency GPS receivers and a navigation-grade INS. In this study, a cost effective GPS/INS integration approach using single-frequency GPS receivers and a tactical-grade SDINS has been developed and tested in Chapter 2. Three field experiments were performed to evaluate the overall system performance and the influence of vehicle dynamics in the filter estimation and navigation accuracy.

The results from the general system performance evaluation have shown that the system is capable of delivering position accuracies at the level of a few centimetres under a benign operational environment, where six GPS measurements are continuously used for the filter updating. On the other hand, results obtained from the tests with the GPS signal blockages have indicated that the INS prediction accuracy is at the sub-decimetres level during the signal blockage lasting up to five seconds, but deteriorates to a few metres after a long blockage of fifty seconds.

The following conclusions can be drawn on the impact analysis of vehicle trajectory & dynamics on the integrated GPS/INS system performance (Section 2.7):

- 1) Vehicle dynamics affect the Kalman filter initialisation time and estimation performance, especially in a heading component.
- 2) The higher the lateral dynamic changes (e.g., the North and East component), the shorter the initialisation time and the more precise the filter estimation.
- 3) A trajectory with the S-turn provides the best system performance for the four trajectories that were considered.

When GPS signal blockages were simulated with respect to each of the designed vehicle trajectories and dynamics, it could be seen that relatively high dynamic changes degraded the system performance. This is because the equilibrant relationship among error parameters in the filter is quickly destroyed, the level of which is dependant on the magnitude of the vehicle dynamic change during the GPS blockages.

### **8.1.2 Integration of Pseudolite Observables with GPS/INS**

A novel kinematic positioning and navigation system based on GPS/Pseudolite/INS integration has been proposed in Chapter 3, to address the drawbacks of the GPS-based positioning and navigation systems. In addition, some of pseudolite measurement modelling issues have been discussed with emphasis on different technical considerations from those of GPS (Section 3.3).

Intensive simulation analyses and field tests have been carried out in order to study the effects of introducing pseudolite measurements on the system performance, in terms of satellite geometric strength, and system accuracy and precision. Based on these analyses, the following conclusions are made:

- 1) The inclusion of pseudolites substantially improves the GPS/INS navigation solutions in terms of precision, reliability, and ambiguity resolution performance. Furthermore the best pseudolite location(s) at a certain time depends on the satellite constellation, and is certainly not continuously the best since satellites are in motion. (Section 3.4)
- 2) Overall, the larger the number of pseudolites, the more accurate the navigation solution is. However, more than three pseudolites used in the GPS/INS system only marginally improve the solution accuracy. The second simulation test ('indoor navigation') demonstrated that pseudolite signals could successfully replace those of satellites in the Kalman filter update (Section 3.5).
- 3) According to field experiments, the two pseudolites included in the GPS/INS system enhanced the precision of positioning, in particular the vertical component. Moreover, the test with simulated GPS signal blockages (under harsh operational environment) demonstrated that the integrated GPS/Pseudolite/INS approach renders centimetre-level accuracy positioning possible, even if there are insufficient GPS signals available (Section 3.6).

### **8.1.3 Impact of Pseudolite Location Errors on Positioning**

Since pseudolites are closely located ('on the ground') to user receivers, their location errors may largely influence positioning solutions. This issue has been studied through theoretical and numerical analysis in Chapter 4, with a view to identifying new characteristics of the impact of the pseudolite location errors on positioning. Taking into account the optimal locations of pseudolites in the tests, the experimental results have shown that the impact of pseudolite location errors in the final solutions could be minimised using a measurement differencing technique. On the contrary, the errors degraded the positioning performance when pseudolites were located at the worst

geometry. As a consequence, the pseudolite sites must be carefully selected, not only to maximise the satellite/pseudolite geometry constellation, but also to minimise the pseudolite location error effects in the position computation. Furthermore, it has been proven from the results that Equation (4.2) could be efficiently used for a thorough analysis of the potential effects of pseudolite location errors for any specific application, thanks to the consistent results between the numerical analysis based on the Equation and simulation tests.

#### **8.1.4 An Integer Ambiguity Resolution Procedure Using Pseudolite and INS**

Since carrier phase measurements are much more precise than pseudo-ranges, the carrier phases are used as primary measurements for updating the integration filter in the proposed GPS/Pseudolite/INS integration. It is a prerequisite, however, that the carrier phase integer ambiguities have to be resolved before they are utilised for the filter updating. In Chapter 5, a new ambiguity resolution procedure using pseudolite observables and an INS-predicted GPS antenna position has been developed and tested. The new procedure adopts stochastic modelling and a statistically rigorous ambiguity validation scheme to enhance the reliability of ambiguity resolution. To study potential benefits of the procedure, a single epoch covariance matrix of float ambiguities within the integrated GPS/Pseudolite/INS system has been derived and discussed in §5.2 and Appendix C.

The following impacts of including pseudolite and INS observations in the AR were determined through simulation studies (Section 5.3):

- 1) The INS predicted-position included in the ambiguity resolution can substantially improve the precision and correlation of the float ambiguities (e.g., enhanced AR performance) as it reduces ADOP values.
- 2) The pseudolite measurements play an import role in the proposed AR procedure, as ADOP values can be largely decreased even if only *one* pseudolite is added to the GPS constellation.

- 3) The relatively rapid change of the line-of-sight vector enhances the performance of the AR process.

The field experiment results have revealed the following aspects of the AR procedure (Section 5.4):

- 1) Stochastic modelling for the satellite and pseudolite measurements is vital to strengthen the AR performance.
- 2) ‘Instantaneous’ AR is feasible if the duration of the signal blockage is within a couple of seconds.
- 3) Even if the signal blockage is up to 50 seconds, the ambiguities can still be fixed within a few tens of seconds, depending on the satellite/pseudolite geometry and the measurements quality.

### **8.1.5 An Effective Cycle Slip Detection and Identification Algorithm**

After being resolved, the integer ambiguities remain constant as long as no loss of signal lock occurs. When a GPS signal loses its lock, the integer counter is reinitialised, and hence a jump in the instantaneous accumulated phase is raised by an integer number of cycles, so-called ‘cycle slip’. In order to maintain high accuracy of carrier phase-based positioning and navigation, the induced cycle slips must be detected and corrected. Hence, an effective cycle slip detection and identification scheme for single-frequency measurements has been developed in Chapter 6, which is used in the architecture of the proposed GPS/Pseudolite/INS integration. The algorithm uses INS-predicted GPS/pseudolites antenna position to generate cycle slip decision signals, and applies a statistical test (e.g., CUSUM) to detect the cycle slip.

The data pre-processing results have revealed that pseudolite signals are more vulnerable to cycle slips than the satellite signals, due to the low pseudolite elevation angles and some obstructions. Moreover, the performance tests have indicated that cycle slips could be effectively detected and instantaneously identified using the proposed algorithm, even if the slips occur at successive epochs.

### **8.1.6 Case Study of GPS/Pseudolite/INS Integration for Aircraft Precision Approach and Landing**

With full GPS operational capability declared in the mid-1990s, the development of a local area augmentation system for GPS has been carried out to establish a precise aircraft landing system, that can fulfil the Required Navigation Performance (RNP) parameters (accuracy, availability, integrity and continuity) for CAT II/III aircraft precision approach and landing. Standalone GPS and conventional code-phase differential GPS are unable to meet the stringent navigation requirements in most airborne applications, because the performance of satellite-based navigation systems are dependent on both the number and geometric distribution of satellites tracked by the receivers. Due to the limited number of GPS satellites, a sufficient number of visible satellites cannot be guaranteed at all times and/or locations. Even if some low elevation satellites are tracked, the measurements from these satellites are contaminated by relatively high atmospheric noise. Hence, the proposed GPS/Pseudolite/INS integration approach would be one option to improve the system performance, particularly in poor operational environments.

Flight tests were conducted in order to evaluate overall system performance of a navigation component in precision aircraft approach and landing (Chapter 7). From the test results it was possible to derive the following conclusions:

- 1) The inclusion of the pseudolite signals can indeed enhance the GPS satellite vertical geometry component, so that remarkable improvement in the navigation solution is observed in the aircraft's altitude. However, the magnitude of the increase from the accuracy assessment is not as much as expected from the satellite/pseudolites geometry and furthermore, was much smaller than that of the filter estimation precision (e.g., RMS errors). This contradiction seems to be attributed to the impact of pseudolite measurement residual errors mainly caused by multipath. Hence if such errors are mitigated and/or modelled, it is expected that further improvement in the accuracy be accomplished.
- 2) The pseudolite signal improves both internal and external reliabilities due to the increase in the redundant measurements. Significant improvement is realised in the

external reliability, especially in the vertical component (e.g., 28 cm to 6 cm and 23 m to 6 m when using carrier phases and pseudo-ranges, respectively).

## 8.2 Recommendations for Future Research

Based on both the theoretical and experimental results obtained in this study, the following recommendations are made for future research work:

- 1) The GPS/Pseudolite/INS integration approach for precise positioning and navigation discussed in this research is operated in the post-processing mode only. However, in order to meet the growing demands for real-time positioning and navigation, a real-time system should be implemented. In real-time systems, the issues of system integrity monitoring and quality control are very important and therefore should be taken into account in the system implementation.
- 2) The GPS/Pseudolite/INS integration through the conventional Kalman filter has shown success in providing centimetre level positioning accuracy. However, it will be possible to achieve a better system performance through improving the filter estimation efficiency. Adaptive filtering can be one option to improve the filter estimation performance, since it tackles the problem of imperfect a priori information on process and measurement noise through a learning process based on the innovation sequence (Mehra, 1970). It will therefore be a challenge to investigate on the advanced estimation techniques for the integrated positioning and navigation.
- 3) Despite performing field experiments with controlled-trajectories (subsection 2.7.1), it is recognised that they are insufficient to profoundly examine their impact on the integration performance. Hence, theoretical and/or simulation studies (e.g., observability analysis and/or covariance simulation) will be useful approaches to further understanding such an impact.



- 4) Pseudolite multipath is still a challenging issue that needs to be addressed for kinematic applications to maximise the usage of pseudolites in positioning and navigation systems (Section 3.3). Note that the accuracy improvement was not as great as expected from the geometry analysis (especially in Chapter 7). Improvement to the hardware, including receivers, receiver antennas and pseudolite transmitter antenna, as well as the development of software-based multipath mitigation techniques will be needed.
- 5) The ambiguity resolution procedure and cycle slip detection/identification algorithm developed in this research (Chapters 5 and 6) are devoted to short baseline applications (less than 15km). It will be a challenge to extend the procedure and algorithm for use in long-baseline applications that must account for atmospheric delay corrections.
- 6) The development of the pseudolites-augmented aircraft precision approach and landing system is still ongoing. It is planned to conduct further tests in the near future. In the next tests, the impact of pseudolite location will be considered to maximise satellite/pseudolite geometry and pseudolite signal acquisition at both reference and mobile receiver, and minimise the impact of pseudolite location errors in navigation solutions.

## REFERENCES

---

---

- Altmayer, C. (2000) Enhancing the integrity of integrated GPS/INS system by cycle slip detection and correction. *IEEE intelligent Vehicles Symposium*, Dearborn, Miami, October 3-5, pp. 174-179.
- Baarda, W. (1968) *A Testing procedure for use in geodesy networks*. Netherlands Geodetic Commission Publications on Geodesy, New Series, 2(5), Delft, Netherlands, 97pp.
- Bar-Itzhak, I. and Berman, N. (1988) Control theoretic approach to Inertial Navigation System. *Journal of AIAA Guidance, Control, and Dynamics*, 11(3), pp. 237-245.
- Barnes, J., Wang, J., Rizos, C. and Tsujii, T. (2002) The performance of a pseudolite-based positioning system for deformation monitoring. *2<sup>nd</sup> Symposium on Geodesy for Geotechnical & Structural Applications*, Berlin, Germany, 21-24 May, pp. 326-327.
- Bartone, C. (1997) Airport pseudolite for precision approach. *10<sup>th</sup> Int. Tech. Meeting of the Satellite Division of the U.S. Inst. of Navigation*, Kansas City, Missouri, 16-19, September, pp. 1719-1728
- Bartrop, K.J., Stafford, J.F. and Elrod, B.D. (1996) Local DGPS with pseudolite augmentation and implementation considerations for LAAS. *9<sup>th</sup> Int. Tech. Meeting of the Satellite Division of the U.S. Inst. of Navigation*, Kansas City, Missouri, 17-20 September, pp. 449-459.
- Basseville, M. (1988) Detecting changes in signals and systems – a survey. *Automatica*, 24(3), pp. 309-326.
- Basseville, M. and Nikiforov, V. (1993) *Detection of Abrupt Changes – Theory and Applications*. Prentice Hall, New Jersey, 441pp.
- Bauersima, I. (1983) *NAVSTAR/Global Positioning Systems (GPS) II*, Mitteilungen der Satellitenbeobachtungsstation Zimmerwald, Nr.10, Astronomical Institute, University of Berne, Switzerland.

- Bevly, D.M., Rekow, A. and Parkinson, B.W. (2000) Comparison of INS vs. carrier-phase DGPS for attitude determination in the control of off-road vehicles, *Navigation, Journal of the U.S. Institute of Navigation*, 47(4), pp. 257-265.
- Beser J. and Parkinson, B.W. (1982) The application of NAVSTAR differential GPS in the civilian community. *Navigation, Journal of the U.S. Institute of Navigation*, 29(2), pp. 107-135.
- Blewitt, G. (1990) An automatic editing algorithm for GPS data, *Geophysical Research Letters*, 17(3), pp. 199-202.
- Porat, B. and Bar-Itzhack, I.Y. (1981) Effects of acceleration switching during INS in-flight alignment. *Journal of AIAA Guidance, Control, and Dynamics*, 4(4), pp. 385-389.
- Boeing Defense and Space Group (1997) *C-MIGITS-II integrated GPS/INS user's guide*. Boeing North American, Anaheim, California, 245pp.
- Britting, K. R. (1971) *Inertial navigation system analysis*. Wiley-Interscience, New York.
- Broxmeyer, C. (1961) *Inertial navigation system*. McGraw-Hill, New York.
- Brown, R. G. and Hwang, P.Y.C. (1992) *Introduction to random signals and applied Kalman filtering*. John Wiley & Sons Inc., 484pp.
- Brunner, F.K. and Welsch, M. (1993) Effect of the troposphere on GPS measurements. *GPS World*, 4(1), pp. 42-51.
- Cannon, M.E. (1987) *Kinematic positioning using GPS pseudoranges and carrier phase observations*. M.Sc. Thesis, Department of Geomatics Engineering, The University of Calgary, Alberta, Canada, 84pp.
- Cross, P.A. (1983) *Advanced Least Squares Applied to Position Fixing*. Working Paper, No. 6, Department of Surveying, Polytechnic of East London, 205pp.
- Cross, P.A., Hawksbee, D.J. and Nicolai, R. (1994) Quality measures for differential GPS positioning. *The Hydrographic Journal*, Hydrographic Society, 72, pp. 17-22.

- Da, R (1997) Investigation of a Low-cost and high-accuracy GPS/IMU system. *ION National Technical Meeting*. Santa Monica, California, 14-16 January, pp. 955-963.
- Dai, L., Wang, J., Tsujii, T. and Rizos, C. (2001) Pseudolite applications in positioning and navigation: modelling and geometric analysis. *International Symposium on Kinematic Systems in Geodesy, Geomatics & Navigation (KIS2001)*, Banff, Canada, 5-8 June, pp. 482-489.
- Dai, L., Wang, J., Rizos, C. and Han, S. (2002) Pseudo-satellite applications in deformation monitoring. *GPS Solutions*, 5(3), pp. 80-87.
- Dedes, G. and Mallett, A. (1995) Effects of the ionosphere and cycle-slips in long baseline dynamic positioning. *Mobile Mapping Symposium*, Columbus, Ohio, May 44-26, pp. 142-152.
- Elrod, B. and Barltrop, K. (1994) Testing of GPS augmented with pseudolites for precision approach applications. *7<sup>th</sup> Int. Tech. Meeting of the Satellite Division of the U.S. Inst. of Navigation*, Salt Lake City, Utah, 20-23, September, pp. 1269-1278.
- Elrod, B.D. and Van Dierendonck, A.J. (1996) *Pseudolites*, In: B.W. Parkinson and J.J. Spilker (eds.), *Global Positioning System: Theory and Applications (Vol. II)*, American Institute of Astronautics, Washington D.C., pp. 51-78.
- Farrell, Jay A. and Barth, M. (1998) *The Global Positioning System & Inertial Navigation*. McGraw-Hill companies, Yew York, 340pp.
- Ford, T., Neumann, J., Tos, N., Petersen, W., Anderson, C., Fenton, P., Holden, T. and Barltrop, D. (1996) HAPPI - High accuracy pseudolite/GPS positioning integration. *9<sup>th</sup> Int. Tech. Meeting of the Satellite Division of the U.S. Inst. of Navigation*, Kansas City, Missouri, 17-20, September, pp. 1719-1728
- Forl, T., Neumann, J., Fenton, P., Bobye, M. and Hamilton, J. (2001) OEM4 Inertial: A tightly integrated decentralised inertial/GPS navigation system, *14<sup>th</sup> Int. Tech. Meeting of the Satellite Division of the U.S. Inst. of Navigation*, Salt Lake City, Utah, 11-14 September, pp. 3153-3163.

- Gao, Y. (1992) *A robust quality control System for GPS navigation and kinematic positioning*. PhD Thesis, Department of Geomatics Engineering, The University of Calgary, Alberta, Canada, 152pp.
- Gao, Y. and Li, Z. (1999) Cycle slip detection and ambiguity resolution algorithms for dual-frequency GPS data processing. *Marine Geodesy*, 22(4), pp. 161-181.
- Goshen-Meskin, D. and Bar-Itzhack, I. Y. (1992a) Unified approach to inertial navigation system error modeling. *Journal of Guidance, Control, and Dynamics*, 15(3), pp. 648-653.
- Goshen-Meskin, D. and Bar-Itzhack, I. Y. (1992b) Observability analysis of piece-wise constant systems –Part I & II. *IEEE Transactions on Aerospace and Electronic Systems*, 28(4), pp. 1056-1067; pp. 1068-1075.
- Greenspan, R.L. (1996) GPS and inertial integration, *In: B.W. Parkinson and J.J. Spilker (eds.), Global Positioning System: Theory and Applications (Vol. II)*, American Institute of Astronautics, Washington D.C., pp. 187-218.
- Grejner-Brzezinska, D., Da, R. and Toth, C. (1998a) GPS error modeling and OTF ambiguity resolution for high-accuracy GPS/INS integrated system. *Journal of Geodesy*, 72, pp. 626-638.
- Grejner-Brzezinska, D., Da, R. and Toth, C. (1998b) Positioning accuracy of the airborne integrated mapping system. *National Technical Meeting of the Institute of Navigation*, Long Beach, California, 21-23 January, pp. 713-721.
- Han, S. (1997) *Carrier phase-based long-range GPS kinematic positioning*. PhD Thesis, School of Surveying and Spatial Information Systems, The University of New South Wales, Sydney, Australia, 185pp.
- Han, S. and Rizos, C. (1997) Comparing GPS ambiguity resolution techniques. *GPS World*, 8(10), pp. 54-61.
- Harrington, R.L. and Dolloff, J.T. (1976) The inverted range: GPS user test facility. *IEEE Position Location and Navigation Symposium (PLANS 76)*, San Diego, California, 1-3 November, pp. 204-211.
- Hein, G. W, Eissfeller, B., Werner, W., Ott, B., Elrod, B.D., Barltrop, K.J. and Stafford, J.F. (1997) Practical investigations on DGPS for aircraft precision approaches

- augmented by pseudolite carrier phase tracking. *10<sup>th</sup> Int. Tech. Meeting of the Satellite Division of the U.S. Inst. of Navigation*, Kansas City, Missouri, 16-19 September, pp. 1851-1860.
- Hawkins, M.D. and Olwell, D.H. (1998) *Cumulative Sum Charts and Charting for Quality Improvement (Statistics for engineering and physical science)*. Berlin/Heidelberg: Springer Verlag, 247pp.
- Henzler, J. and Weiser, M. (1999) Using pseudolites as a flightlanding system. *U.S. Institute of Navigation Annual Meeting*, Cambridge, MA, 28-30, June, pp. 199-207.
- Hewitson, S., Wang, J. and Kearsley, W. (2003) Performance evaluation of inertial navigation systems for surveying. *6<sup>th</sup> Int. Symp. on Satellite Navigation Technology Including Mobile Positioning & Location Services*, Melbourne, Australia, 22-25 July, CD-ROM proc., paper 39.
- Hewitson, S., Lee, H.K. and Wang, J. (2004) Localizability analysis for GPS/Galileo receiver autonomous integrity monitoring. *Journal of Navigation*, 57(2), pp. 245-259.
- Hinkley, D. (1970) Inference about the change point in a sequence of random variables. *Biometrika*, 57(1), pp. 1-17.
- Hofmann-Wellenhof, B., Lichtenegger, H. and Collins, J. (2001) *GPS Theory and Practice*. 5<sup>th</sup> Edition, Springer-Verlag, Wien, 382pp.
- Hopfield, H.S. (1969) Two-quadratic tropospheric refractivity profile for correcting satellite data. *Journal of Geophysical Research*, 74, pp. 4487-4499.
- Kee C.D., Jun, H., Yun, D., Kim, B., Parkinson, B.W., Langestein, T., Pullen, S. and Lee, J. (2000) Development of indoor navigation system using asynchronous pseudolites. *13<sup>th</sup> Int. Tech. Meeting of the Satellite Division of the U.S. Inst. of Navigation*, Salt Lake City, Utah, 19-22 September, pp. 1038-1045.
- Kim, D. and R.B. Langley (2000) GPS ambiguity resolution and validation: Methodologies, trends and issues, *7th GNSS Workshop - International Symposium on GPS/GNSS*, Seoul, Korea, 30 November - 2 December, pp. 213-221.

- Klein D. and Parkinson, B.W. (1984) The use of pseudo-satellites for improving GPS performance. *Global Positioning System (Red book)*, Vol. III, U.S. Institute of Navigation, pp. 135-146.
- Kwon, J.H. and Jekeli, C. (2001) A new approach for airborne vector gravimetry using GPS/INS. *Journal of Geodesy*, 74, pp. 690-700.
- Lachapelle, G., Falkenberg, W., Neufeldt, D. and Keilland, P. (1989) Marine DGPS using code and carrier in a multipath environment. *2<sup>nd</sup> Int. Tech. Meeting of the Satellite Division of the U.S. Inst. of Navigation*, Colorado Springs, Colorado, September 27-29, pp. 343-347.
- Lapucha, D. (1990) *Precise GPS/INS positioning for a highway inventory system*. M.Sc. Thesis, Department of Geomatics Engineering, The University of Calgary, Albert, Canada, 128pp.
- Lee, J.G., Yoon, Y.J., Mark, J.G. and Tazartes, D. A. (1988) Extension of strapdown attitude algorithm for high-frequency base motion. *Journal of AIAA Guidance, Control, and Dynamics*, 12(2), pp. 738-743.
- Lee, H.K., Wang, J., Rizos, C., Grejner-Brzezinska, D. and Toth, C. (2002) GPS/Pseudolite/INS integration: concept and first tests. *GPS Solutions*, 6(1-2), pp. 34-46.
- Leick, A. (1995) *GPS Satellite Surveying*. 2<sup>nd</sup> edition, John Wiley & Sons, Inc., New York, 560pp.
- LeMaster E.A. and Rock, S. (1999) Mars exploration using self-calibrating pseudolite arrays. *12<sup>th</sup> Int. Tech. Meeting of the Satellite Division of the U.S. Inst. of Navigation*, Nashville, Tennessee, 14-17 September, pp. 1549-1558.
- Lück T., Löhnert, E., Eissfeller, B. and Meinke, P. (1997) Track irregularity measurement using an INS-GPS integration technique. *10<sup>th</sup> Int. Tech. Meeting of the Satellite Division of the U.S. Inst. of Navigation*, Nashville, Tennessee, 16-19 September, pp. 71-78.
- Maybeck, P. S. (1979) *Stochastic models, estimation, and control*. Volume I, Academic Press, 397pp.

- Mehra, R.K. (1970) On the identification of variance and adaptive Kalman filtering. *IEEE Transactions on Automatic Control*, 15(2), pp. 175-184.
- Mertikas, S.P. (2001) Automatic and on-line detection of small but persistent shifts in GPS station coordinates and statistical process control. *GPS Solutions*, 5(1), pp. 39-50.
- Mertikas, S.P. and Rizos, C. (1997) Online detection of abrupt changes in the carrier phase measurements of GPS. *Journal of Geodesy*, 71, pp. 469-482.
- Michalson W.M. and Proгри, I.F. (2000) Assessing the accuracy of underground positioning using pseudolites. *13<sup>th</sup> Int. Tech. Meeting of the Satellite Division of the U.S. Inst. of Navigation*, Salt Lake City, Utah, 19-22 September, pp. 1007-1015.
- Mikhail, E.M. (1976) *Observations and Least Squares*, Dun-Donnelley Publisher, New York, 497pp.
- Morley T. and Lachapelle, G. (1997) GPS augmentation with pseudolites for navigation in constricted waterways. *Navigation, Journal of U.S. Institute of Navigation*, 44(3), pp. 359-372.
- Moore, M., Rizos, C. and Wang, J. (2002) Quality control issues relating to an attitude determination system using a multi-antenna GPS array. *Geomatics Research Australasia*, 77, pp. 27-48.
- NovAtel (1993) *GPS Card<sup>TM</sup> user manual*. Novatel Communications Ltd.
- Ogaja, C. (2002) *A framework in support of structural monitoring by RTK-GPS and multisensor data*. PhD Thesis, School of Surveying and Spatial Information Systems, The University of New South Wales, Sydney, Australia, 207pp.
- O'Keefe, K., Sharma, J., Cannon, M.E. and Lachapelle, G. (1999) Pseudolite-based inverted GPS concept for local area positioning. *12<sup>th</sup> Int. Tech. Meeting of the Satellite Division of the U.S. Inst. of Navigation*, Nashville, Tennessee, 20-23 September, pp. 1523-1530.
- Parkinson, B.W. and Spilker, Jr., J.J. (eds.) (1996). *Global Positioning System: Theory and Applications (Vol. 1)*. American Institute of Aeronautics and Astronautics, Inc., Washington D.C., 793pp.



- Parkinson, B.W. and Enge, P. K. (1996). Differential GPS, In *Global Positioning System: Theory and Applications (Vol. 2)*. Edited by Parkinson and Spilker, American Institute of Aeronautics and Astronautics, Inc., Washington D.C., pp. 3-50.
- Pervan, B.S. (1996) *Navigation integrity for aircraft precision landing using the Global Positioning System*, Ph.D. Thesis, Department of Aeronautics and Astronautics, Stanford University, 170pp.
- Ray, J.K. (2000) *Mitigation of GPS code and carrier phase multipath effects using multi-antenna system*. PhD Thesis, Department of Geomatics Engineering, The University of Calgary, Alberta, Canada, 260pp.
- Rhee, I., Abdel-Hafea, M. F. and Speyer, J. L. (2002) On the observability of an integrated GPS/INS during maneuvers. *15<sup>th</sup> Int. Tech. Meeting of the Satellite Division of the Institute of Navigation*, 24-27, September, Portland, Oregon, pp. 1489-1499.
- Rizos, C. (1996) *Principles and Practice of GPS Surveying*. Monograph 17, School of Surveying and Spatial Information Systems, The University of New South Wales, Sydney, Australia, 555pp.
- Rizos, C. (1999) *Quality issues in real-time GPS positioning*. Final Report of the IAG SSG 1.154 (at [http://www.gmat.unsw.edu.au/ssg\\_RTQC/ssg\\_rtqc.pdf](http://www.gmat.unsw.edu.au/ssg_RTQC/ssg_rtqc.pdf)).
- Rizos C. and Satirapod, C. (2001) GPS with SA off: How good is it ? *Measure & Map*, 12, pp. 19-21.
- Rogers, R.M. (2000) *Applied mathematics in integrated navigation systems*. American Institute of Aeronautics and Astronautics, 300pp.
- Saastamoinen, J. (1973) Contributions to the theory of atmospheric refraction. *Bulletin Geodesique*, 197, pp. 13-34.
- Savage, P.G. (1983) *Introduction of inertial navigation systems*, Supplemental material, Geomatics Engineering Department, The University of Calgary, Canada.
- Savage, P.G. (2000a) *Strapdown Analytics: Part I*. Strapdown Associates, Inc., 773pp.
- Savage, P.G. (2000b) *Strapdown Analytics: Part II*, Strapdown Associates, Inc., 650pp.

- Schwarz, K.P., El-Sheimy, N. and Liu, Z. (1994). Fixing GPS cycle slips by INS/GPS – method and experience, *Int. Symp. on Kinematic Systems in Geodesy, Geomatics and Navigation*, Banff, Canada, 30 August – 2 September, pp. 265-275.
- Seeber, G. (1993) *Satellite Geodesy: Foundations, Methods & Applications*. Walter de Gruyter, Berlin New York, 531pp.
- Spilker, Jr., J. J. (1996) Tropospheric effects on GPS. In: Parkinson, B.W et al. (eds.), *Global Positioning System: Theory and Applications, Progress in Astronautics & Aeronautics*, 163, pp. 517-546.
- Stone M.J. and Powell, J.D. (1998) Precise positioning with GPS near obstructions by augmentation with pseudolites. *IEEE PLANS '98, Position Location and Navigation Symposium*, Palm Springs, California, pp. 526-569.
- Stone M.J. and Powell, J.D. (1999) Precise positioning using GPS satellite and pseudolites emphasising open-pit mining applications. *4<sup>th</sup> Int. Symp. on Satellite Navigation Technology & Applications*, Brisbane, Australia, 11-15 April, pp. 562-573.
- Teunissen P.J.G. (1993) A new method for fast carrier phase ambiguity estimation. *IEEE PLANS '93, Position Location and Navigation Symposium*, Las Vegas, 11-15 April, pp. 562-573.
- Teunissen, P.J.G. (1997). A canonical theory for short GPS baselines (Part I-IV). *Journal of Geodesy*, 71, 320-336, 389-401, 486-501, pp. 513-525.
- Teunissen, P.J.G. and Odijk, D. (1997) Ambiguity dilution of precision: definition, properties and application, *10<sup>th</sup> Int. Tech. Meeting of the Satellite Division of the Institute of Navigation*, 16-19 September, Kansas City, MO, pp. 891-900.
- Teunissen P.J.G. (1998). Success probability of integer GPS ambiguity rounding and bootstrapping. *Journal of Geodesy*, 72, pp. 606-612.
- Tiberius, C.C.J.M. (1998). Quality control in positioning, *The Hydrographical Journal*, 90, 3-8.

- Tiberius, C.C.J.M. and de Jonge, P.J. (1995). Fast positioning using the LAMBDA-method, *4<sup>th</sup> Int. Conference on Differential Satellite Navigation System*, Bergen, Norway, 24-28 April, Paper No. 30.
- Townsend, B., Fenton, P., Van Dierendonck, K. and Van Nee, R. (1995) Performance evaluation of the Multipath Eliminating Delay Lock Loop. *Navigation, Journal of the Institute of Navigation*, 42(3), pp. 503-514.
- Tsujii, T., Rizos, C., Wang, J., Dai, L., Roberts, C. and Harigae, M. (2001) A navigation/positioning service based on pseudolites installed on stratospheric airships. *5<sup>th</sup> Int. Symp. on Satellite Navigation Technology & Applications*, Canberra, Australia, 24-27 July, CD-ROM proc., paper 49.
- Van Dierendonck, A.J., Fenton, P. and Ford, T. (1992). Theory and performance of a narrow correlator spacing in a GPS receiver. *Navigation, Journal of the Institute of Navigation*, 39(3), pp. 265-283.
- Wang J, Stewart, M.P. and Tsakiri, M. (1998) A discrimination test procedure for ambiguity resolution on-the-fly. *Journal of Geodesy*, 72, pp. 644-653.
- Wang J, Stewart, M.P. and Tsakiri, M. (1999) A comparative study of the integer ambiguity validation procedures. *Earth, Planets & Space*, 52(10), pp. 813-817.
- Wang, J. (1999) *Modelling and quality control for precise GPS and GLONASS satellite positioning*. PhD thesis, School of Spatial Sciences, Curtin University of Technology, Perth, Australia, 171 pp.
- Wang, J., Tsujii, T., Rizos, C., Dai, L. and Moore, M. (2000) Integrating GPS and pseudolite signals for position and attitude determination: Theoretical analysis and experiment results. *13<sup>th</sup> Int. Tech. Meeting of the Satellite Division of the U.S. Inst. of Navigation*, Salt Lake City, Utah, 19-22 September, pp. 2252-2262.
- Wang, J., Tsujii, T., Rizos, C., Dai, L. and Moore, M. (2001a) GPS and pseudo-satellites integration for precise positioning. *Geomatics Research Australasia*, 74, pp. 103-117.
- Wang, J., Dai, L., Tsujii, T., Rizos, C., Grejner-Brzezinska, D. and Toth, C.K. (2001b) GPS/INS/Pseudolites: Concepts, simulation and testing. *14<sup>th</sup> Int. Tech.*

- Meeting of the Satellite Division of the U.S. Inst. of Navigation*, Salt Lake City, Utah, 11-14 September, pp. 2708-2715.
- Wang, J. and Lee, H.K. (2002) Impact of pseudolite location errors in positioning. *Geomatics Research Australasia*, 77, pp. 81-94.
- Wang, J. (2002) Applications of pseudolites in geodetic positioning: Progress and problems. *Journal of Global Positioning Systems*, 1(1), pp. 48-56.
- Wang, J., Lee, H.K., Hewitson, S. and Lee, H.K. (2003a) Influence of dynamics and trajectory on integrated GPS/INS navigation performance. *Presented in GNSS2003*, Graz, Austria, 22-25 April, CD-ROM proc.
- Wang, J., Lee, H.K., Hewitson, S., Rizos, C. and Barnes, J. (2003b) Sensitivity analysis for GNSS integer carrier phase ambiguity validation test. *Presented in XXIIIth General Assembly of the IUGG*, Sapporo, Japan, 30 June - 11 July, CD-ROM proc.
- Wawrzyniak G., Lightsey, E.G. and Key, K.W. (2001) Ground experimentation of a pseudolite-only method for the relative positioning of two spacecraft. *14th Int. Tech. Meeting of the Satellite Division of the U.S. Inst. of Navigation*, Salt Lake City, Utah, 11-14 September, pp. 1436-1478.
- Wei, M., Cannon, M.E. and Schwarz, K.P. (1992) Maintaining high accuracy GPS positioning 'on the fly'. *IEEE PLANS '92, Position Location and Navigation Symposium*, March 23-27, pp. 403 -411.
- Weiser, M. (1988) Development of a carrier and C/A-code based pseudolite system, *11<sup>th</sup> Int. Tech. Meeting of the Satellite Division of the U.S. Inst. of Navigation*, Nashville, USA, 15-18, September, pp. 1465-1475.
- Wells D.E., Beck, N., Delikaragolou, D., Kleusberg, A., Krakiwsky, E.J., Lachapelle, G., Langley, R.B., Nakiboglu, M., Schwarz, K.P., Tranquilla, J.M. and Vanicek, P. (1987) *Guide to GPS positioning*. 2<sup>nd</sup> corrected printing, Canadian GPS Associates, Fredericton, New Brunswick, Canada, 503pp.
- Zimmerman, K.R., Cohen, C.E., Lawrence, D.G., Montgomery, P.Y., Cobb, H.S. and Melton, W.C. (2000), *11<sup>th</sup> Int. Tech. Meeting of the Satellite Division of the U.S. Inst. of Navigation*, Salt Lake City, Utah, 19-22 September, pp.1024-1033.

**APPENDIX A**

**DERIVATION OF NAVIGATION EQUATIONS FOR STRAPDOWN  
INERTIAL NAVIGATION SYSTEM**

---

In this section, the continuous form of dynamic equations for Strapdown INS navigation parameters are derived. The main references for the following derivation are Farrell and Barth (1998), Savage (2000a), and Rogers (2000).

**A.1 Velocity Equation**

The velocity data in an inertial navigation system is typically computed as an integration of velocity rate described in the  $n$ -frame. The velocity vector  $v^n$  in the rotating  $n$ -frame is defined as the position change rate in the  $e$ -frame  $\dot{r}^e$  and the rotation matrix between two frames  $R_e^n$ :

$$v^n \equiv R_e^n \dot{r}^e \tag{A.1}$$

where  $r^e$  is the position vector of the interest point in the  $e$ -frame.

The derivate of Equation (A.1) yields:

$$\dot{v}^n = \dot{R}_e^n \dot{r}^e + R_e^n \ddot{r}^e \tag{A.2}$$

The position vector  $r^e$  can be written as a function of  $r$  vector in a non-rotating  $i$ -frame:

$$r^e = R_i^e r^i \tag{A.3}$$

The time derivative of Equation (A.3) is:

$$\dot{r}^e = \dot{R}_i^e r^i + R_i^e \dot{r}^i \tag{A.4}$$

The time rate change of the rotation matrix  $R_i^e$  is (Savage 2000; Farrell and Barth, 1998):

$$\dot{R}_i^e = R_i^e \Omega_{ei}^i = -\Omega_{ie}^e R_i^e = -R_i^e \Omega_{ie}^i \quad (\text{A.5})$$

where  $\Omega_{ei}^i$  is the skew-symmetric form of an angular velocity vector of  $i$  (*subscripted*) - frame with respect to  $e$ -frame coordinated in  $i$  (*superscripted*) - frame.

Substituting Equation (A.5) into (A.4) results in:

$$\dot{r}^e = R_i^e \dot{r}^i - R_i^e \Omega_{ie}^i r^i = R_i^e [\dot{r}^i - \Omega_{ie}^i r^i] \quad (\text{A.6})$$

The derivative of Equation (A.6) results in:

$$\begin{aligned} \ddot{r}^e &= \dot{R}_i^e [\dot{r}^i - \Omega_{ie}^i r^i] + R_i^e [\ddot{r}^i - \dot{\Omega}_{ie}^i r^i - \Omega_{ie}^i \dot{r}^i] \\ &= -R_i^e \Omega_{ie}^i [\dot{r}^i - \Omega_{ie}^i r^i] + R_i^e [\ddot{r}^i - \dot{\Omega}_{ie}^i r^i - \Omega_{ie}^i \dot{r}^i] \end{aligned} \quad (\text{A.7})$$

Assuming that the Earth's rotation rate is constants, namely  $\dot{\Omega}_{ie}^i = 0$ ,

$$\ddot{r}^e = R_i^e [\ddot{r}^i - 2\Omega_{ie}^i \dot{r}^i + \Omega_{ie}^i \Omega_{ie}^i r^i] \quad (\text{A.8})$$

The above Equation (A.8) describes how the total acceleration vector  $\ddot{r}^i$  in the non-rotating  $i$ -frame is transformed to the rotating  $e$ -frame. It should be noted that the first, second (including the negative sign) and third term in brackets represents the inertial acceleration, *Coriolis* acceleration, and the local centrifugal acceleration respectively.

Substituting Equation (A.6), (A.8), and the time rate change of the rotation matrix  $R_e^n$  using Equation (A.5) relationship into Equation (A.2) yields:

$$\dot{v}^n = R_i^n [\ddot{r}^i - (\Omega_{en}^i + 2\Omega_{ie}^i) R_n^i v^n - \Omega_{ie}^i \Omega_{ie}^i r^i] \quad (\text{A.9})$$

The above Equation (A.9) describes how the total acceleration vector  $\ddot{r}^i$  in the non-rotating  $i$ -frame is transformed to the rotating the  $n$ -frame. Note that *Coriolis* acceleration term caused by  $n$ -frame rotation with respect to the  $e$ -frame is added, compared with Equation (A.8).

The  $\ddot{r}^i$  term in Equation (A.9) is the total acceleration in the  $i$ -frame. However, as discussed in § 1.2.1, accelerometers measure the specific force, instead of the total acceleration, due to the basic limitations of fundamental physics. The specific  $f^n$  sensed in the accelerometer is expressed as:

$$f^n = R_i^n \ddot{r}^i - G^n \quad (\text{A.10})$$

with:

$$G^n = g^n + \Omega_{ie}^n \Omega_{ie}^n r^n = g^n + R_i^n \Omega_{ie}^i R_n^i R_i^n \Omega_{ie}^i R_n^i r^n$$

where  $g^n$  and  $\Omega_{ie}^n \Omega_{ie}^n r^n$  is the gravity and centripetal acceleration term in  $n$ -frame respectively.

Through manipulating Equation (A.10), the total acceleration in the  $i$ -frame can be expressed as follows:

$$\ddot{r}^i = R_n^i (f^n + g^n) + \Omega_{ie}^i \Omega_{ie}^i r^i \quad (\text{A.11})$$

Substituting Equation (A.11) into (A.9) results in:

$$\begin{aligned} \dot{v}^n &= R_i^n \left[ R_n^i (f^n + g^n) + \Omega_{ie}^i \Omega_{ie}^i r^i - (\Omega_{en}^i + 2\Omega_{ie}^i) R_n^i v^n - \Omega_{ie}^i \Omega_{ie}^i r^i \right] \\ &= f^n - (\Omega_{en}^n + 2\Omega_{ie}^n) v^n + g^n \end{aligned} \quad (\text{A.12})$$

where  $\Omega_{en}^n$  is the skew-symmetric form of the  $n$ -frame rotation rate vector  $\omega_{en}^n$  with respect to the  $e$ -frame coordinated in the  $n$ -frame, and  $\Omega_{ie}^n$  is the skew-symmetric form of the  $e$ -frame rotation rate vector  $\omega_{ie}^n$  with respect to the  $i$ -frame coordinated in the  $n$ -frame. This is the dynamic equation in the continuous form that describes INS velocity evolution in the navigation (Local-Geodetic) frame.

## A.2 Position Equation

The position vector  $r^n$  in a navigation frame can be written as a function of  $r$  vector in the  $e$ -frame with a rotation matrix between two frames  $R_e^n$ :

$$r^n = R_e^n r^e \quad (\text{A.13})$$

After differentiating Equation (A.13) with respect to time, substituting the time rate change of the rotation matrix  $R_e^n$  using Equation (A.5) relationship yields:

$$\begin{aligned} \dot{r}^n &= \dot{R}_e^n r^e + R_e^n \dot{r}^e \\ &= -\Omega_{en}^n R_e^n r^e + R_e^n \dot{r}^e \\ &= -\Omega_{en}^n r^n + v^n \end{aligned} \quad (\text{A.14})$$

This is the dynamic position equation in the continuous form that describes INS position evolution in the navigation (Local-Geodetic) frame.

## A.3 Attitude Equation

The continuous form of the attitude dynamic equation for a strapdown INS can be expressed using Equation (A.5):



$$\dot{R}_b^n = R_b^n \Omega_{nb}^b \quad (\text{A.15})$$

On the other hand, the dynamic equation can be defined in terms of the individual inertial angular rate of the  $b$ -frame and the  $n$ -frame. First of all, the rotation matrix  $R_b^n$  can be rewritten as:

$$R_b^n = R_i^n R_b^i \quad (\text{A.16})$$

and then the derivative of Equation (A.16) becomes:

$$\dot{R}_b^n = R_i^n \dot{R}_b^i + \dot{R}_i^n R_b^i \quad (\text{A.17})$$

According to Equation (A.5), Equation (A.17) can be manipulated as:

$$\begin{aligned} \dot{R}_b^n &= R_i^n R_b^i \Omega_{ib}^b - \Omega_{in}^n R_i^n R_b^i \\ &= R_b^n \Omega_{ib}^b - \Omega_{in}^n R_b^n \end{aligned} \quad (\text{A.18})$$

where  $\Omega_{ib}^b$  and  $\Omega_{in}^n$  is the skew-symmetric form of the angular velocity vector  $\omega_{ib}^b$  in the  $body$  frame sensed by gyroscopes and the  $n$ -frame rotation rate vector  $\omega_{in}^n$  with respect to the  $i$ -frame coordinated in the  $n$ -frame.

## APPENDIX B

### A NUMERICAL QUATERNION-UPDATING ALGORITHM

---

The time differential attitude equation in § 2.2 can be expressed by using a quaternion:

$$\dot{q}_b^n = \frac{1}{2} q_b^n w_{ib}^b - \frac{1}{2} w_{in}^n q_b^n \quad (\text{B.1})$$

where  $w_{ib}^b$ ,  $w_{in}^n$  are quaternion equivalents to  $\omega_{ib}^b$ ,  $\omega_{in}^n$  as indicated below.

$$w_{ib}^b = \begin{bmatrix} 0 \\ \omega_{ib}^b \end{bmatrix}, \quad w_{in}^n = \begin{bmatrix} 0 \\ \omega_{in}^n \end{bmatrix} \quad (\text{B.2})$$

A quaternion for a certain time can be calculated either by integrating the continuous form of Equation (B.1), or by numerical (or digital) quaternion updating algorithm based on two-speed approach. Although the results from both methods are identical, many modern SDINSs use the latter in order to minimise truncation errors in numerical computation and to improve the computation speed. The quaternion-updating algorithm comprises *body frame rotation update* and *navigation frame rotation update*. The former is carried out with  $w_{ib}^b$ , while the latter is performed based on  $w_{in}^n$ . Note that it is not necessary to update the navigation frame rotation at the same instant when the body frame rotation update occurs, since the navigation frame rotation is much slower than that of the body frame. Hence the body frame updates are five to ten times faster than the navigation frame updates.

#### B.1 Body Frame Rotation Update

The updating for the body frame rotation is performed as:

$$q_b^n(j) = q_b^n(j-1)q_i^b(j) \quad (\text{B.3})$$

where

- $q_b^n(j)$  quaternion representing a relation between the  $b$ -frame and the  $n$ -frame at  $j^{\text{th}}$  epoch
- $q_b^n(j-1)$  quaternion representing a relation between the  $b$ -frame and the  $n$ -frame at  $j-1^{\text{th}}$  epoch
- $q_i^b(j)$  attitude quaternion taking into account for the  $b$ -frame rotation with respect to the  $i$ -frame

After integrating angular velocities measured by gyroscopes  $\omega_{ib}^{b_x}$ ,  $\omega_{ib}^{b_y}$ ,  $\omega_{ib}^{b_z}$  to rotation angles  $\Phi_x$ ,  $\Phi_y$ ,  $\Phi_z$ , the quaternion  $q_i^b(j)$  is constructed as:

$$q_i^b(j) = \begin{bmatrix} \cos \frac{\Phi}{2} \\ \frac{\sin 0.5\Phi}{\Phi} \Phi_x \\ \frac{\sin 0.5\Phi}{\Phi} \Phi_y \\ \frac{\sin 0.5\Phi}{\Phi} \Phi_z \end{bmatrix} \quad (\text{B.4})$$

with

$$\Phi = \sqrt{\Phi_x^2 + \Phi_y^2 + \Phi_z^2}$$

Thus, an operation for the Equation (B.3) is made according to the quaternion product rule as:

$$q_b^n(j) = \begin{bmatrix} q_0 & -q_1 & -q_2 & -q_3 \\ q_1 & q_0 & -q_3 & q_2 \\ q_2 & q_3 & q_0 & -q_1 \\ q_3 & -q_2 & q_1 & q_0 \end{bmatrix} \begin{bmatrix} \cos \frac{\Phi}{2} \\ \frac{\sin 0.5\Phi}{\Phi} \Phi_x \\ \frac{\sin 0.5\Phi}{\Phi} \Phi_y \\ \frac{\sin 0.5\Phi}{\Phi} \Phi_z \end{bmatrix} \quad (\text{B.5})$$

## B.2 Navigation Frame Rotation Update

Like the body frame motion updating, the updating for the navigation frame rotation at  $k^{\text{th}}$  epoch is conducted as:

$$q_b^n(k) = q_i^n(k)q_b^n(k-1) \quad (\text{B.6})$$

where  $q_i^n(j)$  is attitude quaternion relating  $n$ -frame rotation with respect to the  $i$ -frame  $\omega_{in}^n$ .

After integrating angular velocities of the  $n$ -frame rotation around the  $i$ -frame  $\omega_{in}^{n_x}$ ,  $\omega_{in}^{n_y}$ ,  $\omega_{in}^{n_z}$  to rotation angles  $\Theta_x$ ,  $\Theta_y$ ,  $\Theta_z$ , the quaternion  $q_i^n(j)$  is constructed as:

$$q_i^b(j) = \begin{bmatrix} \cos \frac{\Phi}{2} \\ -\frac{\sin 0.5\Phi}{\Phi} \Phi_x \\ -\frac{\sin 0.5\Phi}{\Phi} \Phi_y \\ -\frac{\sin 0.5\Phi}{\Phi} \Phi_z \end{bmatrix} \quad (\text{B.7})$$

Hence, the navigation frame motion update with the Equation (B.6) can be accomplished by using the quaternion product rule, like the Equation (B.5).

## B.3 Quaternion Normalisation Correction

Using its characteristic that the sum of the squared quaternion elements is unity, the quaternion normalisation errors can be computed as follows:

$$\delta_q = q_0^2 + q_1^2 + q_2^2 + q_3^2 - 1 \quad (\text{B.8})$$

This normalisation condition should be checked out periodically by  $\delta_q$  and then used to correct the elements to maintain normality. The correction is based on the following equation.

$$q = q - 0.5\delta_q q \tag{B.9}$$

**APPENDIX C**  
**PROOF OF EQUATION (5.22)**

---

The covariance matrix for single epoch float ambiguity estimation within an integrated GPS/Pseudolite/INS system is derived as follows.

From Equation (5.9), we can obtain:

$$\begin{aligned}
 A^T P A &= \begin{bmatrix} A_b^T & A_b^T & I \\ \lambda I & 0 & 0 \end{bmatrix} \begin{bmatrix} P_{\nabla\Delta\phi} & 0 & 0 \\ 0 & P_{\nabla\Delta R} & 0 \\ 0 & 0 & P_{ins} \end{bmatrix} \begin{bmatrix} A_b & \lambda I \\ A_b & 0 \\ I & 0 \end{bmatrix} \\
 &= \begin{bmatrix} N_{11} & N_{12} \\ N_{21} & N_{22} \end{bmatrix}
 \end{aligned} \tag{C.1}$$

with

$$N_{11} = A_b^T P_{\nabla\Delta\phi} A_b + A_b^T P_{\nabla\Delta R} A_b + P_{ins}$$

$$N_{12} = \lambda A_b^T P_{\nabla\Delta\phi}$$

$$N_{21} = \lambda P_{\nabla\Delta\phi} A_b$$

$$N_{22} = \lambda^2 P_{\nabla\Delta\phi}$$

Then, the covariance matrix for the unknown parameters is:

$$\mathcal{Q}_{\hat{X}} = \begin{bmatrix} \mathcal{Q}_{X_b} & \mathcal{Q}_{X_b} \mathcal{Q}_{X_a} \\ \mathcal{Q}_{X_a} \mathcal{Q}_{X_b} & \mathcal{Q}_{X_b} \end{bmatrix} = \begin{bmatrix} N_{11} & N_{12} \\ N_{21} & N_{22} \end{bmatrix}^{-1} \tag{C.2}$$

According to the matrix inversion by partitioning theorem (Mikhail, 1976), the covariance matrix of the float baseline solution (C.3) and of the float ambiguities (C.4) are derived as follows:

$$\begin{aligned}
\mathcal{Q}_{X_b} &= (N_{11} - N_{12}N_{22}^{-1}N_{21})^{-1} \\
&= \left( \underbrace{A_b^T P_{\nabla\Delta R} A_b}_{\mathcal{Q}_{\hat{x}, \nabla\Delta R}^{-1}} + P_{ins} \right)^{-1} \\
&= (\mathcal{Q}_{\hat{x}, \nabla\Delta R}^{-1} + \mathcal{Q}_{ins}^{-1})^{-1}
\end{aligned} \tag{C.3}$$

with

$$\begin{aligned}
N_{12}N_{22}^{-1}N_{21} &= (\lambda A_b^T P_{\nabla\Delta\phi}) \left( \frac{1}{\lambda^2} \mathcal{Q}_{\nabla\Delta\phi} \right) (\lambda P_{\nabla\Delta\phi} A_b) \\
&= A_b^T P_{\nabla\Delta\phi} A_b
\end{aligned}$$

$$\begin{aligned}
\mathcal{Q}_{X_a} &= N_{22}^{-1} + N_{22}^{-1}N_{21} \underbrace{(N_{11} - N_{12}N_{22}^{-1}N_{21})^{-1}}_{\mathcal{Q}_{\hat{x}_b}} N_{12}N_{22}^{-1} \\
&= \frac{1}{\lambda^2} \mathcal{Q}_{\nabla\Delta\phi} + \frac{1}{\lambda^2} \underbrace{A_b \mathcal{Q}_{\hat{x}_b} A_b^T}_{\mathcal{Q}_i} \\
&= \frac{1}{\lambda^2} (\mathcal{Q}_{\nabla\Delta\phi} + \mathcal{Q}_i)
\end{aligned} \tag{C.4}$$

with

$$\begin{aligned}
N_{22}^{-1}N_{21} &= \left( \frac{1}{\lambda^2} \mathcal{Q}_{\nabla\Delta\phi} \right) (\lambda P_{\nabla\Delta\phi} A_b) \\
&= \frac{1}{\lambda} A_b
\end{aligned}$$

$$\begin{aligned}
N_{12}N_{22}^{-1} &= (\lambda A_b^T P_{\nabla\Delta\phi}) \left( \frac{1}{\lambda^2} \mathcal{Q}_{\nabla\Delta\phi} \right) \\
&= \frac{1}{\lambda} A_b^T
\end{aligned}$$

DETAILED FLIGHT EXPERIMENT RESULTS

D.1 GPS/Pseudolite/INS Integration Based on DD Carrier Phases

D.1.1 Navigation solutions

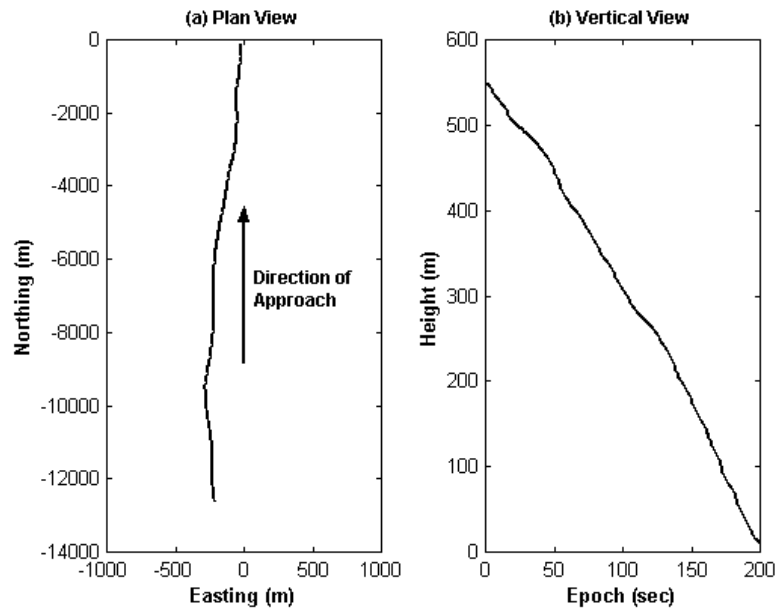


Figure D-1 Plan and vertical views of the flight trajectory in ENU frame (origin at reference station)

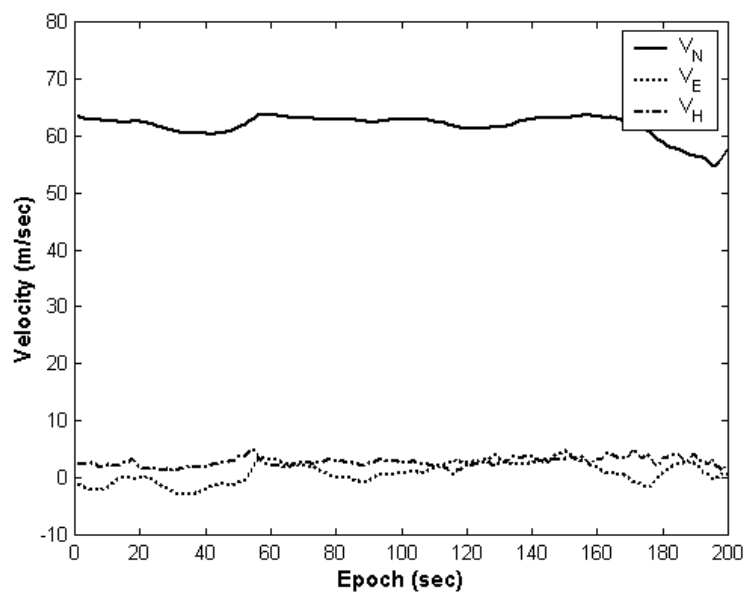


Figure D-2 Velocities in ENU frame for the vehicle



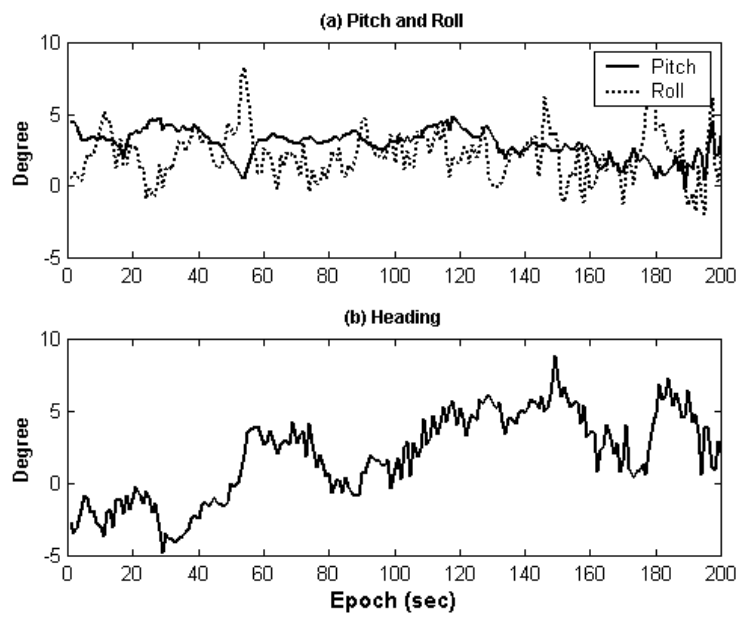


Figure D-3 The estimated attitudes for the vehicle

### D.1.2 Errors of navigation solution

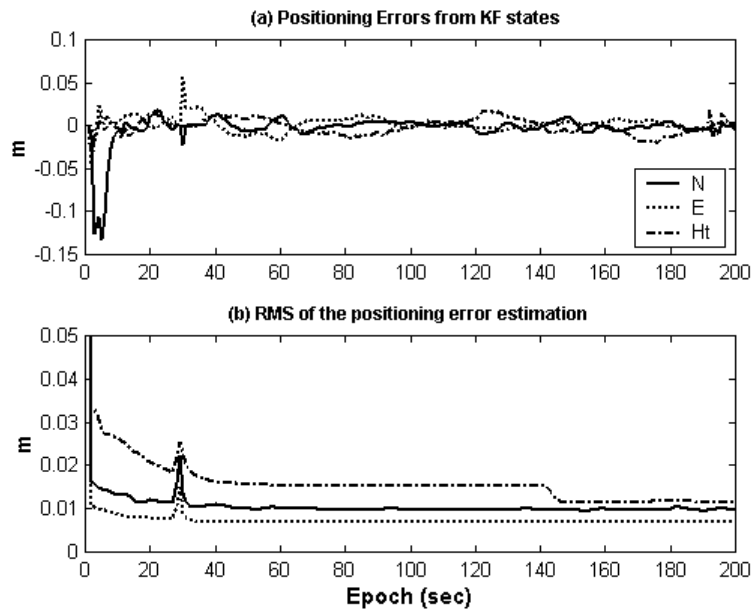


Figure D-4 Estimated position errors from the filter states and their RMS

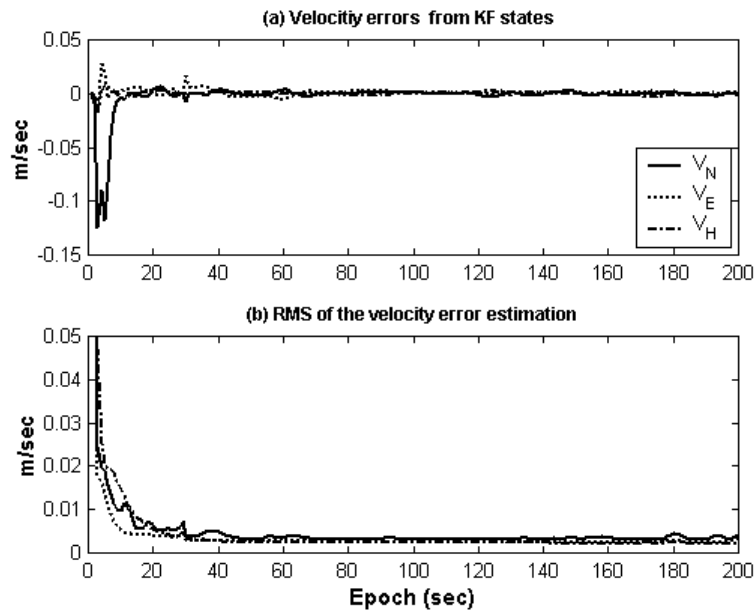


Figure D-5 Estimated velocity errors from the filter states and their RMS

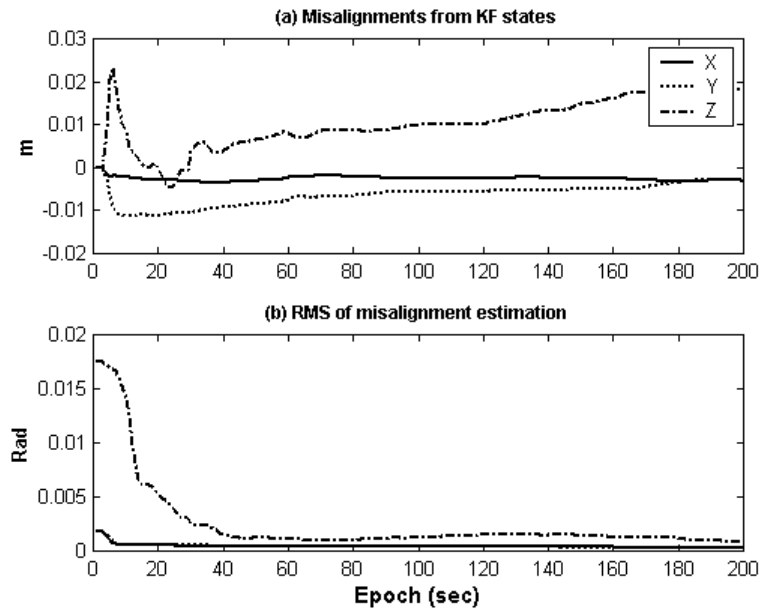


Figure D-6 Estimated three misalignments of the platform frame and their RMS

## D.1.3 Sensor errors

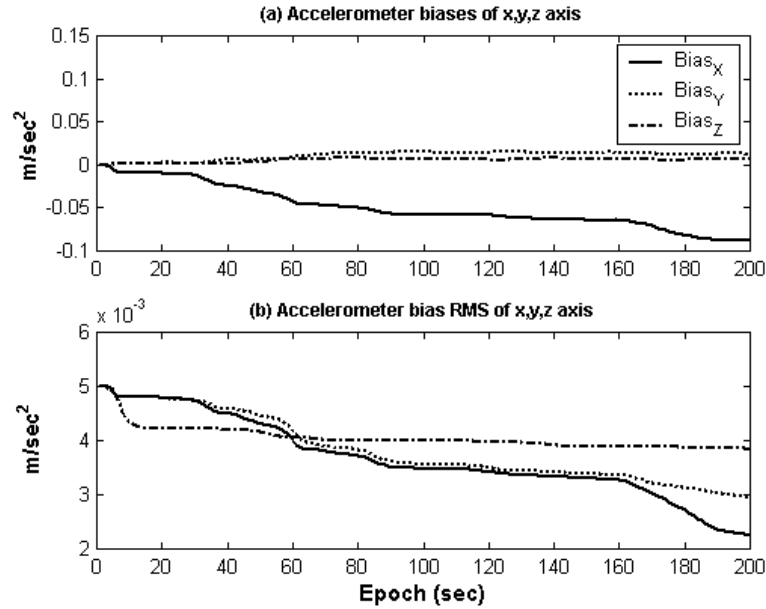


Figure D-7 Estimated accelerometer biases from the filter and their RMS

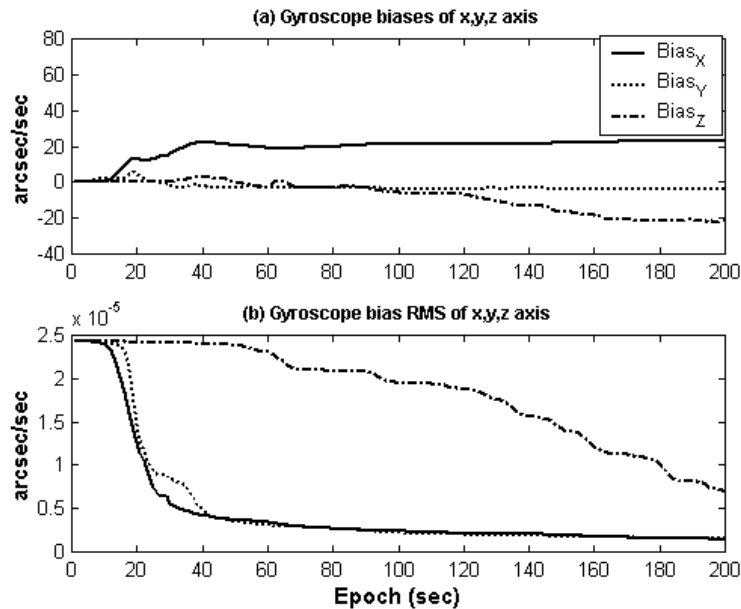


Figure D-8 Estimated gyroscope biases from the filter and their RMS

## D.2 GPS/Pseudolite/INS Integration Based on DD Pseudo-Ranges

### D.2.1 Navigation solutions

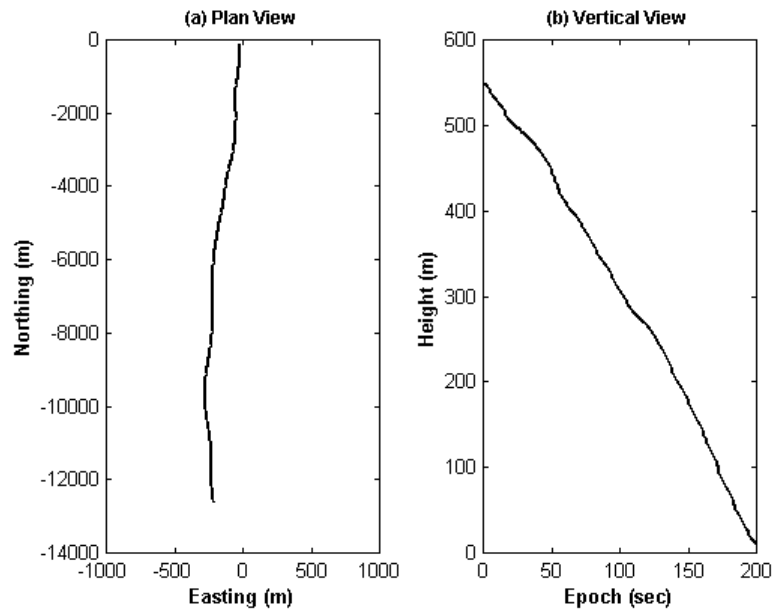


Figure D-9 Plan and vertical view of the flight trajectory in ENU frame (origin at reference station)

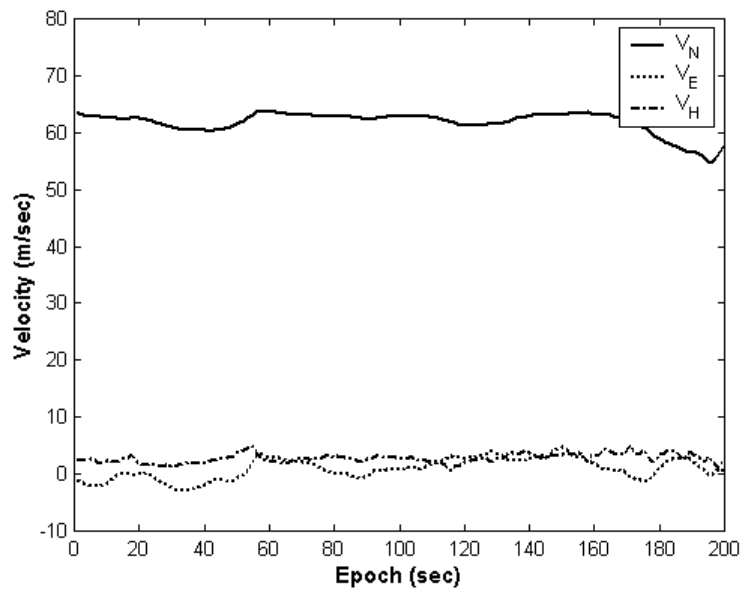


Figure D-10 Velocities in ENU frame for the vehicle

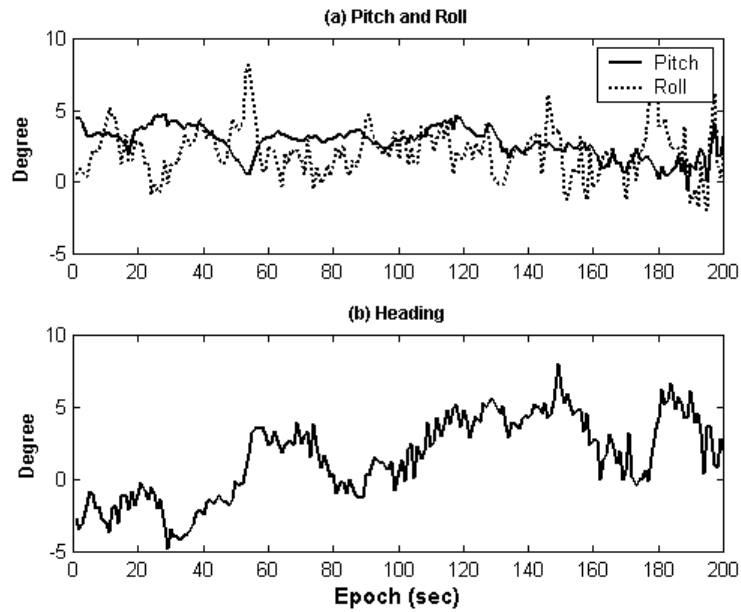


Figure D-11 Attitudes for the vehicle

### D.2.2 Errors of navigation solution

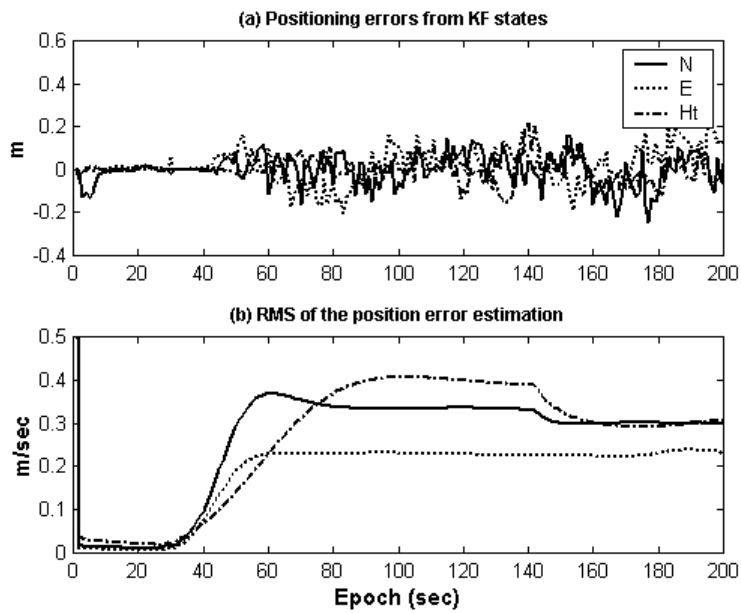


Figure D-12 Estimated position errors from the filter states and their RMS

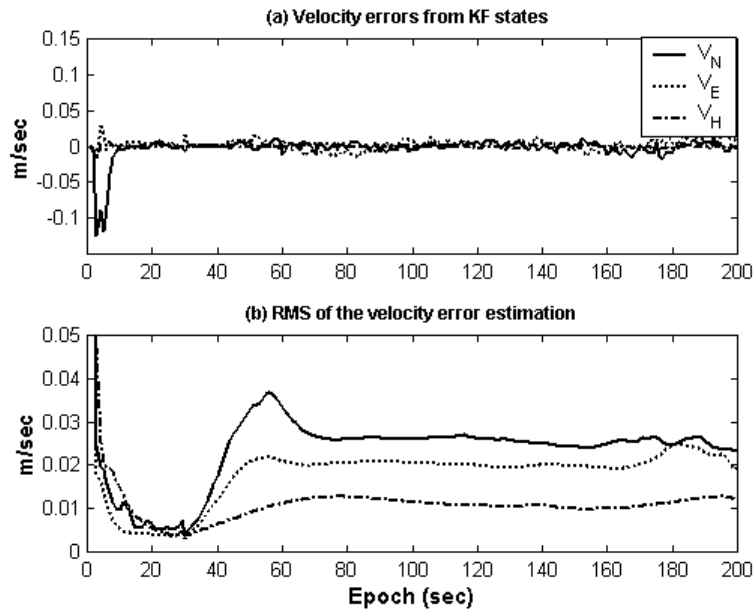


Figure D-13 Estimated velocity errors from the filter states and their RMS

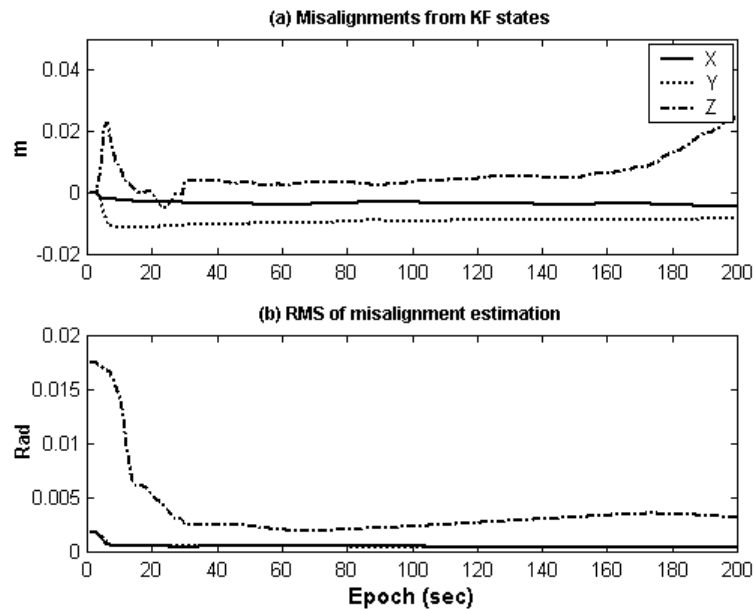


Figure D-14 Estimated three misalignments of the platform frame and their RMS

## D.2.3 Sensor errors

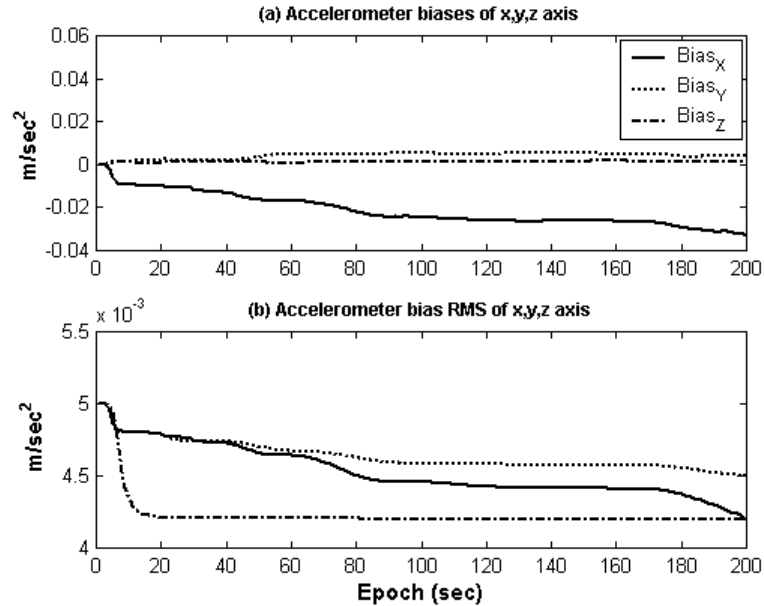


Figure D-15 Estimated accelerometer biases from the filter and their RMS

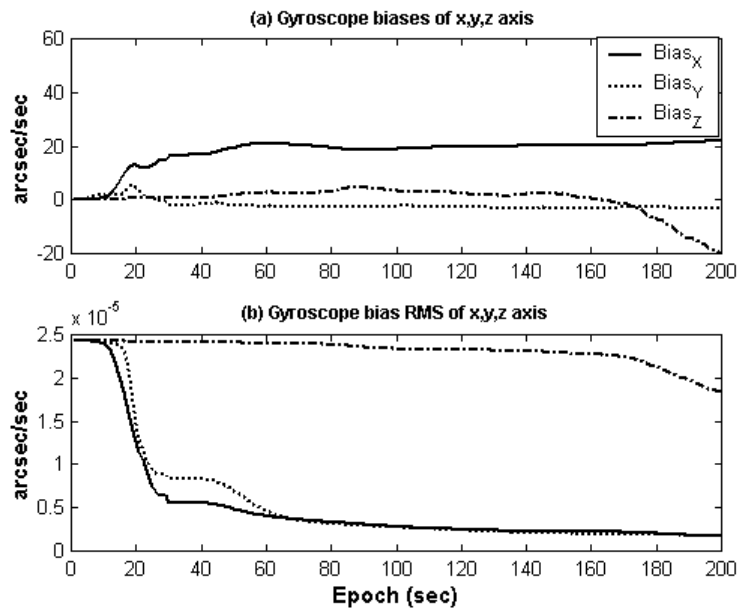


Figure D-16 Estimated gyroscope biases from the filter and their RMS

---

---

**Biodata**

Full name: Hung Kyu Lee  
Gender: Male  
Date of birth: March 13, 1972  
Nationality: Republic of Korea  
Marital status: Married  
Address: School of Surveying and Spatial Information Systems  
University of New South Wales  
Sydney NSW 2052, Australia

**Universities attended and degrees obtained:**

2001-present: Ph.D. Candidate  
School of Surveying and Spatial Information Systems  
*(formerly School of Geomatics Engineering)*  
Faculty of Engineering  
The University of New South Wales  
Sydney, Australia

1998-2000: Master of Science  
Department of Civil Engineering (Geomatics)  
Dong-A University  
Pusan, Republic of Korea

1992-1998: Bachelor of Science  
Department of Civil Engineering  
Dong-A University  
Pusan, Republic of Korea



## **Awards and Prizes**

2002-present: Scholarship from The Kwanjeong Educational Foundation, Seoul, Republic of Korea to undertake PhD studies at the University of New South Wales, Sydney, Australia.

2002: Best Student Paper Award, *Second International Symposium on Geodesy for Geotechnical and Structural Applications*, International Association of Geodesy (IAG), Commission IV, 21-24 April, Berlin, Germany.

2002: Student Paper Competition Award to present the paper at the *15<sup>th</sup> International Technical Meeting of the Satellite Division of the U.S. Institute of Navigation*, 24-27 September, Portland, Oregon, USA.

2002: Second Place Winner of Student paper competition, *Heiskanen Symposium on Geodesy*, Columbus, 1-5 October, Ohio, USA.

## **Professional Membership**

Member, International Association of Geodesy (IAG)

Member, A Joint Working Group of Intercommission on Theory (ICCT) and Commission 4 of the International Association of Geodesy (IAG) – Statistic and Geometry in Mixed Integer Linear Models, with Application to GPS and InSAR

Member, A Working Group 4.1.1 of International Association of Geodesy (IAG) – Advances in Inertial Navigation and Error Modelling Algorithms

Member, U.S. Institute of Navigation (ION)

Member, Australian Global Positioning Systems Society

Member, Institution of Surveyors, Australia (ISA)

Member, The Korean Society of Geodesy, Photogrammetry, and Cartography (KSGPC)

---

Member, The Korean Society of Civil Engineers (KSCE)

## **Academic Contributions (2002-present)**

### **Journal Papers**

1. **Lee, H.K.**, Wang, J., Rizos, C. and Grejner-Brzezinska, D. (2002) GPS/Pseudolite/INS Integration: Concept and First Tests. *GPS Solutions*, Vol. 6 (1-2), ISSN 1080-5370 (print version) 1521-1886 (electronic version), pp. 34-46.
2. Wang, J. and **Lee, H.K.** (2002) Impact of Pseudolite Location Errors in Positioning. *Geomatics Research Australia*, ISSN 0159-8910, Vol. 77, pp. 81-94.
3. **Lee, H.K.**, Wang, J. and Rizos, C., (2003) Effective cycle slip detection and identification for high precision GPS/INS integration systems. *Journal of Navigation*, ISSN 0373-4633, Vol. 56, No. 3, pp. 475-486.
4. Wang, J., **Lee, H.K.** and Rizos, C. (2003) GPS/INS integration: A performance sensitivity analysis. *Journal of Nature Sciences*, ISSN 1007-1202, Vol. 8, No. 2B, pp. 508-516.
5. **Lee, H.K.**, Wang, J., Rizos, C. and Grejner-Brzezinska, D. (2004) Analysing the impact of integrating pseudolite observables into a GPS/INS system. *ASCE Journal of Surveying Engineering*, ISSN 0733-9453, Vol. 130, No. 2, pp. 95-103.
6. **Lee, H.K.**, Wang, J., Rizos, C. and Tsujii, T. (2004) Augmenting GPS by ground-based, pseudolite signals for airborne surveying applications. *Accepted for publication in Survey Review on 25<sup>th</sup> May 2003, To appear in Vol. 38.*
7. Hewitson, S., **Lee, H.K.** and Wang, J. (2004) Localizability analysis for GPS/Galileo receiver autonomous integrity monitoring. *Journal of Navigation*, ISSN 0373-4633, Vol. 57, No. 2, pp. 245-259.

8. **Lee, H.K.**, Wang, J. and RIZOS, C. (2003) An integer ambiguity resolution procedure for GPS/Pseudolite/INS integration, *Submitted to Journal of Geodesy* in October.

### Conference and Symposium Papers

1. **Lee, H.K.**, Wang, J. and Rizos, C. (2002) Kinematic positioning with an integrated GPS/Pseudolite/INS. *Proceeding of 2<sup>nd</sup> Symposium on Geodesy for Geotechnical & Structural Applications*, Berlin, Germany, 21-24 May, pp. 314-325.
2. **Lee, H.K.** (2002) GPS/Pseudolite/SDINS integration approach for kinematic applications. *Proceeding of 15<sup>th</sup> International Technical Meeting of the Satellite Division of the U.S. Institute of Navigation (ION GPS2002)*, Portland, Oregon, 24-27 September, pp. 1464-1473.
3. **Lee, H.K.**, Wang, J., Rizos, C., Barnes, J., Tsujii, T. and Soon, B.K.H. (2002) Analysis of pseudolite augmentation for GPS airborne applications. *Proceeding of 15<sup>th</sup> International Technical Meeting of the Satellite Division of the U.S. Institute of Navigation (ION GPS2002)*, Portland, Oregon, 24-27 September, pp. 2610-2618.
4. **Lee, H.K.** (2002) Effects of introducing pseudolite measurements into an integrated GPS/INS system. *Proceedings of Heiskanen Symposium on Geodesy*. Columbus, Ohio, 1-5 October, CD-ROM Proc.
5. **Lee, H.K.**, Wang, J., Rizos, C., Li, B. and Park, W.Y. (2003) Effective cycle slip detection and identification for high accuracy integrated GPS/INS positioning, *Proceedings of 6<sup>th</sup> International Symposium on Satellite Navigation Technology Including Mobile Positioning & Location Services (SatNav2003)*. Melbourne, Australia, 22-25 July, CD-ROM proc., Paper 43.
6. Soon, B.H.K., Barnes, J., Zhang, J., **Lee, H.K.** and Rizos, C. (2003) Preliminary results of the carrier-smoothed code-phase differential GPS/pseudolite system.

---

*Proceedings of 6<sup>th</sup> International Symposium on Satellite Navigation Technology Including Mobile Positioning & Location Services (SatNav2003)*, Melbourne, Australia, 22-25 July, CD-Rom Proc., Paper 48.

7. Barnes, J., Rizos, C., **Lee, H.K.**, Roberts, G.W., Meng, X., Cosser, E. and Dodson, A.H. (2003) The integration of GPS and pseudolites for bridge monitoring. *Proceedings of XXIIIth General Assembly of the IUGG*, Sapporo, Japan, 30 June-11 July, CD-ROM Proc.
8. Wang, J., **Lee, H.K.**, Hewitson, S., Rizos, C. and Barnes, J. (2003) Sensitive Analysis for GNSS Integer Carrier Phase Ambiguity Validation. *Proceedings of XXIIIth General Assembly of the IUGG*, Sapporo, Japan, 30 June-11 July, CD-ROM Proc.
9. Soon, B.H.K., Poh, E.K., Barnes, J., Zhang, J., **Lee, H.K.**, Lee, H.K. and Rizos, C. (2003) Flight test results of precision approach and landing augmented by airport pseudolites. *Proceedings of 16<sup>th</sup> Int. Tech. Meeting of the Satellite Division of the U.S. Institute of Navigation (ION GNSS2003)*, Portland, Oregon, 9-12 September, 2318-2325.
10. **Lee, H.K.**, Wang, J., Rizos, C. and Park, W.Y. (2003) Carrier phase processing issues for high accuracy integrated GPS/Pseudolite/INS systems. *Proceedings of 11<sup>th</sup> International Association of Institute of Navigation (IAIN) World Congress*, Berlin, Germany, October, CD-Rom Proc., Paper 252.
11. Wang, J., **Lee, H.K.**, Hewitson, S. and Lee, H.K. (2003) Influence of dynamics and trajectory on integrated GPS/INS navigation performance. *European Navigation Conference (GNSS2003)*, Graz, Austria, 22-25 April, CD-ROM proc.
12. Soon, B.K.H., Poh, E.K., Barnes, J., **Lee, H.K.**, Zhang, J., Lee, H.K. and Rizos, C. (2004) Pseudolite augmented GPS navigation for automatic landing of flight vehicles, *New Challenges in Aerospace Technology and Maintenance Conference 2004 (NCATMC 2004)*, Singapore, 20-21 February, CD-ROM proc.

13. Soon, B.K.H., Barnes, J., **Lee, H.K.**, Zhang, J., Rizos, C., Wang, J. and Lee, H.K. (2004) Real-time flight test results of an integrated GPS/INS/pseudolite autolanding system. *European Navigation Conference (GNSS2004)*, Rotterdam, The Netherlands, 16-19 May. CD-ROM proc.